BRITTANY M. DUGGAN

REGULATION OF BLOOD GLUCOSE BY XENOBIOTIC AND MICROBIAL IMPACTORS OF RIPK2 SIGNALLING

By Brittany M. Duggan, B.Sc.

A Thesis Submitted to the School of Graduate Studies in Partial Fulfillment of the Requirements for the Degree Doctor of Philosophy

McMaster University DOCTOR OF PHILOSOPHY (2018) Hamilton, Ontario (Medical Sciences)

TITLE: Regulation of blood glucose by xenobiotic and microbial impactors of RIPK2 signalling

AUTHOR: Brittany M. Duggan

SUPERVISOR: Associate Professor J.D. Schertzer

NUMBER OF PAGES: 219

LAY ABSTRACT

Introduction: Obesity increases the risk of chronic diseases, including Type 2 Diabetes (T2D). Obesity stops insulin from working properly, leading to the inability to lower blood glucose. Obesity and T2D are linked to chronic, low-grade activation of the immune system. The immune system normally defends the body against microbes by inducing a pro-inflammatory response. Inflammation can also be activated or inhibited by drugs (xenobiotics), and different aspects of inflammation can increase or decrease blood glucose and insulin. A major unanswered question was how certain cancer drugs and bacterial components interact with the immune system to change blood glucose or insulin. This work tested how an innate immune pathway that detects bacterial cell wall components is influenced by cancer drugs and alters blood glucose and insulin in pre-clinical models. This work is targeted at understanding how new prebiotics or existing drugs can be tasked as therapeutic strategies for prediabetes and T2D.

ABSTRACT

Obesity is characterized by hyperinsulinemia and chronic inflammation, contributing to insulin resistance and type 2 diabetes (T2D) risk. Pattern recognition receptors (PRRs) of the innate immune system, including Toll-like Receptors (TLRs) and Nod-like Receptors (NLRs), have been identified as propagators of metabolic inflammation. Circulating bacterial components exert distinct effects on inflammation and insulin sensitivity via TLRs and NLRs. Specific types of bacterial peptidoglycan engage NOD1 and NOD2. Activators of NOD1 increase inflammation and insulin resistance, while activators of NOD2 promote immune tolerance and insulin sensitivity. NOD1 and NOD2 use the common downstream adaptor RIPK2 to drive immune responses, but the role of RIPK2 in glucose homeostasis was unknown. RIPK2 is positioned to mediate effects of xenobiotics and microbial components on blood glucose. For example, tyrosine kinase inhibitors (TKIs) are being investigated for diabetes treatment. Improvements in blood glucose control have been observed in diabetic cancer patients receiving TKI therapy but the mechanism underlying these changes remains unclear. Several TKIs inhibit RIPK2. We sought to understand if TKIs that inhibit RIPK2 block inflammatory and metabolic consequences of NOD signalling. We hypothesized inhibition of inflammation via NOD1-RIPK2 by certain TKIs contributes to lowered blood glucose/improved insulin sensitivity in pre-clinical models of obesity. We showed that RIPK2 was required for acute glycemic consequences of NOD1 and NOD2 activation, and RIPK2-specific TKIs attenuated these glycemic effects. We found TKI-mediated improvements in blood glucose are independent of NOD-RIPK2 signalling during diet-induced obesity. However, RIPK2 mediated the effects of certain TKIs on blood insulin. Finally, we tested if RIPK2 mediated the effects of bacterial components derived from commensal microbiota. We found injection of upper intestinal microbe components lowered blood glucose via NOD2-RIPK2 signalling. These findings demonstrate that modulation of RIPK2 signalling by xenobiotic or microbial factors is an important contributor to blood glucose and insulin homeostasis.

ACKNOWLEDGEMENTS

I would first like to acknowledge my supervisor, Dr. Jonathan Schertzer. You have provided me with a unique and special mentorship over the course of my graduate degree that prompted my gradual transition from flustered, frightened and anxious amateur to a well-balanced, analytical scientist with increasingly independent research abilities and aspirations. These experiences have roused in me a spirit of scientific curiosity and integrity that I will long carry with me into an academic future. As I strive to have mentees of my own one day, your thoughtful approach and unwavering support will not be forgotten. Thank you.

I would also like to thank the members of my supervisory committee, Dr. Deborah Sloboda and Dr. Thomas Hawke. Your astute input over the years has provided invaluable research considerations that contributed to the success of this work and to my academic and professional development as a scientist.

Another expression of gratitude is owed to my fellow Schertzer (and neighboring) labmates; over endless glucose tolerance tests, lab meetings, the occasional late-night tissue harvest, lunchtimes in the lounge, hallway coffees, Christmas potlucks, conference travels, and Phoenix beers; the weight of these friendships have tipped the scales heavily in favour of a pleasurable and satisfying PhD experience and I would not hesitate to make the same decision again.

Finally, to my parents. I'm sure you still don't understand what I'm doing (or even why I'm doing it), and trying to read this document surely won't help with that, but your steadfast support and resolute encouragement through it all has provided me a lifetime of intellectual opportunity and exploration that I could not be more grateful for.

STATEMENT OF CONTRIBUTIONS

Chapter 3.1:

Authors: Brittany M. Duggan, Kevin P. Foley, Brandyn D. Henriksbo, Joseph F. Cavallari Akhilesh K. Tamrakar, Jonathan D. Schertzer

Contributions: B.M.D. and J.D.S. conception and design of research; B.M.D., K.P.F., B.D.H., J.F.C. and A.K.T. performed or assisted with experiments; B.M.D. performed all analysis. B.M.D. and J.D.S. interpreted experimental results.

Chapter 3.2:

Authors: Brittany M. Duggan, Kevin P. Foley, Joseph F. Cavallari, Nicole G. Barra, Jonathan D. Schertzer

Contributions: B.M.D. and J.D.S. conception and design of research; B.M.D., K.P.F., N.G.B., and J.F.C. performed or assisted with experiments; B.M.D. performed all analysis. B.M.D. and J.D.S. interpreted experimental results.

Chapter 3.3:

Authors: Brittany M. Duggan, Kevin P. Foley, Nicole G. Barra, Akhilesh K. Tamrakar, Fernando F. Anhê, Jonathan D. Schertzer

Contributions: B.M.D. and J.D.S. conception and design of research; B.M.D., K.P.F., N.G.B., A.K.T. and F.F.A. performed or assisted with experiments; B.M.D. performed all analysis. B.M.D. and J.D.S. interpreted experimental results.

TABLE OF CONTENTS

Title Page		i
Descriptive note		ii
Lay abstract		iii
Abstract		iv
Acknowledgements		v
Statement of contribution		vi
Table of contents		vii
List of figures & tables		x
List of abbreviations		xv
Declaration of academic achievements		xvii

Chapter 1: Introduction

1.1	**Obesity and Type 2 Diabetes**	**2**
	1.1.1 Etiology of obesity and metabolic syndrome	2
	1.1.2 Pathogenesis of T2D	8
	1.1.3 Insulin and insulin signalling	11
	1.1.4 Mechanisms of insulin resistance and β-cell function	14
1.2	**Immunometabolism**	**17**
	1.2.1 Obesity, inflammation and insulin resistance	18
	Adipose	21
	Liver	21
	Skeletal muscle	23
	Pancreas, brain and gastrointestinal tract	23
1.3	**Pattern recognition receptors**	**25**
	1.3.1 NOD1 and NOD2 in immunity and inflammatory disease	26
	1.3.2 Immunometabolism of NODs	29
	1.3.3 Immunometabolism of RIPK2	30
1.4	**Gut microbes, immunity and metabolism**	**32**
	1.4.1 Gut microbes in metabolic disease	34
1.5	**Xenobiotics, immunity and metabolism**	**36**
	1.5.1 Xenobiotics alter innate immunity	36
	1.5.2 Clinically approved kinase inhibitors	38
	1.5.3 Kinase inhibitors regulate blood glucose	42
1.6	**Hypothesis and objectives**	**45**

Chapter 2: Materials and methods

2.1	**Mice and materials**	**48**
2.2	**Cell culture**	**50**
2.3	**Glycerol assay and ELISA**	**51**
2.4	**NF-κB activity**	**52**
2.5	**Immunoblotting**	**52**
2.6	**Gene expression analysis**	**53**
2.7	***In vivo* Glucose and insulin tests**	**54**
2.8	**Inflammatory, dietary and intestinal injection mouse models**	**55**
	2.8.1 Acute NOD1 activation model	55
	2.8.2 Acute NOD2 activation model	56
	2.8.3 TKI Intervention models	56
	2.8.4 Collection and preparation of intestinal extracts	57
	2.8.5 Chow Intestinal injection model	59
	2.8.6 HFD Intestinal injection model	59
2.9	**TKI serum quantification**	**59**
	2.9.1 Quantification of serum TKI concentration after single administration in chow diet fed mice	59
	2.9.2 Quantification of serum TKI concentration during repeated administration in obese mice	60
	2.9.3 TKI serum sample processing and quantification	60
2.10	**Quantification of 16S rRNA in intestinal extracts**	**61**
2.11	**Statistical analysis**	**62**

Chapter 3: Results

3.1	**Kinase inhibitors of RIPK2 attenuate NOD-mediated immunometabolism**	**66**
	3.1.1 Kinase inhibitors of RIPK2 attenuate NOD1-mediated lipolysis	66
	3.1.2 Kinase inhibitors of RIPK2 attenuate NOD1-mediated inflammation in metabolic and immune cells	72
	3.1.3 Kinase inhibitors of RIPK2 attenuate NOD1-mediated insulin resistance in adipocytes	79
	3.1.4 Kinase inhibitors of RIPK2 attenuate NOD1-mediated inflammation *in vivo*	80
	3.1.5 RIPK2 is required for NOD1-mediated changes in blood glucose *in vivo* and kinase inhibitors of RIPK2 mitigate dysglycemia caused by NOD1 activation	84

	3.1.6 RIPK2 is required for NOD2-mediated changes in blood glucose *in vivo* and kinase inhibitors of RIPK2 attenuate glycemic effects of NOD2 activation	86
3.2	**Metabolic effects of kinase inhibitors during obesity**	**92**
	3.2.1 Kinase inhibitor gefitinib attenuates obesity-induced glucose and insulin tolerance	92
	3.2.2 Kinase inhibitor gefitinib attenuates obesity-induced glucose intolerance independent from NOD1, NOD2 and RIPK2	101
	3.2.3 RIPK2-selective kinase inhibitors lower insulin, but only in *Ripk2*$^{-/-}$ mice	106
	3.2.4 Kinase inhibitor imatinib attenuates obesity-induced glucose intolerance but induces hyperinsulinemia	116
3.3	**Upper intestinal commensal microbe components alter glucose homeostasis via NOD-RIPK2 signalling**	**126**
	3.3.1 Injection of mice with diluted ileal luminal contents improves blood glucose control in a dose-dependent manner	128
	3.3.2 Injection of ileal extracts improves glucose control in lean and obese mice, independent of diet fed to donor or recipient mice	133
	3.3.3 Intestinal extracts from upper gut segments alter blood glucose	145
	3.3.4 Injection of mice with ileal extracts does not alter insulin secretion in lean or obese mice	150
	3.3.5 Bacteria are required for intestinal extracts to lower blood glucose	153
	3.3.6 Intestinal extract injection requires NOD2-RIPK2 to alter blood glucose	155
	3.3.7 Quantification of bacterial 16S rRNA in intestinal extracts	167

Chapter 4: Discussion

4.1	**Kinase inhibitors of RIPK2 attenuate NOD-mediated immunometabolism**	**169**
4.2	**Metabolic effects of kinase inhibitors during obesity**	**178**
4.3	**Upper intestinal commensal microbe components alter glucose homeostasis via NOD-RIPK2 signalling**	**183**
4.4	**Research limitations & future directions**	**189**
4.5	**Summary**	**195**

Chapter 5: References **197**

List of Figures & Tables

Figure 1.1	The causes underlying weight gain and the development of obesity are complex and multifactorial	6
Figure 1.2	Progression from impaired glucose tolerance to development of Type 2 Diabetes	10
Figure 1.3	The domain structures of NOD1, NOD2 and RIPK2	28
Figure 1.4	Immunometabolism of NOD-RIPK2 signalling	32
Figure 1.5	Binding modes of reversible small molecule kinase inhibitors	40
Figure 1.6	Distinct TKIs and overlapping TKI targets manifest effects on blood glucose, blood insulin and pancreatic β-cell survival in clinical reports and animal models	44
Figure 3.1.1	Experimental design of 3T3-L1 adipocyte and bone marrow-derived macrophage treatment to investigate inhibition of NOD1 immunometabolism by TKIs	67
Figure 3.1.2	Select TKIs inhibit bacterial cell wall-mediated lipolysis in adipocytes	68
Figure 3.1.3	TKI gefitinib, but not imatinib, inhibits bacterial cell wall-mediated glycerol release rate in adipocytes	69
Figure 3.1.4	TKI gefitinib inhibits bacterial cell wall-mediated, but not adrenergic lipolysis	70
Figure 3.1.5	NOD1-mediated changes in gene expression of molecular markers of lipid oxidation, transport and synthesis	72
Figure 3.1.6	TKI gefitinib, but not imatinib, inhibits bacterial cell wall-mediated cytokine responses in adipocytes	75
Figure 3.1.7	TKI gefitinib does not inhibit endotoxin-induced cytokine responses in adipocytes	76
Figure 3.1.8	RIPK2 is required for macrophage inflammation induced by bacterial cell wall muropeptides, but not endotoxin	77
Figure 3.1.9	NOD1 activation does not potently stimulate IL-6 release in macrophages	78
Figure 3.1.10	TKI gefitinib inhibits NF-κB activity induced by bacterial cell wall components, but not endotoxin	79
Figure 3.1.11	TKI gefitinib attenuates bacterial cell wall-mediated insulin resistance in adipocytes	80

Figure 3.1.12	Experimental design to investigate inhibition of NOD1 immunometabolism by TKIs *in vivo*	82
Figure 3.1.13	TKI gefitinib inhibits RIPK2-mediated inflammation *in vivo*	83
Figure 3.1.14	RIPK2 mediates bacterial cell wall-mediated dysglycemia *in vivo*	85
Figure 3.1.15	TKI gefitinib inhibits bacterial cell wall-induced dysglycemia *in vivo*	86
Figure 3.1.16	RIPK2 is required for NOD2-mediated glycemic effects during acute endotoxemia *in vivo*	89
Figure 3.1.17	TKI gefitinib attenuates NOD2-mediated glycemic effects during endotoxemia challenge *in vivo*	90
Figure 3.1.18	TKI imatinib does not attenuate NOD2-mediated glycemic effects during endotoxemia challenge *in vivo*	91
Figure 3.2.1	Experimental design for investigating metabolic effects of TKI gefitinib during obesity	93
Figure 3.2.2	Intervention with 50 mg/kg gefitinib does not alter body mass, food consumption or tissue morphology across treatment period	94
Figure 3.2.3	TKI gefitinib improves obesity-induced glucose and insulin intolerance independently of body mass or adiposity	96
Figure 3.2.4	TKI gefitinib does not improve insulin signalling in adipose or liver tissue during obesity	97
Figure 3.2.5	TKI gefitinib does not alter blood glucose control in lean mice	98
Figure 3.2.6	TKI gefitinib improves blood glucose control independently of body mass or adiposity in obese *Wt/N* mice	100
Figure 3.2.7	TKI gefitinib improves blood glucose control during obesity independently of NOD1	103
Figure 3.2.8	TKI gefitinib improves blood glucose control during obesity independently of NOD2	104
Figure 3.2.9	TKI gefitinib improves blood glucose control during obesity independently of RIPK2	105
Figure 3.2.10	TKI gefitinib does not alter insulin secretion or insulin resistance in *Wt/J* or *Wt/N* mice	107
Figure 3.2.11	TKI gefitinib attenuates insulin secretion and insulin resistance in *Ripk2*$^{-/-}$, but not *Nod1*$^{-/-}$ or *Nod2*$^{-/-}$ mice	109

Figure 3.2.12	TKI gefitinib does not alter inflammatory or ER-stress related gene profiles in adipose, and is not dictated by RIPK2	112
Figure 3.2.13	TKI gefitinib does not alter inflammatory or ER-stress related gene profiles in liver, and is not dictated by RIPK2	113
Figure 3.2.14	TKI gefitinib does not alter inflammatory or ER-stress related gene profiles in muscle, and is not dictated by RIPK2	114
Figure 3.2.15	TKI gefitinib does not alter inflammatory or ER-stress related gene profiles in pancreas, and is not dictated by RIPK2	115
Figure 3.2.16	Experimental design for investigating metabolic effects of TKI imatinib during obesity	117
Figure 3.2.17	Equimolar treatment with TKI imatinib does not attenuate obesity-induced glucose intolerance or insulin resistance	118
Figure 3.2.18	High-dose imatinib improves blood glucose control but induces hyperinsulinemia during obesity	120
Figure 3.2.19	TKI imatinib does not alter inflammatory or ER-stress related gene profiles in pancreas	121
Figure 3.2.20	Quantification of TKI gefitinib and imatinib serum concentration levels after a single administration in lean *Wt* mice	124
Figure 3.2.21	Quantification of TKI gefitinib and imatinib serum concentration levels after repeated administration in obese *Wt* mice	125
Figure 3.3.1	Ripk2 is required for MDP-mediated glycemic effects during diet-induced obesity	127
Figure 3.3.2	Published model of intestinal injection protocol in HFD-fed mice	129
Figure 3.3.3	Experimental design for preparation of intestinal extracts and injection protocol in recipient mice	130
Figure 3.3.4	Specific concentration of intestinal extracts is a critical factor for promoting blood glucose control following intestinal injection	132
Figure 3.3.5	Injection with ileal extracts promotes blood glucose control in chow-fed mice regardless of intestinal donor diet	134

Figure 3.3.6	Injection with ileal extracts promotes blood glucose control independent of sex	135
Figure 3.3.7	Previous injection with ileal extracts does not protect against the onset of glucose intolerance after 4 weeks of HFD feeding	138
Figure 3.3.8	Previous injection with ileal extracts does not alter progression of glucose intolerance after 8 weeks of HFD feeding	139
Figure 3.3.9	Injection with ileal extracts at 8 weeks of HFD reverses diet-induced glucose intolerance at 12 weeks	140
Figure 3.3.10	A single injection with ileal extracts at 8 weeks of HFD is insufficient to reverse diet-induced glucose intolerance	143
Figure 3.3.11	A second injection with ileal extracts at 12 weeks of HFD is sufficient to reverse diet-induced glucose intolerance	144
Figure 3.3.12	Glycemic effects of intestinal extracts are restricted to upper gut segments	146
Figure 3.3.13	Injection with intestinal extracts doesn't alter insulin tolerance after 6 weeks	148
Figure 3.3.14	Delayed onset of glycemic control phenotype following injection with upper gut segments	149
Figure 3.3.15	Intestinal extract injection does not alter insulin secretion in chow-fed mice	151
Figure 3.3.16	Intestinal extract injection does not alter insulin secretion in obese mice	152
Figure 3.3.17	Glucose tolerizing properties of intestinal extracts require an intact intestinal microbiota	154
Figure 3.3.18	NOD2 is required for glycemic effects following ileal extract injection	157
Figure 3.3.19	Absence of glucose phenotype is maintained after 8 weeks of high-fat feeding in *Nod2*$^{-/-}$ mice	158
Figure 3.3.20	Repeat MDP treatment acutely decreases blood glucose levels during a GTT in obese mice and persists for 4 weeks	159
Figure 3.3.21	A single MDP injection acutely increases blood glucose levels during a GTT in obese mice	160
Figure 3.3.22	RIPK2 protects against deleterious glucose control following ileal extract injection	162

Figure 3.3.23	Changes in blood glucose control persist after 8 weeks of HFD in *Ripk2*$^{-/-}$ mice	163
Figure 3.3.24	NOD1 protects against deleterious glucose control following ileal extract injection	165
Figure 3.3.25	Changes in blood glucose control are absent after 8 weeks of HFD in *Nod1*$^{-/-}$ mice	166
Figure 3.3.26	Quantification of 16S rRNA in intestinal extracts	167
Figure 4.1	Tyrosine kinase inhibitors of RIPK2 attenuate NOD1-mediated immunometabolism	173
Figure 4.2	Inhibition of RIPK2 limits the insulin sensitizing potential of a TKI	182
Figure 4.3	Postbiotic components derived from the microbiota can alter blood glucose homeostasis and is influenced by distinct NOD-RIPK2 signalling pathways	190
Table 1.1	Common TKIs inhibit numerous kinase targets	41
Table 2.1	Antibody reagent list	62
Table 2.2	TaqMan qPCR probe list	62

List of Abbreviations

AS160	Akt substrate of 160 kDa
β	beta
BMI	body mass index
ER	endoplasmic reticulum
FMT	fecal microbial transfer
FFA	free fatty acid
FOXO1	forkhead box protein O1
GLP-1	glucagon-like peptide-1
GLP-1R	glucagon-like peptide-1 receptor
GS	glycogen synthase
GSIS	glucose-stimulated insulin secretion
GSK	glycogen synthase kinase
HGP/HGO	hepatic glucose production/hepatic glucose output
IGT	impaired glucose tolerance
IL	interleukin
ILC	innate lymphoid cell
IR	insulin receptor
IRS	insulin receptor substrate
IKK	inhibitor of κB kinase
IκB	inhibitor of nuclear factor kappa B
JNK	c-Jun N-terminal kinase
LPS	lipopolysaccharide
mTORC	mammalian target of rapamycin complex
NF-κB	nuclear factor kappa B
NK	natural killer
NLR	NOD-like receptor
NOD1	nucleotide oligomerization domain-containing protein 1
NOD2	nucleotide oligomerization domain-containing protein 2
OGSIS	oral glucose-stimulated insulin secretion
PDK	phosphoinositide-dependent kinase
PI3K	phosphatidylinositol 3-kinase
PIP_2	phosphatidylinositol 4,5-diphosphate
PIP_3	phosphatidylinositol 3,4,5-triphosphate
PKB	protein kinase B
PKCθ	protein kinase C theta
PRR	pattern recognition receptor
PTB	phosphotyrosine-binding
PTEN	phosphatase and tensin homolog
RIPK2	receptor-interacting serine/threonine-protein kinase 2
ROS	reactive oxygen species
S6K	S6 kinase β-1
T1D	Type 1 Diabetes

T2D	Type 2 Diabetes
TKI	tyrosine kinase inhibitor
TLR	Toll-like receptor
TNFα	tumor necrosis factor alpha
Wt	wild type

Declaration of Academic Achievement

The 2 first-author peer-reviewed papers listed below comprise the majority of results described in Section 3.1 and 3.2 of this thesis, respectively. A manuscript is currently in preparation for the results described in Section 3.3, pending completion of a minor series of final experiments that were initially disrupted by the global pandemic.

First-author peer reviewed contributions

Duggan BM, Foley KP, Henriksbo BD, Cavallari JF, Tamrakar AK, Schertzer JD. Tyrosine kinase inhibitors of Ripk2 attenuate bacterial cell wall-mediated lipolysis, inflammation and dysglycemia. *Scientific Reports,* May 2017.

Duggan BM, Foley KP, Cavallari JC, Barra NG, Schertzer JD. RIPK2 dictates insulin-responses to tyrosine kinase inhibitors in obese male mice. *Endocrinology,* June 2020.

Co-author peer-reviewed contributions

Henriksbo BD, Lau TC, Cavallari JF, Denou E, Chi W, Lally JA, Crane JD, **Duggan BM**, Foley KP, Fullerton MD, Tarnopolsky MA, Steinberg GR, Schertzer JD. Fluvastatin causes NLRP3 inflammasome-mediated adipose insulin resistance. *Diabetes,* June 2014.

Denou E, Lolmede K, Chabo C, Lau TC, Fullerton MD, Nigro G, Zakaroff-Girard A, Luche E, Garret C, Serino M, Amar J, Courtney M, Cavallari JF, Henriksbo BD, Barra NG, Foley KP, McPhee JB, **Duggan BM**, O'Neill HM, Lee AJ, Sansonetti P, Ashkar AA, Khan WI, Surette MG, Bouloumie A, Steinberg GR, Burcelin R, Schertzer JD. Defective NOD2 peptidoglycan sensing promotes diet-induced inflammation, dysbiosis and insulin resistance. *EMBO Molecular Medicine,* Mar 2015.

Cavallari JF, Fullerton MD, **Duggan BM,** Foley KP, Denou E, Smith BK, Desjardins EM, Henriksbo BD, Kim KJ, Tuinema BR, Stearns JC, Prescott D, Rosentiel P, Coombes BK, Steinberg GR, Schertzer JD. Muramyl dipeptide-based postbiotics mitigate obesity-induced insulin resistance via IRF4. *Cell Metabolism*, May 2017.

Foley, KP, Zlitni S, Denoi E, **Duggan BM**, Chan RW, Stearns JC, Schertzer JD. Long term but not short-term exposure to obesity-related microbiota promotes host insulin resistance. *Nature Communications,* Nov 2018.

Henriksbo BD, Tamrakar AK, Xu J, **Duggan BM**, Cavallari JF, Phulka J, Stampfli MR, Ashkar AA, Schertzer JD. Statins promote interleukin-1β-dependent adipocyte insulin resistance through lower prenylation, not cholesterol. *Diabetes*, July 2019.

Cavallari JF, Barra NG, Foley KP, Lee A, **Duggan BM**, Henriksbo BD, Anhê FF, Ashkar AA, Schertzer JD. Postbiotics for NOD2 require nonhematopoietic RIPK2 to improve blood glucose and metabolic inflammation in mice. *American Journal of Physiology Endocrinology and Metabolism,* Mar 2020.

CHAPTER 1: Introduction

1.1 Obesity and Type 2 Diabetes

1.1.1 Etiology of obesity and metabolic disease

Obesity has more than doubled within the past three decades in high and low-income countries and it is estimated that there are more than 1.6 billion overweight and 600 million obese individuals worldwide[1]. Obesity is often defined as a body mass index (BMI) of 30 kg/m^2 or higher, and the World Health Organization also recognizes a BMI as 25 kg/m^2 or higher as overweight. Higher BMIs in overweight or obese individuals are associated with increased morbidity and decreased life expectancy[2,3]. The global rise in overweight and obese individuals is paralleled by an increase in the prevalence of chronic diseases, including (but not limited to) sleep apnea, non-alcoholic fatty liver disease, cardiovascular disease, hypertension, obesity-related cancers and Type 2 Diabetes (T2D)[2,3]. Obesity increases an individual's risk for developing metabolic syndrome, defined as the clustering of 3 or more of the following conditions; High blood pressure, high blood glucose levels, high triglycerides, low HDL-cholesterol, and higher visceral adiposity[2]. Obesity is one of the highest risk factors for T2D[4]. The rising prevalence, morbidity and mortality that is associated with obesity and T2D have sparked intensive research efforts into understanding the etiology of the connection between obesity and blood glucose control.

The causes underlying weight gain and the development of obesity are complex and multifactorial. Significant lifestyle shifts over the past several decades have played a role in the prevalence of obesity. Food availability, variety and

processing level have all increased and influenced contemporary dietary patterns, where many calorically dense foods are highly processed to include additional fat and sugar, enhancing palatability and overconsumption, contributing to increases in energy intake[5]. In addition, an increase in sedentary behaviour following the improvement of manufacturing, technology, transportation and automation has lowered daily energy expenditure in the average individual[6,7]. However, changes in overall energy balance cannot entirely explain the rising occurrence of obesity and additional environmental and genetic factors have been shown to play a role[8,9]. Mutations in genes coding for leptin[10], leptin receptor[11], melanocortin 4 receptor[12], and pro-opiomelanocortin[13] that result in severe early-onset obesity all highlight the important role that genetics can play in food seeking behaviour and energy homeostasis. While monogenic forms of obesity like these are rare, individual predisposition to weight gain has a strong genetic basis and genome-wide association studies have identified as many as loci that can collectively contribute to overall risk of obesity and T2D[14,15]. The heritability of BMI has been estimated as 40-70%, and observations from twins and adoption studies further support the notion that obesity is, partly, an inherited disorder of energy homeostasis[16,17]. Intrauterine environment and epigenetic intergenerational effects have also been shown to influence body weight and composition. For example, maternal diet during pregnancy can affect DNA methylation patterns that persist over decades in offspring[18] and maternal obesity and gestational weight gain have been shown to predispose offspring to developing obesity[19]. Furthermore, early epigenetic

association studies identified several DNA methylation sites that are associated with obesity in peripheral blood leukocytes[20] and subsequent studies have confirmed epigenetic modification of several of these sites in other cells and tissues, including T-cells, neutrophils and subcutaneous adipose tissue[21–23]. Other biological factors such as brown fat function, inadequate sleep and use of medications with weight gain as a side effect all have been shown to contribute to BMI and obesity risk [24–27].

Additional psychological, social and environmental factors and circumstances can also have an important effect on weight gain and BMI. Built neighborhood factors such as sidewalks and walkability, proximity to green space, and traffic density have been shown to be associated with body weight in children and adults[28,29]. Environmental exposure to various chemicals and pesticides that have been shown to interfere with endocrine signalling can disrupt hormonally regulated metabolic homeostasis and may predispose individuals to weight gain and obesity, especially with early life exposure. These chemicals are now deemed 'obesogens', and include cigarette smoke, polycyclic aromatic hydrocarbons as a result of air pollution, bisphenol A present in many plastic products, phthalates present in cosmetic products, and flame retardants used in furniture and electronics production[30]. This research raises the important question of how xenobiotics, substances that are foreign to the body, alter endocrine control of metabolism during obesity.

Finally, research in the past decade has revealed how metabolic disease is characterized by a shift in gut microbial ecology, while diet-induced weight loss is accompanied by a restoration of a healthy microbial composition, suggesting a link between altered composition of the intestinal microbiota and obesity[31–35]. Furthermore, colonizing germ-free mice with microbiota from obese mice transfers part of the increased adiposity seen in obese mice[33,36]. The critical importance of gut microbes in metabolic homeostasis and adiposity will be discussed in greater detail in subsequent sections of this thesis.

The complex environmental, biological and societal factors underlying body weight regulation and the development of obesity are depicted in Figure 1.1.

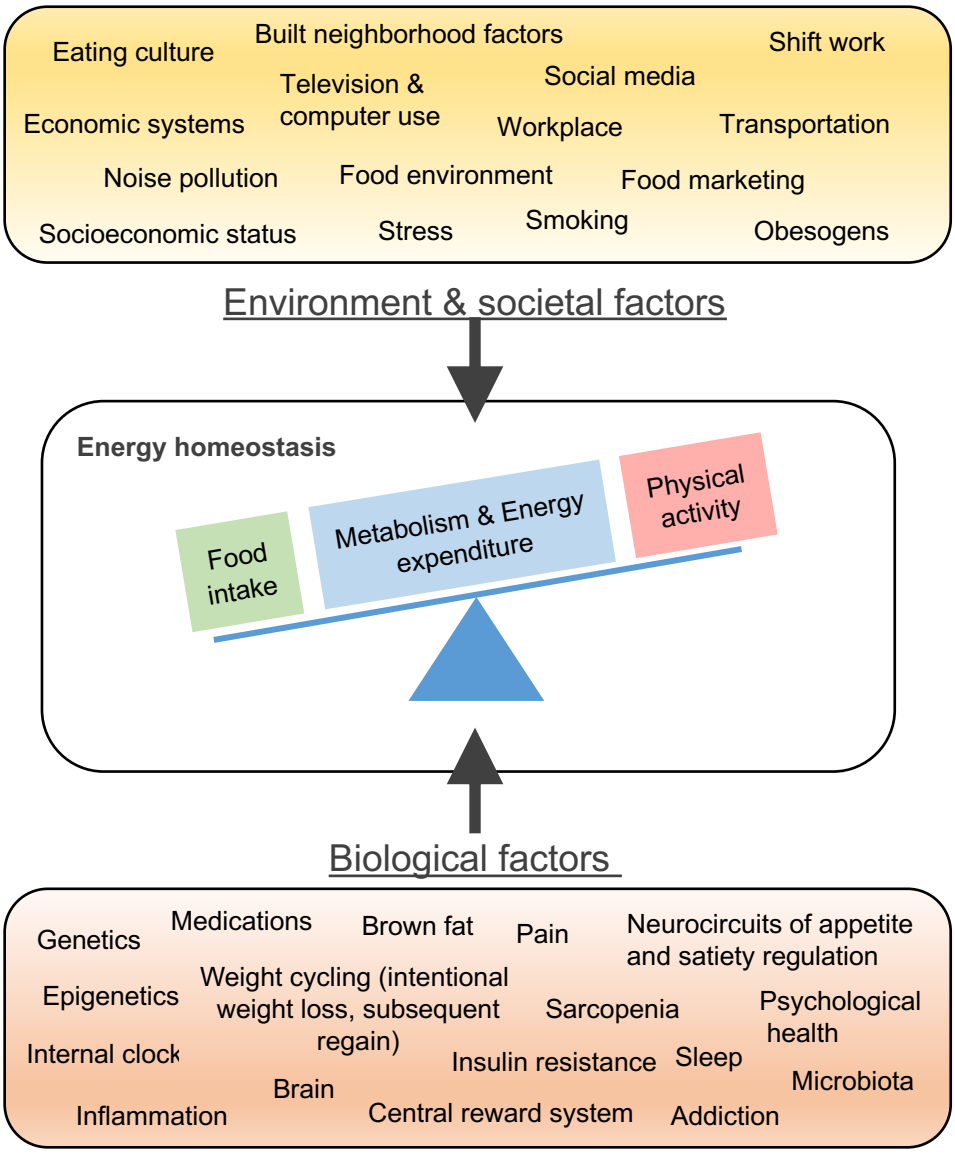

Figure 1.1 The causes underlying weight gain and the development of obesity are complex and multifactorial.

Complex interactions between numerous environmental, societal and biological factors regulate overall energy homeostasis in an individual and contribute to the development of obesity. Adapted from Blüher, 2019.

Current approaches to obesity and metabolic disease treatment include behavioural interventions, pharmacotherapy and bariatric surgery. Behavioural interventions are aimed at reducing energy intake and increasing energy expenditure through lifestyle changes. However, studies indicate that lifestyle interventions alone are often not durable and often insufficient to reduce the burden of morbidity and mortality. Therefore, current strategies of reducing caloric consumption and increasing physical activity have repeatedly proven ineffective for many people[37]. Considerable metabolic and behavioural compensatory responses to caloric restriction or increased energy expenditure through exercise attenuate the ability to sustain a negative energy balance, posing a barrier for long-term maintenance of weight loss[38–43]. Furthermore, targeting individual decision-making around food and exercise as an obesity prevention and treatment strategy disregards important research insights into the regulation of energy homeostasis and appetite by subconscious neurophysiological circuits[44–46]. Beyond lifestyle intervention, the majority of currently available pharmacotherapies designed to induce weight loss via decreased appetite, increased satiety or interference with nutrient absorption have had limited success in producing substantial long-term weight loss in obese patients[47]. Some therapeutic strategies, such as pharmacological activation of the glucagon-like peptide-1 receptor (GLP-1R) with GLP-1 agonists, originally designed for T2D, have shown promise in reducing appetite and adiposity in individuals with obesity, and liraglutide, a GLP-1 agonist, has recently been approved for the treatment of obesity[48,49]. Beyond

pharmacological intervention, invasive bariatric surgery is remarkably effective for causing durable weight loss and ameliorating obesity-related comorbidities in patients with metabolic disease, but this approach is not a scalable solution for addressing the worldwide increase in obesity prevalence[50].

Visceral obesity and ectopic fat deposition are directly related to insulin resistance and precipitates factors that culminate in the progression from prediabetes to T2D. Indeed, obesity has been posited at the leading cause of diabetes, and is a major cause of death and disability worldwide[4,51]. Elevated levels of free fatty acids (FFA), inflammatory mediators such as cytokines and lipid intermediates in adipose and non-adipose tissues are hallmarks of the obese state, and inflammation can contribute to impaired insulin-signalling and subsequent insulin resistance, which are factors in the progression to T2D. The findings presented in this thesis will focus on the relationship between the development of obesity, inflammation and insulin resistance.

1.1.2 Pathogenesis of Type 2 Diabetes

There are two main types of Diabetes mellitus (DM), Type 1 Diabetes (T1D) and T2D. Obesity increases the risk of T2D. Whereas both types of DM are characterized by elevated blood glucose levels and insufficient insulin production by the pancreatic β-cells, many of the mechanisms leading to T1D versus T2D are distinct. T1D is caused by autoimmune destruction of pancreatic β-cells, resulting in *impaired insulin secretion*. In contrast to impaired insulin secretion, T2D is a

disease that is associated with *impaired insulin action* and insulin insufficiency relative to insulin sensitivity. In fact, the progression of prediabetes to T2D is characterized by increased insulin secretion. Higher levels of insulin can contribute to obesity and insulin resistance[52–55]. Insulin is an important anabolic hormone whose pleiotropic actions will be discussed in greater detail in subsequent sections of this thesis. One of the primary purposes of insulin is to decrease blood glucose levels by increasing glucose uptake into insulin-sensitive tissues and inhibiting hepatic glucose production and output (HGP/HGO) into circulation. In T2D, progressive insulin resistance in target tissues such as adipose, liver and muscle can propagate a response that results in an impaired ability to control blood glucose levels. The early stages of development, often described as impaired glucose tolerance (IGT) or pre-diabetes, is characterized by higher blood insulin as pancreatic β-cells respond and contribute to progressive tissue insulin resistance. However, as T2D develops pancreatic β-cells eventually cannot secrete enough insulin to control blood glucose, an effect that may manifest as relative insulin insufficiency and/or progressive decline in β-cell function. Interestingly, pancreatic β-cell mass is increased in obese non-diabetic humans compared to lean controls, but decreased in obese diabetic humans, supporting a role for β-cell involvement in the early stages of the development of insulin resistance, which eventually progresses to β-cell dysfunction and even cell death[56]. This progressive relationship is depicted in Figure 1.2.

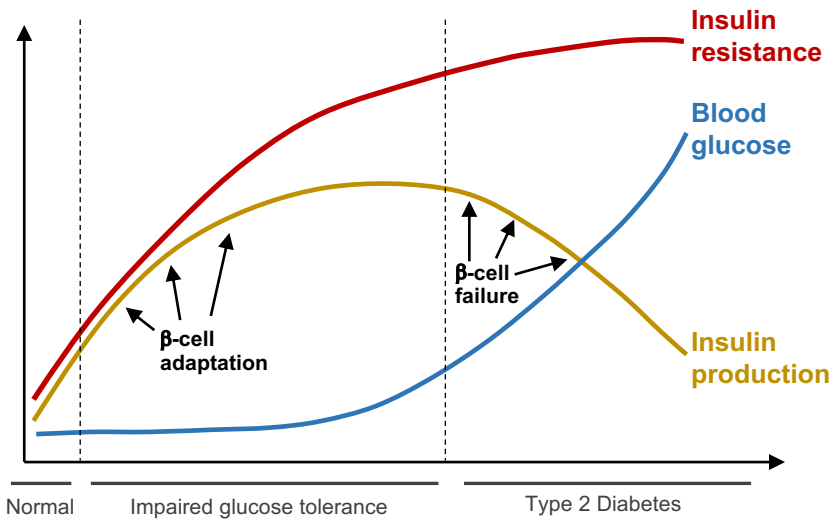

Figure 1.2 Progression from impaired glucose tolerance to development of Type 2 Diabetes

Increasing tissue insulin resistance is countered by increasing levels of insulin production from the pancreatic β-cells to maintain blood glucose levels. As the β-cells become exhausted and fail, insulin production decreases and hyperglycemia manifests, leading to the diagnosis of T2D. Adapted from Henry, 1998.

In healthy individuals, blood glucose levels in the body are tightly maintained between 3.3 and 8.3 mmol/L to maintain homeostasis and ensure normal glucose levels within cells. Elevated blood glucose can result in damage to nerve, kidney and retinal cells and blood vessels. Chronic hyperglycemia is hypothesized to be responsible for many diabetic-related complications, such as neuropathy and limb amputation, diabetic retinopathy and blindness, kidney failure, cardiovascular complications and increased susceptibility to infection which together contribute to the approximately 1.5 million annual deaths worldwide[57,58]. Understanding how obesity contributes to the development of hyperinsulinemia, insulin resistance, hyperglycemia and progression of T2D may lead to new

treatments and approaches to alleviate morbidity, mortality and the resultant global healthcare burden of T2D and its complications.

1.1.3 Insulin and insulin signalling

Insulin is an important anabolic hormone secreted from pancreatic β-cells with pleiotropic effects in multiple tissues of the body. Insulin is the primary regulator of blood glucose by promoting peripheral glucose uptake and inhibiting HGO. Insulin increases glucose uptake into cells by inducing the translocation of glucose transporter GLUT4 to the cell surface[59]. The major tissues responsible for postprandial glucose uptake are muscle, brain and kidney and liver, while only a small amount occurs in adipose tissue, although the increased mass of adipose in obesity can increase the relative amount of glucose that enters adipose tissue. Insulin also promotes glucose and lipid substrate storage in liver, fat and muscle. In adipocytes, insulin acts to inhibit lipolysis[60] and promote lipid storage by stimulating the uptake, synthesis and storage of triglycerides[61]. Thus, insulin deficiency or insulin resistance can result in elevations in circulating lipid levels in addition to hyperglycemia[62]. Insulin also suppresses glycogenolysis and protein breakdown and stimulates glycogen and protein synthesis in liver and muscle and promotes cell growth and differentiation[63].

Insulin secretion from the β-cells is a tightly regulated process. Following ingestion of a carbohydrate-containing meal, the rise in blood glucose concentrations promotes insulin secretion in a biphasic secretion pattern. While

there are many insulin secretagogues that can induce insulin release, such as glucose, fatty acids, amino acids, nucleotides and incretin hormones like GLP-1, glucose is the primary stimulator of insulin release. The other secretagogues can serve as insulin-secretion potentiators that require a threshold level of blood glucose to exert their effects[63]. Uptake and metabolism of glucose by β-cells leads to an increase in intracellular ATP:ADP ratio and results in β-cell membrane depolarization, opening of voltage-gated Ca^{2+} channels, and subsequent insulin granule exocytosis[64–66]. A small number of readily-releasable granules docked to the plasma membrane of β-cells contributes to the first, acute phase of insulin release that occurs in the 10 min of glucose stimulation, followed by a secondary, sustained phase of insulin release beginning about 15 minutes after initial glucose stimulation[65–67].

Upon release into circulation, insulin travels to target tissues and binds the α-subunit of the insulin receptor (IR), inducing dimerization and tyrosine autophosphorylation of the β-subunit, which stimulates a complex signalling transduction network that can be examined as three main signalling nodes: 1) Insulin receptor substrate (IRS) proteins, 2) Phosphatidylinositol 3-kinase (PI3K) and 3) Akt/protein kinase B (PKB)[65–67]. Phosphorylated tyrosine residues at the IR β-subunit are recognized by the phosphotyrosine-binding (PTB) domains of IRS proteins, promoting activation via tyrosine phosphorylation of docked IRS proteins. Tissue- and function-specific isoforms of the IRS proteins can influence cell-specific functions of insulin. IRS-1 is found predominantly in muscle and adipose

and IRS-2 is found predominantly in liver[68,69]. The second critical node of insulin signalling, lipid kinase PI3K, binds the phosphotyrosine sites of IRS proteins, and synthesizes phosphatidylinositol 3,4,5-triphosphate (PIP_3), from phosphatidylinositol 4,5-diphosphate (PIP_2) which in turn recruits phosphoinositide-dependent kinase (PDK), responsible for phosphorylating the Thr^{308} residue of Akt/PKB, a third critical node in the insulin signalling cascade. Full activation of Akt/PKB requires secondary phosphorylation of Akt/PKB at Ser^{473} residues by mammalian target of rapamycin complex (mTORC)2[63,70,71]. Activated Akt/PKB mediates several signalling transduction events that ultimately mediate the various metabolic consequences of insulin signalling.

Akt/PKB inhibits Akt substrate of 160 kDa (AS160) leading to the translocation of intracellular stores of GLUT4-containing vesicles to the cell membrane for glucose uptake[72,73]. In the liver, Akt/PKB inhibits Forkhead box protein O1 (FOXO1) to suppress gluconeogenesis and glycogen synthase kinase 3 (GSK3). Glycogen synthase (GS) is an important enzyme in glycogen synthase and is inhibited by GSK3. Thus, inhibition of GSK promotes GS activity and subsequent glycogen synthesis[74]. Akt/PKT also contributes to the activation of mTORC1 and S6 kinase β-1 (S6K) to increase ribosomal activity and protein synthesis[75]. Negative feedback mechanisms attenuate the prolonged insulin action. For example, activation of phosphatase and tensin homolog (PTEN) protein, which converts PIP_3 back to PIP_2, effectively "resetting" the PI3K signalling cascade[76]. In addition to negative regulation by PTEN, inhibitory serine or threonine

phosphorylation of key insulin signalling intermediates, such as the IR, IRS proteins and Akt/PKB is another mechanism of negative feedback[77–79].

1.1.4 Mechanisms of insulin resistance and β-cell dysfunction

Insulin resistance is often characterized as a reduction in signal transduction in response to insulin binding the IR in target tissues. As discussed in Section 1.1.2, the progression from prediabetes to T2D is typified by increased secretion and insulin resistance in target tissues. β-cell dysfunction can manifest as relative insulin insufficiency and/or impaired insulin secretion, leading to hyperglycemia. Peripheral tissue insulin resistance can precede relative insulin insufficiency and β-cell dysfunction by many years in humans. This period represents a therapeutic window where the progression to T2D can be reversed. It is noteworthy that increased insulin secretion can be thought of as a form of β-cell adaptation (that helps control blood glucose) or dysfunction (that promotes obesity an insulin resistance) during the early stages of T2D progression. Understanding the precipitating factors and underlying mechanisms that contribute to the progression from insulin resistance, impaired glucose tolerance to β-cell dysfunction and hyperglycemia is critical for informing therapeutic strategies to halt disease progression. Significant research efforts in the last few decades have delineated various complex and overlapping inflammatory and non-inflammatory mechanisms that underlie insulin resistance and β-cell dysfunction[80–82].

Several factors have been associated with inhibitory phosphorylation of key insulin signalling intermediates, including fatty acids, hyperglycemia, mitochondrial dysfunction, endoplasmic reticulum (ER) stress, drug metabolites, bacterial components and inflammatory molecules[83–92]. For example, the inflammatory cytokine tumor necrosis factor-α (TNFα) causes activation of the stress kinase c-Jun N-terminal kinase (JNK), which can phosphorylate IRS-1 at Ser^{307} and inhibit IRS-1 tyrosine phosphorylation, effectively mitigating downstream signal transduction in insulin responsive tissues that participate in blood glucose control[93]. Inhibitor of κB kinase (IKK) and protein kinase C-θ (PKCθ) has also been shown to phosphorylate IRS-1 at Ser^{307} [86,94]. IKK is part of the nuclear factor kappa B (NF-κB) signal transduction cascade and is an important point of convergence for multiple immune pathways from diverse inflammatory stimuli.

A growing body of evidence suggests that inflammation in pancreatic islets may also be an important contributor to β-cell dysfunction. β-cell dysfunction can involve a decrease in β-cell mass or failure of specific β-cell functions such as glucose-stimulated insulin secretion (GSIS). An elevated number of resident islet macrophages and increased expression of interleukin (IL)-1β have been reported in diabetic patients and depletion of resident macrophages in diabetic rodents reduced IL-1β expression and improved β-cell insulin secretion[95–97]. IL-1β neutralization also has also been shown to improve β-cell function in clinical trials of T2D patients[98].

Other factors including genetic susceptibility to β-cell deterioration, metabolic overload, ER stress, oxidative stress and amyloid fibril formation have also been identified as prominent contributors to β-cell dysfunction[99–101]. Chronic exposure of pancreatic islets to elevated levels of glucose and fatty acids can impair GSIS[102], raising the possibility of a role for 'glucolipotoxicity' in β-cell functional impairment. Indeed, elevated glucose or FFA exposure has been shown to induce a pro-inflammatory response in pancreatic islets via IL-1 signalling[103,104], linking glucolipotoxicity to inflammatory mechanisms that potentiate β-cell dysfunction and apoptosis. Moreover, islet sections taken from T2D patients contain amyloid fibril deposits, and amyloid in human islets have been shown to impair β-cell function and initiate apoptotic pathways[105–107]. Interestingly, increasing amyloid formation closely correlates with local IL-1β levels in pancreatic islets of humans and transgenic mice expressing human amylin[108].

Inflammation has been identified as a prominent feature of obesity-induced insulin resistance. Many cellular mechanisms contributing to insulin resistance and β-cell dysfunction have been identified[77,92], including endoplasmic reticulum (ER) stress and oxidative stress. This thesis investigates the relationship between insulin resistance and inflammation with a focus on xenobiotic (i.e. drug) and microbial triggers of immune responses that alter blood glucose and insulin.

1.2 Immunometabolism

In 1993, the seminal discovery by Spiegelman and colleagues that obese adipose tissue produces TNFα, a proinflammatory factor that promotes insulin resistance formed the cornerstone for the field of immunometabolism[109]. Decades of research have identified complex immunometabolic signalling networks that are critical to maintaining immune and metabolic homeostasis relevant to endocrine control of metabolism, including insulin resistance. Altered nutrient supply and changes in energy balance influence the connections between immunity and metabolism and can contribute to aspects of chronic metabolic disease, including obesity and T2D. A number of different immune cell populations and signalling pathways have been implicated in the pathogenesis of metabolic disease[110–113].

As early as 1884, clinical observations linking immunity to metabolism were made in meningitis patients who exhibited a transient diabetic syndrome[114], and it has also been known for the past century that high-dose salicylate treatment can reverse insulin resistance[115]. Elevated blood glucose and insulin resistance during infection continued to be observed in patients throughout the early and mid-1900s but it wasn't until experiments performed in the 1980s in canines when some of the mechanisms underlying metabolic alterations during infection were revealed. Work from Raymond and colleagues demonstrates that lipopolysaccharide (LPS) treatment in dogs induced acute insulin resistance by mitigating insulin-stimulated glucose uptake in skeletal muscle[116]. Shortly thereafter, it was found that acute bacterial infection in human patients resulted in decreased binding of insulin to the

IR in isolated blood cells, and that high doses of salicylates block NF-κB providing another mechanistic link for aspirin-induced improvements in insulin resistance[117–119].

From an evolutionary perspective, two paramount tasks for an organism is to evade predators and external environmental threats (immunity), and to obtain energy for sustaining cellular processes (metabolism), and current opinion holds that immunometabolism represents a highly conserved and interwoven relationship between these two conserved functions, with tissue specialization occurring progressively over the course of evolution[120]. Indeed, functions of multiple cells types and tissues are performed by one or two cell types in organisms, such as *Caenorhabditis elegans* or *Drosophila melanogaster*[121,122]. It has been proposed that the Drosophila fat body together serves as the human orthologues of adipose, liver and haematopoietic cells[123,124].

1.2.1 Obesity, inflammation, and insulin resistance

Obesity is associated with chronic low-grade inflammation. Importantly, obesity-related changes in immunity are compartmentalized in different tissues and cell types. For example, obesity can be associated with impairments in specific immune responses in certain upper gut segments, but also associated with increased immune responses in the adipose tissue[125,126].

Since the findings that obese adipose tissue expresses TNFα, two decades of intensive research effects have characterized many of the inflammatory and immune changes that accompany obesity, insulin resistance and metabolic disease. It is now appreciated that in addition to TNFα, a number of other pro-inflammatory molecules cytokines are increased during obesity, such as acute phase proteins, IL-6, IL-1β and CCL2, among others[127,128]. This is significant because, as discussed in section 1.1.4, stress kinase responses that are engaged by immune responses and upregulated in obesity have been directly shown to interfere with the insulin signalling cascade, thus providing a plausible link to insulin resistance at the level of the tissues. In support of this model, neutralization or genetic deletion of inflammatory signalling nodes and cytokines, such as IKK-β or TNFα yields partial protection from obesity-induced insulin resistance in mice[129–131].

Although the inflammatory and immune cell changes in specific tissues in obese and insulin resistant states have been well characterized, the fundamental source or triggers of inflammation in obesity are not yet well understood. Obesity is associated with dyslipidemia, changes in immunogenic bacterial molecules, reactive oxygen species (ROS), and ER stress responses, all of which can engage pro-inflammatory pathways and can contribute to insulin resistance[128,132]. For example, acute infusion of FFA can impair whole body insulin-stimulated glucose uptake. Cellular lipid metabolism synergizes with activation of the innate immune receptor Toll-like receptor 4 (TLR4) by LPS and activation of various inflammasomes[133–137]. The mechanisms of lipid-induced inflammation are still

somewhat contentious, but other inflammatory triggers have been associated with fat-laden diets and obesity. A single fat-containing meal in lean subjects can increase bacterial endotoxin in circulation, and obesity has been associated with increased systemic levels of bacterial endotoxin and the bacterial cell wall component peptidoglycan (PGN)[89,138,139]. Moreover, production of ROS is increased selectively in obese adipose tissue, which promotes production of pro-inflammatory adipokines[140,141]. Finally, ER stress is increased in liver and adipose tissues in both dietary and genetic obesity models[142]. Two ER stress pathways, inositol-requiring enzyme 1 (IRE-1) and PKR-like endoplasmic reticulum kinase (PERK) have been linked to the activation of JNK and NF-κB[143,144].

It has been proposed that the compartmentalization of immune responses in different tissues during obesity is an important dictator of inflammation and insulin resistance status. For example, IKK deletion in myeloid, liver and hypothalamic neurons improves glucose homeostasis but loss of IKK in adipocytes impairs glucose homeostasis[145–147]. This highlights complexity of immunometabolic interfaces; there is not a direct line from adipose inflammation to insulin resistance and glucose intolerance. Importantly, IKK-NFκB plays a crucial role in resolution of inflammation, in part by the production of IL-10 and IL-13[148]. While chronic tissue inflammation in obese states has been identified in liver, adipose and muscle, the three classical insulin target tissues, elevated pro-inflammatory signalling has also been identified in the pancreas, brain and certain segments of the intestine[128]. The precise role inflammation in these tissues plays with respect to insulin

resistance and pathogenesis of T2D will be discussed in detail in subsequent sections.

Adipose tissue

Inflammatory alterations in obesity have been most extensively studied in adipose tissue. Following the pioneer finding that cells in adipose tissue produce TNFα, which is elevated in obesity, it was also identified that obese adipose tissue is also infiltrated with macrophages that are skewed towards a pro-inflammatory M1 polarization state versus the anti-inflammatory M2 polarization state[149,150]. In rodents, macrophage infiltration of adipose tissue occurs within 1 week of high fat feeding and can comprise up to half of the cells in an obese adipose tissue depot [151,152]. In addition to pro-inflammatory macrophage accumulation, adipose tissue during obesity has elevated CD8+ T cells, Th1 T cells, B cells, natural killer (NK) cells, and neutrophils coincident with a reduced proportion of regulatory T cells, eosinophils, and type 2 innate lymphoid cells (ILCs)[128]. Taken together, these studies provide a strong evidence for a mechanistic role of adipose tissue inflammation in obesity-induced insulin resistance.

Liver

The liver plays an important role in blood glucose homeostasis by storing glycogen (glycogen synthesis) and synthesizing glucose from non-glucose precursors (gluconeogenesis). In the fasted state, the liver helps to maintain euglycemia by increasing HGO into the bloodstream and in the fed state, insulin inhibits endogenous HGP[153]. Insulin resistance in the liver results in a failure to

suppress HGO, which can contribute to hyperglycemia. The liver contains a large number of hepatic-resident immune cells including macrophages, known as Kupffer cells, dendritic cells, NK cells, and CD4 and CD8 T cells[154]. In contrast to adipose tissue, the liver does not experience an infiltration of macrophages during obesity, but rather an activation of resident Kupffer cells and inflammatory cytokine expression is increased in obese livers compared to lean controls[155]. Furthermore, dyslipidemia and ectopic lipids from expanding adipose tissue during obesity results in the accumulation of hepatic lipids. Excess lipid storage results in elevated lipid species, such as diacylglycerols (DAGs) and ceramide species, that can activate PKCθ and interfere with insulin signalling via inhibitory serine phosphorylation of IRS proteins[156,157].

The liver is an important site of drug and macronutrient metabolism and detoxification. The liver is positioned to conduct first pass metabolism of xenobiotics, microbial components and metabolites due to the direct connection between the intestine and the liver via the portal circulation, comprised of blood returning from the gastrointestinal tract via the hepatic portal vein in combination with arterial flow[158]. Thus, the liver is a primary interface for receiving bacterial, drug metabolite and nutritional content from the GI tract, and the relationship between the gut, the microbiota and metabolic tissues has recently been the subject of intensive research.

Skeletal muscle

Skeletal muscle is a primary site of postprandial glucose clearance from the skeletal muscle, accounting for up to 75% of insulin-dependent glucose uptake and is an important mediator of glucose homeostasis[59,159]. Skeletal muscle appears to be a minor contributor to inflammation in obesity, as increased expression of TNFα, IL-6 or other inflammatory mediators are not observed in muscle fibers, and muscle-specific disruption of NF-κB signalling has no effect on muscle insulin sensitivity or systemic glucose homeostasis[160,161]. These results suggest that autocrine inflammatory signalling in muscle is not a major contributor to muscle insulin resistance. However, circulating inflammatory cytokines can induce muscle insulin resistance and interfere with insulin-stimulated glucose uptake and glycogen synthesis[162,163]. Furthermore, inflammation can promote adipocyte lipolysis and elevated blood lipids (i.e. dyslipidemia) during obesity leads to enlargement of intramuscular lipid stores that are associated with insulin resistance[164,165]. Similar to excess hepatic lipid storage, it has been proposed that elevated intramuscular lipid stores equates to higher fatty acid intermediates, such as DAGs and ceramide species, which can activate PKCθ and interfere with insulin signalling via inhibitory serine phosphorylation of IRS proteins[166].

Pancreas, brain and gastrointestinal tract

Mounting evidence now implicates a role for elevated immune responses in the pancreas, brain and GI tract in the pathogenesis of T2D. Islet inflammation has been recognized as a potential contributor to β-cell dysfunction[167]. Across the

development of obesity, the pancreas is subject to increases in inflammatory cytokine production and infiltration of macrophage cells, and an IL-1β–NF-κB pathway has been shown to mediate β-cell apoptosis[168,169]. The hypothalamus is a key center of appetite control and regulation and responds to metabolic and endocrine signals, including insulin. Insulin resistance has been observed in the hypothalamus of obese patients and contributes to disordered feeding behaviour and impaired appetite suppression[170]. There is also evidence for hypothalamic control of HGP, and insulin resistance in the hypothalamus can impair insulin-mediated suppression of HGO[171].

The gastrointestinal tract represents an important barrier between the external environment and internal organs of the host that is critical for protecting the host from penetration by pathogenic bacteria and bacterial components that can elicit immune responses. The intestinal immune system is highly specialized to deal with a high burden of bacteria, including a robust mucosal barrier and antimicrobial responses that regulate the gut resident microbiota[172]. Obesity is associated with altered intestinal immunity, including changes in innate and adaptive immune cells within certain segments of the gut, and obesity is often associated with impaired intestinal barrier function[172]. Increased levels of pro-inflammatory cytokines, such as TNFα, IL-1β and IL-12p40 have been reported in the intestine and decreased proportions of specific ILCs, T cells and eosinophils have been observed in mouse models of obesity[173–175]. In rodents, an obesogenic high-fat diet impairs intestinal Th17 immune responses, which have been linked to maintenance of intestinal

epithelial integrity and penetration of microbial components that can activate tissue-specific immune responses[125,176,177]. Thus, altered intestinal immunity (i.e. lower immune responses in the gut) can be associated with increased intestinal permeability, which may allow for increased penetration of immunogenic bacterial components, such as LPS or others, that can contribute to pro-inflammatory signalling in other metabolic tissues and impair insulin sensitivity[89,172,178].

1.3 Pattern recognition receptors

Pattern recognition receptors (PRRs) of the innate immune system are one of the first lines of host detection and defense against invading pathogens and endogenous tissue damage. Specific PRRs have evolved to protect against a variety of non-host conserved molecular patterns, referred to as pathogen-associated molecular patterns (PAMPs) and endogenous host molecular patterns, referred to as damage-associated molecular patterns (DAMPs) that initiate context-dependent signalling cascades for pathogen elimination or tissue repair.

PRRs of the innate immune system include transmembrane Toll-like receptors (TLRs) and RIG-I-like receptors, and intracellular NOD-like receptors (NLRs) and C-type lectin receptors. As the front line of defense against cellular pathogen invasion, these receptors are expressed in “professional” innate immune cells (such as macrophages and neutrophils), but also cells within tissues that are not traditionally thought of as key immune regulators (such as adipocytes, hepatocytes and muscle cells)[179,180]. The sensing of PAMPS or DAMPS by PRRs induces gene transcription for pro-inflammatory cytokines and chemokines, type I

interferon and antimicrobial proteins, and the specific patterns of induced genes differ amongst the various PRRs[179].

1.3.1 NOD1 and NOD2 in immunity and inflammatory disease

The Nucleotide-binding oligomerization domain-containing (NOD) proteins, NOD1 and NOD2, are PRRs that sense bacterial cell wall muropeptides and induce an inflammatory response upon binding of bacterial PGN-containing fragments. NOD1 detects D-glutamyl-meso-diaminopimelic acid (meso-DAP)-containing PGN found predominantly in Gram-negative bacteria and NOD2 detects the muramyl dipeptide (MDP) PGN motif found predominately in Gram-positive bacteria[181–183]. NOD proteins are composed of N-terminal caspase-activation and recruitment domains (CARDs), a central NOD, and a C-terminal leucine-rich repeat (LRR) domain that is responsible for ligand recognition and binding. NOD1 contains a single CARD while NOD2 contains a dual CARD, to facilitate downstream signalling via homotypic CARD-CARD interactions[184].

Upon specific PGN ligand binding, NOD1 or NOD2 undergoes self-oligomerization and interaction with a common downstream adaptor, Receptor-interacting serine/threonine protein kinase 2 (RIPK2). RIPK2 mediates downstream signalling for both the NOD1 and NOD2 proteins[185,186]. Upon interaction with ligand-bound NOD1 or NOD2, RIPK2 subsequently undergoes autophosphorylation and polyubiquitylation, inducing downstream activation of NF-κB and mitogen-activated protein kinase (MAPK) signalling pathways[185,186].

While activation of NOD1 and NOD2 lead to distinct inflammatory outcomes, it is not known how the common adapter RIPK2 mediates these distinct outcomes, but assembly of different downstream accessory molecules has been suggested. The protein domain structures and binding of NOD1, NOD2 and RIPK2 are depicted in Figure 1.4.

Aberrant NOD1 or NOD2 signalling are associated with altered response to infection and inflammatory diseases. For example, NOD1-mediated responses regulate important neutrophil-mediated bacterial killing during infection, while mutations in the *Nod2* gene is associated with Crohn's disease in humans and susceptibility to experimental colitis in mice[187–189], highlighting the critical role of these innate immune sensors in balancing host-microbe interactions and inflammatory signalling.

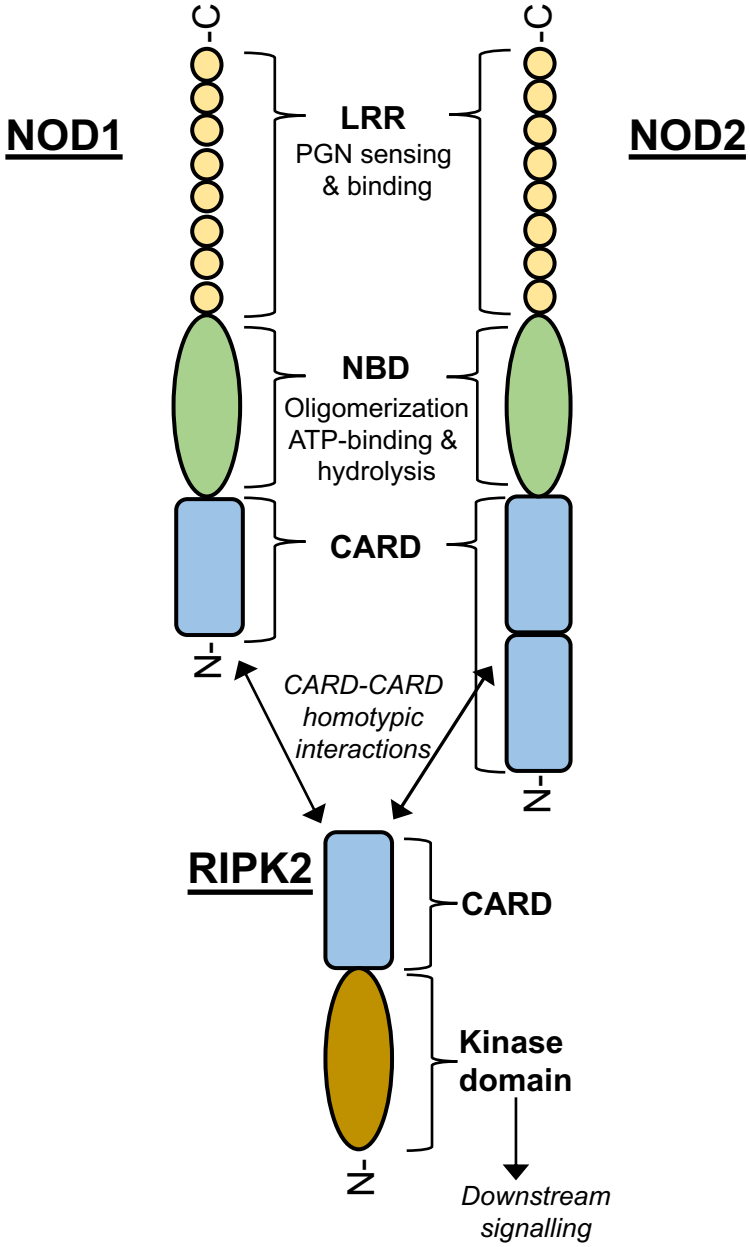

Figure 1.3 The domain structures of NOD1, NOD2 and RIPK2

NOD1 and NOD2 contain a C-terminal leucine-rich repeat (LRR) domain that mediates peptidoglycan (PGN) sensing and binding, and a nucleotide binding domain (NBD) that undergoes oligomerization and mediates ATP hydrolysis. NOD1 contains a single N-terminal caspase activation and recruitment domain (CARD) and NOD2 contains dual-CARDs that interact with RIPK2's C-terminal CARD domain. RIPK2 has a N-terminal kinase domain that dimerizes and phosphorylates downstream factors. Adapted from Murherjee, et al. 2019 and Philpott, et al. 2014.

1.3.2 Immunometabolism of NODs

PRRs of the innate immune system, have been identified as a critical point of convergence between immunity and metabolism. Specifically, PRRs such as the TLR family of receptors, and the NLR family of receptors, can propagate paracrine and autocrine inflammatory signals that promote insulin resistance[60,134,190–192]. For example, elevated levels of circulating bacterial components such as higher LPS load during metabolic endotoxemia in obesity can elicit inflammation and insulin resistance through TLR4[89,134,178]. Further, endotoxin can synergize with lipid metabolism of saturated fat to exacerbate TLR4-mediated inflammation in metabolic tissues[134,136]. In addition to LPS, work from our lab and others have shown how distinct bacterial muropeptides, sensed by NOD1 and NOD2, can differentially mediate inflammation, glucose and insulin homeostasis[60,139,190,193,194].

Work from our lab and others showed that bacterial PGN-mediated activation of NOD1 induces inflammatory and metabolic changes relevant to blood glucose control and lipid metabolism. For example, *in vitro* treatment with the NOD1-specific synthetic PGN ligand FK565 increases lipolysis in adipocytes[194] and inflammation in adipocytes and macrophages[60,190]. *In vivo* administration of NOD1 ligand prior to hyperinsulinemic euglycemic clamps or insulin or glucose tolerance tests in mice showed that NOD1 activation induces insulin resistance and glucose intolerance[60,190]. Interestingly, there is evidence for

increased NOD1 activity in subcutaneous adipose of metabolic syndrome patients[195].

In contrast to NOD1, activation of intracellular PRR NOD2 promotes immune tolerance and better glucose control under conditions of both bacterial and nutritional stress. Specifically, administration of NOD2-specific PGN ligand muramyl dipeptide (MDP) improves insulin sensitivity and glucose tolerance during low-dose endotoxin challenge and diet-induced obesity[196]. Furthermore, published work from our lab has demonstrated the deletion of NOD2 during diet-induced obesity significantly worsens gut dysbiosis, inflammation and insulin resistance in mice[196]. In stark contrast to NOD1 signalling, these data position NOD2 signalling in obesity as a therapeutic target for managing gut microbial homeostasis, inflammation and metabolic defects such as obesity-induced insulin resistance.

1.3.3 Immunometabolism of RIPK2

RIPK2, also known as RICK, CARDIAK, CCK and CARD3, was originally classified as an serine/threonine protein kinase but was later identified to have tyrosine kinase activity that is required for maximal NF-κB activation and downstream signalling[185,186,197]. RIPK2 has been implicated as an important mediator for integrated innate and adaptive immune signalling, as *Ripk2*$^{-/-}$ cells are deficient for inflammatory signalling through NOD proteins and *Ripk2*$^{-/-}$ T cells show impaired NF-κB activation, proliferation and differentiation[185,198–200].

Current models suggest that RIPK2 is recruited to ligand-bound NOD1 or NOD2 and undergoes autophosphorylation at tyrosine residues, inducing K63-polyubiquination of RIPK2 by E3 ubiquitin ligases cIAP1, cIAP2 and xIAP[201,202]. K63-polyubiquinated RIPK2 induces the K63-linked polyubiquitination of IKKγ, and together allow binding of the TAK1-TAB1/2/3 complex, resulting in phosphorylation and degradation of inhibitor of nuclear factor kappa B (IκB) kinase and resultant activation and translocation of NF-κB to the nucleus[203–206]. The E3 ubiquitin ligase ITCH specifically downregulates activated RIPK2 to terminate NOD-induced signal transduction events[207].

Work from our lab and others have established divergent glycemic and metabolic consequences of NOD1 versus NOD2 signalling[60,139,190,193,196]. While RIPK2 has been established as an obligate component of NOD1- and NOD2-driven immune responses, it is not known if or how RIPK2 is required to mediate the glycemic effects downstream of NOD1 or NOD2 activation. The metabolic consequences of NOD1 and NOD2 signalling and a potential role for RIPK2 is depicted in Figure 1.4.

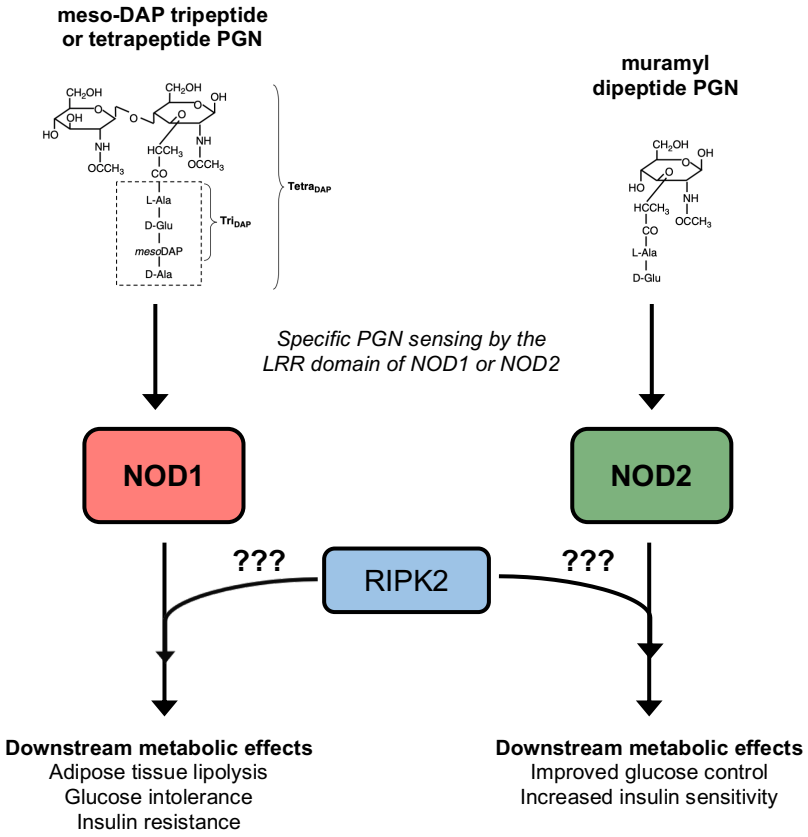

Figure 1.4 Immunometabolism of NOD-RIPK2 signalling

Activation of NOD1 with specific meso-DAP-containing PGN increases lipolysis in adipocytes, and insulin resistance and glucose intolerance *in vivo*. In contrast, activation of NOD2 with specific muramyl dipeptide PGN promotes better glucose control and insulin sensitivity. It is not known if RIPK2 mediates the downstream metabolic effects of NOD1 or NOD2 activation. Molecular structures of meso-DAP type PGN and muramyl dipeptide type PGN adapted from Kaparakis, et al. 2007.

1.4 Gut microbes, immunity, and metabolism

The gut microbiota of the gastrointestinal (GI) tract have a profound effect on host physiology and are part of a critical relationship between the gut microbiota, immunity and metabolism. The integrated host-microbe response has emerged as a

modifier of the mechanisms that underpin aspects of obesity and diabetes. The GI tract is home to commensal microorganisms that reside at the initial site of digestion, metabolism and absorption of dietary nutrients and perfectly positioned to interact with ingested food, the immune system and consequent changes in host endocrine and metabolic responses. The gut microbiota alter nutrient metabolism by synthesizing vitamins and enzymes involved in energy extraction and fermenting carbohydrates that aren't digestible by the host[208]. In addition, the gut microbiota produce various metabolites that have emerged as important signalling molecules, such as short chain fatty acids (SCFAs) and secondary bile acids (BAs), involved in maintenance of homeostasis in host metabolic and immune function[32,209,210]. Much has been learned from studies in germ-free mice over the past several decades.

Germ-free mice are typically very lean and exhibit significant substantial differences in immunity, including altered antibody production by B cells, deficient Th1 and Th17 responses, and reduced T regulatory (Treg) cell populations in the large intestine, suggesting a role for gut microbiota in the development and maintenance of host immune responses[210]. As there is a growing recognition of the important of commensal intestinal microbiota on host physiology, germ-free mice are excellent tools allowing for the study of the complete absence of microbes, or for the generation of exclusively colonized animals with specific microbes (i.e. monocolonization or specific microbial community transfer). For example, monocolonization of germ-free mice with *E. coli* can promote macrophage accumulation in adipose, and colonization of germ-free mice with microbiota from

HFD-fed animals results in increased adiposity[33,211], providing evidence for an important causal link between the microbiota contributing to obesity and adipose tissue inflammation. However, the principal advantage of gnotobiotic mice are in proof-of-principle studies, and the artificial nature of organismal development in the absence of microbes must be considered as an important limitation. Germ-free mice exhibit several alterations in behavior and development, such as increased anxiety behaviours, impaired learning and memory responses and increased locomotor behaviours[212], and these changes must be carefully considered when deeming if a germ-free mouse model is suitable for a specific line of scientific inquiry.

1.4.1 Gut microbes in metabolic disease

Diet is a significant factor in metabolic disease risk[213,214]. Diet also plays a huge role in shaping the composition of the gut microbiota and even short-term changes in the relative amounts of macronutrients that are ingested produces rapid and distinct shifts in the microbial populations. Switching from a low-fat plant-based diet to a high-fat, high-sugar diet can shift the structure of the microbiota within a single day[215] and specific macronutrient compositions have been shown to promote changes in bacterial species abundance[216]. Macronutrient composition clearly plays a distinct role in overall microbiota composition, but other modern dietary components can also play a definitive role. For example, dietary emulsifiers have been shown to impact the mouse gut microbiota and promotes colitis and metabolic syndrome[217].

Some clear and reproducible shifts in gut microbiota have been observed in rodents and humans during obesity. Bacteria present in the distal gut and feces of mice and humans have been shown to belong to two main phyla; Firmicutes and Bacteroidetes. During obesity, an increased ratio of Firmicutes to Bacteroidetes is observed in genetically obese *ob/ob* rodents and obese humans[31,218]. Interestingly, transfer of the gut microbiota from obese mice to lean mice induced weight gain in lean mice even when fed a regular diet[33]. Transmissibility of obesity phenotypes by gut microbial transfer supports the notion that gut dysbiosis can play a causal role in metabolic disease. Additional consequences associated with metabolic disease, including hepatic steatosis, and atherosclerosis have all been shown , at least in part, to be regulated by changes in the microbiota[219,220]. Direct and indirect manipulation of the microbiome through fecal transplant, administration of specific bacterial populations or dietary alterations (i.e. pre- or probiotic supplementation), have been proposed as potential treatments for metabolic disease and insulin resistance.

Fecal microbial transplant (FMT) has been shown to alter glucose metabolism in obese humans. Specifically, FMT from lean donors into obese males with metabolic syndrome improved peripheral insulin sensitivity and lowered glycated hemoglobin[221,222]. In animals, administration of specific bacterial populations, such as *Akkermansia muciniphilia*, have been shown to mitigate inflammation and insulin resistance in diet-induced obesity[223,224] and a recent study in humans demonstrated that daily oral supplementation of *Akkermansia muciniphilia* improved insulin sensitivity and reduced hyperinsulinemia[225]. In

addition to FMT or other methods to modify bacterial populations, emerging data demonstrate how bacterial components can alter immunity and subsequent metabolic homeostasis. It has long been known that live bacteria are not required to elicit an immune response. Further, it has known that sepsis causes insulin resistance and that LPS alters blood glucose[116,226,227]. Recently published work demonstrates that subcutaneous injection with luminal contents collected from ileal segments improves glucose control in high fat-fed mice[228]. Injection of the bacterial extracts from the ileum of mice activated an adaptive immune response that was required to improve blood glucose[228]. However, the innate immune sensors involved in sensing these conglomerates of bacterial factors are not known. These results, along with our findings that bacterial-derived postbiotic MDP protects against diet-induced glucose intolerance and insulin resistance[193] are consistent with a model where the microbiota contain glucose-lowering and insulin-sensitizing compounds which are mediated by innate immune components that can alter endocrine control of metabolism.

1.5 Xenobiotics, immunity & metabolism

1.5.1 Xenobiotics influence innate immunity

The gut microbiota and microbial components have been established as important regulators of innate immunity, but xenobiotics have also been shown to influence innate immunity. Interestingly, xenobiotics can also alter the microbiota and bacteria can metabolize xenobiotics providing evidence for bidirectional interactions between bugs, drugs and the immune system. It has been long

understood that NF-κB, an important integrator of innate immune signalling downstream of multiple PRRs, is inhibited by aspirin and sodium salicylate[118,119]. Metformin is a widely prescribed first-line therapeutic for T2D that inhibits HGP via AMP-activated protein kinase (AMPK)-dependent and AMPK-independent mechanisms. Recent studies have revealed that metformin can also influence the gut microbiota and the immune system, which were previously unappreciated mechanisms of action of this drug with various physiological outcomes[229,230]. For example, metformin has been shown to enrich *Akkermansia* microbial populations in the intestines of obese mice coincident with reduced adipose tissue inflammation and improved blood glucose control, and has also been shown to alter gut microbial populations in diabetic humans[231,232]. Irrespective of diabetic status, metformin also has direct effects on inflammation, by inhibiting NF-κB activation in primary hepatocytes and impairing monocyte differentiation *in vivo*[233,234]. Metformin treatment extends lifespan in *C. Elegans* by promoting intestinal microbial growth[235]. Furthermore, work from our lab and others have shown how statins, another class of widely prescribed drugs that lower cholesterol and triglycerides, can also alter immunity. Statins are generally considered to be anti-inflammatory, and statin treatment results in decreased C-reactive protein and other inflammatory processes in cardiovascular patients and healthy individuals alike[236,237]. In contrast, given adequate "immune priming", statins increase IL-1β secretion in bone marrow derived macrophage (BMDM) cells and activate the NLRP3 inflammasome, leading to adipose tissue insulin resistance[192,238,239].

Small molecule kinase inhibitors, well established therapeutic agents in oncology practices, have also emerged as having significant immunomodulatory effects. Recent attention has been focused on the anti-inflammatory actions of kinase inhibitors, and several kinase inhibitors are currently being investigated as potential therapeutics for autoimmune and inflammatory conditions[240,241]. These drugs will be discussed in greater detail in the subsequent section.

1.5.2 Clinically approved small molecule kinase inhibitors

With more than 500 protein kinases confirmed in the human genome, this class of enzymes mediate the majority of signal transductions and are critical regulators of all cellular activities, including proliferation, differentiation, survival, metabolism and immunity[242,243]. Kinase enzymes regulate the biological activity of other proteins by transferring the γ-phosphate group from an ATP molecule to a serine/threonine residue or a tyrosine residue on the substrate protein. Some protein kinases are serine/threonine-specific, some are tyrosine-specific and some are dual-specificity[244]. The ATP-binding catalytic subunit of protein kinases is highly conserved and includes a flexible activation loop beginning with an Asp-Phe-Gly (DFG) sequence that regulates access to the active site[245,246]. Mutations or dysregulation of protein kinases play causal roles in human disease[247]. Pathological and pharmacological evidence positions aberrant kinase activity as a promising drug target for disease treatment. Subsequently, the past twenty years has seen small molecule kinase inhibitors as the subject of intense drug discovery and development. At present, more than 50 small-molecule

kinase inhibitors have been approved for clinical use in the treatment of cancerous malignancies[246,248] and many are now being investigated as a potential therapeutic for autoimmune and inflammatory conditions[240,241]. In 2012, tofacitinib was the first TKI to be approved for clinical use in a non-cancerous pathology, rheumatoid arthritis[241]. Current research efforts are further directed at the efficacy of kinase inhibitors in other conditions, such as asthma[249], psoriasis[250], inflammatory bowel diseases[251,252], peritonitis[253], multiple sclerosis[254], pulmonary fibrosis[255], and interestingly, T1D and T2D[256–258].

Among the approved small molecule kinase inhibitors, the majority are tyrosine kinase inhibitors (TKIs), a few are serine/threonine kinase inhibitors, and Idelalisib is a lipid kinase inhibitor. Kinase inhibitors can also be classified based on their mode of binding: reversible and irreversible. Irreversible kinase inhibitors covalently bond with reactive cysteine residue adjacent to the ATP-binding site to effectively block the ATP site in an irreversible manner[259]. The majority of kinase inhibitors are reversible and can be further classified into four main types based on conformation of the target kinase binding pocket and the conserved DFG region of the activation loop. Type I inhibitors are ATP-competitive inhibitors that bind to the active form of a kinase with the aspartate residue of the DFG motif facing inwards to the active site, while Type II inhibitors are non-ATP competitive inhibitors that bind to the inactive form of a kinase with the aspartate residue facing outwards. In contrast, Type III and Type IV inhibitors work by binding to an allosteric site without making any interaction with the ATP binding

pocket[246,259–261]. Due to the similar 3D structure and highly conserved ATP binding pocket across the mammalian kinome, specificity issues are a concern in the design and development of small molecule kinase inhibitors. Despite intended selectivity and specificity, clinically approved kinase inhibitors have many off-target effects and inhibit a range of kinases[262]. The binding modes and overlapping tyrosine kinase targets of some common reversible kinase inhibitors are depicted in Figure 1.5 and Table 1.2 respectively.

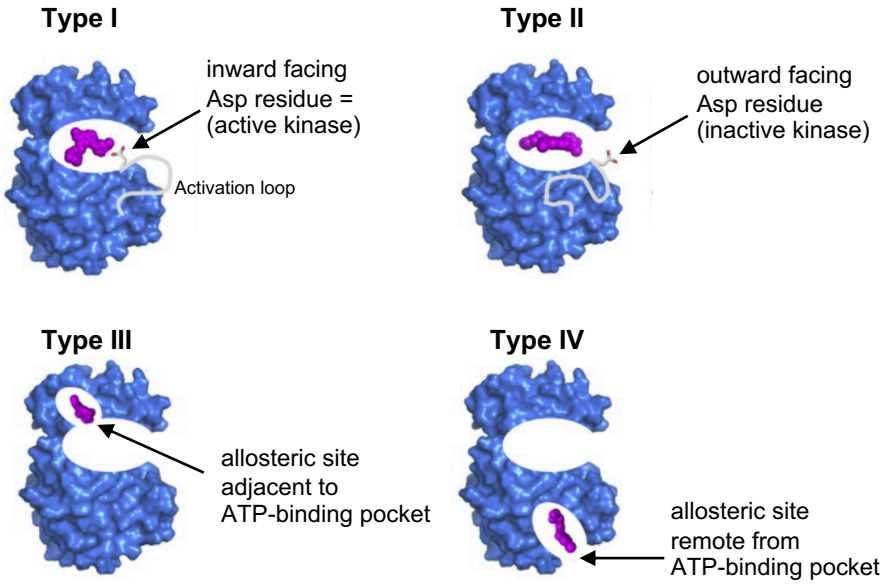

Figure 1.3 Binding modes of reversible small molecule kinase inhibitors

Type 1 inhibitors are ATP-competitive inhibitors that bind to the active site of the kinase when the Asp residue of the activation loop in facing inwards. Type II-IV inhibitors are non-ATP competitive inhibitors. Type II inhibitors bind to the active site of an inactive kinase (when the activation loop is facing outwards). Type III inhibitors bind to an allosteric site adjacent to the active site while Type IV inhibitors bind to an allosteric site remote from the active site.

Table 1.1 Common TKIs inhibit numerous kinase targets

Compound	Tyrosine kinase targets:				
	RIPK2	**c-Kit**	**c-Abl** (phosphorylated)	**PDGFRβ**	**EGFR**
gefitinib	530 nM	-	480 nM	-	1.0 nM
erlotinib	680 nM	1700 nM	76 nM	1400 nM	0.7 nM
imatinib	-	13 nM	21 nM	14 nM	-
sunitinib	-	0.4 nM	150 nM	0.1 nM	-
sorafenib	1300 nM	28 nM	1400 nM	37 nM	-
dasatinib	31 nM	0.81 nM	0.05 nM	0.63 nM	120 nM
lapatinib	3600 nM	-	-	-	2.4 nM

The majority of kinase inhibitors are rapidly absorbed and reach peak plasma concentration within 3-7 hours after an oral dose. Food consumption only marginally increases the extent of bioavailability, or does not significantly affect the bioavailability of most kinase inhibitors, including gefitinib and imatinib[263–266]. Kinase inhibitors are primarily metabolized by cytochrome P450 (CYP) 3A4 with other CYP enzymes playing a secondary role in the metabolism of some inhibitors. Kinase inhibitors are predominantly excreted in feces, and a minor amount is also excreted in urine[263].

1.5.3 Kinase inhibitors regulate blood glucose

TKI treatment in diabetic cancer patients revealed that certain TKIs improved blood glucose control and reversed insulin dependence or diabetic medication requirements. These initial clinical observations spurred interest in re-tasking clinically approved kinase inhibitors for aspects of diabetes. Clinically approved tyrosine kinase inhibitors (TKIs) are now being investigated for treatment of diabetes and diabetic complications, including retinopathy and diabetic kidney disease[267,268]. However, it is still not well understood how TKIs alter blood glucose or insulin. Several TKIs lower blood glucose in humans, but the target kinases and molecular signals responsible for changes in glucose or insulin are unknown[256–258,269,270]. Further, the effects of TKIs on immune responses that are relevant to metabolic disease are ill-defined. TKIs can improve glycemic control in animal models of obesity and diabetes, but it is still not clear if inhibition of the intended kinase or off-target kinase inhibition underpins changes in glucose or insulin[271–280]. Furthermore, a subset of TKIs, including nilotinib, rociletinib and ceritinib, have been associated with hyperglycemia due to impaired insulin secretion, inhibition of the IR, or development of insulin resistance[281–286]. TKIs have also been reported to have opposing effects on insulin levels. Some clinical reports demonstrate increased c-peptide levels during TKI therapy[287–291] or increased β-cell insulin secretion *in vitro*[274,290], while other TKIs may impair insulin secretion[292,293]. Difficulty in interpreting the mechanism of action underlying TKI's ability to regulate blood glucose can be at least partly attributed

to the numerous off-target actions of these compounds, despite intended selectivity and specificity. For example, many of the TKIs reported to alter blood glucose share many overlapping targets, such as c-Abl, c-Kit and platelet-derived growth factor receptor β (PDGFRβ)[287] (see Table 1.1).

We became interested in regulation of blood glucose by TKIs when it was reported that gefitinib and erlotinib inhibit RIPK2 with a similar efficacy as their designated target, epidermal growth factor receptor (EGFR). Considering the immune underpinnings of obesity-induced metabolic disorder and the known anti-inflammatory effects of TKIs, this represents a viable mechanism by which TKIs may influence blood glucose. Specifically, activation of the NOD1 signalling axis triggers key features of metabolic syndrome, including lipolysis, inflammation and dysglycemia. Given the reported inhibition of RIPK2 by various TKIs, this may be representative of a specific pro-inflammatory signalling pathway that is targeted by TKIs, resulting in improved blood glucose control. In contrast, activation of NOD2 signalling axis can alleviate metabolic dysfunction during nutritional or bacterial stress. Thus, inhibition of NOD2 signalling via RIPK2-specific TKIs, is an aspect of these drugs that could limit their therapeutic application. The novel use of TKIs for the treatment of T2D is a promising avenue to investigate, but more research is needed to elucidate the efficacy of these compounds, and the potential mechanisms of the actions of these drugs via RIPK2 signalling pathways. A summary of TKIs and kinase targets with reported effects on blood glucose in humans and animals are depicted in Figure 1.6.

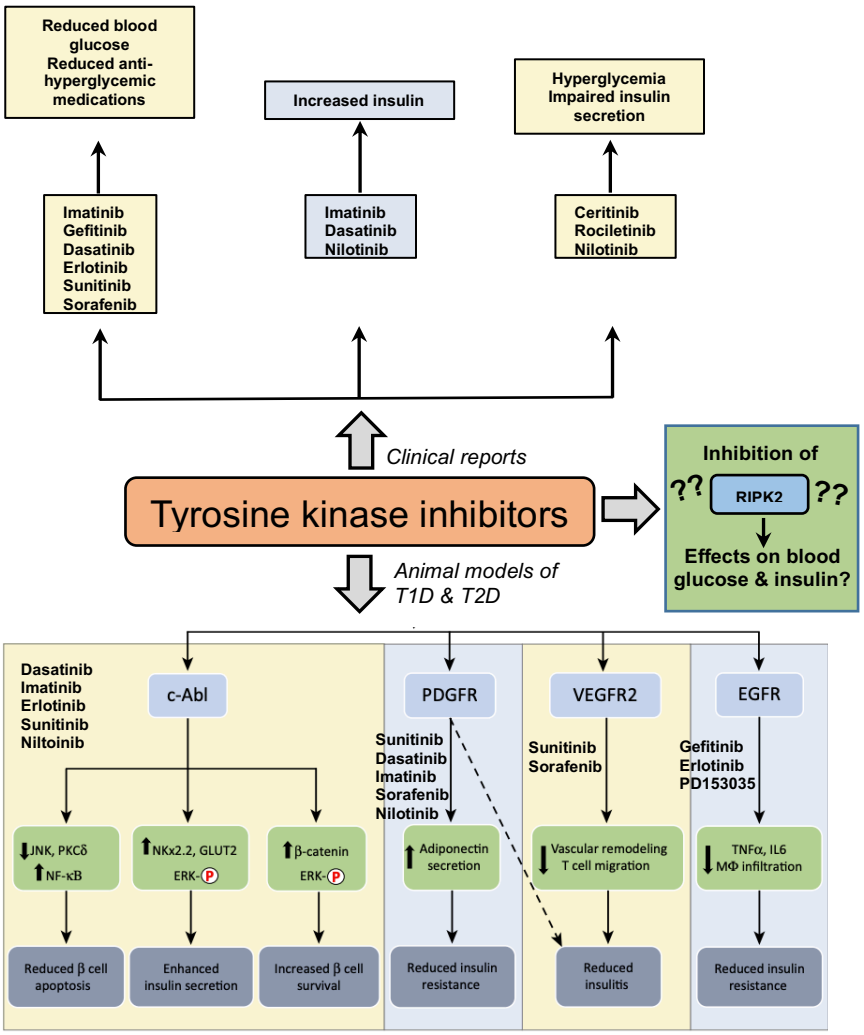

Figure 1.6 Distinct TKIs and overlapping TKI targets manifest effects on blood glucose, blood insulin and pancreatic β cell survival in clinical reports and animal models

TKIs such as imatinib, gefitinib, erlotinib, dasatinib, suninitib and sorafenib have been reported to lower blood glucose and reduce anti-hyperglycemic or diabetic medication requirements in patients. TKIs imatinib and dasatinib have been shown to increase fasting and postprandial insulin levels, while there are conflicting reports of nilotinib increasing insulin in some patients and impairing insulin secretion in others, leading to hyperglycemia. TKIs ceritinib and rociletinib have also been reported to cause hyperglycemia and impair insulin secretion in patients. Prelimninary animal models have investigated various kinase targets of TKIs that could be mediating the observed clinical effects on blood glucose and insulin, including c-Abl, PDGFR, VEGFR2 and EGFR. The TKIs that inhibit each target with a Kd value <300nM are listed beside each target. A current role for RIPK2 inhibition in mediating TKIs' glycemic effects was unknown. Adapted from Fountas, et al. 2015.

1.6 Hypotheses and objectives

The over-arching hypothesis is that RIPK2 mediates specific metabolic consequences of TKIs and microbes by regulating NOD1 and NOD2 immune responses. We hypothesized that RIPK2-specific TKIs would attenuate acute effects of NOD1, including NOD1-mediated lipolysis, inflammation, and dysglycemia. We initially hypothesized that TKIs specific for RIPK2, such as gefitinib, would improve inflammatory and metabolic parameters using a NOD1-dependent and RIPK2-dependent mechanism in adipocytes and during diet-induced obesity in mice. Based on results showing that NOD2 required RIPK2 to improve glucose control, we also tested if TKIs that inhibit RIPK2 prevented NOD2-mediated improvements in glucose control. We hypothesized that the relevance of RIPK2 to metabolic control extended beyond TKIs and that RIPK2 was also important in the integrated host-microbe responses that alter immunity and metabolism. We hypothesized that an innate immune response involving the NOD2-RIPK2 axis was required to mediate improved glucose control that can be elicited by injecting the luminal contents of the ileum into mice.

The objectives of this thesis were:

1) Investigate how kinase inhibitors of RIPK2 influence NOD1- and NOD2-immunometabolism in adipocytes and macrophages
2) Determine if RIPK2 dictates how certain TKIs alter blood glucose or insulin during obesity in mice
3) Determine if NOD1, NOD2 or RIPK2 are required for upper gut bacterial components to alter blood glucose or insulin during obesity in mice

CHAPTER 2: Methods

2.1 Mice and materials

All animal procedures for this study were approved by the McMaster University Animal Research Ethics Board in accordance with the guidelines of the Canadian Council of Animal Care. All mice were a minimum of 8 weeks old before dietary intervention or experiment initiation. Animals were maintained on a 12-hour light/dark cycle, and experiments were performed on multiple cohorts of mice born from different parents at different times of the year. Except where indicated, male mice were used for experiments. The majority of experiments were conducted on wild-type (*Wt*) C57BL/6J mice from our in-house colony born under specific pathogen-free conditions at McMaster University, and originally established from C57BL/6J mice received from The Jackson Laboratory (strain 000664). Occasionally, cohorts of C57BL/6J mice of the same strain were obtained from The Jackson Laboratory for performing experiments. *Nod1*$^{-/-}$, *Nod2*$^{-/-}$, and *Ripk2*$^{-/-}$ mice were born under specific pathogen-free conditions at McMaster University. Genotyping analysis based on nucleotide transhydrogenase (*Nnt)* gene was used to identify the substrains of our knockout models (*Nod1*$^{-/-}$, *Nod2*$^{-/-}$ and *Ripk2*$^{-/-}$ mice) because mutant forms of the *Nnt* gene have been shown to influence glucose and insulin levels during a glucose challenge[294]. All mice used in these studies were typical of the C57BL/6J (*WT/J*) or C57BL/6N (*WT/N*) background. We did not compare results between substrains or different knockout mice in any study. A cohort of diet-induced obese C57BL/6N mice used in gefitinib HFD intervention studies (Figure 3.2.6) were received from Taconic

Biosciences (Model# DIO-B6-M). Age-matched mice were used for all *in vivo* experiments. Germ-free mice were obtained from the Farncombe Gnotobiotic Unit of McMaster University, which are C57BL/6N germ free mice originally from Taconic Biosciences. Animals were fed a chow diet (17% kcal from fat, 29% kcal from protein, 54% kcal from carbohydrate; cat# 8640 Teklad 22/5, Envigo) or one of two obesity-promoting low fibre, HFDs (60% HFD; 60% kcal from fat, 20% kcal from protein, 20% kcal from carbohydrate; cat# D12492, Research Diets; or 45% HFD; 45% kcal from fat, 20% kcal from protein, 35% kcal from carbohydrate; cat# D12451, Research Diets).

NOD1 ligand FK565 (heptanoyl-γ-D-glutamyl-L-*meso*-diamino-pimelyl-D-alanine) was obtained from Astellas Pharma (Tokyo, Japan). NOD2 ligand MDP (tlrl-mdp), ultrapure lipopolysaccharide (LPS; tlrl-3pelps), Normocin™ (ant-nr-1), Blasticidin™ (ant-bl-1), Zeocin™ (ant-zn-1), HEK-Blue™ Detection media (hb-det3), HEK-Blue™ mNOD1 (hkb-mnod1) cells and HEK-Blue™ mTLR4 (hkb-mtlr4) cells were obtained from Invivogen (San Diego, CA). Gefitinib and erlotinib were from AbMole Bioscience (Houston, TX). SB203580, Compound 56, neratinib, lapatinib, and PD153035 hydrochloride were from ApexBio (Houston, TX). Tyrphostin AG 1478 was from Cell Signalling Technology (Boston, MA). Ponatinib, dasatinib, dabrafenib, vandetanib, ruxolitinib, ibrutinib sorafenib, crizotinib, imatinib and sunitinib were from AdooQ Bioscience (Irvine, CA). Methylcellulose (M0512), isoproterenol (I6504), (-)-N^6-(2-phenylisopropyl)adenosine (PIA; P4532) and fatty acid-free

bovine serum albumin (BSA) were from Sigma-Aldrich (St. Louis, MO). GlutaMAX, Dulbecco's modified Eagle medium (DMEM), Dulbecco's phosphate-buffered saline (DPBS) and fetal bovine serum (FBS) were from Life Technologies (Burlington, ON). Insulin was Novorapid (#02245397) from Novo Nordisk (Mississauga, ON). Antibodies were from Cell Signalling Technologies.

2.2 Cell culture

Murine 3T3-L1 preadipocytes (American Type Culture Collection, Rockville, MD) were cultured in DMEM containing 10% FBS, 1% GlutaMAX and 1% penicillin-streptomycin (complete culture medium). When cells reached 80% confluence, differentiation was induced by incubating with complete culture medium containing 0.5 mM 3-isobutyl-1methylxanthine, 0.25 µM dexamethasone, 10 µg/mL insulin and 2 µM rosiglitazone for 48 hours (day 0 to 2) and then changed to complete culture medium containing only 10 µg/mL insulin for 48 hours (day 2 to 4). Complete culture medium containing only 10 µg/mL insulin was replaced every 48 hours and experiments were performed on adipocytes he differentiated for 8–12 days. Bone marrow derived macrophage (BMDM) cells were harvested from femur and tibia of C57Bl/6J (WT) or RIPK2$^{-/-}$ mice and cultured for 7–10 days in DMEM containing 10% FBS and 15% L929 conditioned media, as described[192]. On day 4, media was replenished with additional 15% L929 conditioned media. Prior to treatment, adipocytes were washed twice with warmed DPBS and maintained in serum-free DMEM

containing 0.5% fatty-acid free BSA and 1% pen/strep (treatment media). BMDM cells were washed twice with warmed DPBS and maintained in DMEM containing 0.5% FBS and 1% pen/strep. Adipocytes and BMDM cells were pre-incubated for 1 h with inhibitors and subsequently treated with or without 10 μg/mL FK565 or 0.5 μg/mL LPS. Supernatant media samples were collected prior to stimulation with ligands (0 h) and at 24 h and 48 h post-stimulation.

HEK-Blue™ NOD1 cells were grown in media containing DMEM, 10% FBS, 1% Glutamine, 1% p/s, 100 μg/mL Normocin™, 30 μg/mL Blasticidin™ and 10 μg/mL Zeocin™ (HEK-NOD1 media). Cells were seeded at a density of 30,000 cells/well into a 96-well plate and incubated for 24 hours prior to treatment.

2.3 Glycerol assay and ELISA

Free glycerol concentrations in supernatant media of 3T3-L1 adipocytes were determined using a free glycerol determination kit from Sigma-Aldrich (St. Louis, MO). Free glycerol concentrations at 0, 24 and 48 h were quantified and used to calculate glycerol release rate, as described[194].

CXCL1, CXCL9 and IL-6 were quantified by ELISA from R&D Systems (Denver, CO) in adipocyte or macrophage supernatant media, mouse serum and protein isolates from epididymal adipose depots at specified time points, according to manufacturer's instructions.

2.4 NF-κB activity

At time of HEK cell treatment, cells were switched into HEK-Blue™ detection media supplemented with 1 or 5 μM gefitinib, as appropriate. Cells were incubated for 1 hour with or without gefitinib, before stimulation with 10 μg/mL FK565 or 0.5 μg/mL LPS. 24 hours later, the secreted alkaline phosphatase (SEAP) reporter of NF-κB activity was detected by measuring absorbance at 630 nM on a Synergy H4, Hybrid Reader (BioTek, Winooski, VT). All cells were maintained at 37 °C and 5% CO_2.

2.5 Immunoblotting

For insulin signalling in adipocytes, following 1 h pre-incubation with 5 μM gefitinib and 48 hour treatment with 10 μg/mL FK565, adipocytes were stimulated for 10 minutes with 100 nM insulin and washed twice in ice-cold PBS. Cell lysates were prepared in SBJ lysis buffer (0.05M HEPES, 0.15M NaCl, 0.1M NaF, 0.01M Na pyrophosphate, 0.0005M EDTA*2H20, 0.25M Sucrose, 1mM DTT, 1% Triton-X, 1 mM Na-orthovanadate, and 1% Protease inhibitor solution) by passing through a 25G syringed needle 10 times. For insulin signalling in murine adipose tissue, protein was extracted from ~50mg epididymal adipose depots in SBJ lysis buffer using mechanical homogenization at 4.5 m/s for 1 min using a FastPrep-24 tissue homogenizer (MP Biomedicals) and one plastic bead.

Samples were centrifuged (4°C, 13000xg, 15 min) and supernatant was transferred to clean sample tubes. Protein concentration was quantified with the Pierce BCA protein assay (cat# 23225, Thermo Fisher Scientific). Equal amounts of protein were prepared in Laemmli sample buffer and resolved on 7.5% poly-acrylamide gels using the Bio-Rad Mini-PROTEAN Tetra Cell Western blotting system. Samples were transferred to PVDF membrane (0.45 μM, Millipore Immobilon-P, #IPVH00010) using the Bio-Rad Trans-Blot Turbo transfer system. Following transfer, membrane was blocked for 1 hour while rocking using a 5% BSA solution, followed by overnight incubation with the designated antibody. A list of antibodies and dilutions can be found in Table 2.1. Following overnight incubation, membranes were washed in TBS-Tween 0.05% (4 x 15 min) followed by 1 h incubation with Anti-Rabbit Secondary antibody and a repeat washing step. Membranes were then incubated in Clarity Max ECL reagent (cat#1705062) while rocking for 5 minutes at room temperature and immediately imaged using the Bio-Rad ChemiDoc XRS+. Quantification of immuno-reactive signals 9(i.e. bands) for specific proteins was performed using the Bio-Rad ImageLab software (6.0.1).

2.6 Gene expression analysis

For transcript analysis, total RNA was prepared using Trizol (Invitrogen; Carlsbad, CA) from 3T3-L1 adipocyte lysates or from ~50 mg of liver, epididymal adipose and tibialis anterior muscle via mechanical homogenization at 4.5 m/s for

30 s using a FastPrep-24 tissue homogenizer (MP Biomedicals) and ceramic beads, followed by phenol-chloroform extraction. Total RNA was prepared from ~25 mg murine pancreas using a Qiagen RNeasy Mini Kit (Qiagen, cat#74104; Germantown, MD) according to manufacturer's instructions. All RNA was treated with DNase I (Thermo Fisher Scientific) and cDNA was prepared using 500-1000 ng total RNA and SuperScript III Reverse Transcriptase (Thermo Fisher Scientific). Transcript expression was measured using TaqMan Assays with AmpliTaq Gold DNA polymerase (Thermo Fisher Scientific) and target genes were compared to the mean of *Rplp0* and *18S* housekeeping genes using the $\Delta\Delta C_T$ method. A list of target probe sequences can be found in Table 2.2.

2.7 *In vivo* Glucose and insulin tests

Glucose tolerance tests (GTTs) and insulin tolerance tests (ITTs) were performed in 6 h-fasted, conscious mice and oral glucose-stimulated insulin secretion tests (OGSIS) were performed in 12 h-fasted, conscious mice. The dose of D-glucose (Sigma-Aldrich) or insulin (NovoRapid, Novo Nordisk) and route of administration is indicated in each figure caption for each experiment. Blood glucose was determined by tail vein blood sampling using a handheld glucometer (Roche Accu-Check Performa). During OGSIS tests, blood samples were collected via tail-vein sampling at t=0, 10 and 60m post-glucose gavage (4g/kg). Blood was centrifuged for 10 min at 4°C and 10,000 g, and plasma fraction was collected and stored at -80°C. Plasma insulin was assessed using high sensitivity mouse insulin

ELISA kit (Toronto Bioscience, Cat# 32270) and measured with a Synergy H4 Hybrid reader (Biotek Instruments). Area under the curve (AUC) of blood glucose or blood insulin vs. time was calculated for GTT, ITT and OGSIS using GraphPad Prism 6 software (with baseline Y values set to 0). HOMA-IR was calculated by multiplying blood glucose values (mmol/L) by insulin values (μU/mL) and dividing this by 22.5, as described[295]. Insulin resistance index (IRI) was calculated by multiplying the AUC for glucose by the AUC for insulin during OGSIS and then multiplying by 10^{-4}, as described[224].

2.8 Inflammatory, dietary, and intestinal injection mouse models

2.8.1 Acute NOD1 activation model: *WT/J* or *Ripk2*$^{-/-}$ mice were administered gefitinib or methylcellulose vehicle for 4 days across a range of doses (5-200mg/kg/day, *p.o.*). Specific doses are indicated in each respective graph or figure legends. For all experiments, the dose of gefitinib was based on body mass measured on Day 1 and Day 3. Gefitinib was suspended in 1% methylcellulose with brief sonication followed by thorough vortexing to achieve a homogenous colloid. Concentration of gefitinib in suspension was based on body mass and the desired dose (in mg/kg) such that maximal oral gavage volume per mouse per day did not exceed 200μL. Following four consecutive days of gefitinib administration, mice were injected with NOD1 ligand FK565 (10 μg, *i.p.*). For quantification of inflammatory cytokines in adipose and serum, blood samples were collected via tail-vein sampling at t = 0, 2, and 6 h post-injection. Blood was incubated at RT for

20 min, centrifuged (4°C, 7500rpm, 5 min), and the serum fraction was collected and stored at -80°C until analysis. Immediately following collection of 6 h serum samples, mice were euthanized by cervical dislocation and epididymal adipose tissue depots were rapidly excised and snap frozen in liquid nitrogen. For GTTs, *WT/J* mice were administered with gefitinib (100mg/kg/d, *p.o.*) for 4 days as described, and injected with FK565 (10 μg, *i.p.*) after 4 days of gefitinib treatment. A GTT was performed 24 h later in 6 h fasted *WT/J* mice. *Ripk2*$^{-/-}$ mice were injected with FK565 (10 μg, *i.p.*) and 24 h later, a GTT was performed.

2.8.2 Acute NOD2 activation model: *WT/J* mice were gavaged with equimolar doses of gefitinib (100mg/kg, *p.o.*), imatinib (110mg/kg, *p.o.*) or methylcellulose vehicle, prepared as described above, and then 4 hours later mice were injected with MDP (100μg, *i.p.*) or saline, every day for 3 consecutive days. On the 4th day, all mice were injected with ultrapure LPS (0.2mg/kg, *i.p.*), fasted for 6 h, and a GTT was performed (2g/kg, *i.p.*). *Ripk2*$^{-/-}$ mice were injected with MDP (100μg, *i.p.*) or saline, every day for 3 consecutive days. On the 4th day, all mice were injected with ultrapure LPS (0.2mg/kg, *i.p.*), fasted for 6h, and a GTT was performed (2g/kg, *i.p.*).

2.8.3 TKI Intervention models: All mice were 8-12 weeks of age before being placed on an obesogenic HFD containing 60% kcal from fat (Research Diets, D12492). Where indicated, age-matched mice were also maintained on a control (chow) diet (Teklad 22/5, 17% kcal from fat). TKIs were prepared as a homogenous

suspension and administered as described above, and after 10 weeks of HFD feeding, gefitinib (50 mg/kg) or imatinib (250 mg/kg) were gavaged every second day for 8 treatments. Subsequently, a 6h-fasted glucose tolerance test (GTT) or insulin tolerance (ITT) was performed (HFD; 1g/kg, *i.p.*, or 2g/kg, *p.o.*, Chow diet; 2g/kg, *i.p.*) the day following the 8th TKI treatment. Body composition was measured using whole body MRI (Bruker Minispec, LF90-II) after gavage of TKIs two more times every second day (i.e. the 10th TKI treatment). Mice were treated for 11 total treatments over 22 days before assessing OGSIS as detailed in Figure 3.2.1. Following OGSIS, mice were euthanized by cervical dislocation and liver, epidydimal adipose, pancreas and tibialis anterior muscles were rapidly excised, weighed and snap frozen in liquid nitrogen. For insulin signalling experiments, after 11 total treatments over 22 days, mice were fasted overnight and injected with insulin (2 IU/kg, *i.p.*). Liver and epidydimal adipose tissues were excised at 15 and 16 min, respectively, after insulin injection. Protein lysates were prepared and immunoblotting was performed as described in Section 2.5.

2.8.4 Collection and preparation of intestinal extracts for injection: Groups of 3 *WT/J* donor mice, aged 10-14 weeks, used for preparation of intestinal extracts were placed on a 60% HFD for 4 weeks, or groups of 3 age-matched mice fed a chow diet, were euthanized via cervical dislocation and entire length of the small and large intestine were carefully removed with sterile tools. Each intestinal extract contained the luminal contents of 3 donor mice. The pooled intestinal extract from

3 mice was combined and used to inject multiple mice for each experiment. Luminal contents of each intestinal section were collected via gentle and thorough pressurization into a clean tube containing 500µL DPBS on ice, using separate tools for each section. Duodenal/jejunal section was defined as the proximal 15cm of small intestine, measured distally from the pyloric sphincter. Ileal section was defined as distal 10cm of small intestine, starting from cecum and measuring proximally. The entire contents of cecal sack was collected for cecum extracts. The entire length of colon from cecum to rectum was collected for colon extracts. Upon collection, all luminal contents were vigorously vortexed for 1 min to ensure thorough mixing. For fecal extracts, a single fecal pellet was collected from each of the 3 donor mice prior to euthanization, and mechanically homogenized at 4.5 m/s for 1 min using a FastPrep-24 tissue homogenizer (MP Biomedicals) and two plastic beads. Germ-free intestinal extracts were prepared from 3 age-matched germ-free mice immediately upon export from the Farncombe Gnotobiotic Unit at McMaster University. Euthanization and intestinal extracts were prepared only in the level II biosafety hood to prevent contamination with ambient microbes. All extracts were centrifuged (4°C, 7500rpm, 5 min) to pellet debris and supernatant was transferred into fresh tubes. Supernatant was sonicated for 1 min (Fisher Scientific 20kHx sonicator), aliquoted and stored at -80° until use). Extracts were stored for a maximum of 4 months, and multiple separate collections of extracts were tested across multiple studies to ensure reproducibility. Diluted ileal extracts were prepared fresh on the day of injection in recipient mice in dPBS (50-20,000x).

2.8.5 Chow diet intestinal injection model: *WT/J*, *Nod1*$^{-/-}$, *Nod2*$^{-/-}$ and *Ripk2*$^{-/-}$ recipient mice, aged 10-18 weeks old, received a single injection of intestinal extract (200μL, *s.c.*, of duodenal/jejunal, ileal, cecal, colon or fecal extract) and glucose tolerance or oral glucose-stimulated insulin secretion was assessed 35 days after injection. Insulin tolerance was assessed 42 days after injection.

2.8.6 HFD intestinal injection model: Following 35-day post-injection GTT or OGSIS, *WT/J*, *Nod1*$^{-/-}$, *Nod2*$^{-/-}$ and *Ripk2*$^{-/-}$ mice were switched to a 60% HFD for 12 weeks. After 8 weeks of HFD-feeding, recipient mice received a second injection of intestinal extract (200μL, *s.c.*) and a GTT or OGSIS was performed after 12 weeks of HFD-feeding. recipient mice. In a single cohort of HFD-fed mice that did not receive an injection of intestinal extract during chow-feeding (see Figure 3.3.10-11), a first injection of intestinal extract was administered after 8 weeks of HFD-feeding, and a second injection was administered after 12 weeks of HFD-feeding. Glucose tolerance was assessed after 12 and 16 weeks of HFD-feeding in this cohort of mice.

2.9 TKI serum quantification

2.9.1 Quantification of serum TKI concentration after single administration in chow diet-fed mice: *WT/J* mice were gavaged with an equimolar dose of gefitinib (100mg/kg, *p.o.*), imatinib (110mg/kg) or methylcellulose (vehicle control). These

doses correspond to the doses used in chow-fed mice during acute NOD2 activation experiments. Blood samples were collected via tail vein sampling at t=0, 2 and 6 h post-administration.

2.9.2 Quantification of serum TKI concentration during repeated administration in obese mice: Obese *WT/J* mice fed the HFD for 10 weeks were gavaged with gefitinib (50mg/kg, *p.o.*), imatinib (250mg/kg, *p.o.*) or methylcellulose (vehicle control). These doses correspond to the doses used in obese mice in our HFD intervention model. Blood samples were collected via tail vein sampling 2h after the 1st, 4th and 8th administration (on TKI treatment days 1, 7, and 15).

2.9.3 TKI serum sample processing and quantification: All blood samples were clotted for 20 min, then centrifuged for 10 min (4°C at 10,000 g) and serum fraction was collected and stored at -80°C until analysis. Quantification was accomplished using liquid chromatography coupled to tandem mass spectrometry based on a previously published method[262]. In brief, an acetonitrile precipitation was performed prior to sample analysis by an Agilent 1290 Infinity II HPLC with an Agilent 6550 iFunnel Q-TOF mass spectrometer for detection (Agilent, Santa Clara, CA, USA). Gefitinib and deuterated gefitinib (gefitinib-d6, Cayman Chemicals, Ann Arbour, MI), imatinib and deuterated imatinib (imatinib-d3, Cayman Chemicals, Ann Arbour, MI) were used to generate a matrix-matched standard curve and determine sample recovery. Method detection was confirmed in a linear

concentration range, reproducibility was verified, matrix effects were tested for and three TKI concentrations were validated (0.1ppm-20ppm). No gefitinib or imatinib was detected in control samples above the method detection limit of 0.02ppm.

2.10 Quantification of 16S rRNA in intestinal extracts

Sonicated, undiluted intestinal extract (300uL) was processed using ZymoBIOMICS DNA kit (cat# D4300, Zymo Research Corporation), according to manufacturer's instructions, with the addition of 2 enzymatic lysis steps following mechanical homogenization. These additions to the protocol consisting of an incubation with lysis solution 1 (50 mg/mL lysozyme and 20% RNase), rocked at 37°C for 1 hour and then incubation with lysis solution 2 (25 µL of 25% SDS, 25 µL of 5M NaCl, 50 µL of 10 mg per mL Proteinase K) at 60° C for 30 min. qPCR for bacterial 16S rRNA gene was then conducted, as described[296]. In brief, master mix was comprised of 50% BioRad SsoFast EvaGreen supermix (cat#172-5200), 0.5% forward primer 926f* (AAACTCAAKGAATTGACGG), 0.5% reverse primer 1062r (CTCACRRCACGAGCTGAC), 5% 10 mg/mL BSA, 39% ultrapure H_20, and 1% standard or unknown sample (purified intestinal extract). Purified genomic DNA from *Escherichia coli* were used to generate a standard curve between 10-100 ng/µL. The qPCR was performed using a Bio-Rad CFX96 thermocycler and all calculations were performed on the Bio-Rad CFX96 software.

2.11 Statistical analysis

Data is expressed as mean ± standard error of the mean (SEM). Comparisons were made using unpaired, two-tailed Student's t-test where 2 variables are compared. ANOVA, was used for comparison of more than 2 variables and Tukey's post-hoc test was used when appropriate. Multiple t-tests, one per row, using the Holm-Sidak method, were used to determine differences between individual time-points during a GTT, ITT or OGSIS (GraphPad Prism 6 Software). Differences were considered statistically significant at $p < 0.05$.

Table 2.1: Antibody reagent list
CS – Cell Signalling Technologies (Danvers, MA)

Antibody	Species	Dilution	Company
pAKT (Ser473)	Rabbit	1:1000	CS-#4058
Total AKT	Rabbit	1:1000	CS-#9272
Secondary Anti-rabbit	Goat	1:5000	CS-#7074

Table 2.2: TaqMan qPCR probe list
From Thermofisher TaqMan Gene Expression Assays

Gene	Probe catalog #
acc1	Mm01304257_m1
acc2	Mm01204671_m1
arg1	Mm01190441_g1
atf6	Hs00232586_m1
b-had	Mm00840109_m1
bip	Mm00517691_m1
ccl2	Mm00441242_m1
ccr7	Mm01301785_m1
cd3e	Mm01179194_m1
cd4	Mm00442754_m1

cd8	Mm01182107_g1
cd36	Mm00432403_m1
c-idea	Mm00432554_m1
chop	Mm01135937_g1
cox2	Mm03294838_g1
cox8b	Mm00432648_m1
cpt-1	Mm01231183_m1
cxcl1	Mm04207460_m1
cxcl9	Mm00434946_m1
cxcl10	Mm00445235_m1
emr1	Mm00802529_m1
fabp4	Mm00445878_m1
il1b	Mm00434228_m1
il1rn	Mm00445260_m1
il4	Mm00445260_m1
il6	Mm00446190_m1
il10	Mm00439616_m1
irak3	Mm00518541_m1
ire-1	Mm00469005_m1
itgam	Mm00434455_m1
itgax	Mm00498701_m1
nlrp3	Mm00840904_m1
nod1	Mm00805062_m1
nod2	Mm00467543_m1
nos2	Mm00440502_m1
rplp0	Mm01974474_gH
sxbp1	Mm03464496_m1
tgfb1	Mm01178820_m1
tgfb2	Mm00436955_m1
tgfb3	Mm00436960_m1
tlr4	Mm00445273_m1
tnf	Mm00443258_m1
xbp1	Mm00457357_m1
18s	Mm03928990_g1

CHAPTER 3: Results

3.1 Kinase inhibitors of RIPK2 and NOD-mediated immunometabolism

We designed a series of experiments in adipocytes and bone marrow derived macrophages to investigate whether tyrosine kinase inhibitors that are reported to inhibit RIPK2 could attenuate various immune or metabolic consequences of NOD1 signalling, such as lipolysis, inflammation and insulin resistance. The experimental design is depicted in Figure 3.1.1.

3.1.1 Kinase inhibitors of RIPK2 attenuate NOD1-mediated lipolysis

Previous work from our lab has shown activation of NOD1 with 10 μg/mL of the muramyl tetrapeptide, heptanoyl-γ-D-glutamyl-(L)-meso-diaminopimelyl-(D)-alanine (FK565) augments lipolysis in 3T3-L1 adipocytes and murine adipose tissue[194]. As an initial screen to investigate if TKIs with reported inhibitory activity against RIPK2 attenuate NOD1-mediated lipolysis, we pre-treated adipocytes with increasing concentrations (1-10μM) of a broad panel of TKIs prior to stimulation of NOD1 with FK565 (10μg/mL) and measured glycerol release into the cell culture media. Our results show that select TKIs (with diverse intended target kinases) inhibit NOD1-mediated lipolysis in a dose-dependent manner (Figure 3.1.2, A). FK565-stimulated glycerol release was lower in 3T3-L1 adipocytes pre-incubated with TKIs ponatinib, dasatinib, dafabranib, vandetanib, ruxolitinib, SB203580, ibrutinib, gefitinib, sorafenib, neratinib, erlotinib at concentrations of 1–10 μM. FK565-sitmulated glycerol release was lower in 3T3-L1 adipocytes pre-incubated with AG1478, crizotinib and PD153035 at concentrations of 5–10 μM, while

Compound 56 and lapatinib only inhibited FK565-stimulated lipolysis when present at 10 μM. However, imatinib and sunitinib, which do not have reported inhibitory activities against RIPK2[262], did not alter FK565-stimuluated glycerol release after 48 hours (Figure 3.1.2).

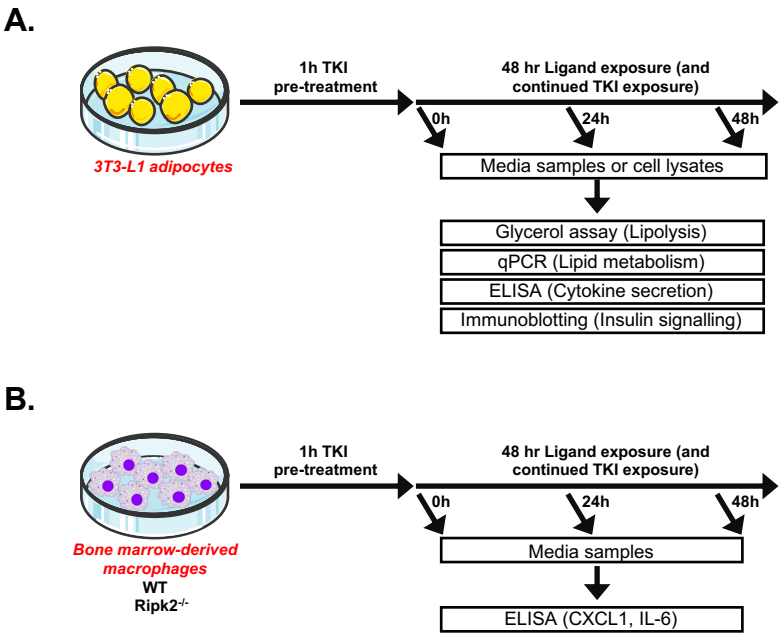

Figure 3.1.1 Experimental design of 3T3-L1 adipocyte and bone marrow-derived macrophage treatment to investigate inhibition of NOD1 immunometabolism by TKIs

A) Experimental model for investigating the effects of TKIs on NOD1-mediated immunometabolism in cultured 3T3-L1 adipocytes. To assess inhibitor specificity for NOD1 responses, cells were treated with various TKIs and then stimulated with FK565 (NOD1 ligand), LPS (TLR4 ligand), or isoproterenol. Lipolysis was measured by glycerol assay in and gene expression for molecular marks of lipid oxidation, transport and synthesis were assessed by qPCR. Cytokine secretion in response to NOD1 or TLR4 stimulation was measured by ELISA. Insulin signalling was determined by immunoblotting for phosphorylation of AKT at Ser473. B) Experimental model for investigating the effects of TKIs on NOD1-mediated immunometabolism in bone marrow-derived macrophages derived from *Wt* and *Ripk2*$^{-/-}$ mice. Cells were pre-treated with various TKIs and stimulated with FK565 or LPS (NOD1 and TLR4 ligands, respectively).

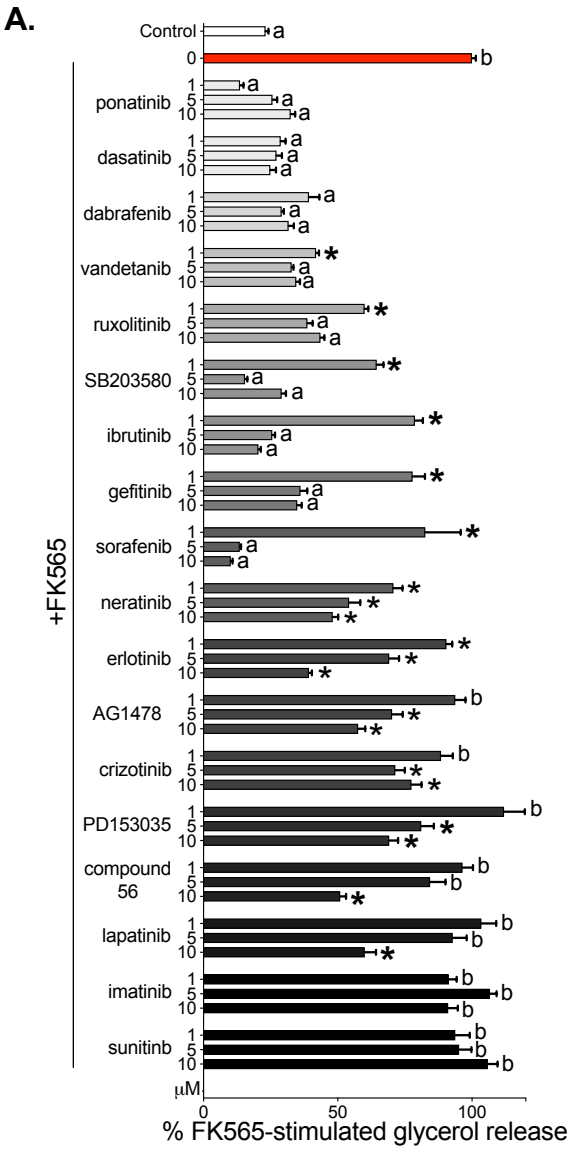

Figure 3.1.2 Select TKIs inhibit bacterial cell wall-mediated lipolysis in adipocytes

A) Relative levels of glycerol released from 3T3-L1 adipocytes after stimulation with the NOD1 ligand FK565 (10 μg/mL) for 48 h and pre-incubated for 1 h with 1, 5 or 10 μM of various TKIs (n = 6–69/group) Values are mean ± SEM. Conditions with different letters (a, b, c) denotes a statistical difference compared to all other conditions without the same letter. *Denotes partial inhibition that is statistically lower than FK565-stimulated glycerol release, but significantly higher than basal glycerol release for a given TKI ($p < 0.05$)

We next used the rate of glycerol release to model adipocyte lipolysis over 48 hours. We determined the rate of glycerol release that was stimulated by FK565 between 0 and 48 hours with pre-incubation of gefitinib, SB203580 (a known RIPK2 inhibitor) and imatinib, a TKI which did not display inhibitory activity against NOD1-mediated lipolysis. Only 1 or 5 µM gefitinib and 1 or 5 µM SB203580 dose-dependently attenuated the increased rate of glycerol release induced by FK565. Again, imatinib did not alter the rate of FK565-induced glycerol release over 48 hours (Figure 3.1.3)

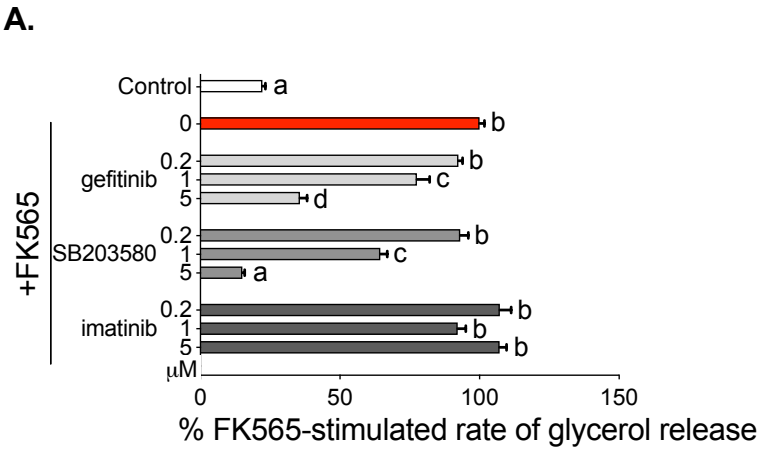

Figure 3.1.3 TKI gefitinib, but not imatinib, inhibits bacterial cell wall-mediated glycerol release rate in adipocytes

A) Rate of glycerol release over 48 h in 3T3-L1 adipocytes after stimulation with NOD1 ligand FK565 (10 µg/mL) for 48 h and pre-incubated for 1 h with 0.2, 1 or 5 µM gefitinib, SB203580, and imatinib n = 8–49/group). Values are mean ± SEM. Conditions with different letters (a, b, c) denotes a statistical difference compared to all other conditions without the same letter ($p < 0.05$).

Because of the robust effects that certain TKIs had on NOD1-mediated lipolysis, we sought to differentiate the effects of TKIs on inflammatory-induced

lipolysis versus hormonal/adrenergic lipolytic programs. We tested effects of (-)-N^6-(2-phenylisopropyl)adenosine (PIA) on glycerol release from adipocytes treated with NOD1 ligand. PIA is an analogue of adenosine that is a well-established inhibitor of catecholamine-induced lipolysis at low concentrations[297–299]. PIA (1–10 μM) pre-treatment did not alter FK565-stimulated lipolysis. Furthermore, we tested the ability of the TKI gefitinib to attenuate isoproterenol-induced lipolysis. We used gefitinib at 1 or 5 μM, which are doses we have shown to be lower NOD1-mediated lipolysis, but gefitinib had no effect on isoproterenol-induced lipolysis (Figure 3.1.4).

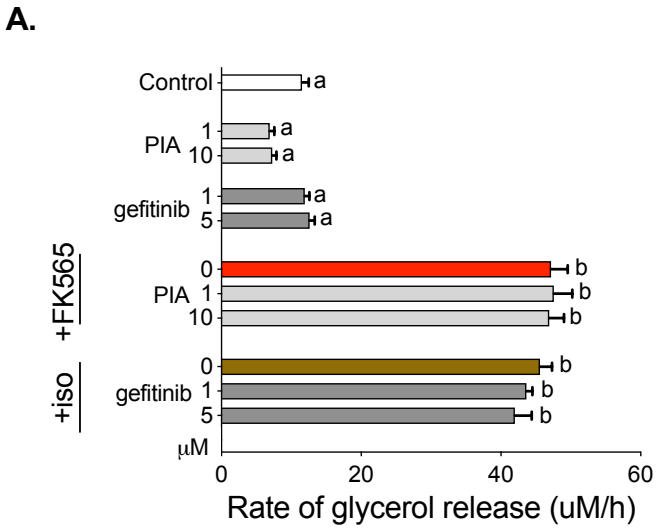

Figure 3.1.4 TKI gefitinib inhibits bacterial cell wall-mediated, but not adrenergic lipolysis
Rate of glycerol release over 48 h in 3T3-L1 adipocytes pre-incubated for 1 h with PIA (1 or 10 μM) and stimulated with FK565 (10 μg/mL), or pre-incubated with gefitinib (1 or 5 μM) and stimulated with isoproterenol (2 μM) respectively (n=6-10/group). Values are mean ± SEM. iso = isoproterenol. Conditions with different letters (a, b, c) denote a statistical difference compared to all other conditions without the same letter ($P < 0.05$).

Our results show that distinct pathways are engaged by NOD1-mediated inflammatory-related lipolysis versus adrenergic or hormonal lipolysis, and TKIs are specific for attenuating NOD1-mediated lipolysis only.

To determine if effects of TKIs on NOD1-mediated lipolysis were coincident with changes in molecular markers of lipid metabolism, we assessed gene expression for a range of genes associated with lipid uptake, oxidation and storage. In particular, our results show that stimulation with FK565 significantly decreased the majority of markers in these processes. We found significant decreases in *B-had*, *Cox2*, *Cox8b*, *Cd36*, *Fabp4*, *Acc2* in 3T3-L1 adipocytes and that pre-treatment with gefitinib partially or completely restored changes in the transcript levels of all of these indices of lipid metabolism at 24 and 48 hours (Figure 3.1.5)

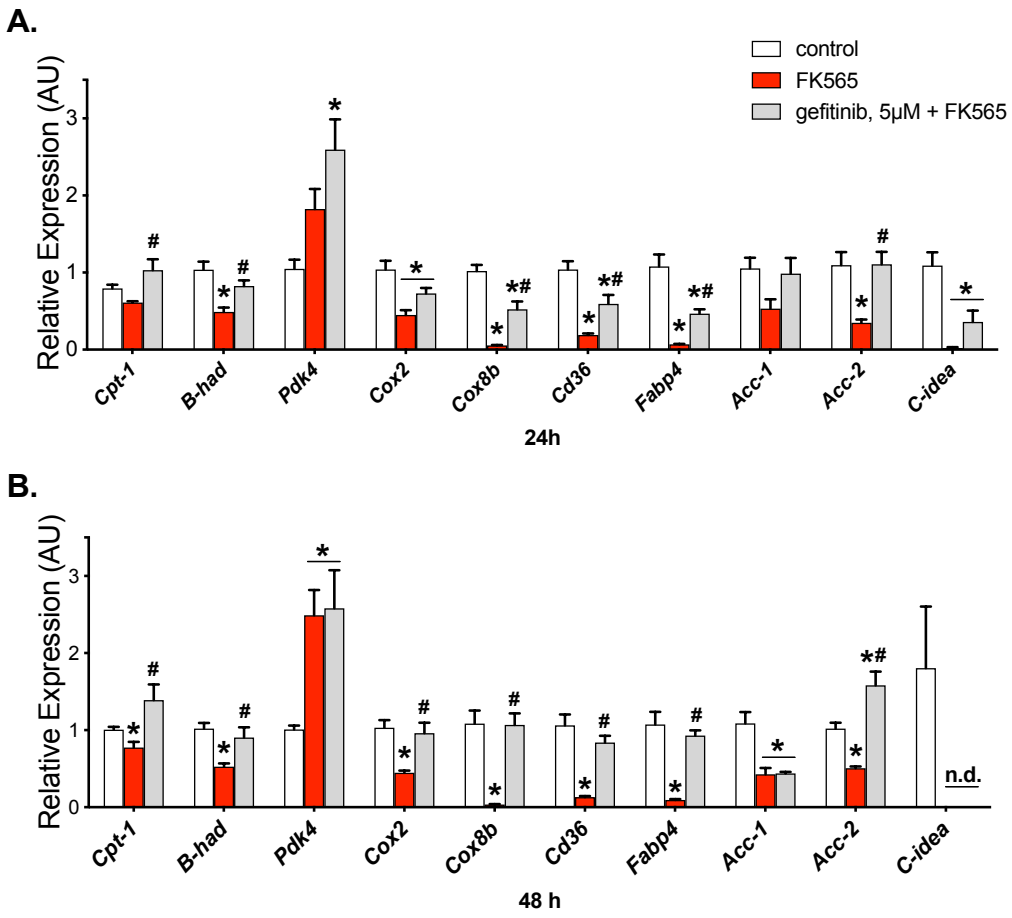

Figure 3.1.5 NOD1-mediated changes in gene expression of molecular markers of lipid oxidation, transport and synthesis Changes in gene expression of molecular markers of lipid oxidation, transport and synthesis A) 24h and B) 48 h after stimulation with the NOD1 ligand FK565 (10μg/mL) in 3T3-L1 adipocytes preincubated with 5μM gefitinib (n=7-8/group) Values are mean + SEM. * denotes statistically different from Control condition, # denotes statistically different from FK565 condition ($p<0.05$).

3.1.2 Kinase inhibitors of RIPK2 attenuate NOD1-mediated inflammation in metabolic and immune cells

We next determined if certain TKIs also attenuated NOD1-mediated inflammatory mediators in 3T3-L1 adipocytes and bone marrow derived

macrophages (BMDM). We used secretion of the chemokine CXCL1 and cytokine IL-6 as pro-inflammatory indicators of NOD1 signalling, as previously published[60]. We used the p38 MAPK inhibitor SB203580 as a positive control that is known to inhibit LPS-induced inflammation, Our results show that pre-incubation with 1–5 μM gefitinib or 1–5 μM SB203580, but not 1–5 μM imatinib significantly attenuated FK565-induced CXCL1 and IL-6 release in a dose-dependent manner in adipocytes (Figure 3.1.6).

In order to assess specificity of RIPK2 inhibitors for different components of the bacterial cell wall, we next tested these selected TKIs at their highest proven effective concentration on LPS-mediated CXCL1 and IL-6 secretion. Our results show that 5 μM gefitinib or 5 μM imatinib did not alter LPS-induced secretion of CXCL1 or IL-6 in 3T3-L1 adipocytes (Figure 3.1.7). However, 5 μM SB203580 significantly lowered LPS-induced CXCL1 and IL-6 concentration in 3T3-L1 adipocytes (Figure 3.1.7). These results show that gefitinib inhibits NOD1-ligand, but not LPS-induced inflammation in adipocytes.

We also tested these same TKIs in primary bone marrow-derived macrophages and took advantage of macrophages derived from *Ripk2*$^{-/-}$ mice to confirm that RIPK2 is required for NOD1-mediated inflammation. Similar to adipocytes, gefitinib lowered FK565-induced, but not LPS-induced CXCL1 secretion from BMDMs (Figure 3.1.8, A-B). BMDMs from *Ripk2*$^{-/-}$ mice were refractory to FK565-induced CXCL1 secretion (Figure 3.1.8, A, right panel). However, LPS-mediated cytokine responses were intact in BMDMs from *Ripk2*$^{-}$

$^{-/-}$ mice. LPS significantly increased CXCL1 secretion in BMDMs derived from *Ripk2*$^{-/-}$ mice and consistent with results from *Wt* BMDM cells, gefitinib did not alter LPS-induced CXCL1 secretion in BMDMs from *Ripk2*$^{-/-}$ mice (Figure 3.1.8, C-D). Interestingly, BMDMs did not secrete a detectable level of IL-6 in response to FK565 (Figure 3.1.9). gefitinib did not alter LPS-induced IL-6 secretion in BMDMs (Figure 3.1.9).

To further examine the specificity of gefitinib for NOD1-mediated inflammatory responses, we assessed NF-κB activity using HEK293 cells stably over-expressing *Nod1* or *Tlr4* and stimulated with NOD1 or TLR4 ligands, respectively. Consistent with cytokine secretion in adipocytes and macrophages, we find that treatment of HEK-Nod1 cells with FK565 (10 μg/mL) increases NF-κB activation, which is attenuated in a dose-dependent manner by pre-incubation with gefitinib at 1 and 5 μM (Figure 3.1.10, A). Conversely, gefitinib has no effect on NF-κB activation in response to LPS-induced TLR4 activation in HEK-Tlr4 cells (Figure 3.1.10, B).

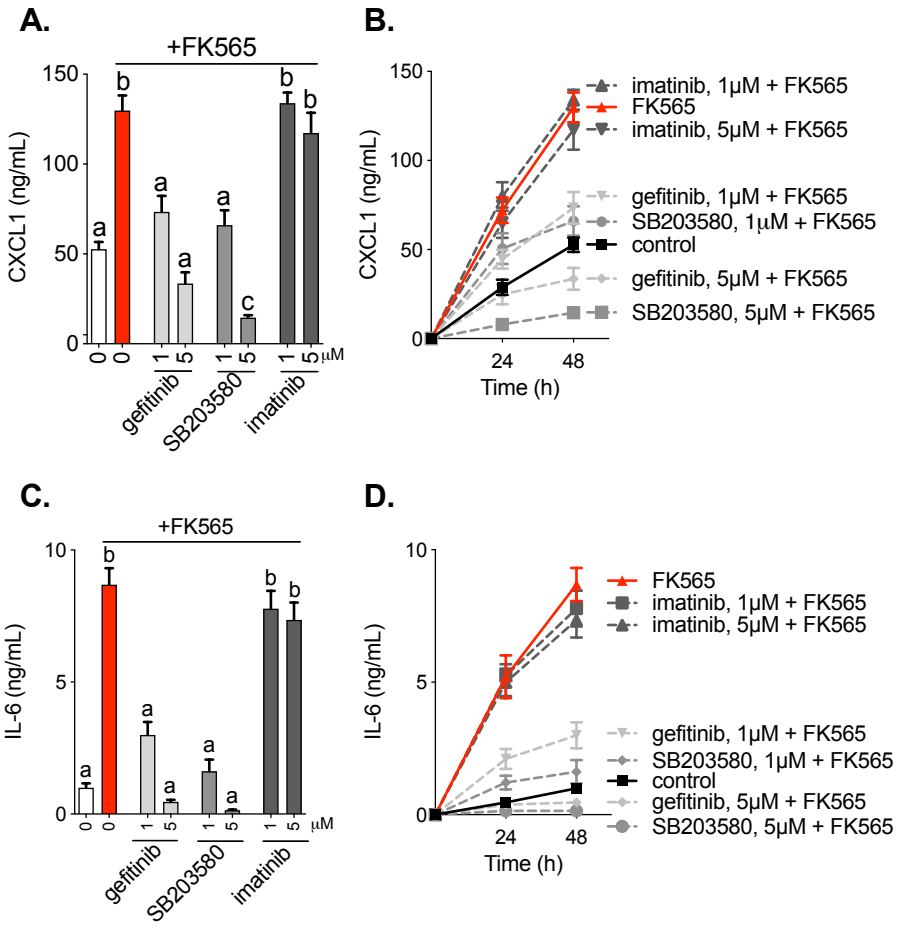

Figure 3.1.6 TKI gefitinib, but not imatinib, inhibits bacterial cell wall-mediated cytokine responses in adipocytes

A) Cumulative levels of CXCL1 released from 3T3-L1 adipocytes 48 h after stimulation with the NOD1 ligand FK565 (10 µg/mL) and pre-incubated for 1 h with 1 or 5 µM of the TKIs gefitinib, SB203580 or imatinib, and B) Time course of FK565-stimulated CXC1 secretion in 3T3-L1 adipocytes (n = 6/group). C) Cumulative levels of IL-6 released from 3T3-L1 adipocytes 48 h after stimulation with the NOD1 ligand FK565 (10 µg/mL) and pre-incubated for 1 h with 1 or 5 µM of the TKIs gefitinib, SB203580 or imatinib, and D) time course of FK565-stimulated IL-6 secretion in 3T3-L1 adipocytes (n = 6/group). Values are mean ± SEM. Conditions with different letters (a, b, c) denote a statistical difference compared to all other conditions without the same letter ($P < 0.05$).

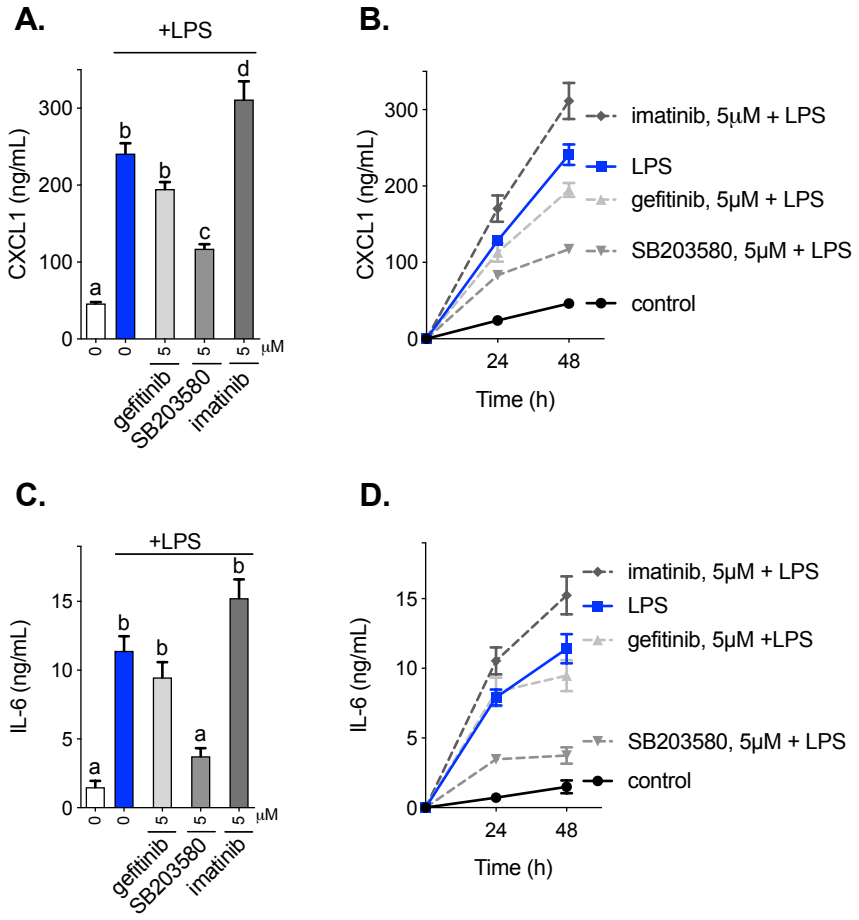

Figure 3.1.7 TKI gefitinib does not inhibit endotoxin-induced cytokine responses in adipocytes

A) Cumulative levels of CXCL1 released from 3T3-L1 adipocytes 48 h after stimulation with the TLR4 ligand LPS (0.5 μg/mL) and pre-incubated for 1 h with 5 μM of the TKIs gefitinib, SB203580 or imatinib, and B) Time course of LPS-stimulated CXC1 secretion in 3T3-L1 adipocytes (n = 6/group). C) Cumulative levels of IL-6 released from 3T3-L1 adipocytes 48 h after stimulation with the TLR4 ligand LPS (0.5 μg/mL) and pre-incubated for 1 h with 5 μM of the TKIs gefitinib, SB203580 or imatinib, and D) time course of LPS-stimulated IL-6 secretion in 3T3-L1 adipocytes (n = 5/group). Values are mean ± SEM. Conditions with different letters (a, b, c) denote a statistical difference compared to all other conditions without the same letter ($P < 0.05$).

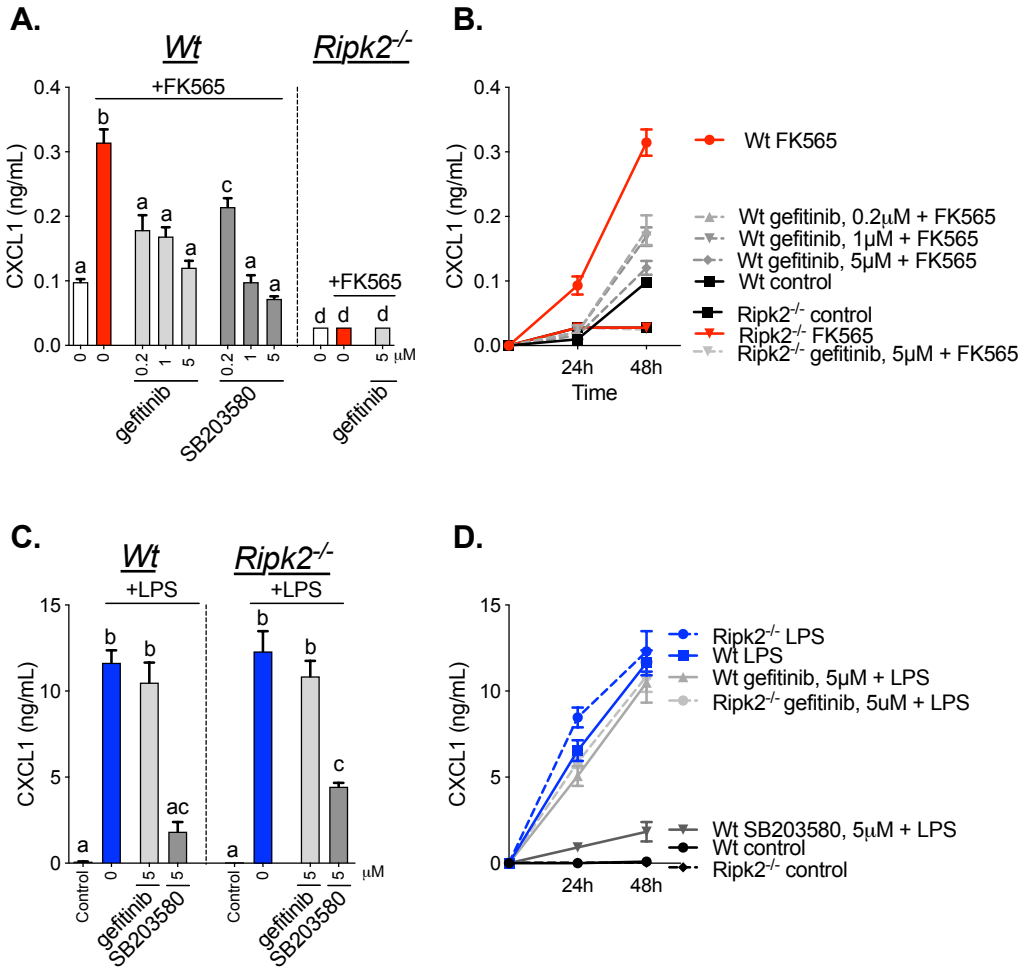

Figure 3.1.8 RIPK2 is required for macrophage inflammation induced by bacterial cell wall muropeptides, but not endotoxin

A) Cumulative levels of CXCL1 released from bone marrow derived macrophages derived from *Wt* (left panel) or *Ripk2*$^{-/-}$ mice (right panel) 48 h after stimulation with the NOD1 ligand FK565 (10 μg/mL) and pre-incubated for 1 h with 0.2, 1 or 5 μM of the TKIs gefitinib, SB203580 or imatinib, and B) Time course of FK565-stimulated CXC1 secretion in *Wt* and *Ripk2*$^{-/-}$ macrophages (n = 4-12/group). C) Cumulative levels of CXCL1 released from released from bone marrow derived macrophages derived from *Wt* (left panel) or *Ripk2*$^{-/-}$ mice (right panel) 48 h after stimulation with the TLR4 ligand LPS (0.5 μg/mL) and pre-incubated for 1 h with 5 μM of the TKIs gefitinib, SB203580 or imatinib, and D) time course of LPS-stimulated CXCL1 secretion in secretion in *Wt* and *Ripk2*$^{-/-}$ macrophages (n = 4-12/group). Values are mean ± SEM. Different letters assigned to each condition (a, b, c) denote statistical differences between groups ($p < 0.05$).

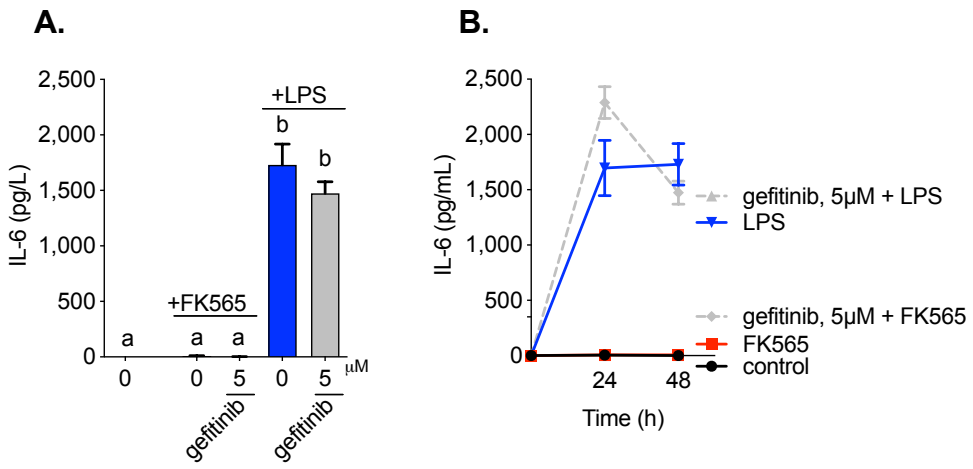

Figure 3.1.9 NOD1 activation does not potently stimuate IL-6 release in macrophages

A) Cumulative levels of IL-6 secreted from bone marrow derived macrophages derived from *Wt* mice 48 hours after stimulation with FK565 (10 µg/mL) or LPS (0.5 µg/mL) and pre-incubated for 1h with gefitinib. B) Time course of FK565-stimulated or LPS-stimulated IL-6 secretion (n=5/group). Values are mean ± SEM. Different letters assigned to each condition (a, b, c) denote statistical differences between groups ($p < 0.05$).

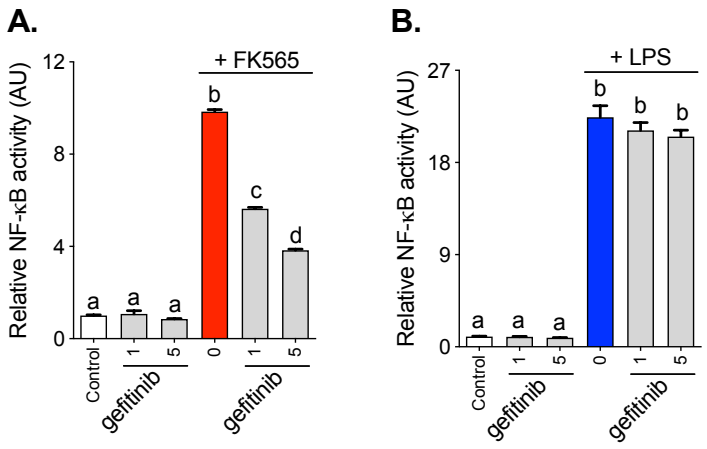

Figure 3.1.10 TKI gefitinib inhibits NF-κB activity induced by bacterial cell wall components, but not endotoxin

Relative NF-κB activity A) in HEK293 cells stably expressing *Nod1*, pre-incubated with gefitinib (1 or 5 μM) and stimulated with FK565 (10 μg/mL), or B) HEK293 cells stably expressing *Tlr4*, pre-incubated with gefitinib (1 or 5 μM) and stimulated with LPS (0.5 μg/mL) (n = 12/group). Values are mean ± SEM. Different letters assigned to each condition (a, b, c) denote statistical differences between groups ($p < 0.05$).

3.1.3 Kinase inhibitors of RIPK2 attenuate NOD1-mediated insulin resistance in adipocytes

Because of the recognized contributions of dyslipidemia and inflammation to insulin resistance, we sought to test if TKI-mediated inhibition of RIPK2 could attenuate NOD1-induced impairments in insulin signalling in adipocytes. Previous work has shown that FK565 impaired insulin signalling in primary hepatocytes via NOD1[60]. Here, we demonstrate that stimulation of 3T3-L1 adipocytes with FK565 impairs the ability of insulin to phosphorylate AKT at serine[473], and that pre-incubation with 5 μM gefitinib restores this aspect of insulin signalling in the

presence of FK565 such that it is not statistically different from insulin stimulation alone (Figure 3.1.11).

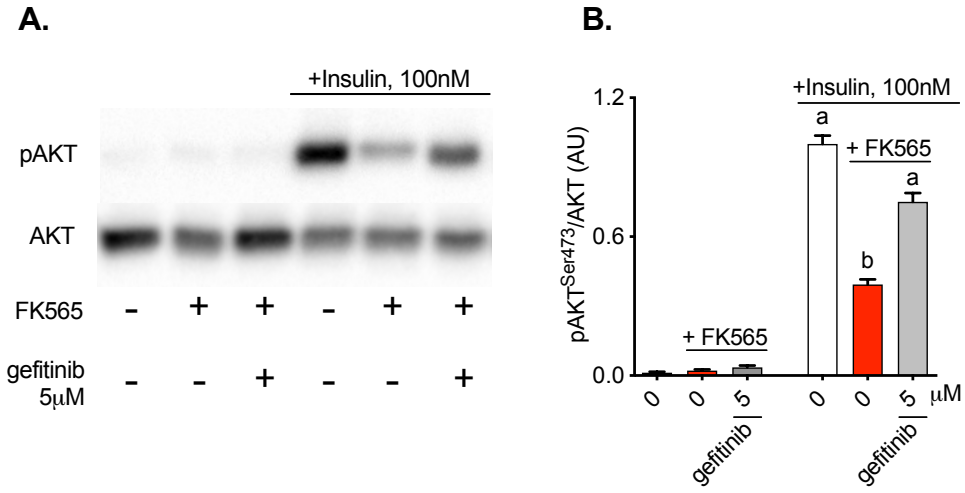

Figure 3.1.11 TKI gefitinib attenuates bacterial cell wall-mediated insulin resistance in adipocytes

A) Representative immunoblots and B) quantification of basal (i.e. no insulin) and 100 nM insulin-stimulated pAKT (Ser473) relative to total AKT in 3T3-L1 adipocytes after 1 h pre-incubation with gefitinib (5 μM) and treatment with FK565 (10 μg/mL) for 48 h. Quantitative comparison was conducted between samples from 4 different blots derived from the same experiment and processed in parallel. (n = 8 total/group). Values are mean ± SEM. Different letters assigned to each condition (a, b) denote statistical differences between groups ($p < 0.05$).

3.1.4 Kinase inhibitors of RIPK2 attenuate NOD1-mediated inflammation *in vivo*

In order to extend these cell-based results, we developed an *in vivo* model to examine the effects of TKI gefitinib on immunometabolic consequences of NOD1 activation. Mice were administered gefitinib (5–200 mg/kg/day) for 4 days, prior to injection of the NOD1 ligand FK565 (10 ug, *i.p.*). Peak plasma levels of

gefitinib occur within 3-7 hours of administration[266]. Therefore, mice were administered the last dose of gefitinib 6 hours prior to NOD1 activation. Tail vein sampling and adipose tissue depots were collected in order to assess cytokine production (Figure 3.1.12, A) or a glucose tolerance test was performed (Figure 3.1.12, B) to investigate gefitinib's effects on dysglycemia following NOD1 activation.

Our results show that treatment of mice with gefitinib at doses equal or greater than 50 mg/kg attenuated NOD1-mediated CXCL1 protein levels in the circulation in C57Bl/6J *Wt* mice in a dose-dependent manner (Figure 3.1.13, A, left panel). We also confirmed that FK565 did not increase CXCL1 serum levels in *Ripk2*$^{-/-}$ mice (Figure 3.1.13, A, right panel). These *in vivo* cytokine results are based on a previous assessment of the time-course of serum CXCL1 levels, where peak serum cytokines levels occurred at 2 h after *i.p*. injection of FK565 in *Wt* mice (data not shown). To distinguish between systemic and adipose-specific inflammation, we assessed transcript levels of several inflammatory genes (*Cxcl1*, *Cxcl9*, *Cxcl10*, *Il-6*) in adipose tissue. Transcript levels of all of these inflammatory markers were increased by FK565 in the adipose tissue but were not significantly altered by pre-treatment of mice with 100 mg/kg gefitinib (Figure 3.1.13, B). Furthermore, protein levels of CXCL9 were also increased by FK565 in the adipose tissue, but CXCL9 was not altered by pre-treatment of mice with 100 mg/kg gefitinib (Figure 3.1.13, C).

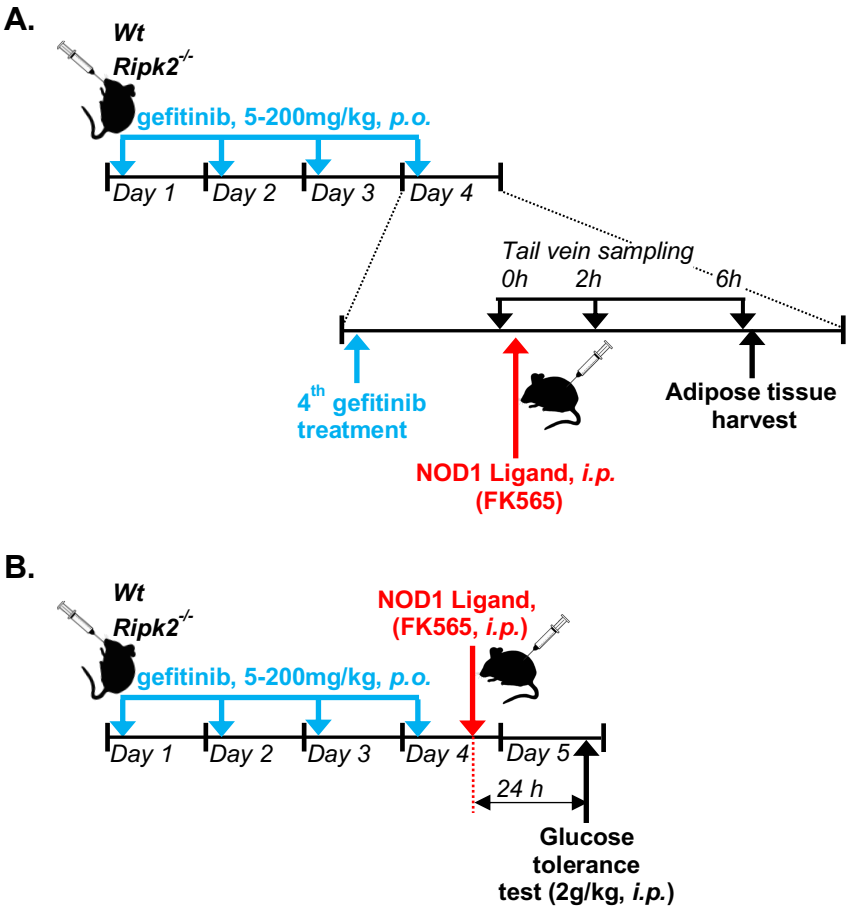

Figure 3.1.12 Experimental design to investigate inhibition of NOD1 immunometabolism by TKIs *in vivo*

A) Experimental model for investigating the effects of TKIs on NOD1-mediated cytokine production in *Wt* or *Ripk2*$^{-/-}$ mice. Mice were pre-treated with various doses of gefitinib (5-200mg/kg) or methylcellulose vehicle for 4 days. On the 4th day, mice were injected with FK565 (10 µg, i.p.), and blood was collected via tail vein sampling at t=0, 2 and 6 h post-FK565. Gonadal adipose tissue depots were also collected at the 6 h time point. B) Experimental model for investigating the effects of TKIs on NOD1-mediated dysglycemia in *Wt* or *Ripk2*$^{-/-}$ mice. Mice were treated with gefitinib and injected with FK565 as described above, and a GTT was performed on the 5th day, 24 h post-FK565 injection.

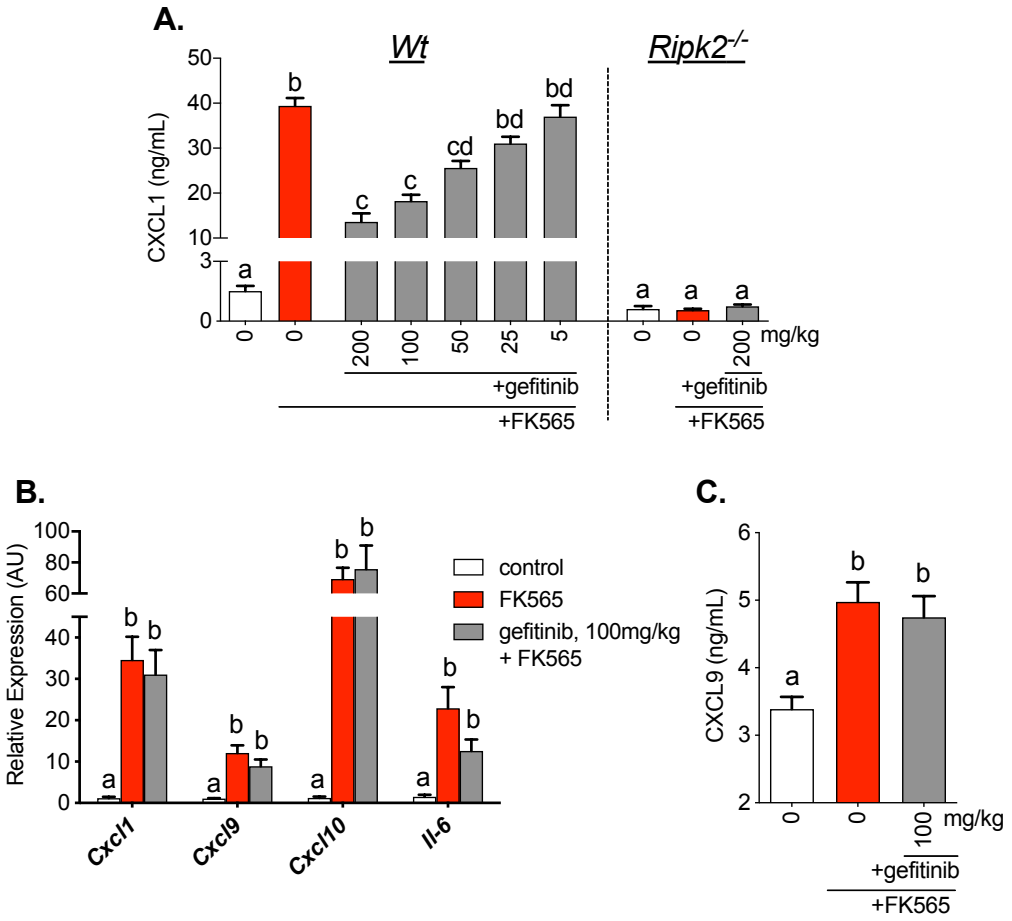

Figure 3.1.13 TKI gefitinib inhibits RIPK2-mediated inflammation *in vivo*

A) CXCL1 secretion 2 h after injection with the NOD1 ligand FK565 (10 µg, i.p.) in *Wt* or *Ripk2*$^{-/-}$ mice pre-treated with various doses of gefitinib (5-200mg/kg) or methylcellulose vehicle for 4 days (n=4-60/group). B) Transcript analysis of *Cxcl1*, *Cxcl9*, *Cxcl10* and *Il-6* in adipose tissue and C) protein levels of CXCL9 6 h after injection of FK565 (10 µg, i.p.) in mice pre-treated with 100mg/kg gefitinib or vehicle (n=7-8/group). Values are mean ± SEM. Different letters assigned to each condition (a, b, c) denote statistical differences between groups ($p < 0.05$).

3.1.5 RIPK2 is required for NOD1-mediated changes in blood glucose *in vivo* and kinase inhibitors of RIPK2 mitigate dysglycemia caused by NOD1 activation

Previous work has shown that injection of NOD1 ligands caused acute insulin resistance and dysglycemia in mice[60]. While RIPK2 is well-known to propagate inflammatory signals in response to NOD1 activation, the role of RIPK2 in propagating metabolic perturbations downstream of NOD1, to this date, remained to be defined, so we first wanted to confirm that RIPK2 is required for NOD1-mediated dysglycemia, and then subsequently assess if gefitinib attenuates dysglycemia induced by NOD1 activation. Our results show that *Ripk2*$^{-/-}$ mice were completely refractory to changes in blood glucose caused by NOD1 activation. Injection with FK565 did not alter body mass, fasting blood glucose after 6 or 24 hours, or glucose tolerance in *Ripk2*$^{-/-}$ mice (Figure 3.1.14).

Next, we chose the lowest dose of gefitinib (100 mg/kg, daily gavage for 4 days) that was able to achieve maximal inhibition of systemic CXCL1 inhibition *in vivo (*Figure 3.1.13, A) to test if a TKI that inhibits RIPK2 can mitigate dysglycemia caused by NOD1 activation. Neither gefitinib nor injection of FK565 (10 µg, *i.p.*) altered body mass (Figure 3.1.15, A). FK565 lowered fasting blood glucose, but pre-treatment with gefitinib attenuated the decline in fasting blood glucose at 6 h post-FK565 injection (Figure 3.1.15, B). At the time of the glucose tolerance test (24 h after FK565 injection) gefitinib pre-treatment did not alter fasting blood

glucose but, pre-treatment with gefitinib prevented FK565-induced relative increases in blood glucose during a GTT (Figure 3.1.1.15, C-E).

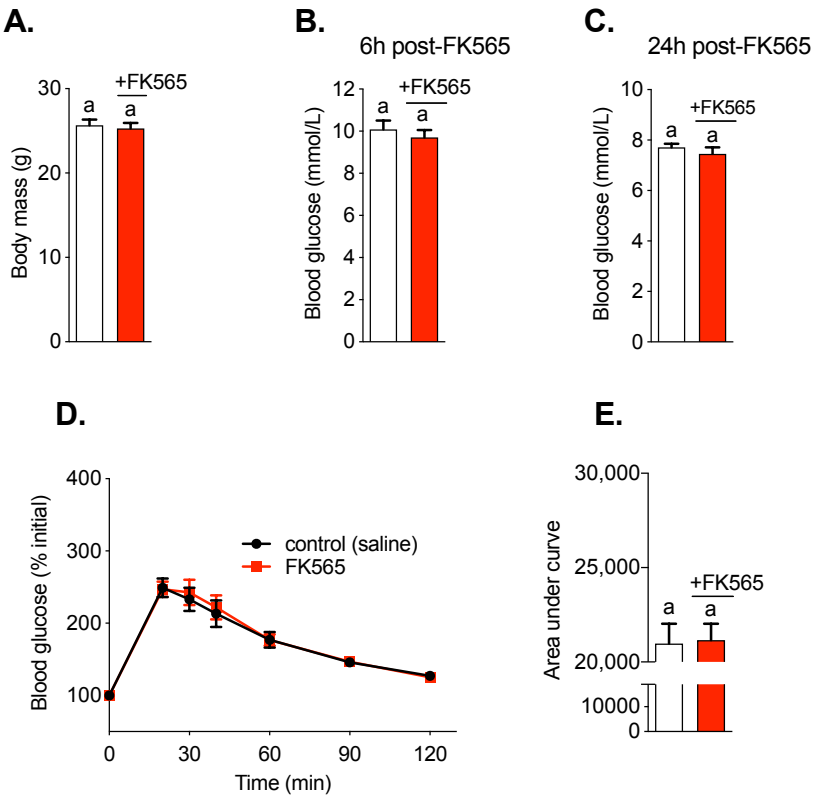

Figure 3.1.14 RIPK2 mediates bacterial cell wall-induced dysglycemia *in vivo*

A) Body mass, B) fasting blood glucose 6 h after and C) 24 h after FK565 (10 µg, *i.p.*) in Ripk2$^{-/-}$ mice. D) Percentage change in blood glucose over time and E) Area under the curve for a glucose tolerance test performed 24 h after FK565 injection (n=9-12/group). Values are mean ± SEM. Different letters assigned to each condition (a, b, c) denote statistical differences between groups ($p < 0.05$)

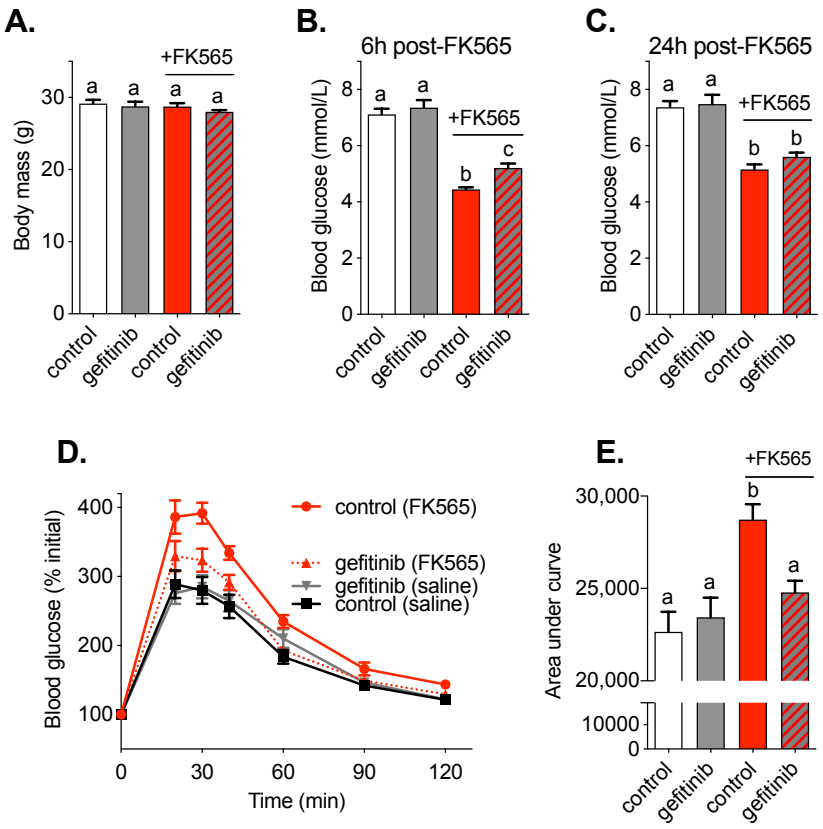

Figure 3.1.15 TKI gefitinib inhibits bacterial cell wall-mediated dysglycemia *in vivo*

Wt mice pre-treated with TKI gefitinib (100 mg/kg) or methylcellulose vehicle for 4 days before injection of NOD1 ligand. A) Body mass, B) fasting blood glucose 6 h after and C) 24 h after FK565 (10 µg, *i.p.*) in gefitinib and vehicle pretreated mice. D) Percentage change in blood glucose over time and E) Area under the curve for a glucose tolerance test performed 24 h after FK565 injection (n=9-12/group). Values are mean ± SEM. Different letters assigned to each condition (a, b, c) denote statistical differences between groups ($p < 0.05$).

3.1.6 RIPK2 is required for NOD2-mediated changes in blood glucose and kinase inhibitors of RIPK2 mitigate improved glucose control caused by NOD2 activation

The TKI gefitinib clearly inhibits many immunometabolic consequences of NOD1 activation, including changes in blood glucose. Hence, we next sought to

test if gefitinib inhibits the metabolic consequences of NOD2 signalling. We took advantage of an established model in our lab that has already demonstrated that activation of the NOD2 signalling pathway causes lower blood glucose during a GTT if mice are subjected to an acute, low-grade endotoxemia challenge. We found that 3 days of MDP treatment (100μg, *i.p.*) lowers fasting blood glucose and lowers blood glucose during a GTT following an low dose of LPS (0.1mg/kg, *i.p.*) in *Wt* mice[193].

We first tested if RIPK2 was a required signalling node for these glucose-lowering effects (Figure 3.1.16, data collected in collaboration with Dr. J.F. Cavallari). We found that *Ripk2*$^{-/-}$ mice were refractory to changes in blood glucose caused by NOD2 activation with MDP (Figure 3.1.16). Next, we sought to test if TKI gefitinib attenuates NOD2-mediated lowering of glucose levels during a GTT in mice given an endotoxemia challenge. We found that MDP decreased fasting blood glucose and the area under the curve of blood glucose x time during a GTT (Figure 3.1.17). We found that both of these MDP-induced changes in glucose control are blunted in mice pre-treated with gefitinib (100mg/kg/day, *p.o.*) prior to MDP administration, without affecting body mass (Figure 3.1.17). Finally, we also tested how an equimolar dose of TKI imatinib, which has no reported inhibitory activity against RIPK2, alters MDP-induced changes in blood glucose. We already showed that imatinib did not alter NOD1/RIPK2 metabolic responses (see Figure 3.1.3, 3.1.6). Here, we found that imatinib does not change any of the blood glucose responses caused by MDP activation, including lowering of fasting blood glucose

or area under the curve during a GTT in mice given an acute endotoxin challenge (Figure 3.1.18). Overall, these results show that the TKI gefitinib blocks both worse glucose control caused by caused by NOD1 activation, but gefitinib also blocks better glucose control caused by NOD2 activation. RIPK2 is required for these NOD1 and NOD2 mediated effects on blood glucose and the TKI imatinib does not influence blood glucose upon NOD1/2 activation.

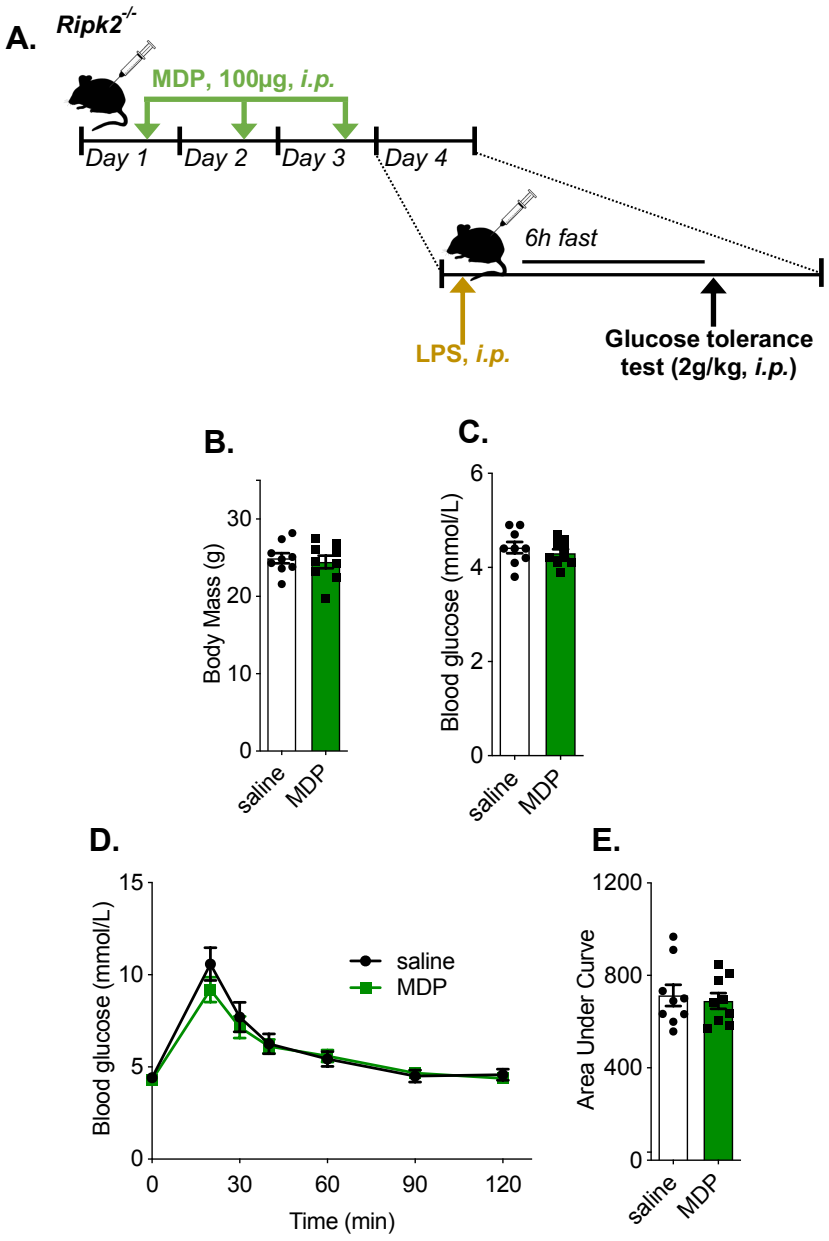

Figure 3.1.16 RIPK2 is required for NOD2-mediated glycemic effects during acute endotoxemia *in vivo*

A) Experimental model for determining if RIPK2 is required for NOD2-mediated glycemic effects during acute endotoxemia. *Ripk2*$^{-/-}$ mice were injected with NOD2 ligand MDP (100 µg, *i.p.)* for 3 days before receiving a low-dose LPS injection (0.1 mg/kg, *i.p.*). Immediately following LPS injection, mice were fasted for 6 h and a glucose tolerance test was performed (2g/kg. *i.p.)*. B) Body mass, C) Fasting blood glucose, D) Blood glucose vs. time and E) Area under curve during a glucose tolerance test (2g/kg, *i.p.).* Values are mean ± SEM. * denotes statistical differences between groups ($p<0.05$)

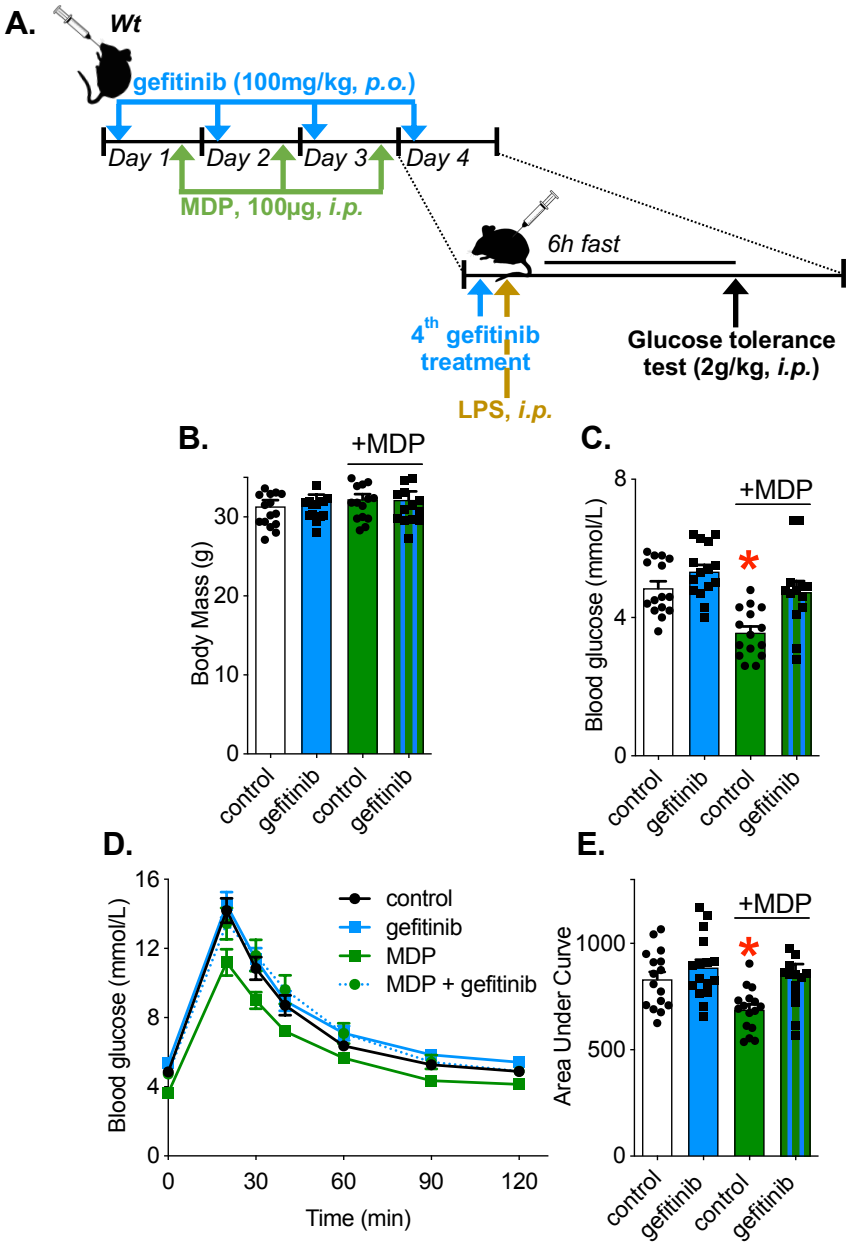

Figure 3.1.17 TKI gefitinib attenuates NOD2-mediated glycemic effects during endotoxemia challenge *in vivo*

A) Experimental model for determining if TKI gefitinib can attenuate NOD2-mediated glycemic effects during acute endotoxemia. WT mice were treated with gefitinib (100mg/kg, *p.o.)* injected with NOD2 ligand MDP (100 µg, *i.p.)* for 3 days before receiving a 4th gefitinib treatment and a low-dose LPS injection (0.1 mg/kg, *i.p.*). Immediately following LPS injection, mice were fasted for 6 h and a glucose tolerance test was performed (2g/kg. *i.p.)*. B) Body mass, C) Fasting blood glucose, D) Blood glucose vs. time and E) Area under curve during a glucose tolerance test (2g/kg, *i.p.).* Values are mean ± SEM. * denotes statistical differences between groups ($p<0.05$)

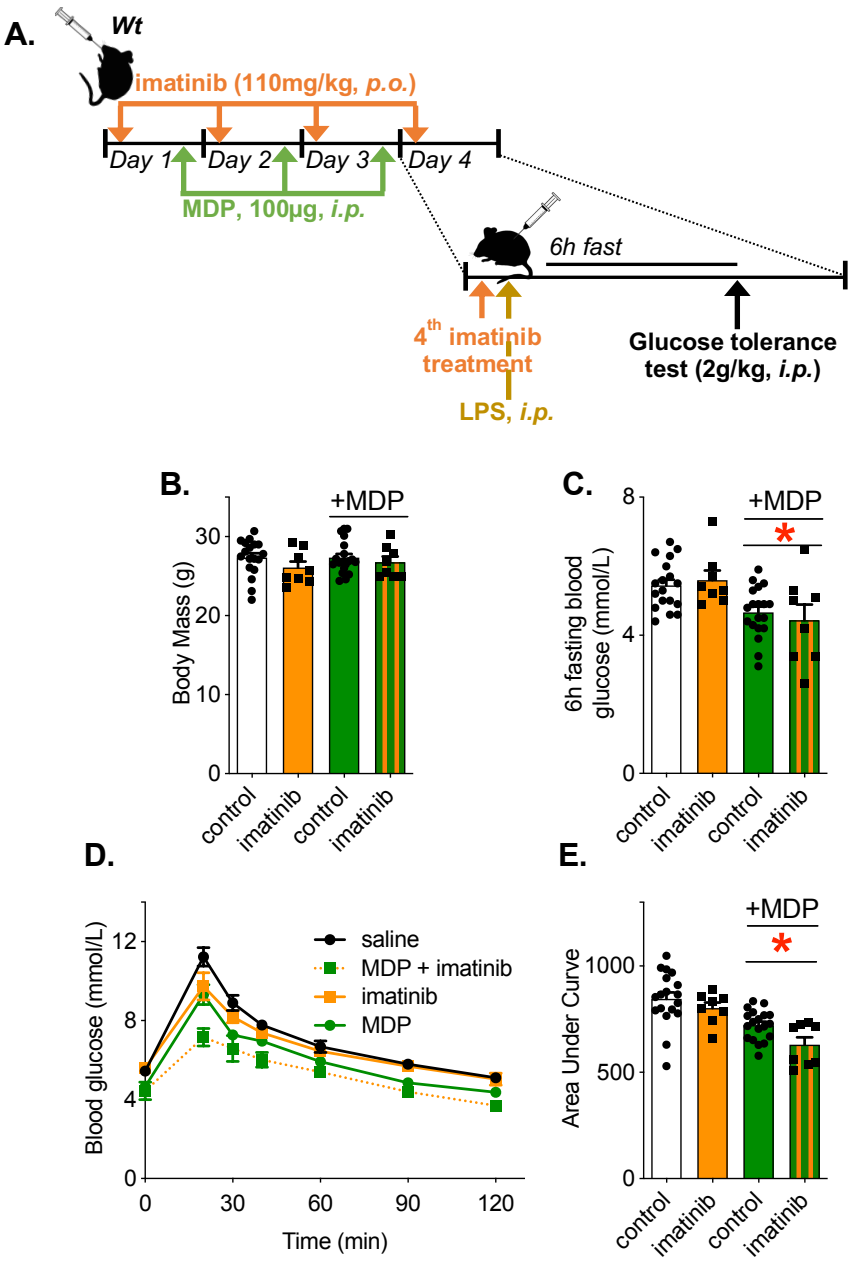

Figure 3.1.18 TKI imatinib does not attenuate NOD2-mediated glycemic effects during endotoxemia challenge *in vivo*

A) Experimental model for determining if TKI imatinib attenuates NOD2-mediated glycemic effects during acute endotoxemia. *Wt* mice were treated with imatinib (110mg/kg, *p.o.)* injected with NOD2 ligand MDP (100 µg, *i.p.)* for 3 days before receiving a 4th imatinib treatment and a low-dose LPS injection (0.1 mg/kg, *i.p.*). Immediately following LPS injection, mice were fasted for 6 h and a glucose tolerance test was performed (2g/kg. *i.p.)*. B) Body mass, C) Fasting blood glucose, D) Blood glucose vs. time and E) Area under curve during a glucose tolerance test (2g/kg, *i.p.).* Values are mean ± SEM. * denotes statistical differences between groups ($p<0.05$)

3.2 Metabolic effects of kinase inhibitors during obesity

3.2.1 Kinase inhibitor gefitinib attenuates obesity-induced glucose and insulin intolerance

To investigate the metabolic effects of the TKI gefitinib during obesity, we established an 'intervention-style' experiment by treating with gefitinib after the mice had already been on a HFD for sufficient time to develop obesity (Figure 3.2.1). All mice were placed on a HFD containing 60% kcal from fat for 10 weeks before commencing treatment with gefitinib. In brief, after 10 weeks on a HFD, a 6-hr fasting "baseline" GTT was performed and mice were separated into experimental groups based on body mass, fasting blood glucose and area under the curve during a GTT before commencing treatment. 8 treatments (gefitinib, 50mg/kg, or vehicle, *p.o.*, every other day) were administered and then glucose or insulin tolerance tests were performed in all mice. Then, three more gefitinib treatments were administered to all mice before glucose-stimulated insulin secretion was assessed and tissues were harvested for subsequent analysis.

Our initial preliminary testing and model-building studies indicated high-dose gefitinib treatment has an anorexigenic effect and rapidly induces weight loss in diet-induced obese mice (Figure 3.2.2, A). These experiments allowed us to establish a gefitinib treatment regime that avoided the confounding factors of weight loss or reduced food consumption between treatment and control groups.

Once we optimized the dose of this TKI, we found that treatment with 50mg/kg, gefitinib. *p.o.*, every other day did not induce weight loss or changes in

food consumption in obese *Wt/J* mice over the course of 11 treatments (22 days total), covering the duration of our 'intervention-style' HFD mouse model (Figure 3.2.2, B-C). Furthermore, this dose and treatment period did not alter epididymal fat, liver, or spleen tissue mass, or whole-body lean mass assessed by Bruker MRI in obese *Wt/J* mice (Figure 3.2.2 D-G). Thus, 50mg/kg *p.o.*, gefitinib was used in all subsequent studies.

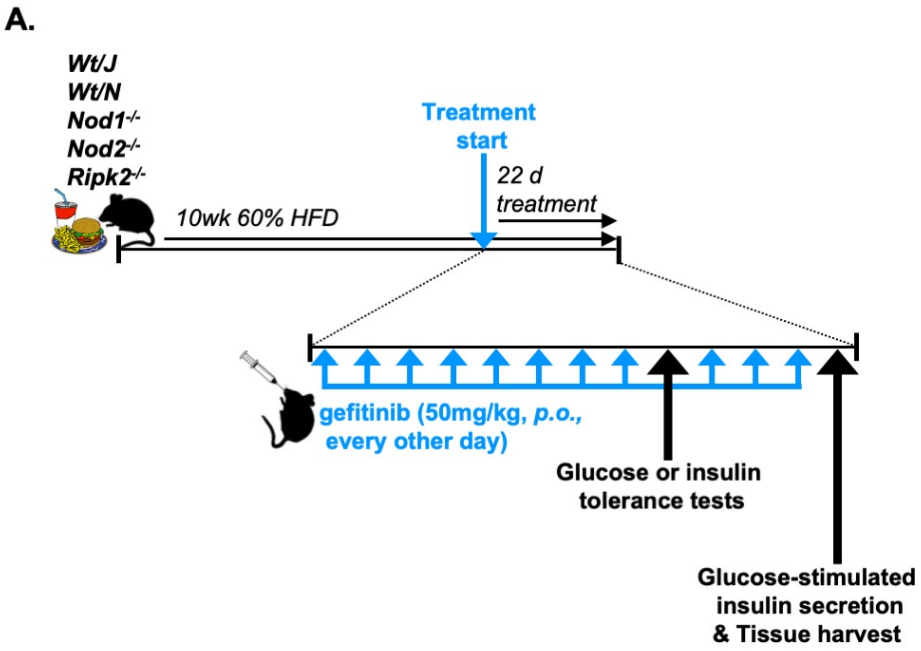

Figure 3.2.1 Experimental design for investigating metabolic effects of TKI gefitinib during obesity

A) Experimental model for investigating the effects of TKI gefitinib on glucose and insulin homeostasis, and tissue inflammation. *Wt/J, Wt/N, Nod1*$^{-/-}$*, Nod2*$^{-/-}$, and *Ripk2*$^{-/-}$ mice were placed on a 60% HFD for 10 week before intervention with gefitinib treatment (50mg/kg, *p.o.*, every other day). Mice received 8 treatments over 16 days before glucose or insulin tolerance was assessed. Then mice received 3 more treatments before glucose-stimulated insulin secretion was assessed and selected tissues were harvested immediately following cervical dislocation.

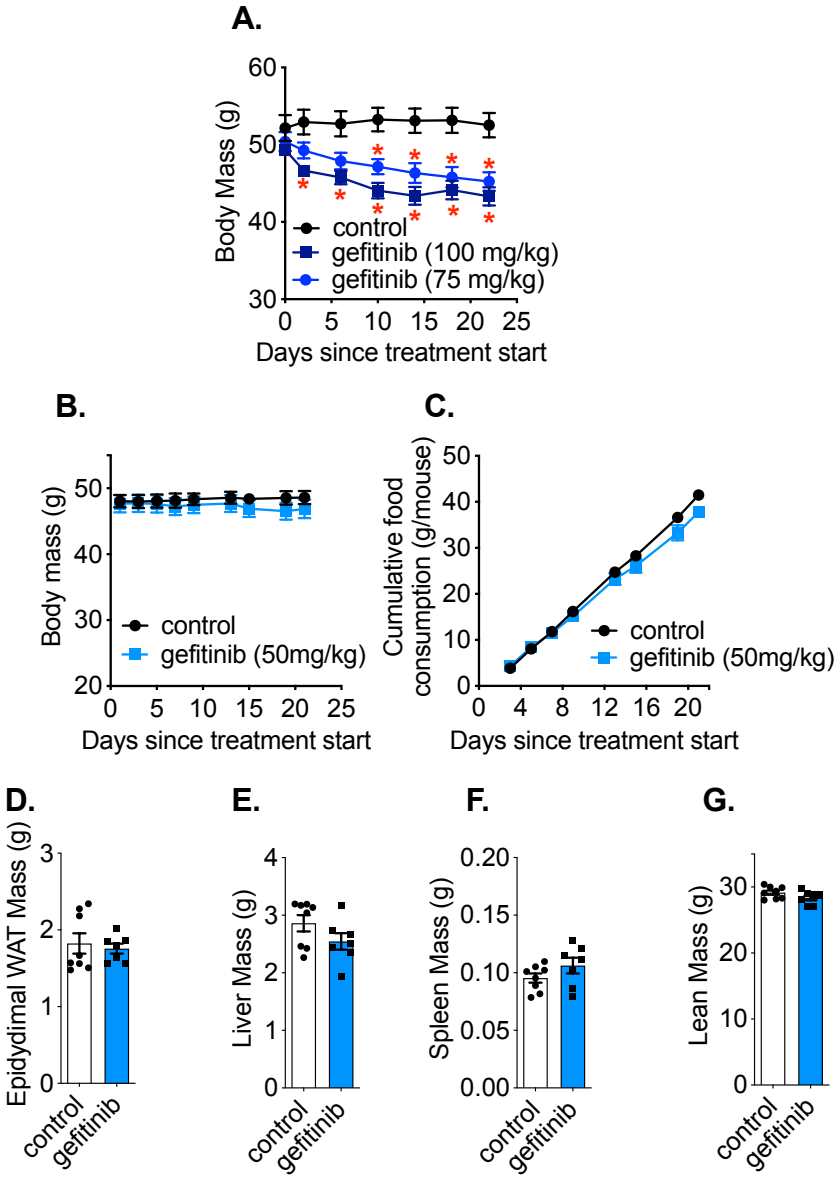

Figure 3.2.2 Intervention with 50 mg/kg gefitinib does not alter body mass, food consumption or tissue morphology across treatment period

A) Body mass in a pilot study of obese mice treated with 100 mg/kg or 75 mg/kg gefitinib (p.o., every other day) for 22 days. B) Body mass, C) Cumulative food consumption during gefitinib treatment (50mg/kg, *p.o.*, every other day for 22 days) in obese *Wt/J* mice, treated according to the Intervention model detailed in Figure 3.2.1. D) Epididymal white adipose tissue mass, E) Liver mass, F) Spleen mass and G) Total body lean mass assessed at the completion of the 22 day treatment period. Values are mean ± SEM (n=7-12/group). * denotes statistical differences between groups ($p<0.05$).

Glucose tolerance was assessed by GTT after 8 gefitinib treatments (50mg/kg, *p.o.*, every other day). Importantly, gefitinib did not alter body mass or adiposity in obese mice fed high fat diet (Figure 3.2.3, A-B). We found that an intervention-style treatment with gefitinib lowers blood glucose during both a GTT and during an ITT independent of changes in fasting blood glucose, and independently of any effects on body weight and adiposity, demonstrated by a significant reduction in the area under the blood glucose curve during both tests (Figure 3.2.3, D-E).

A previous report demonstrated how TKI imatinib improved insulin signalling in liver and adipose tissues in a *db/db* mouse model[281]. Therefore, we also sought to test if gefitinib improved insulin signalling in these tissues in our intervention-model of obesity-induced glucose and insulin intolerance. We next established an experiment to assess insulin signalling based on methodologies in the literature[300–303]. Obese *Wt/J* mice treated with vehicle or gefitinib (50mg/kg *p.o.*) were fasted overnight and injected with 2 IU/kg insulin, *i.p.*, and liver and epididymal adipose tissues were excised at 15m and 16m, respectively, after insulin injection. Protein lysates were prepared for both tissues and insulin signalling was assessed by immunoblotting for phosphorylation of Akt at the Ser^{437} residue. Insulin injection induced a significant increase in insulin signalling in both adipose tissue and liver, as evidenced by a significant increase in $pAKT^{Ser427}$/total AKT in insulin-injected controls compared to saline-injected ('basal') animals (Figure 3.2.4, A-B). However, intervention with gefitinib did not improve insulin signalling in

adipose or liver tissue at the level of this serine-phosphorylation site on AKT at this dose of an insulin bolus (Figure 3.2.4).

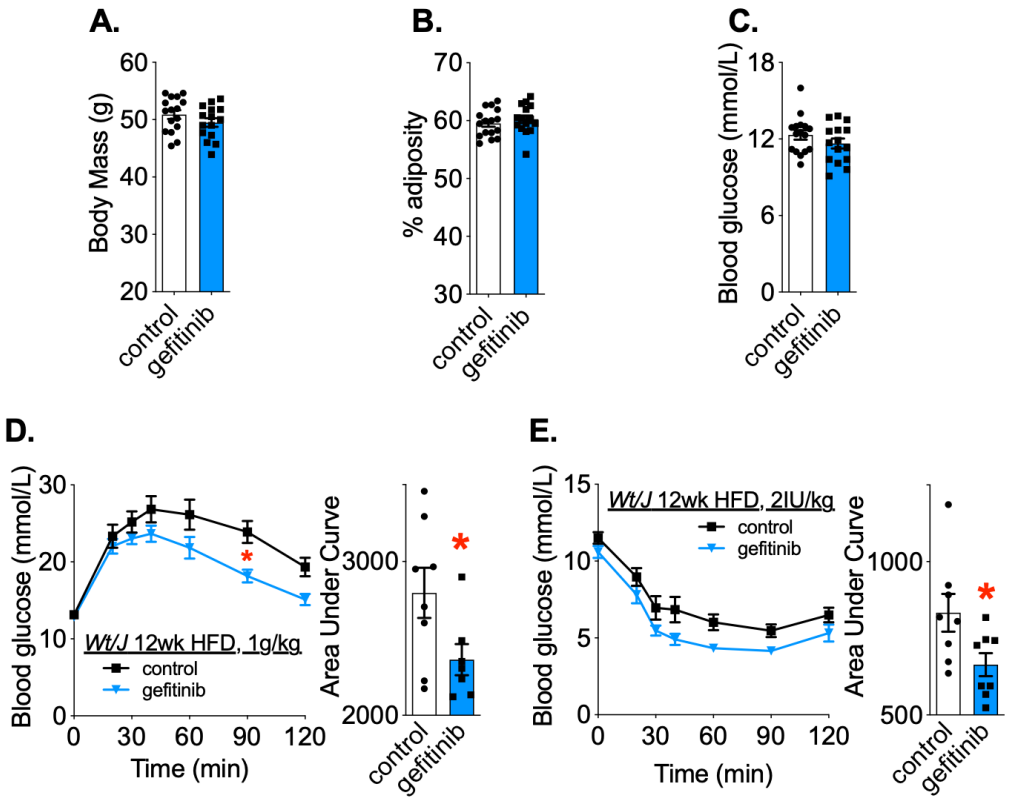

Figure 3.2.3 TKI gefitinib attenuates obesity-induced glucose and insulin intolerance independently of body mass or adiposity

A) Body mass, B) % adiposity and C) 6 h fasting blood glucose after 8x treatments of gefitinib (50mg/kg, *p.o.,* every other day) or vehicle, in obese *Wt/J* mice fed a HFD for 10 weeks before initiating treatment (see Figure 3.2.1). D) Blood glucose vs. time during a glucose tolerance test (1g/kg, *i.p.*) and area under the curve and E) Blood glucose vs. time during an insulin tolerance test (2 IU/kg, *p.o.*) and area under the curve. Values are mean ± SEM (n=8-9/group). * denotes statistical differences between groups ($p<0.05$).

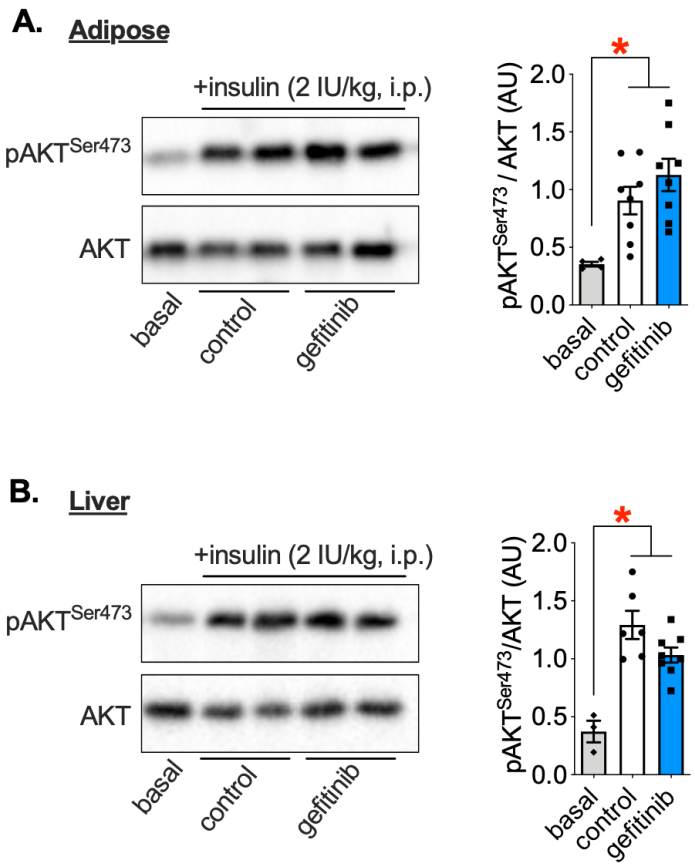

Figure 3.2.4 TKI gefitinib does not alter insulin signalling in adipose or liver tissue during obesity

Representative immunoblot (left) and quantification (right) of phosphorylated Akt (serine 473)/total Akt in A) epididymal adipose tissue and B) liver tissue of obese *Wt/J* mice treated with (50mg/kg, *p.o.,* every other day) or vehicle according to the Intervention model detailed in Figure 3.2.1. Values are mean ± SEM (n=7-8/group). * denotes statistical differences between groups ($p<0.05$).

Given that glucose control during a glucose bolus (i.e. GTT) was improved by gefitinib in diet-induced obese mice, we also tested our a similar gefitinib injection protocol in age-matched, chow diet-fed mice. The goal was to determine if glucose metabolism was altered by gefitinib in lean mice. In contrast to obese mice, our results show that glucose levels during a GTT were not different after

gefitinib treatment in lean mice fed a chow diet (Figure 3.2.5). This is consistent with reports showing the TKI imatinib does not alter glucose control in lean mice, but improves glucose in *db/db* mice[281], suggesting that glucose-lowering capacity of TKIs are limited to mitigating obesity-specific metabolic perturbations. It is noteworthy that gefitinib actually increased fasting blood glucose in chow diet-fed lean mice but did not change body mass or adiposity (Figure 3.2.5).

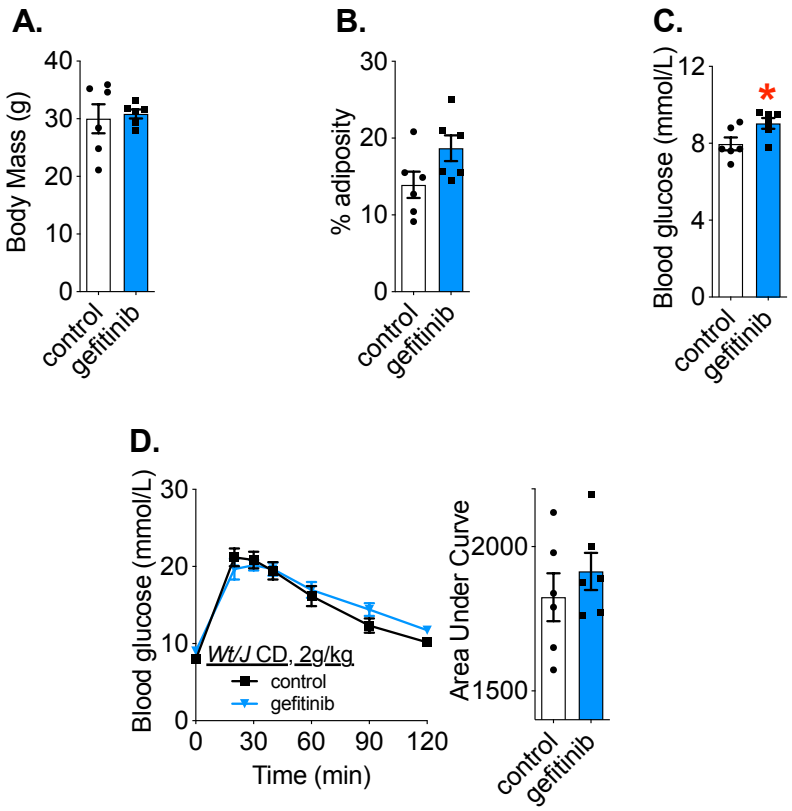

Figure 3.2.5 TKI gefitinib does not alter blood glucose control in lean mice

A) Body mass, B) % adiposity, and C) 6 h fasting blood glucose after 8x treatments of gefitinib (50mg/kg, *p.o.,* every other day) or vehicle, in age-matched *Wt/J* mice fed a chow diet. D) Blood glucose vs. time during a glucose tolerance test (2g/kg, *i.p.)*, and area under the curve. Values are mean ± SEM (n=6/group). * denotes statistical differences between groups ($p<0.05$).

Recent awareness surrounding the genotypic and phenotypic differences in substrains of C57BL/6 mice, used ubiquitously in metabolic biomedical research, has identified the critical importance of properly addressing the background substrain used in 'wild-type' and genetically modified mouse models[294,304,305]. One study found that more than half of published articles involving genetically modified mouse models do not completely address background strain[294]. Indeed, many researchers are not aware of fundamental differences between the substrains, and the shorthand C57BL/6 is often used to describe *Wt* mice. To reconcile any influence of the substrain background on the metabolic effect of TKIs, we evaluated TKI treatment in a HFD intervention model in C57BL6/J (*Wt/J*) and C57BL6/N mice (*Wt/N*) to ensure there were no discrepancies in the metabolic effects of gefitinib treatment, including glucose levels during a GTT. Hence, C57BL6/N mice (*Wt/N*) mice were fed an obesogenic diet (HFD, containing 60% kcal from fat) for 10 weeks and separated into experimental groups based on body weight, fasting blood glucose and area under the glucose curve during a glucose tolerance test before commencing TKI treatment. Glucose tolerance was assessed by GTT after 8 gefitinib treatments (50mg/kg, *p.o.*, every other day). Similar to obese *Wt/J* mice, gefitinib intervention did not alter body weight or adiposity in obese *Wt/N* mice (Figure 3.2.6, A-B), but lowered blood glucose levels during a GTT, independently of any changes in fasting blood glucose (Figure 3.2.6, C-D). We took advantage of an additional cohort of obese *Wt/N* mice treated with gefitinib to assess effects on oral glucose tolerance, as we had not previously assessed glucose tolerance

following oral administration of glucose in *Wt/J* mice, and found that similar to with an intraperitoneal glucose challenge, gefitinib lowered blood glucose levels following an oral glucose challenge (Figure 3.2.6, E).

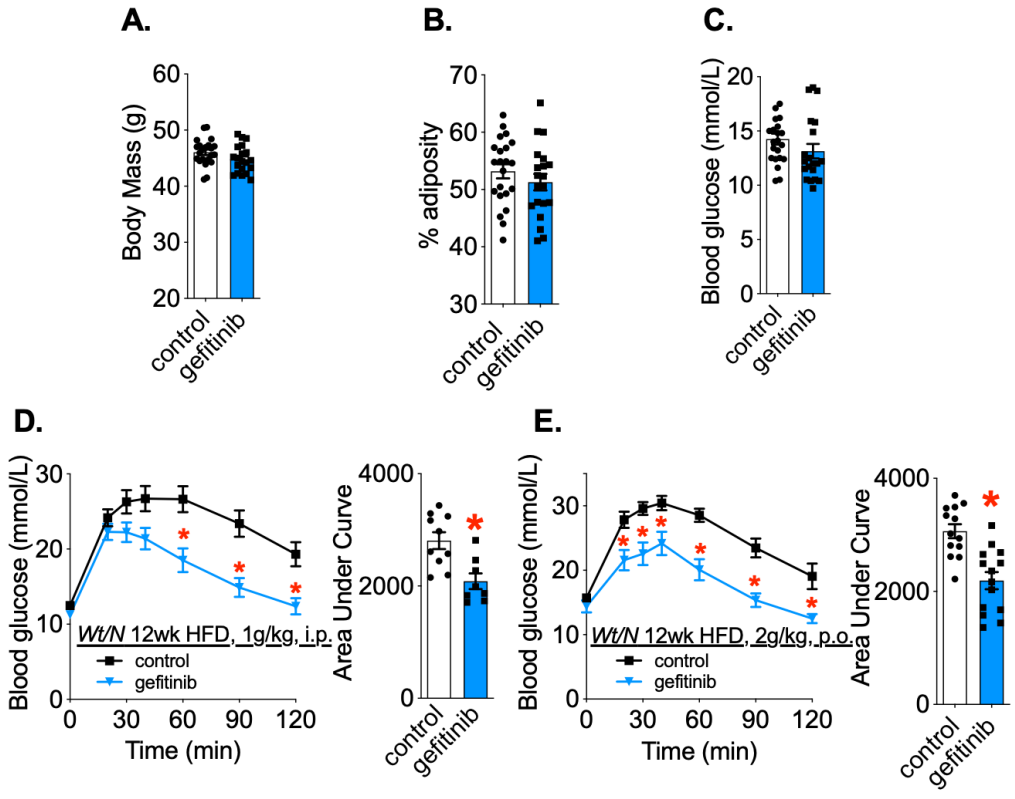

Figure 3.2.6 TKI gefitinib improves obesity-induced glucose intolerance independently of body mass or adiposity in *Wt/N* mice

A) Body mass, B) % adiposity, and C) 6 h fasting blood glucose after 8x treatments of gefitinib (50mg/kg, *p.o.,* every other day) or vehicle, in obese *Wt/N* mice fed a HFD for 10 weeks before initiating treatment. D) Blood glucose vs. time during an intra-peritoneal glucose tolerance test (1g/kg, *i.p.)*, and area under the curve. E) Blood glucose vs. time during an oral glucose tolerance test, (2g/kg, *p.o.*), and area under the curve. Values are mean ± SEM (n=9-14/group). * denotes statistical differences between groups ($p<0.05$).

3.2.2 Kinase inhibitor gefitinib attenuates obesity-induced glucose intolerance independent from NOD1, NOD2 and RIPK2

Next, we set out to determine if the effects of gefitinib were dependent on NOD1, NOD2 or RIPK2. We already knew that RIPK2 was required for the acute NOD1- and NOD2-mediated effects on blood glucose and that TKI gefitinib, but not imatinib influenced blood glucose upon NOD1/2 activation. Here, we employed a series of genetic whole-body knock-out mouse models and applied the same HFD intervention paradigm as used in obese *Wt/J* and *Wt/N* mice (see Figure 3.2.1). In brief, *Nod1*$^{-/-}$, *Nod2*$^{-/-}$ and *Ripk2*$^{-/-}$ mice were fed HFD for 10 weeks and separated into experimental groups based on body weight, fasting blood glucose and area under the glucose curve after a glucose tolerance test before commencing TKI treatment. Glucose tolerance was assessed after 8 gefitinib treatments (50mg/kg, *p.o.*, every other day). Consistent with results in obese *Wt* mice, gefitinib treatment did not alter body mass or adiposity in *Nod1*$^{-/-}$ (Figure 3.2.7, A-B), *Nod2*$^{-/-}$ (Figure 3.2.8, A-B), and *Ripk2*$^{-/-}$ mice (Figure 3.2.9, A-B). A consistent reduction in blood glucose concentrations at specific time-points, and area under the glucose curve during the GTT was observed in all gefitinib-treated mice, regardless of genotype (Figures 3.2.7-9, D). These results show that gefitinib improves glucose control during a GTT in the absence of NOD1, NOD2 and RIPK2 and suggest that this TKI alters blood glucose independent of NOD1-RIPK2 or NOD2-RIPK2 signalling axes. Our results replicate the blood-glucose lowering effects of TKIs observed in clinical studies and various animal models of T1D and T2D, but contrary to our initial

hypothesis, these studies provide strong evidence that inhibition of the NOD-RIPK2 pathway is not required for specific TKIs to alter blood glucose regulation during obesity, even though a given TKI is known to inhibit RIPK2. Taken together, this data suggests that TKIs engage targets beyond RIPK2 to alter blood glucose. This concept requires further investigation if re-tasking of certain TKIs from cancer to diabetes is considered.

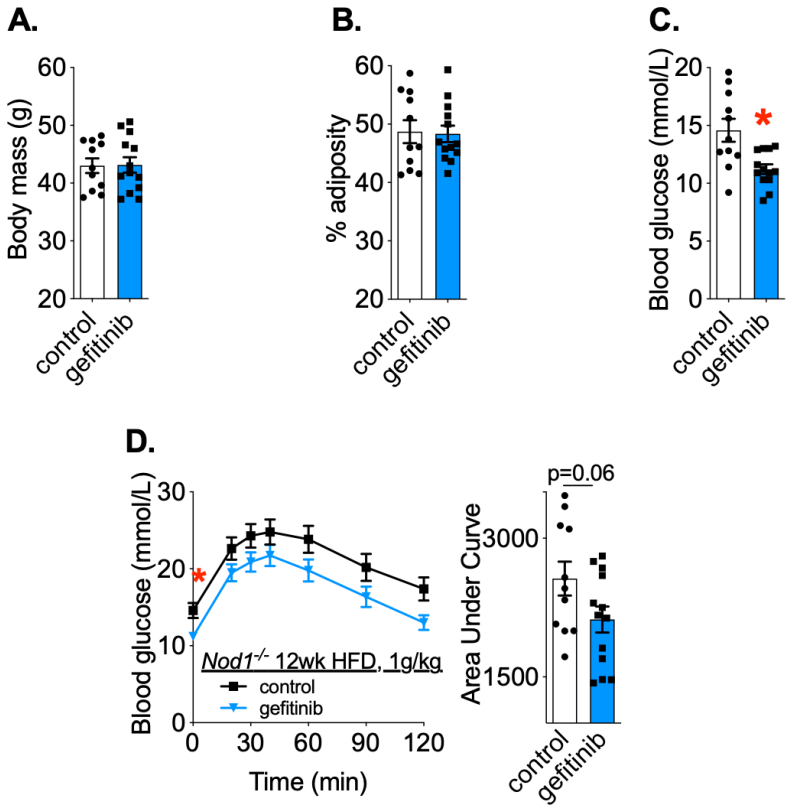

Figure 3.2.7 TKI gefitinib improves obesity-induced glucose intolerance independently of NOD1

A) Body mass, B) % adiposity, and C) 6 h fasting blood glucose after 8x treatments of gefitinib (50mg/kg, *p.o.,* every other day) or vehicle, in obese *Nod1*$^{-/-}$ mice fed a HFD for 10 weeks before initiating treatment. D) Blood glucose vs. time during a glucose tolerance test (1g/kg, *i.p.)*, and area under the curve. Values are mean ± SEM (n=11-13/group). * denotes statistical differences between groups ($p<0.05$).

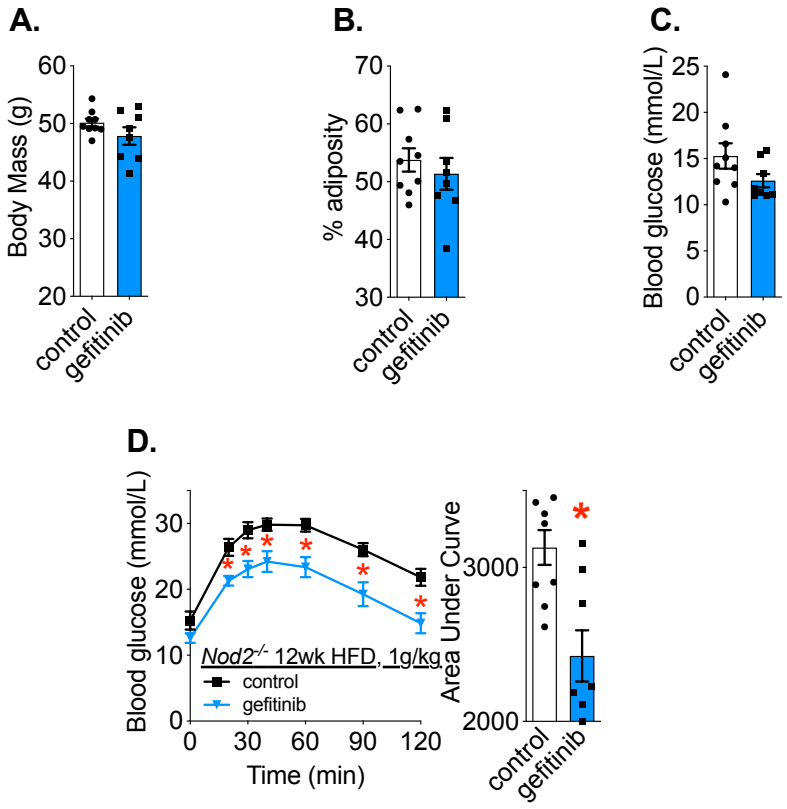

Figure 3.2.8 TKI gefitinib improves obesity-induced glucose intolerance independently of NOD2

A) Body mass, B) % adiposity, and C) 6 h fasting blood glucose after 8x treatments of gefitinib (50mg/kg, *p.o.,* every other day) or vehicle, in obese *Nod2*$^{-/-}$ mice mice fed a HFD for 10 weeks before initiating treatment. D) Blood glucose vs. time during a glucose tolerance test (1g/kg, *i.p.)*, and area under the curve. Values are mean ± SEM (n=8-9/group). * denotes statistical differences between groups ($p<0.05$).

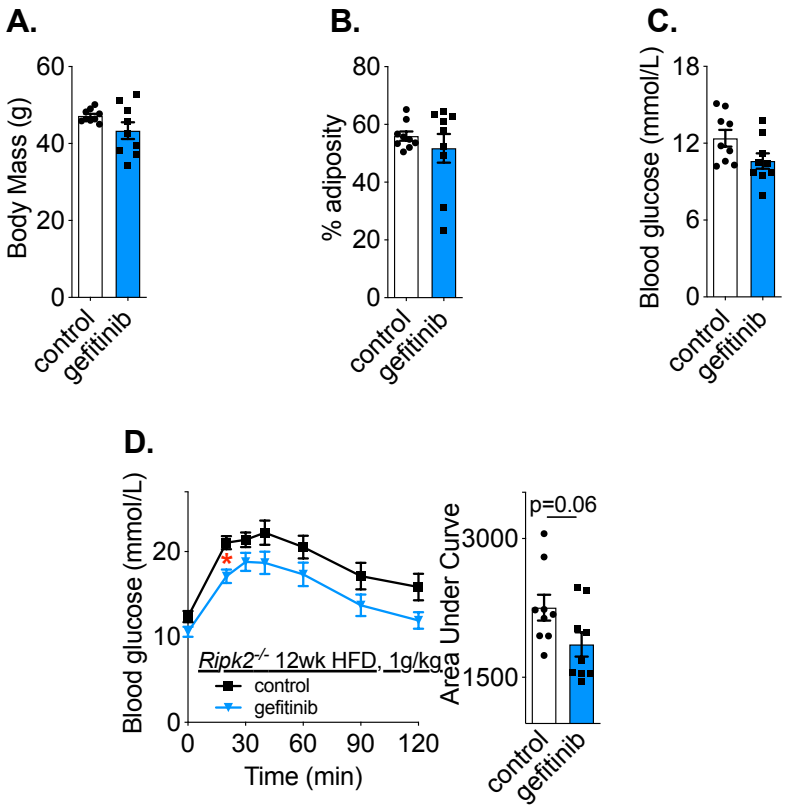

Figure 3.2.9 TKI gefitinib improves obesity-induced glucose intolerance independently of RIPK2

A) Body mass, B) % adiposity, and C) 6 h fasting blood glucose after 8x treatments of gefitinib (50mg/kg, *p.o.,* every other day) or vehicle, in obese *Ripk2*$^{-/-}$ mice mice fed a HFD for 10 weeks before initiating treatment. D) Blood glucose vs. time during a glucose tolerance test (1g/kg, *i.p.)*, and area under the curve. Values are mean ± SEM (n=9/group). * denotes statistical differences between groups ($p<0.05$).

3.2.3 RIPK2-selective kinase inhibitors lower insulin, but only in *Ripk2*$^{-/-}$ mice

We next tested glucose stimulated insulin secretion in *Wt*, *Nod1*$^{-/-}$, *Nod2*$^{-/-}$ and *Ripk2*$^{-/-}$ mice treated with gefitinib. After the GTT, all mice received 3 more treatments of gefitinib (50mg/kg, *p.o.*, every other day for 11x total treatments) before OGSIS was assessed (Figure 3.2.1). Mice were fasted 12 hours overnight, and fasted blood samples were collected before, and 10 and 60 minutes after, administration of an oral glucose challenge (4g/kg, *p.o.*). Plasma insulin was quantified using a high sensitivity mouse insulin ELISA kit, and Homeostatic Model Assessment of Insulin Resistance (HOMA-IR) was calculated using fasting blood glucose and fasting insulin levels. Additionally, we chose to calculate Insulin Resistance Index (IRI), an established metric of insulin resistance in obese animal models[224], by using the calculated area under the glucose curve from the GTT and area under the insulin curve from the OGSIS. Importantly, this metric captures the dynamic relationship between circulating glucose *and* insulin during a glucose challenge, in contrast to the HOMA-IR metric, which only considers the relationship between glucose and insulin in the fasting state.

No differences in fasting insulin levels, glucose-stimulated insulin secretion at 10m and 60m, IRI or HOMA-IR were observed in chow-fed *Wt/J,* obese *Wt/J*, or obese *Wt/N* mice treated with gefitinib compared to controls (Figure 3.2.10, A-I).

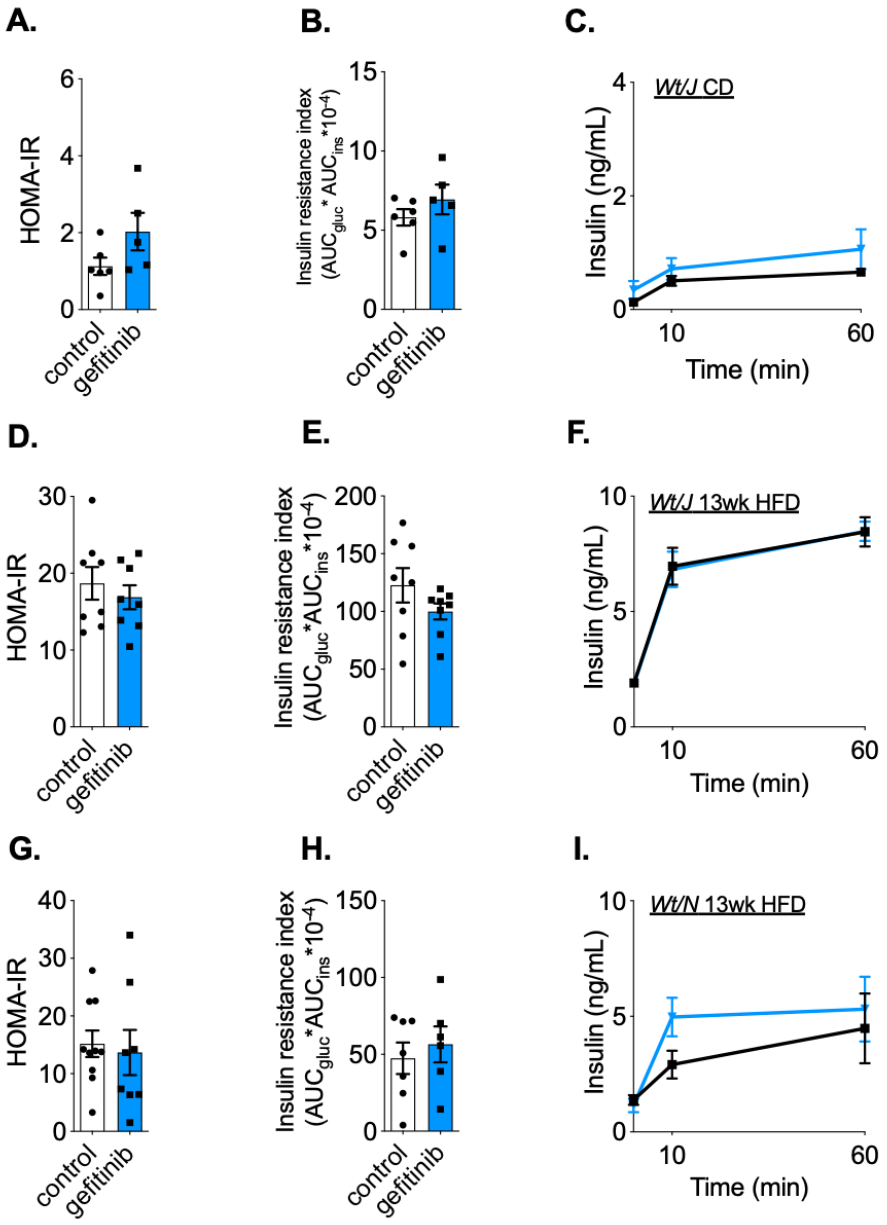

Figure 3.2.10 TKI gefitinib does not alter insulin secretion or insulin resistance in *Wt/J* or *Wt/N* mice

Calculated homeostatic model assessment of insulin resistance (HOMA-IR), insulin resistance index (IRI), and glucose-stimulated insulin secretion (4g/kg, *p.o.*) in A-C) chow diet-fed *Wt/J* mice, D-F) obese *Wt/J* mice, and G-I) obese *Wt/N* mice fed a HFD for 10 weeks before initiating gefitinib treatment according to the model detailed in Figure 3.2.1. Values are mean ± SEM (n=5-10/group).

Next, we assessed OGSIS in obese *Nod1*$^{-/-}$, *Nod2*$^{-/-}$ and *Ripk2*$^{-/-}$ mice, treated 11x with gefitinib. We found no change in fasting insulin levels, glucose-stimulated insulin secretion at 10m and 60m, IRI or HOMA-IR in obese *Nod1*$^{-/}$ or *Nod2*$^{-/-}$ mice (Figure 3.2.11, A-F). However, gefitinib-treated *Ripk2*$^{-/-}$ mice had significantly lower glucose-stimulated insulin secretion at 10m and 60m post-glucose challenge. Gefitinib treatment caused a significant improvement in Insulin Resistance Metric only in *Ripk2*$^{-/-}$ mice. Importantly, this metric highlights that *Ripk2*$^{-/-}$ mice treated with gefitinib exhibited lower blood glucose levels during a GTT (Figure 3.2.9, D), but also require significantly less insulin to achieve this lower blood glucose control (Figure 3.2.11, H-I). The reduced insulin resistance index observed only in *Ripk2*$^{-/-}$ mice suggest that deletion of RIPK2 equates to more pervasive benefits of gefitinib when compared to *Wt* mice or deletion of either NOD1 or NOD2. This supports the notion that RIPK2 is a kinase target that limits the insulin-sensitizing potential of certain TKIs in the treatment of metabolic disease and represents an important consideration when selecting TKIs to re-task for effective treatment of metabolic disease.

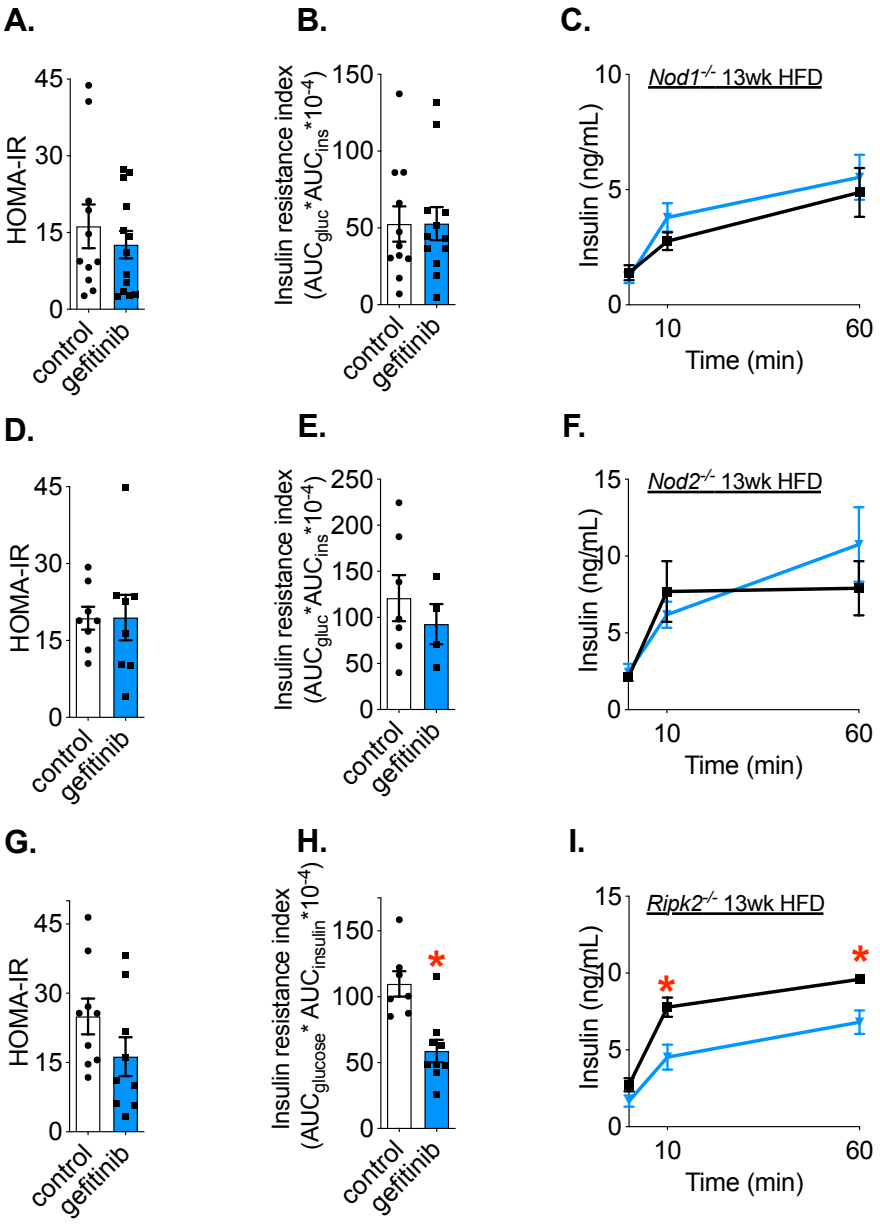

Figure 3.2.11 TKI gefitinib attenuates insulin secretion and insulin resistance in *Ripk2*$^{-/-}$, but not *Nod1*$^{-/-}$ or *Nod2*$^{-/-}$ mice

Calculated homeostatic model assessment of insulin resistance (HOMA-IR), insulin resistance index (IRI), and glucose-stimulated insulin secretion (4g/kg, *p.o.*) in A-C) obese *Nod1*$^{-/-}$, D-F) obese *Nod2*$^{-/-}$, and G-I) obese *Ripk2*$^{-/-}$ mice fed a HFD for 10 weeks before initiating gefitinib treatment according to the model detailed in Figure 3.2.1. Values are mean ± SEM (n=7-13/group). * denotes statistical differences between groups ($p<0.05$).

At the time of this investigation, we based our next analysis on two reports in the literature (one which has since been retracted), which demonstrated decreased inflammation in liver, adipose and muscle, and decreased ER stress in liver and adipose, in obese mice treated with TKIs[281,283]. We measured gene expression of a panel of inflammatory-related genes and ER stress-related genes in liver, adipose, hindlimb skeletal muscle and pancreas (Figure 3.2.12, 3.2.13, 3.2.14, 3.2.15, respectively). To address the divergence in insulin responses in *Wt* mice versus *Ripk2*$^{-/-}$ mice, we assessed gene expression in *Wt* and *Ripk2*$^{-/-}$ mice in the pancreas and several insulin responsive tissues. We hypothesized that gefitinib treatment would alter certain markers of inflammation or ER stress, in *Ripk2*$^{-/-}$ mice, which would parallel the metabolic differences in insulin secretion or insulin sensitivity.

There was no clear pattern of a RIPK2 dependent effect of gefitinib on inflammatory or ER stress markers in the pancreas or in these insulin responsive tissues. Decreased expression of *cxcl1* in liver and pancreas and *il1b* in pancreas was observed in *Wt* and *Ripk2*$^{-/-}$ mice treated with gefitinib, and decreased expression of *Tnf* in liver and *Cxcl1* in muscle was observed in *Wt* mice treated with gefitinib. Overall, only minor differences in pro-inflammatory cytokine expression were observed in gefitinib-treated mice and no robust pattern of changes between *Wt* vs. *Ripk2*$^{-/-}$ was observed (Figure 3.2.13-15, A, E). Minor changes in expression of some anti-inflammatory markers (*irak3, tgfb1, arg1)* were observed in adipose, muscle and pancreas of *Wt* or *Ripk2*$^{-/-}$ mice, but overall, no consistent or robust increases in anti-inflammatory markers were observed in either *Wt* vs. *Ripk2*$^{-/-}$ mice

(Figure 3.2.12-15, B, F). Similarly, no significant changes in gene expression of immune cell markers were observed in any tissue (Figure 3.2.12-15, C, G). Finally, a decrease in the spliced form of *xbp1 (sxbp1)* was observed in liver of *Ripk2*$^{-/-}$ mice (Figure 3.2.13, H). Importantly, no differences in ER-related gene expression was observed in the pancreas of *Wt* vs. *Ripk2*$^{-/-}$ mice (Figure 3.2.15, D, H) that could have accounted for the observed decrease in glucose-stimulated insulin secretion in *Ripk2*$^{-/-}$ mice. In conclusion, changes in a very limited number of inflammatory-related or ER stress-related genes in metabolic tissues are not likely to account for the robust improvements in glucose control observed with gefitinib treatment in diet-induced obese mice. Further, we found no correlation between markers of inflammation or ER stress in the pancreas and the robust effect of gefitinib to lower glucose stimulated insulin secretion in *Ripk2*$^{-/-}$ mice.

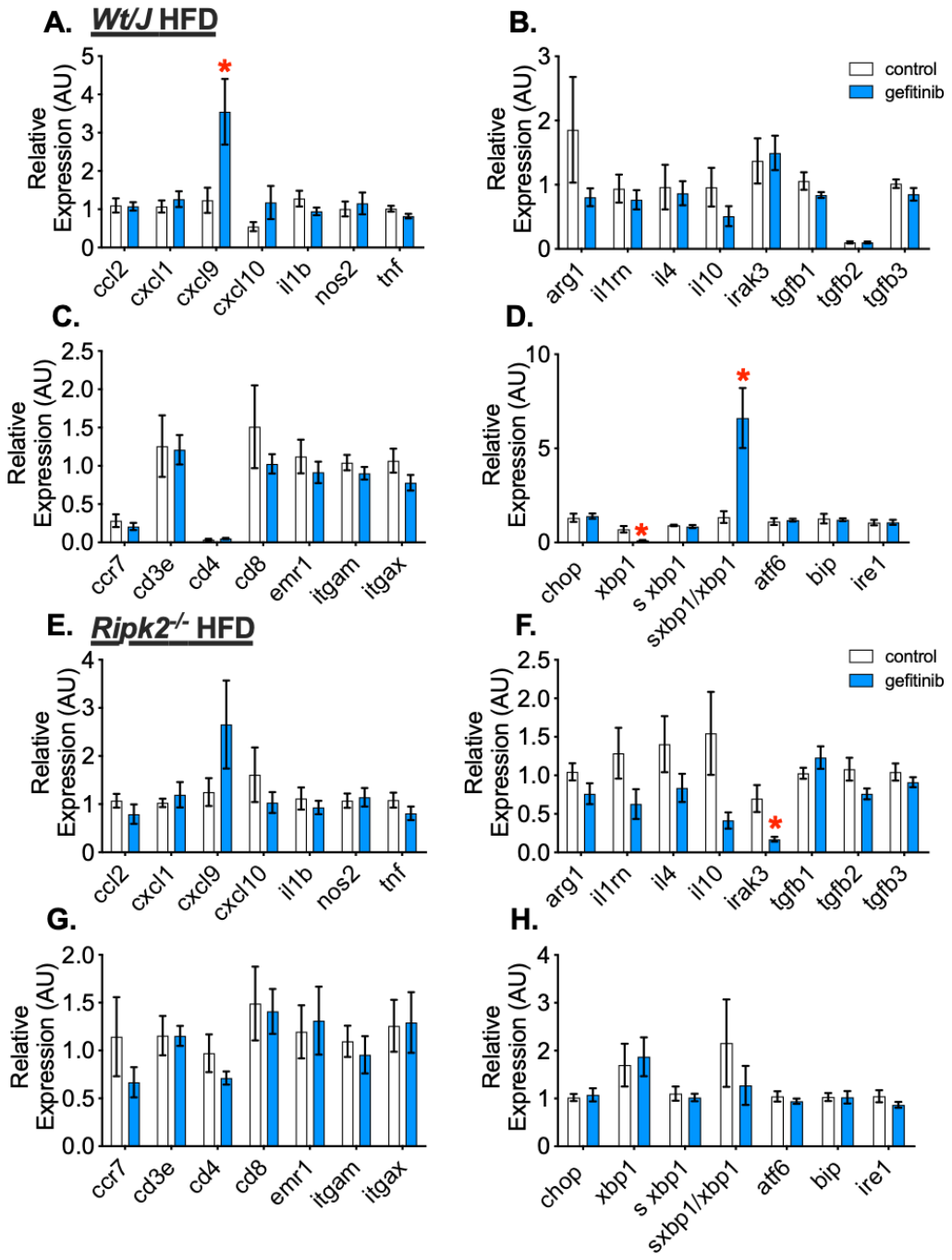

Figure 3.2.12 TKI gefitinib does not alter inflammatory or ER-stress related gene profiles in adipose, and is not dictated by RIPK2

Transcript analysis of pro-inflammatory cytokines (A, E), anti-inflammatory cytokines (B, F), immune cell markers (C, G) and ER-stress related genes in epididymal white adipose tissue of obese *Wt/J* (A-D) and obese *Ripk2*$^{-/-}$ mice (E-H). Values are mean ± SEM. * denotes statistical differences between groups ($p<0.05$).

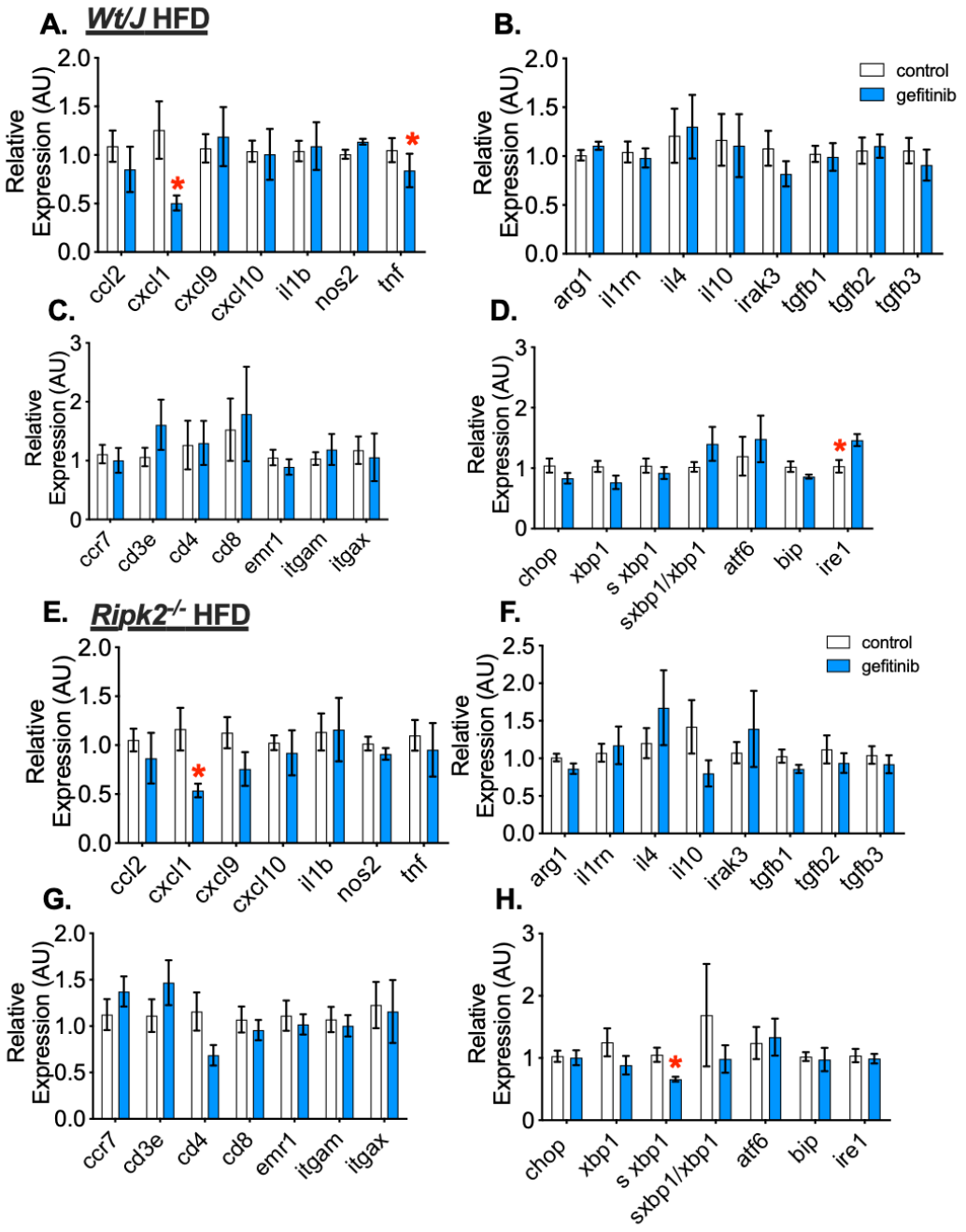

Figure 3.2.13 TKI gefitinib does not alter inflammatory or ER-stress related gene profiles in liver, and is not dictated by RIPK2

Transcript analysis of pro-inflammatory cytokines (A, E), anti-inflammatory cytokines (B, F), immune cell markers (C, G) and ER-stress related genes in liver tissue of obese *Wt/J* (A-D) and obese *Ripk2*$^{-/-}$ mice (E-H). Values are mean ± SEM. * denotes statistical differences between groups ($p<0.05$).

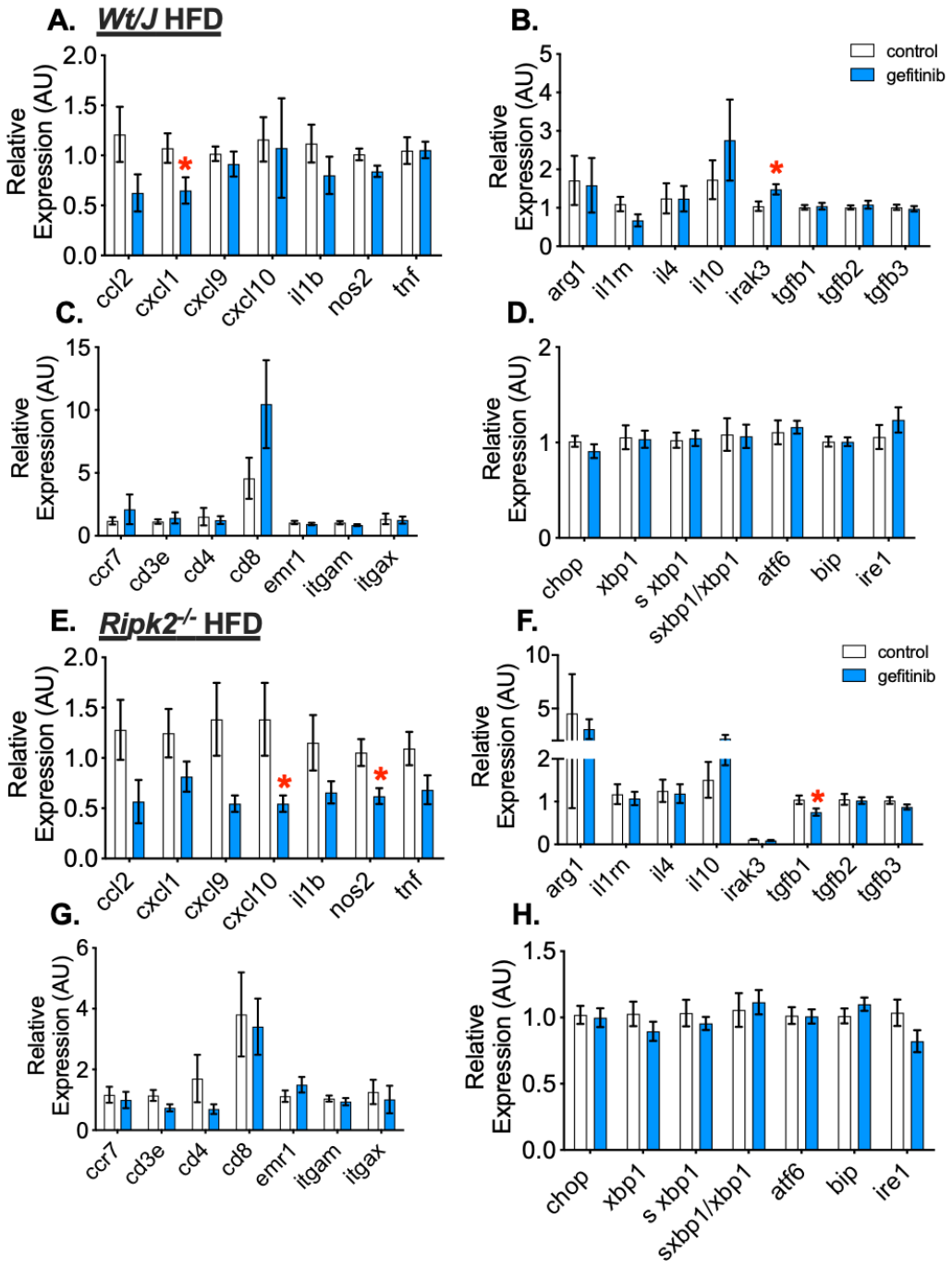

Figure 3.2.14 TKI gefitinib does not alter inflammatory or ER-stress related gene profiles in muscle, and is not dictated by RIPK2

Transcript analysis of pro-inflammatory cytokines (A, E), anti-inflammatory cytokines (B, F), immune cell markers (C, G) and ER-stress related genes in tibialis anterior muscle tissue of obese *Wt/J* (A-D) and obese *Ripk2*$^{-/-}$ mice (E-H). Values are mean ± SEM. * denotes statistical differences between groups ($p<0.05$).

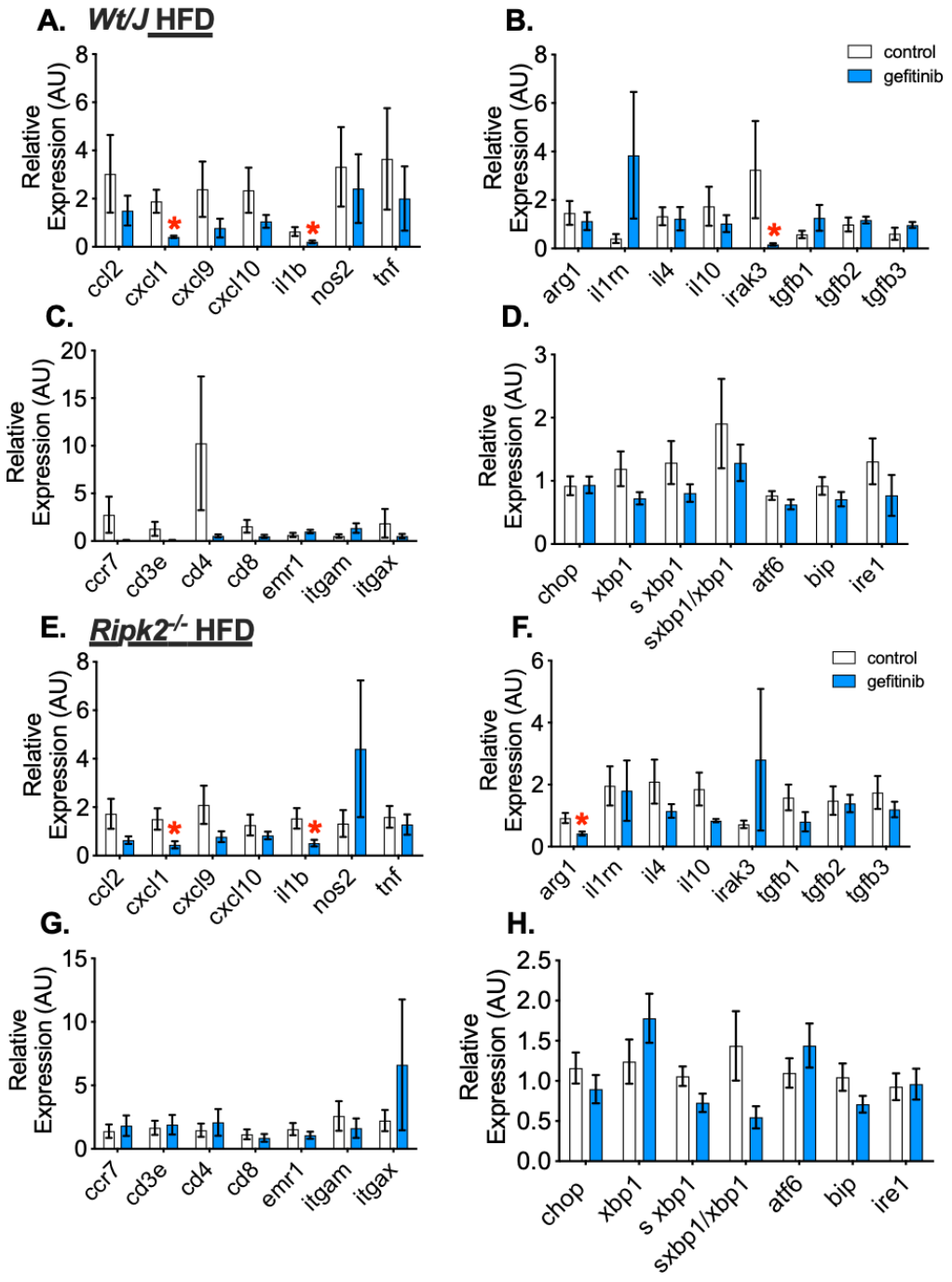

Figure 3.2.15 TKI gefitinib does not alter inflammatory or ER-stress related gene profiles in pancreas, and is not dictated by RIPK2

Transcript analysis of pro-inflammatory cytokines (A, E), anti-inflammatory cytokines (B, F), immune cell markers (C, G) and ER-stress related genes in pancreas tissue of obese *Wt/J* (A-D) and obese *Ripk2*$^{-/-}$ mice (E-H). Values are mean ± SEM. * denotes statistical differences between groups ($p<0.05$).

3.2.4 Kinase inhibitor imatinib attenuates obesity-induced glucose intolerance but induces hyperinsulinemia

Based on our data demonstrating that presence of RIPK2 actually inhibits the ability of gefitinib to improve glucose control for a given amount of insulin secretion, we next sought to test another TKI that does not inhibit RIPK2, such as imatinib. The TKI Imatinib has no reported inhibitory effects against RIPK2 and we confirmed that imatinib does not inhibit acute metabolic effects of NOD1 signalling[190] or NOD2 signalling (Figure 3.1.18). Accordingly, we initially hypothesized that imatinib treatment would lower both blood glucose and insulin levels in obese mice, mimicking our findings in *Ripk2*$^{-/-}$ mice treated with gefitinib. We employed an identical HFD intervention model to treat obese *Wt/J* mice with imatinib (Figure 3.2.16). A small pilot study determined this dose did not induce weight loss or changes in food consumption compared to controls (data not shown). However, we found that, contrary to gefitinib, intervention with an equimolar dose of imatinib did not lower blood levels during a GTT after 8 treatments (Figure 3.2.17, E). We next tested oral glucose-stimulated insulin secretion and did not find any reductions in insulin secretion with this dose of imatinib (Figure 3.12.17, F). Similar to *Wt/J* mice treated with gefitinib, there were no effects on body weight, adiposity, fasting blood glucose, HOMA-IR or IRI in *Wt/J* mice treated with this equimolar dose of imatinib.

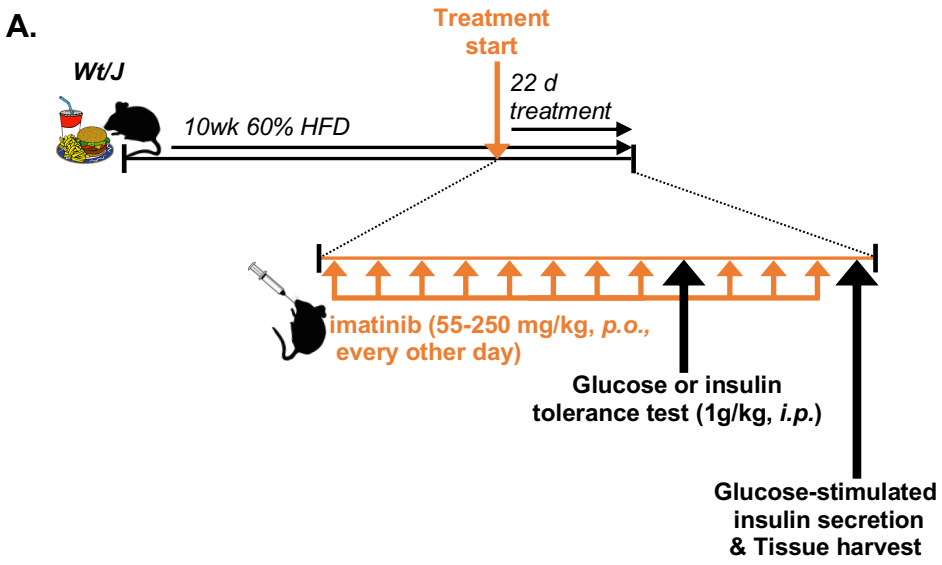

Figure 3.2.16 Experimental design for investigating metabolic effects of TKI imatinib during obesity

A) Experimental model for investigating the effects of TKI imatinib on glucose and insulin homeostasis, and tissue inflammation. *Wt/J* mice were placed on a 60% HFD for 10 week before intervention with imatinib treatment (55-250mg/kg, *p.o.*, every other day). Mice received 8 treatments over 16 days before glucose or insulin tolerance was assessed. Then mice received 3 more treatments before glucose-stimulated insulin secretion was assessed and selected tissues were harvested immediately following cervical dislocation.

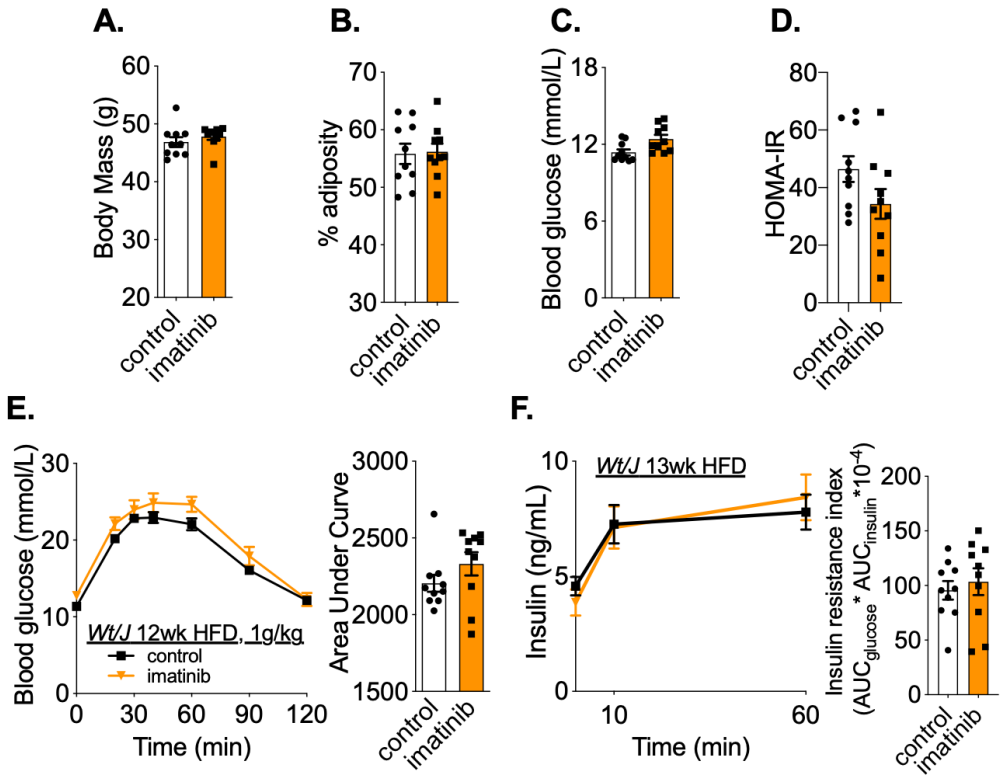

Figure 3.2.17 Equimolar treatment with TKI imatinib does not attenuate obesity-induced glucose intolerance or insulin resistance

A) Body mass, B) % adiposity, and C) 6 h fasting blood glucose after 8x treatments of imatinib (55mg/kg, *p.o.,* every other day) or vehicle, in obese *Wt/J* mice mice fed a HFD for 10 weeks before initiating treatment. D) HOMA-IR after 11x treatments of imatinib. E) Blood glucose vs. time during a glucose tolerance test (1g/kg, *i.p.)*, and area under the curve, and F) glucose stimulated insulin secretion (4g/kg, *p.o.*) after 8x and 11x treatments, respectively, as per experimental model detailed in Figure 3.2.12. Values are mean ± SEM (n=10/group). * denotes statistical differences between groups ($p<0.05$).

Because we had previously chosen our dose of gefitinib to administer in our HFD intervention model based on the maximal dose that could be given without altering food consumption or body weight with repeated administration, we next chose to establish the maximal dose of imatinib that could be administered to mice without altering food consumption or body weight. A pilot study found that

250mg/kg, but not 300mg/kg, of imatinib could be administered without altering food consumption or body weight in mice (data not shown), and thus, the dose of 250mg/kg was chosen for a subsequent HFD intervention study. In contrast to the lower dose of 55mg/kg, we found that diet-induced obese mice treated with imatinib (250mg/kg, *p.o.*, every other day) exhibited significantly lower blood glucose during a GTT, independent of changes in body weight, adiposity, or fasting blood glucose (Figure 3.2.18, A-D). However, contrary to our initial hypothesis, we found that imatinib significantly increased fasting blood insulin levels and insulin secretion at 60m after an oral glucose challenge, compared to vehicle treated obese mice (Figure 3.2.18, E). The increase in fasting blood insulin resulted in a significantly increased HOMA-IR in treated mice, suggesting imatinib increases insulin resistance in the fasted state, despite lowering blood glucose during a glucose challenge. Thus, the improvements in blood glucose regulation during a GTT after imatinib treatment can be, at least partially attributed to, increased insulin secretion. This data supports a model where various TKIs achieve their effects on blood glucose regulation via different mechanisms. Based on the numerous kinases inhibited by each TKI, it is plausible that each specific TKI influence metabolism through different mechanisms to exert segregated effects on insulin secretion from the pancreas versus improved insulin sensitivity at the level of the tissues to manifest their apparent effects on blood glucose regulation.

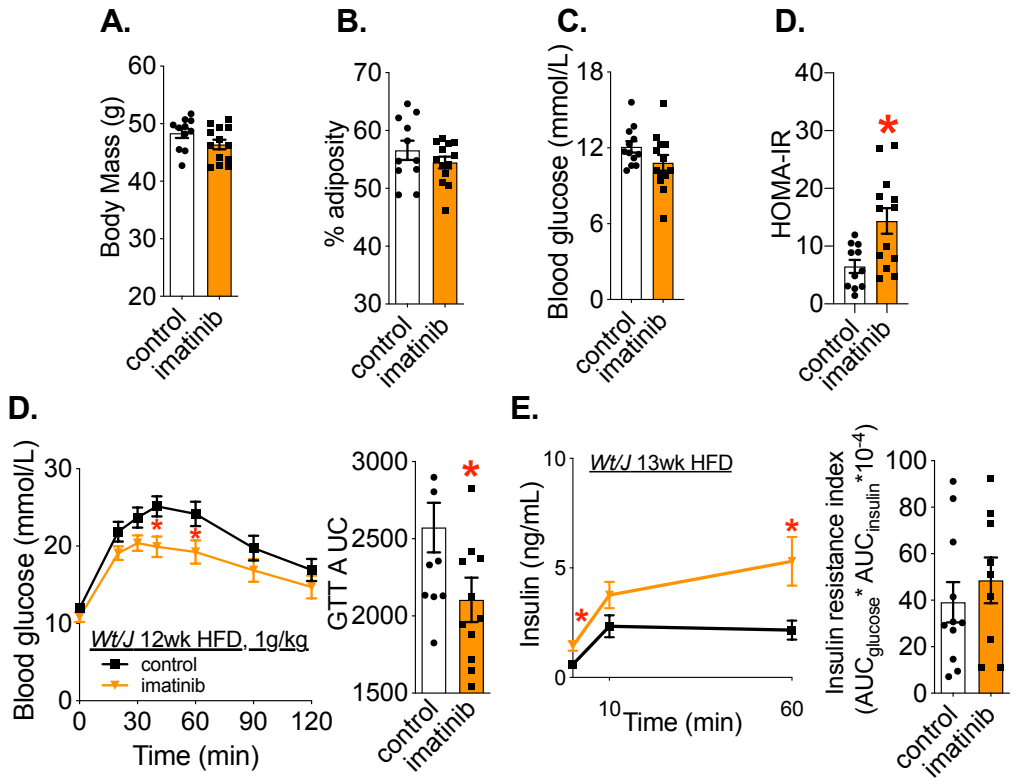

Figure 3.2.18 High-dose imatinib improves glucose tolerance but induces hyperinsulinemia during obesity

A) Body mass, B) % adiposity, and C) 6 h fasting blood glucose after 8x treatments of imatinib (250mg/kg, *p.o.,* every other day) or vehicle, in obese *Wt/J* mice mice fed a HFD for 10 weeks before initiating treatment. D) HOMA-IR after 11x treatments of imatinib. E) Blood glucose vs. time during a glucose tolerance test (1g/kg, *i.p.)*, and area under the curve, and F) glucose stimulated insulin secretion (4g/kg, *p.o.*) after 8x and 11x treatments, respectively, as per experimental model detailed in Figure 3.2.12. Values are mean ± SEM (n=11-13/group). * denotes statistical differences between groups ($p<0.05$).

To further investigate the disparity in insulin secretion observed in imatinib-treated mice vs. gefitinib-treated mice, we chose to analyze the same panel of inflammatory and ER-stress related genes in the pancreas tissue of imatinib-treated mice. We found that while imatinib significantly reduced transcript levels of *cxcl10*

and significantly increased transcript levels of *il4*, no robust pattern of changes in gene expression of inflammation or ER stress-related markers were observed at the transcript level (Figure 3.2.19).

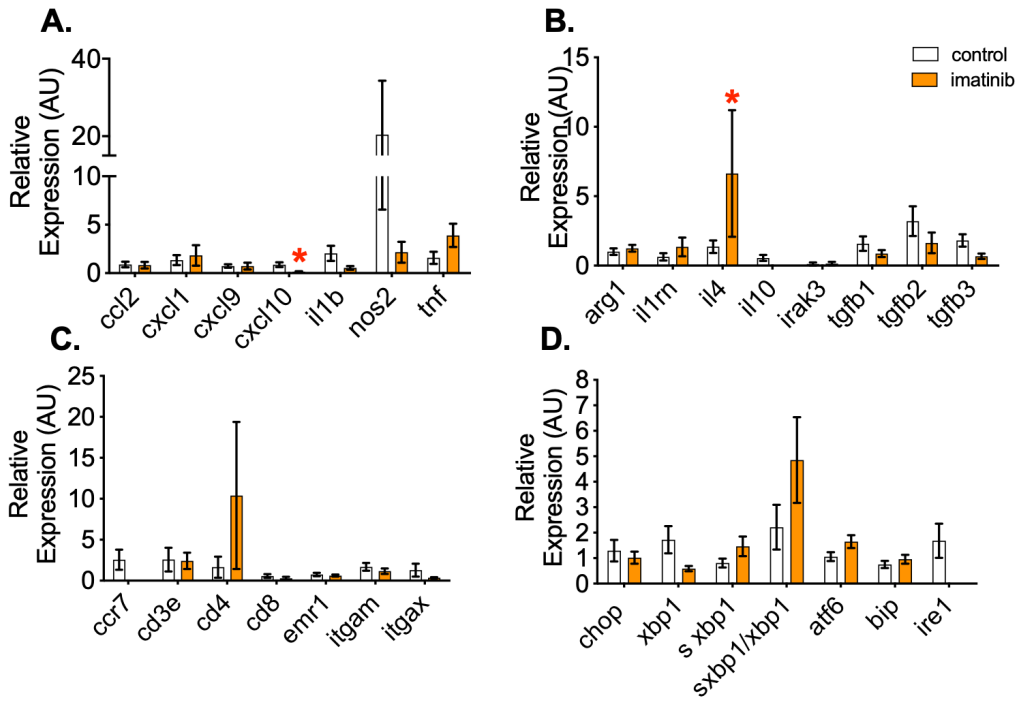

Figure 3.2.19 TKI imatinib does not alter inflammatory or ER-stress related gene profiles in pancreas
Transcript analysis of A) pro-inflammatory cytokines, B) anti-inflammatory cytokines, C) immune cell markers and D) ER-stress related genes in pancreas of obese *Wt/J* mice treated with imatinib. Values are mean ± SEM. * denotes statistical differences between groups ($p<0.05$).

We next quantified the serum concentrations of each TKI during our HFD intervention mouse model in order to address the disparity between the doses of gefitinib and imatinib, 50mg/kg vs. 250mg/kg, respectively, which were required to lower blood glucose levels during a GTT in obese mice. The pharmacokinetic and pharmacodynamic properties of TKI gefitinib and imatinib have been well

studied in lean mice, but to the best of our knowledge, no published report in the literature exists of blood concentrations following TKI gefitinib and imatinib administration to obese mice. Furthermore, understanding how TKIs may potentially accumulate with repeated administration, as in our HFD intervention model is important to understand when comparing two different drugs that required different doses to achieve lowered blood glucose. First, we sought to quantify serum TKI concentration after a single TKI administration in lean, chow-fed mice to compare to other published results in the literature. Mice were given a single administration of gefitinib (100mg/kg, *p.o.*) or imatinib (110mg/kg, *p.o.*), the doses that were used in Section 3.1 (Figures 3.1.13, 3.1.15, 3.1.17, 3.1.18), and are commonly used in many published mouse xenograft models[306–309].

Gefitinib serum concentration was 3.857 ± 0.263 μg/mL and 1.463 ± 0.349 μg/mL 2 and 6 hours after administration, respectively, and imatinib serum concentration was 11.683 ± 1.086 μg/mL and 1.432 ± 0.353 μg/mL 2 and 6 hours after administration, respectively. These results are consistent with results published by other groups that used comparable TKI doses in lean mice[308–310]. Next, we quantified serum concentrations 2h after gefitinib and imatinib administration in obese mice after the first, fourth and eighth treatment, with 8 treatments (gefitinib, 50mg/kg; imatinib, 250mg/kg) corresponding to the number of treatments before glucose tolerance was assessed in our HFD intervention model (Figure 3.2.1, 3.2.16). Gefitinib serum concentration was 4.157 ± 0.546 μg/mL, 4.114 ± 0.108 μg/mL and 4.257 ± 0.165 μg/mL after the first, fourth and eighth administration,

respectively, demonstrating how gefitinib administration reached steady-state concentrations after the first administration, and did not accumulate across the treatment duration (Figure 3.2.21, B). The serum concentration of gefitinib in obese mice 2h after the first administration (4.157 ± 0.546 μg/mL) was comparable to the serum concentration of gefitinib achieved 2h after a single dose of gefitinib in lean mice (3.857 ± 0.263 μg/mL). In contrast, serum concentration of imatinib was 1.432 ± 0.353 μg/mL, 5.700 ± 1.404 μg/mL and 6.167 ± 1.308 μg/mL after the first, fourth and eighth administration, respectively, demonstrating how imatinib administration accumulates across the treatment window (Figure 3.2.21, C). The serum concentration of imatinib in obese mice 2h after the first administration (1.432 ± 0.353 μg/mL) was significantly lower than the serum concentration achieved 2h after a single dose of imatinib in lean mice (11.683 ± 1.086 μg/mL), suggesting that HFD-feeding affects the metabolism of imatinib. By the eighth administration of TKI in obese mice, at which time we demonstrated both gefitinib and imatinib treatment lowered blood glucose during a GTT, a comparable serum concentration of each TKI had been achieved (4.257 ± 0.165 μg/mL for gefitinib vs. 6.167 ± 1.308 μg/mL), thus partially explaining the five-fold higher dose of imatinib required to achieve changes in host glucose metabolism.

A.

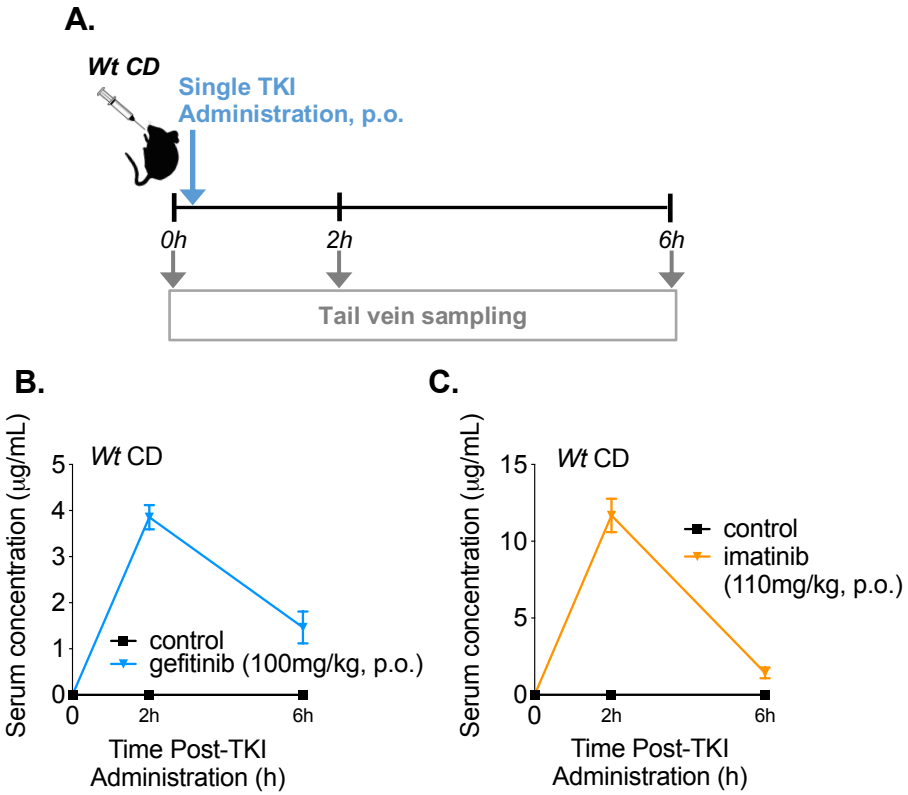

Figure 3.2.20 Quantification of TKI gefitinib and imatinib serum concentration levels after a single administration in lean *Wt* mice

A) Quantification of TKI levels in mouse serum using liquid chromatography coupled to tandem mass spectrometry in chow-fed *Wt* mice before, 2h and 6h after a single administration of B) gefitinib (100mg/kg, p.o.) or C) imatinib (110mg/kg, p.o.). Values are mean ± SEM (n=1/control group and n=6-7 in TKI treatment groups).

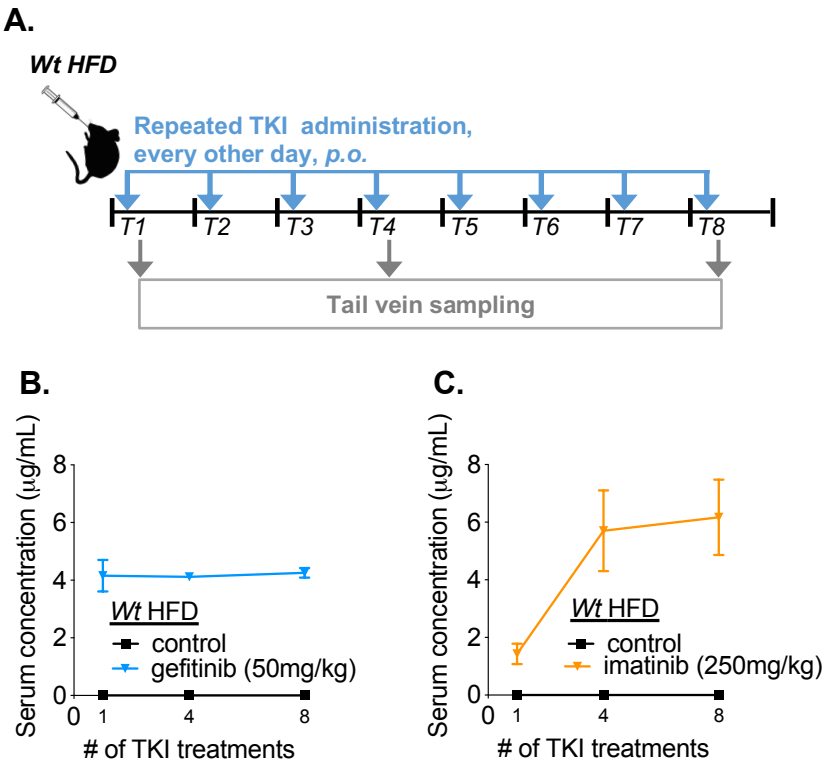

Figure 3.2.21 Quantification of TKI gefitinib and imatinib serum concentration levels after repeated administration in obese *Wt* mice

A) Quantification of TKI levels in mouse serum using liquid chromatography coupled to tandem mass spectrometry in HFD-fed *Wt* mice after 1, 4 and 8 treatments of B) gefitinib (50mg/kg, p.o., every other day) or C) imatinib (250mg/kg, p.o., every other day). Values are mean ± SEM (n=1/control group and n=6-7 in TKI treatment groups).

3.3 Upper intestinal commensal microbe components alter glucose homeostasis via NOD-RIPK2

Previous work from our lab has already identified a potent microbial-derived insulin sensitizing postbiotic (i.e. the bacterial cell wall component MDP) that lowered blood glucose after injection and required intact NOD2 signalling to improve obesity-induced inflammation and metabolic dysfunction in mice[193]. Our work has also demonstrated that MDP's effects on glucose homeostasis are also dependent on RIPK2 (Figure 3.3.1, data collected in collaboration with Dr. J.F. Cavallari)[311]. Work from other labs has also identified novel postbiotics that can influence obesity and glucose tolerance[224,312]. Furthermore, work published by our collaborators demonstrated that injection of mice with the luminal contents collected from ileal segments elicited an adaptive immune response that results in protection against diet-induced glucose intolerance and insulin resistance[228]. However, the identity of the factor that promoted improved glucose control in the extracts from luminal gut contents remained unknown. Further, the host receptors required for ileal lumen contents to alter immunity and blood glucose were not defined. Taken together, these data are consistent with a model where gut luminal contents, including postbiotics derived from microbiota, contain *insulin sensitizing components*. Based on these results, we sought to further test the luminal contents from each intestinal segment influenced blood glucose and insulin. Importantly, given our lab's data demonstrating that microbial-derived MDP promotes lower blood glucose and insulin sensitivity via NOD2-RIPK2 signalling,

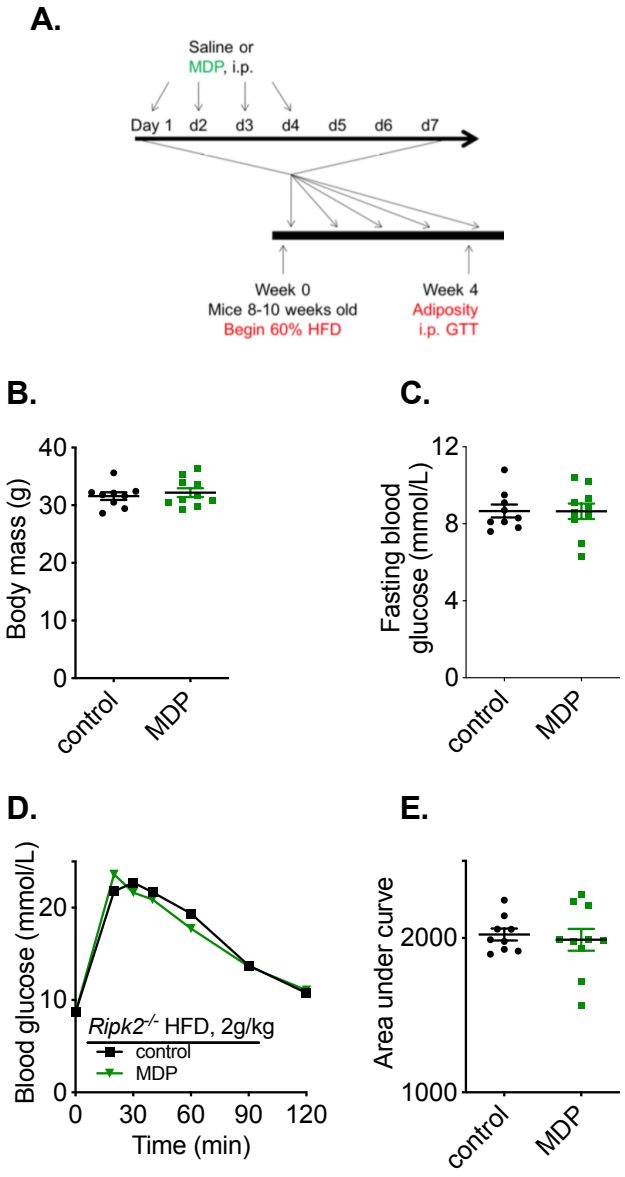

Figure 3.3.1. Ripk2 is required for MDP-mediated glycemic effects during diet-induced obesity

A) Experimental design of *Ripk2*$^{-/-}$ mice fed a 60% HFD for 4 weeks and treated with saline or MDP (100µg, i.p.) 4 days/week for the duration of HFD-feeding prior to a glucose tolerance test, adapted from Cavallari, et al. B) Body mass, C) Fasting blood glucose, D) Blood glucose vs. time, and E) Quantified area under the curve during a glucose tolerance test (2g/kg, n=9-10/group). Values are mean ± SEM. *denotes statistical differences between groups ($p<0.05$).

we sought to determine if changes in blood glucose after injection of gut luminal contents is dependent on presence of gut microbes, and if these effects are mediated by a NOD1-RIPK2 or NOD2-RIPK2 signalling axis.

3.3.1 Injection of mice with diluted ileal luminal contents improves blood glucose control in a dose-dependent manner

Recent publication from Pomie, et al[228] demonstrated that a 'vaccination' using luminal gut contents can improve blood glucose control in mice fed a diabetogenic HFD. This previous work was achieved by subcutaneous injection of diluted ileal contents. In brief, luminal contents from 10 cm segments of ileum were collected from donor mice and used for subcutaneous injection into a cohort of recipient mice. 35 days after injection, mice were switched to a diabetogenic HFD containing 72% fat and <1% carbohydrate, a diet that favours rapid development of hyperglycemia without significant body weight gain[313–315]. Glucose tolerance tests were done after 1 and 2 months of HFD feeding (Figure 3.3.2).

We first sought to replicate these experiments from our collaborators with a few modifications. We chose a distinct injection and diet-induced obesity model and probed these effects in lean and obese mice. We adapted the protocol of Pomie, et al[228] by using a different HFD to study the impact of obesity, and also extended the duration of HFD with intermittent assessment of glucose tolerance to determine the persistence of the ileal injection phenotype over time. While Pomie, et al.[228] used a HFD intended for studying the impact of a fat-enriched diet independent of

obesity, we used an obesogenic HFD comprised of 60% fat and 20% carbohydrate which induces rapid and sustained weight gain in addition to development of insulin resistance and moderate hyperglycemia. In our model, intestinal "donor mice" were fed a normal chow or obesogenic HFD for 4 weeks before luminal contents of ileal segments were collected, as described[228]. Age-matched mice were injected once with diluted ileal contents, as described[228]. 35 days later, a post-injection glucose tolerance test was done during chow diet feeding, then recipient mice were switched to an obesogenic HFD. In our adapted model, we performed a glucose tolerance test after 4 weeks and 8 weeks of HFD feeding (approximately corresponding to 1 and 2-month timepoints). Based on data collected at this point, we chose to inject the recipient mice a second time with an identical injection protocol and dose of intestinal extract, and another glucose tolerance test was done 12 weeks later (Figure 3.3.3).

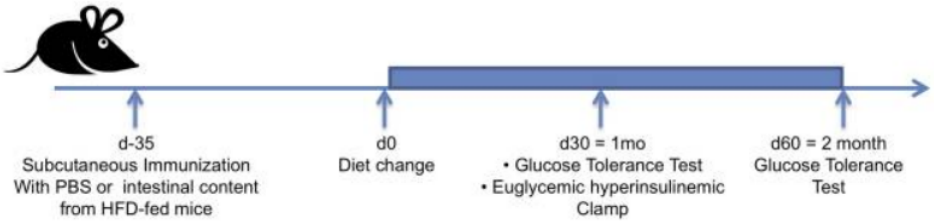

Figure 3.3.2. Published model of intestinal injection in HFD-fed mice

Wt mice were immunized with diluted, sonicated ileal extracts 35 days before beginning a HFD containing 72% fat (corn oil, lard), 28% protein, <1% carbohydrate. Glucose tolerance tests were performed after 1 and 2 months of HFD feeding. Adapted from Pomie et al. 2016

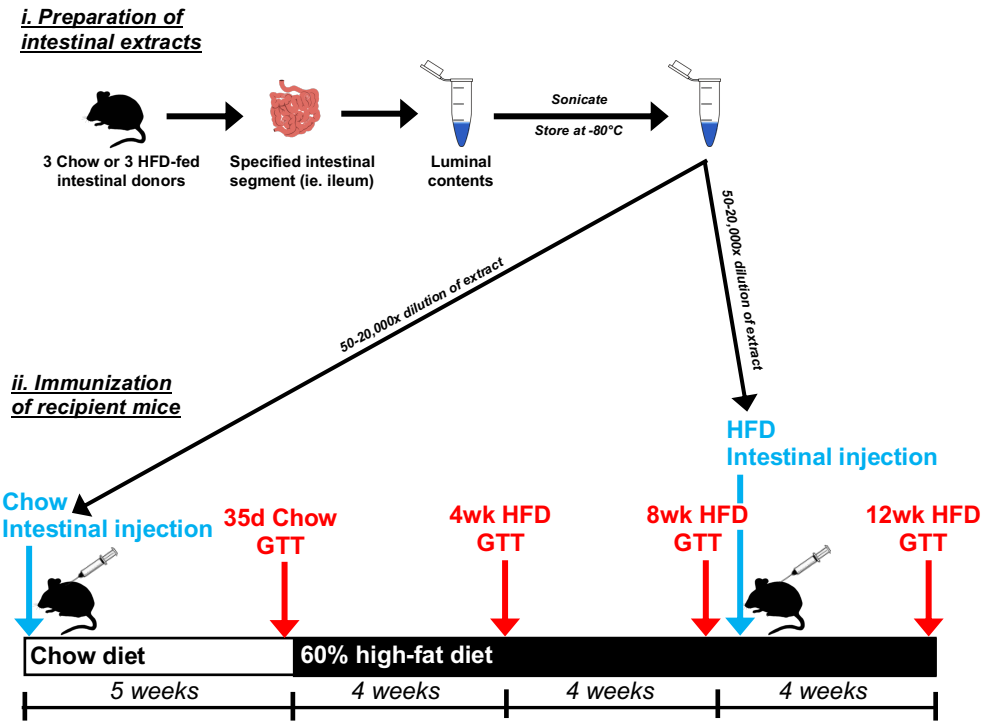

Figure 3.3.3. Experimental design for preparation of intestinal extracts and injection protocol in recipient mice

i. Preparation of intestinal extracts. Intestinal segments (15cm duodenum/jejenum; 10cm ileum; cecum; entire length of colon) or fecal samples were collected from 3 *Wt* Chow-fed or 3 *Wt* 60% HFD-fed mice. Luminal contents of specified intestinal segments from all 3 intestinal donor mice were collected in 500µL PBS and vortexed thoroughly. Fecal samples from all 3 intestinal donor mice were also collected in 500µL PBS and homogenized using ceramic beads. Debris was removed by centrifugation from all segments/fecal samples. Supernatants were sonicated and stored at -80ºC until the time of immunization.
ii. Intestinal injection of recipient mice. Chow-fed recipient mice were injected with specified dilution of intestinal extract or vehicle, 200µL s.c., and 35 days later, glucose metabolism was assessed by GTT (2g/kg, i.p.). Following the 35d Chow GTT, recipient mice began a 60% HFD for a total of 12 weeks. Glucose metabolism was assessed by GTT at 4 weeks and 8 weeks. Following the 8wk HFD GTT, mice were injected a second time and four weeks later, a 12wk HFD GTT was performed.

We first tested a range of dilutions of ileal luminal contents (i.e. extracts) collected from chow diet-fed mice. We found that injection of luminal contents caused a dose-dependent change in blood glucose during a GTT (Figure 3.3.4). Diluting ileal extracts by 5000x lowered blood glucose during a GTT, compared to less dilute (50x, 500x) and more dilute (20,000x) preparations of extract, demonstrating that a critical concentration of luminal contents was required for glycemic effects. Reductions in blood glucose following a glucose load in mice injected with 5000x diluted ileal extracts occurred independent of any changes in body weight or fasting blood glucose (Figure 3.3.4). A specific concentration of intestinal extract required for lowering blood glucose following ileal injection is consistent with published results[228]. This dilution (1/5000) was used for all subsequent experiments.

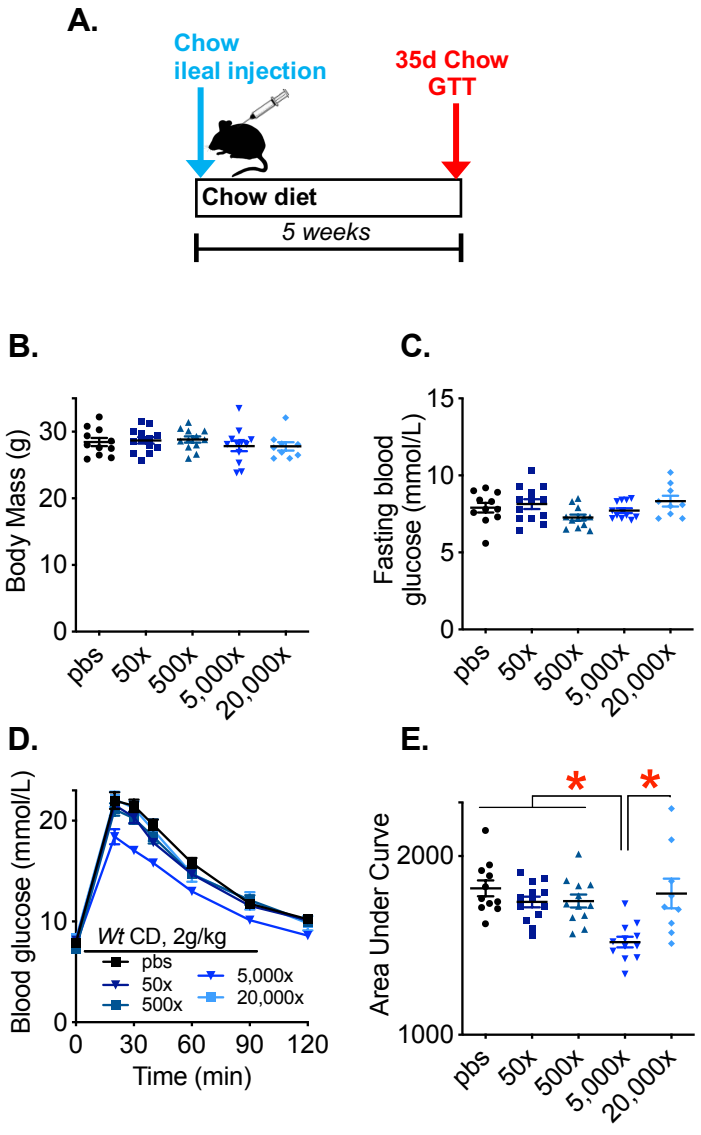

Figure 3.3.4. Specific concentration of intestinal extracts is a critical factor for promoting blood glucose control following intestinal injection

A) Experimental model of *Wt* recipient mice fed a chow diet injected with ileal extracts (200µL, s.c., diluted 50-20,000x) collected from chow-fed donor mice. Glucose metabolism was assessed by GTT 35 days after immunization. B) Body mass, C) Fasting blood glucose, D) Blood glucose vs. time, and E) Quantified area under the curve during GTT (2g/kg, n=9-13/group). Values are mean ± SEM. *denotes statistical differences between groups ($p<0.05$).

3.3.2 Injection of ileal extracts improves glucose control in lean and obese mice, independent of the diet fed to donor or recipient mice

Next, we sought to test the effects of ileal extracts derived from HFD-fed mice. Ileal extracts were prepared from mice fed a HFD for 4 weeks ('HFD ileum') or age-matched chow diet-fed mice ('chow ileum') and ileal luminal contents were injected into in chow diet-fed mice (Figure 3.3.5, A). Our results demonstrate that 35 days after injection with ileal extracts from either HFD-fed or chow diet-fed mice resulted in lower glucose levels during a GTT in mice compared to PBS-injected controls (Figure 3.3.5, D-E). Additionally, the ileal extracts from HFD-fed mice produced a lowered fasting glycemia in chow diet-fed recipient mice, while the extracts derived from chow diet-fed mice did not have this effect on fasting blood glucose (Figure 3.3.5, C). Importantly, no differences in body weight were induced by the ileal injection protocol (Figure 3.3.5, B).

We also repeated this experiment in a cohort of chow-fed female recipient mice to determine if the glucose-tolerizing properties of ileal extracts were sex dependent. Similar to male mice, injection of mice with ileal extracts lowered glucose during a GTT in female recipient mice, compared to PBS-injected controls, regardless of whether the ileal extract was derived from HFD-fed or chow-fed donor mice. No differences in body weight or fasting blood glucose were observed between groups (Figure 3.3.6).

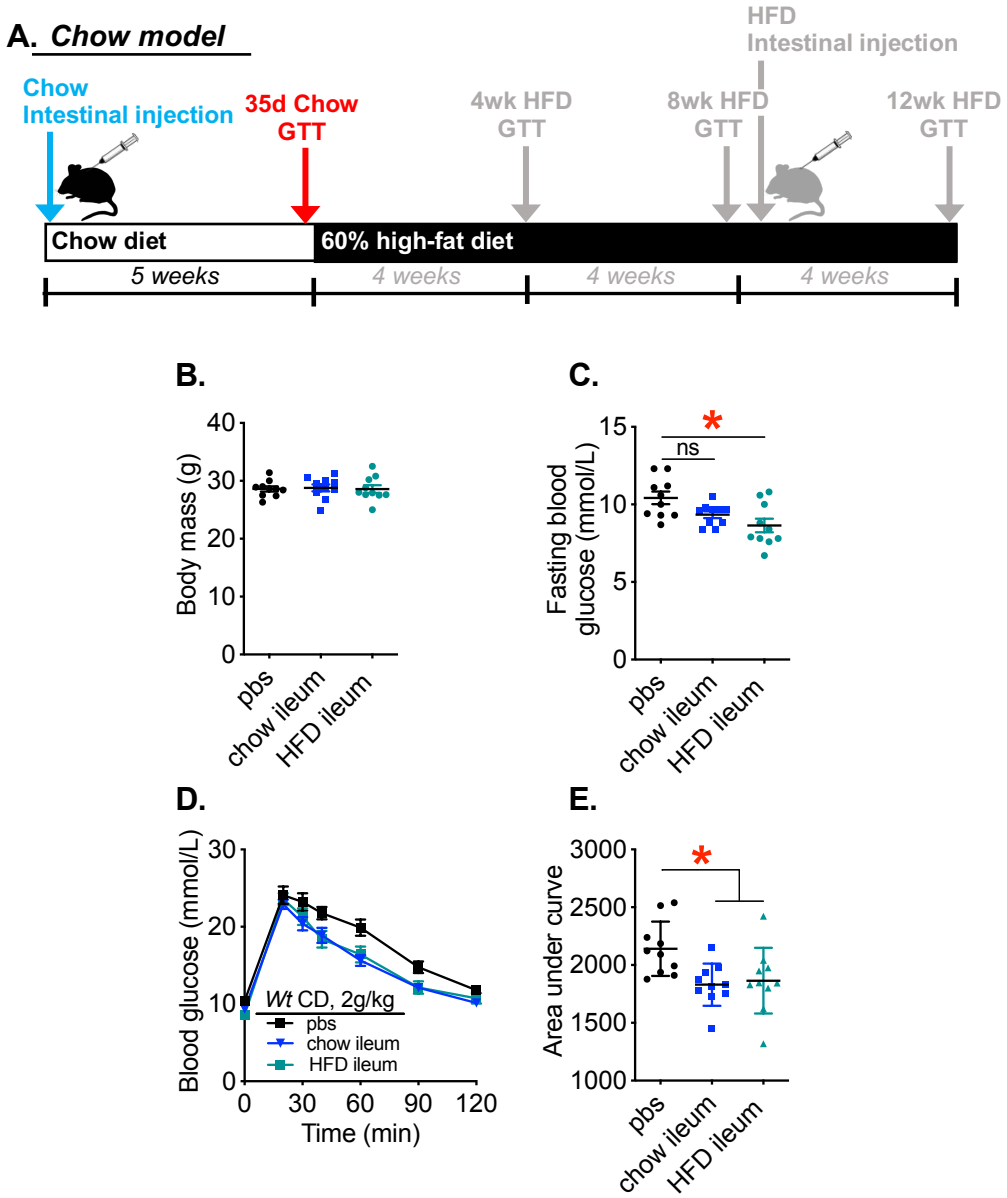

Figure 3.3.5. Injection with ileal extracts promotes blood glucose control in chow-fed mice regardless of intestinal donor diet

A) Experimental model of *Wt* recipient mice fed a chow diet injected with ileal extracts (200µL, s.c., diluted 5000x) collected from chow- or HFD-fed donor mice. Glucose metabolism was assessed by GTT 35 days after immunization. B) Body mass, C) Fasting blood glucose, D) Blood glucose vs. time, and E) Quantified area under the curve during a GTT (2g/kg, n=10/group). Values are mean ± SEM. *denotes statistical differences between groups ($p<0.05$).

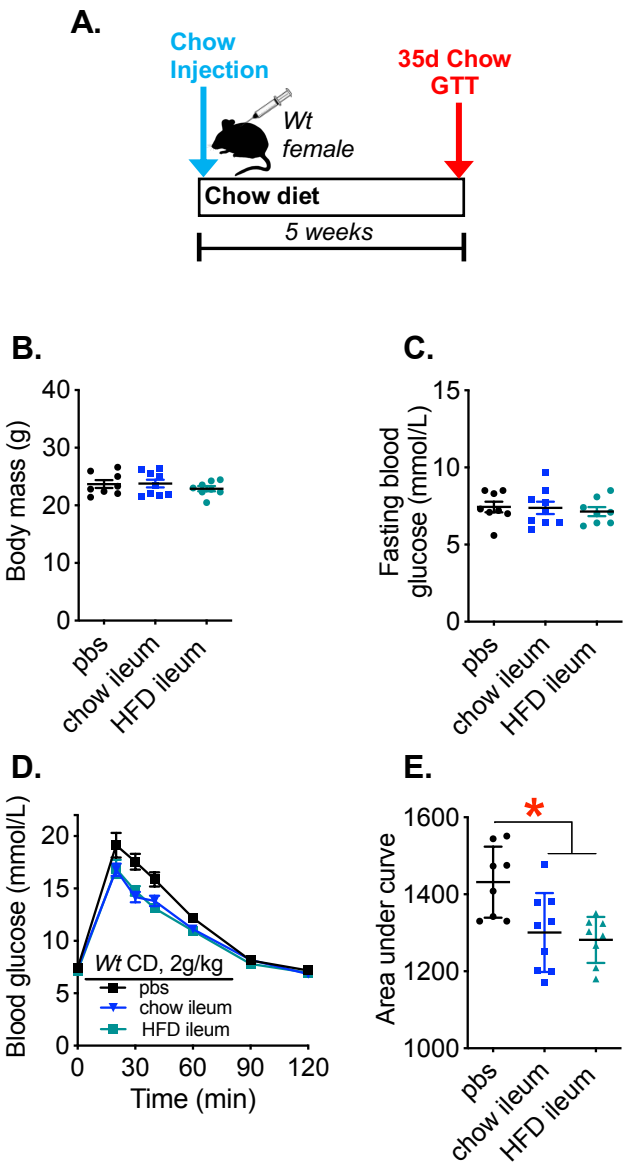

Figure 3.3.6 Injection with ileal extracts promotes blood glucose control independent of sex

A) Experimental model of female *Wt* recipient mice fed a chow diet injected with ileal extracts (200µL, s.c., diluted 5000x) collected from chow- or HFD-fed donor mice B) Body mass C) Fasting blood glucose, D) Blood glucose vs time and E) Quantified area under the curve during a GTT (2g/kg, n= 8-9). Values are mean ± SEM. *denotes statistical differences between groups ($p<0.05$).

35 days after injection with ileal luminal contents, mice were switched to an obesogenic HFD and glucose tolerance was assessed after 4 and 8 weeks of HFD feeding. However, in contrast to our collaborators who used a diabetogenic HFD that does not induce significant weight gain, we found that the effects of ileal extract injection on blood glucose during chow diet-feeding did not persist after 1 month of HFD feeding (Figure 3.3.7). Mice injected with ileal extracts had similar glucose levels during a GTT compared to PBS-injected controls after 35 days on a chow diet plus an additional 4 weeks of HFD feeding. These results suggest that the previous injection of luminal contents in chow-diet fed mice does not protect against the onset of glucose intolerance during the development of obesity (Figure 3.3.7). Recipient mice were tested again after 8 weeks of HFD feeding and no differences in blood glucose were observed (Figure 3.3.8). Our results show that that a single injection of chow-fed mice with ileal extracts does not result in durable changes in glucose control during 1 or 2 month of diet induced obesity in mice. There were also no differences in body mass were observed in any mice at a given time point of HFD feeding (Figure 3.3.7-8, B).

We next tested if a second injection of ileal contents during diet-induced obesity could alter blood glucose. Mice, previously injected during chow diet-feeding, were injected again after 8 weeks of HFD-feeding, and glucose tolerance was assessed 4 weeks later, after 12 weeks of HFD-feeding in total (Figure 3.3.9, A). A second injection with ileal extracts resulted in lower blood glucose during the GTT, evidenced by significantly lower area under the blood glucose vs. time curve,

which occurred despite no change in body mass or fasting blood glucose (Figure 3.3.9, B-E). We already established that injection with ileal contents from both chow diet-fed or HFD-fed intestinal donor mice promotes glucose control in lean mice and reverses diet-induced glucose intolerance in obese mice, intestinal extracts from chow diet-fed donor mice were used for all subsequent experiments.

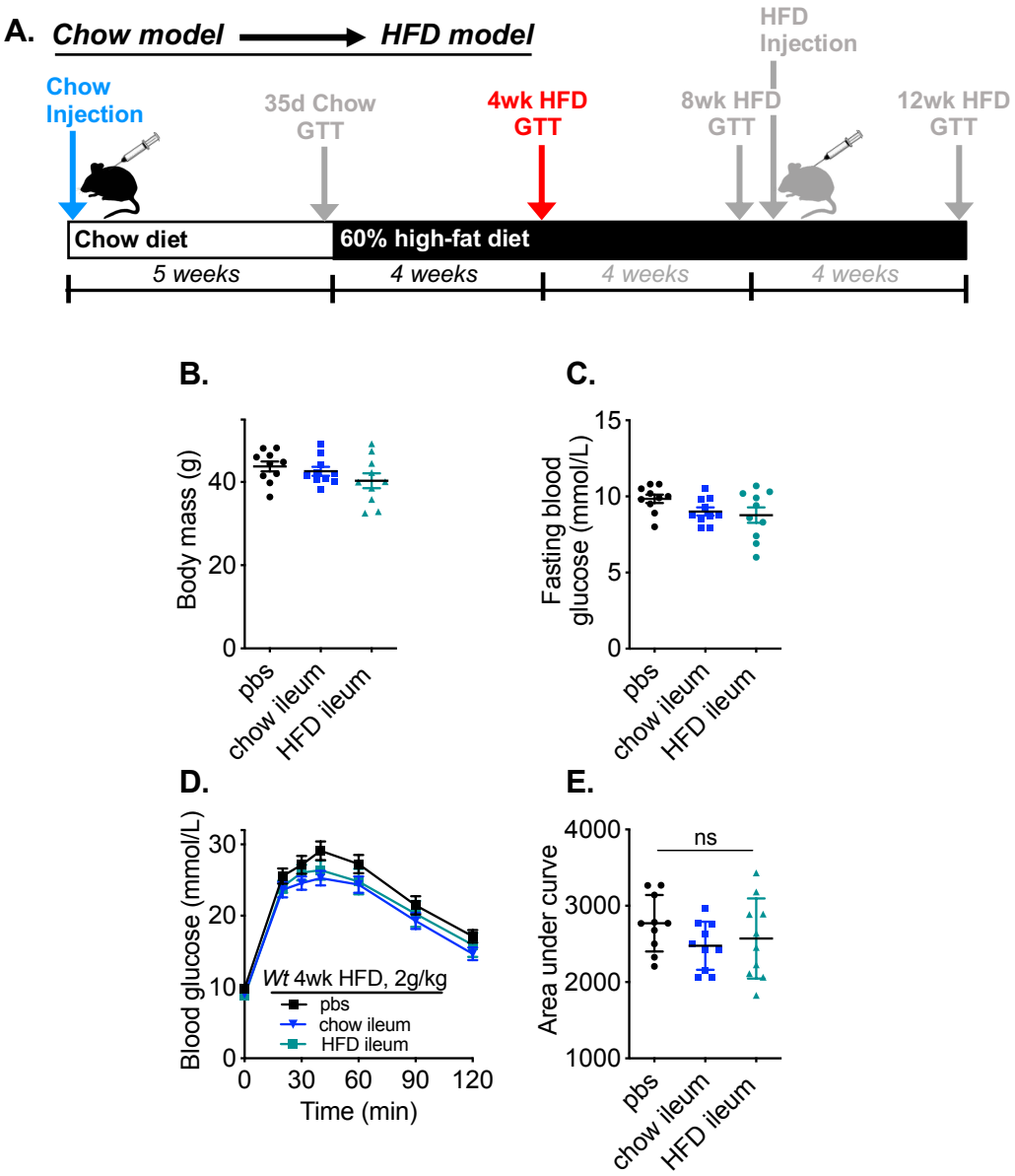

Figure 3.3.7. Previous injection with ileal extracts does not protect against the onset of glucose intolerance after 4 weeks of HFD feeding

A) Experimental model of *Wt* recipient mice previously injected with ileal extracts during chow-feeding (as described in Figure 3.3.4). 35 days later, mice were switched to HFD for 4 weeks before glucose metabolism was again assessed by GTT. B) Body mass, C) Fasting blood glucose, D) Blood glucose vs. time, and E) Quantified area under the curve during GTT (2g/kg, n=10/group). Values are mean ± SEM. *denotes statistical differences between groups ($p<0.05$).

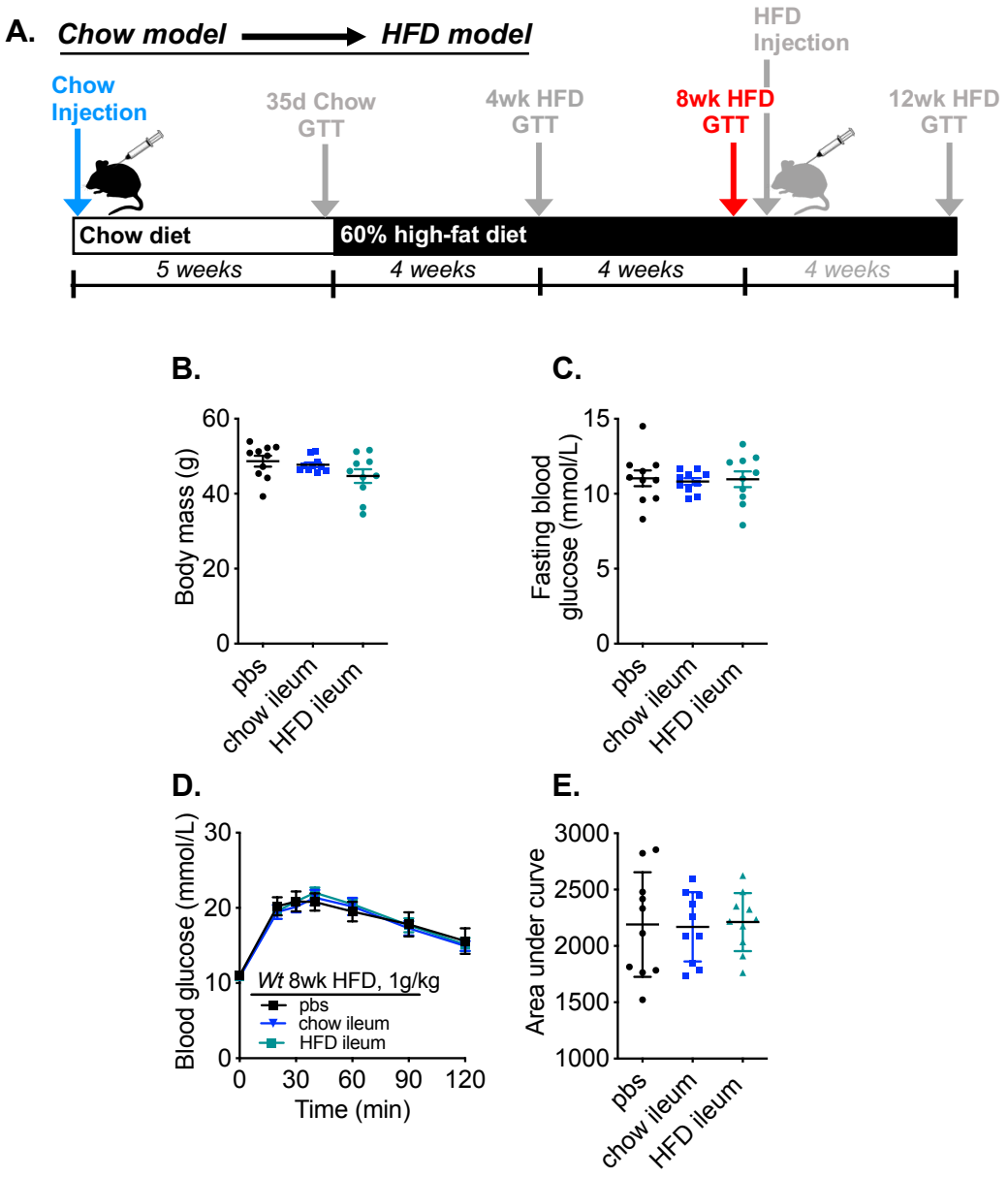

Figure 3.3.8. Previous injection with ileal extracts does not alter progression of glucose intolerance after 8 weeks of HFD feeding

A) Experimental model of *Wt* recipient mice previously injected with ileal extracts during chow-feeding (as described in Figure 3.3.4). 35 days later, mice were switched to a HFD for 8 weeks and glucose metabolism was assessed by GTT. B) Body mass, C) Fasting blood glucose, D) Blood glucose vs. time, and E) Quantified area under the curve during GTT (1g/kg, n=10/group). Values are mean ± SEM. *denotes statistical differences between groups ($p<0.05$).

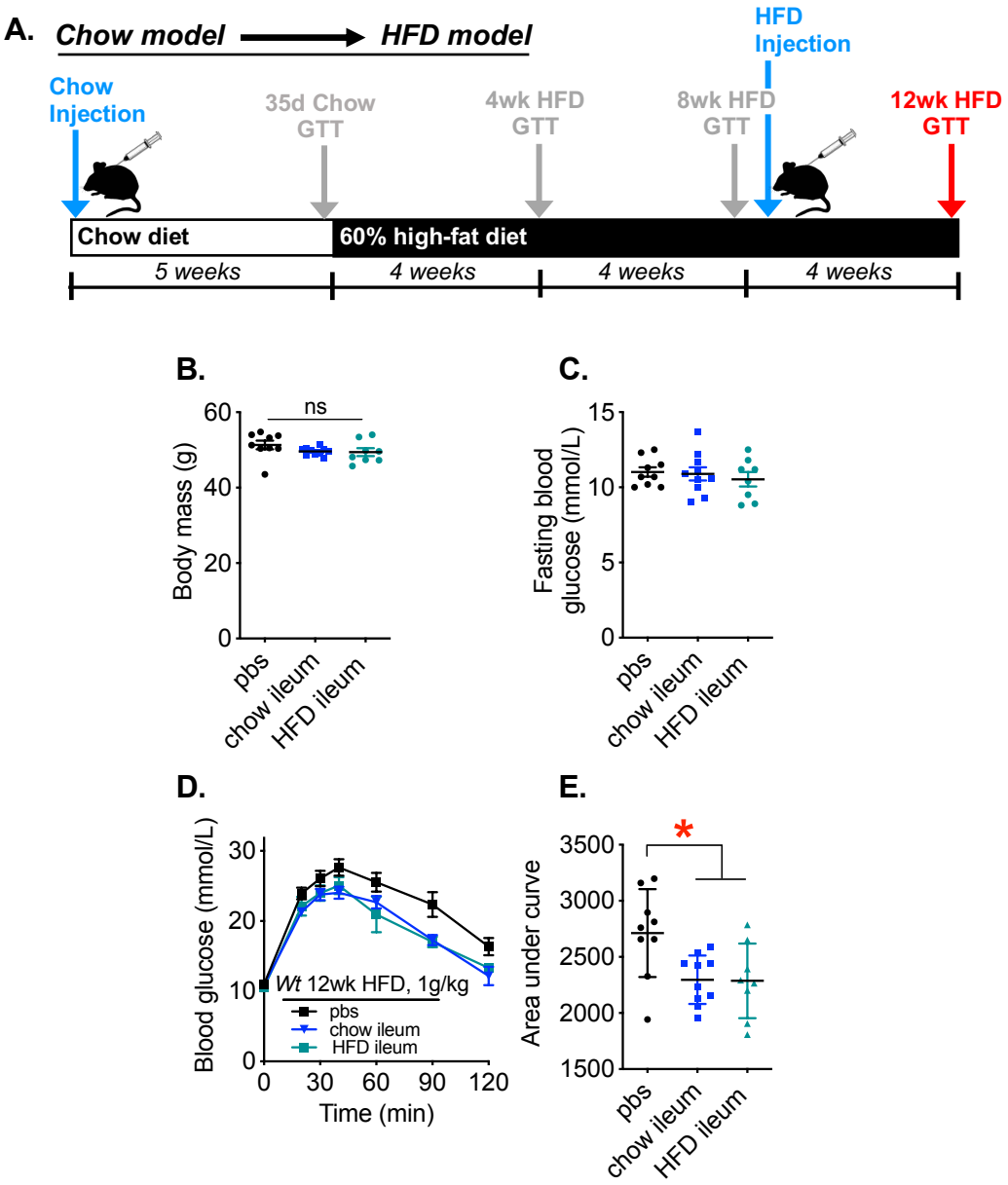

Figure 3.3.9. Injection with ileal extracts at 8 weeks of HFD reverses diet-induced glucose intolerance at 12 weeks

A) Experimental model of *Wt* recipient mice previously injected with ileal extracts during chow-feeding (as described in Figure 3.3.4). 35 days later, mice were switched to a HFD for 8 weeks before receiving a second injection of ileal extracts (200µL, s.c., diluted 5000x). 4 weeks later, after 12 weeks total of HFD-feeding, glucose metabolism was assessed by GTT. B) Body mass, C) Fasting blood glucose, D) Blood glucose vs. time, and E) Quantified area under the curve during GTT (1g/kg, n=8-10/group). Values are mean ± SEM. *denotes statistical differences between groups ($p<0.05$).

Next, we tested a cohort of HFD-fed mice that had not received an injection prior to the onset of HFD-feeding to determine if a single injection of ileal extract during HFD-induced obesity is sufficient to reverse lower blood glucose. Interestingly, a single injection with ileal extracts did not alter blood glucose during a GTT in obese mice that had not been previously injected during chow diet-feeding (Figure 3.3.10). Published results show that injection with ileal extracts induces activation of CD4 and CD8 T cells, followed by development of immunological memory[228]. Based on these results and our data demonstrating that a secondary injection with ileal extracts is required to mitigate diet-induced glucose intolerance in obese mice, we tested if a second injection in these obese mice would be sufficient to lower blood glucose during a GTT. Thus, mice were injected once after 8 weeks of HFD and again after 12 weeks of HFD-feeding and a GTT was done was assessed 4 weeks later, after a total of 16 weeks of HFD-feeding (Figure 3.3.11, A). Two injections of ileal extracts during HFD-feeding, equated to lower blood glucose during a GTT in obese mice compared to PBS-injected controls, as evidenced by a significant reduction in the area under the blood glucose vs. time curve, an effect that occurred despite not change in body mass or fasting blood glucose (Figure 3.3.11, B-E). Taken together, our data suggests that while a single ileal injection and subsequent activation of the adaptive immune response is sufficient to promote glucose control in lean mice, triggering immunological memory (or another unidentified response) via a secondary injection during obesity is required for protection against glucose intolerance during HFD-induced obesity in mice. This is consistent with previous

published work demonstrating that the glycemic effects of ileal injection are mediated by generation of memory T cells[228], but more work is needed to fully elucidate the immunological changes underlying the effects of ileal injection.

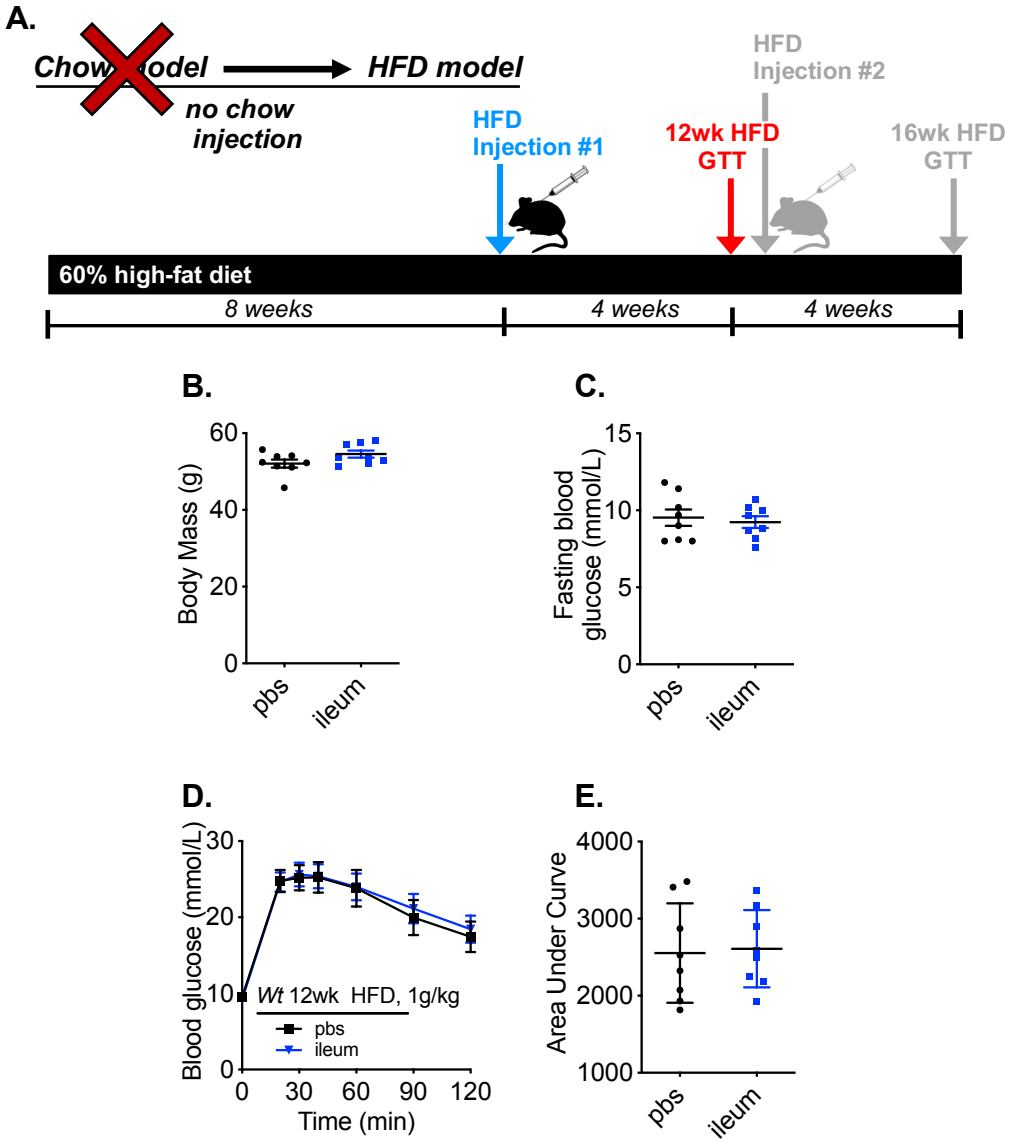

Figure 3.3.10 A single injection with ileal extracts at 8 weeks of HFD is insufficient to reverse diet-induced glucose intolerance

A) Experimental model of *Wt* recipient mice that *did not receive an injection of ileal extracts during chow feeding.* Mice were fed a HFD for 8 weeks before receiving an injection of ileal extract (200µL, s.c., diluted 5000x). 4 weeks later, after 12 weeks total of HFD-feeding, glucose metabolism was assessed by GTT. B) Body mass, C) Fasting blood glucose, D) Blood glucose vs. time, and E) Quantified area under the curve during GTT (1g/kg, n=8/group). Values are mean ± SEM. *denotes statistical differences between groups ($p<0.05$).

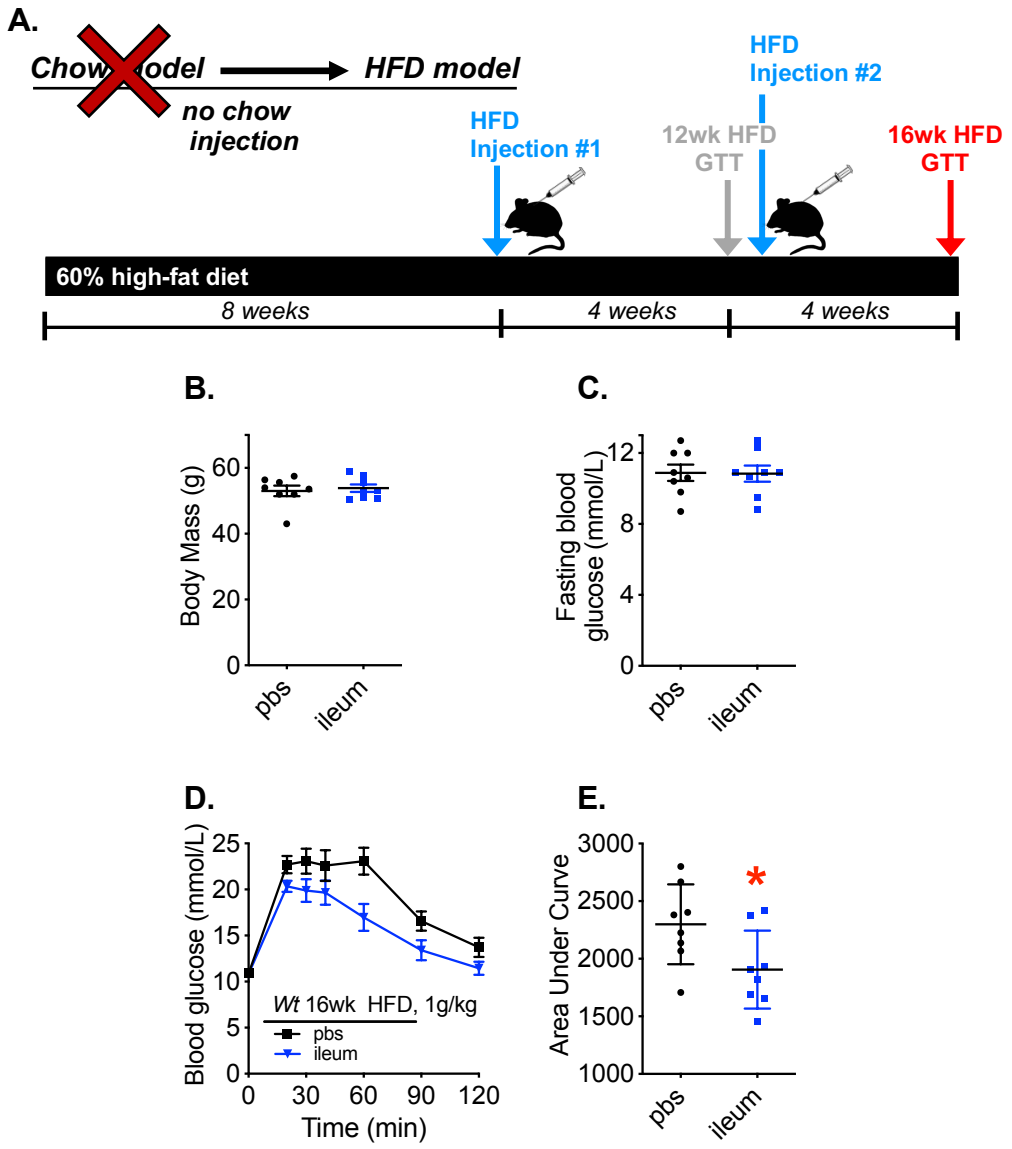

Figure 3.3.11 A second injection with ileal extracts at 12 weeks of HFD is sufficient to reverse diet-induced glucose intolerance

A) Experimental model of *Wt* recipient mice that *did not receive an injection of ileal extracts during chow feeding,* but received 2x injections of ileal extract during HFD-feeding, once at 8 weeks and again at 12 weeks. (200µL, s.c., diluted 5000x). 4 weeks later, after 16 weeks total of HFD-feeding, glucose metabolism was assessed by GTT. B) Body mass, C) Fasting blood glucose, D) Blood glucose vs. time, and E) Quantified area under the curve during GTT (1g/kg, n=8/group). Values are mean ± SEM. *denotes statistical differences between groups ($p<0.05$).

3.3.3 Intestinal extracts from upper gut segments alter blood glucose

It is known that the ecology of the gut microbiota, along with host intestinal immunity varies according to the intestinal segment[316–318]. After finding that intestinal segments collected from the ileal segments of chow diet or HFD-fed mice lower blood glucose during a GTT in lean mice and obese mice, we next determine if this effect was restricted to extracts derived from specific intestinal segments. Intestinal contents were collected from the duodenum/jejunum ('duod/jej'), cecum, colon, in addition to supernatants of fecal homogenates, from chow diet-fed donor mice. Diluted extracts (1/5000) from each of these gut segments (and the feces) were injected in chow diet-fed *Wt* recipient mice. Consistent with previous results, the injection protocol did not affect body mass (Figure 3.3.12, B). We found that mice injected with only the duodenal/jejunal extract, but not cecal, colonic or fecal extracts, caused lower fasting glycemia and lower glucose levels during the GTT, evidenced by a significantly lower area under the blood glucose vs. time curve compared to PBS-injected controls (Figure 3.3.12, B-E). One week later, 42 days after intestinal injection, we also assessed insulin tolerance in these mice but no differences between PBS-injected controls and mice injected with any gut segment were observed (Figure 3.3.13).

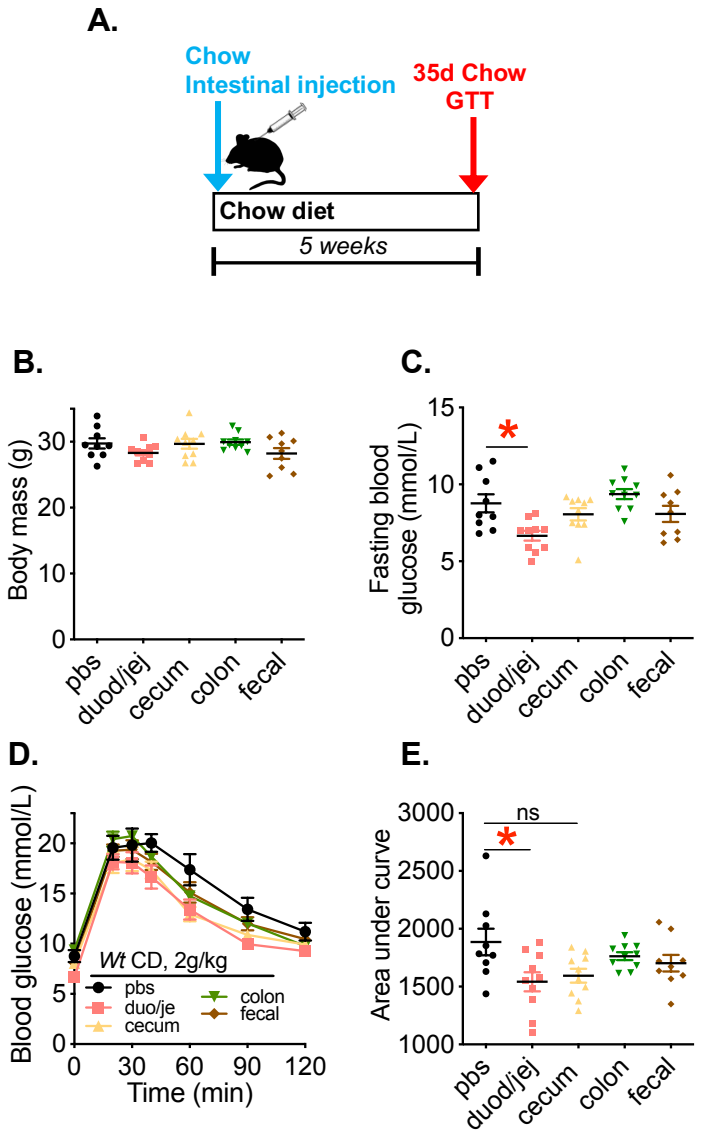

Figure 3.3.12. Glycemic effects of intestinal extracts are restricted to upper gut segments

A) Experimental model of *Wt* recipient mice fed a chow diet injected with intestinal extracts from duodenum/jejunum, cecum, colon or fecal supernatants, (200µL, s.c., diluted 5000x) collected from chow-fed donor mice. Glucose metabolism was assessed by GTT 35 days after injection. B) Body mass, C) Fasting blood glucose, D) Blood glucose vs. time, and E) Quantified area under the curve during GTT (2g/kg, n=9-10/group). Values are mean ± SEM. *denotes statistical differences between groups ($p<0.05$).

These data show that upper gut segments such as the duodenal, jejunal and ileum, contain factors that can lower blood glucose, but the factors or the dose used in cecum and large intestine extracts does not alter blood glucose. This information may help elucidate the identity of intestinal and/or microbial components that improve blood glucose control.

Because published data[228] demonstrated that injection of intestinal extracts elicits an adaptive immune (memory) response, we also wanted to assess glucose tolerance at an early time-point post-intestinal injection that would precede activation of adaptive immunity. Specifically, increased proliferation of CD4+ and CD8+ T cells, and an increased proportion of IFNγ-producing and TNFα-producing T cells were detectable 10 days after the ileal injection procedure, and these differences were maintained at 35 days[228]. Additionally, increased concentrations of plasma IgG1, IgG2a and IgG2b were observed at 35 days[228]. However, our collaborators did not report any assessment of glucose tolerance at any time-points earlier than 65 days post-ileal injection. Thus, we sought to glucose tolerance 7 days after intestinal injection, a time-point that precedes the proliferation of T cells as characterized by Pomie, et al.[228]. Consistent with the lag time required to generate an adaptive immune response, we did not observe any changes in blood glucose levels during a GTT 7 days after injection of mice with duodenal/jejunal extracts or extracts from any other intestinal segment (Figure 3.3.14).

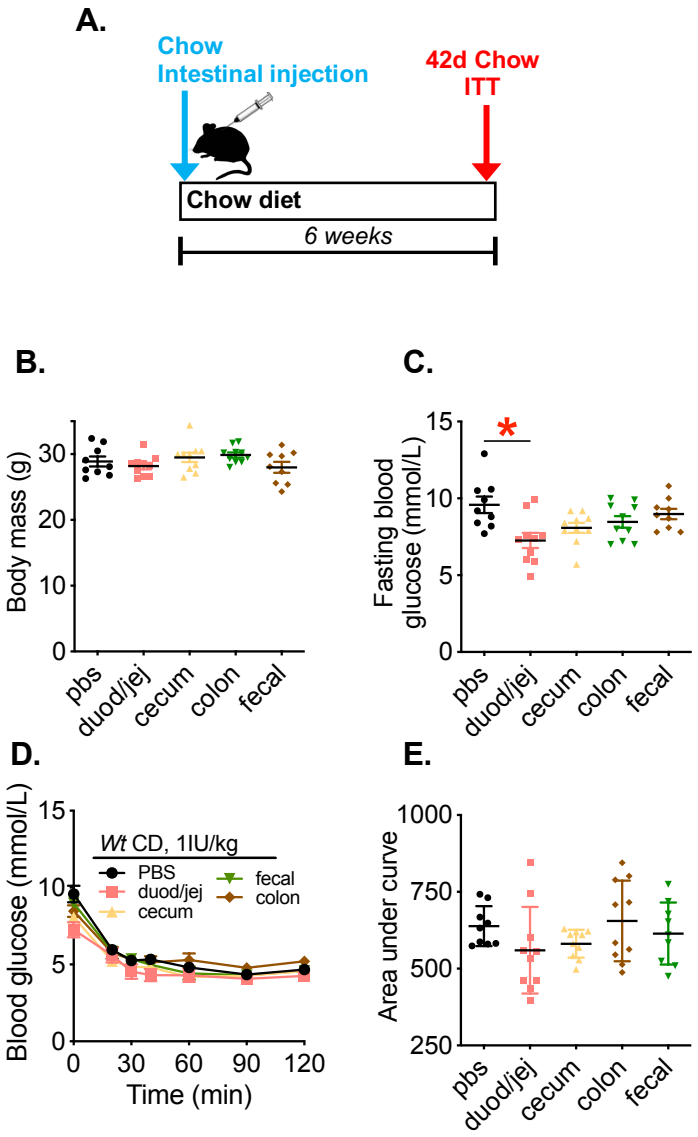

Figure 3.3.13 Injection with intestinal extracts does not alter insulin tolerance after 6 weeks

A) Experimental model of *Wt* recipient mice fed a chow diet injected with intestinal extracts from duodenum/jejunum, cecum, colon or fecal supernatants, (200µL, s.c., diluted 5000x) collected from chow-fed donor mice. Insulin tolerance was assessed by GTT 42 days after injection. B) Body mass, C) Fasting blood glucose, D) Blood glucose vs. time, and E) Quantified area under the curve during GTT (2g/kg, n=9-10/group). Values are mean ± SEM. *denotes statistical differences between groups ($p<0.05$).

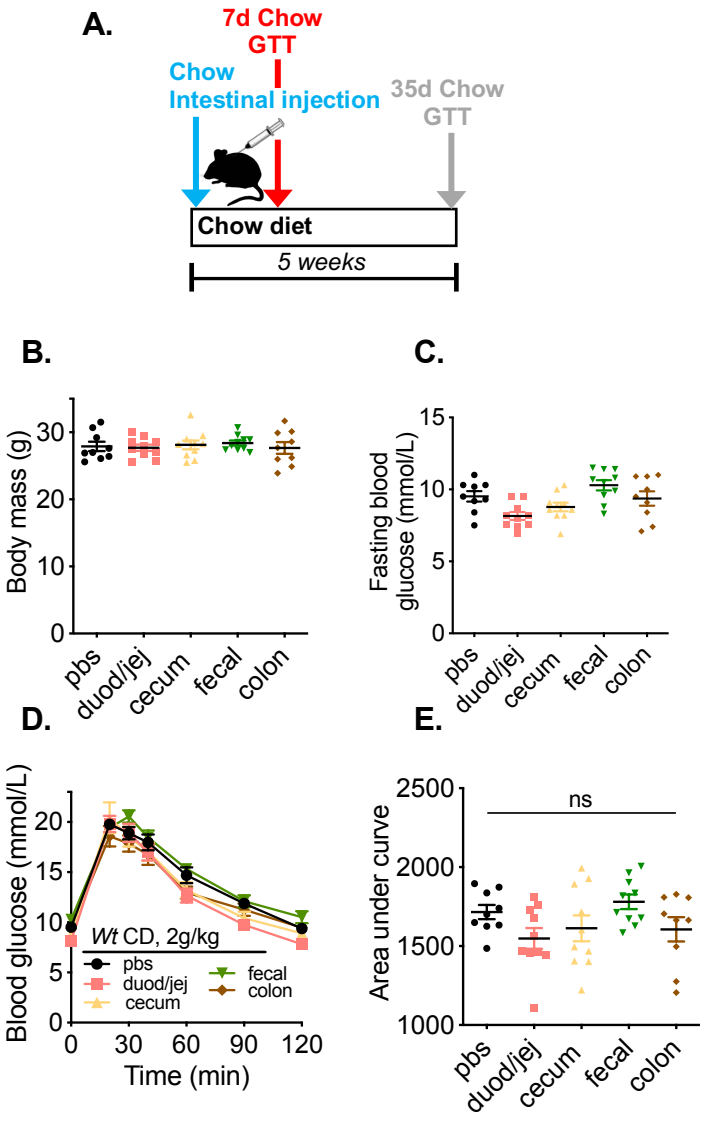

Figure 3.3.14 Delayed onset of glycemic control phenotype following injection with upper gut segments

A) Experimental model of *Wt* recipient mice fed a chow diet injected with intestinal extracts from duodenum/jejunum, cecum, colon or fecal supernatants, (200µL, s.c., diluted 5000x) collected from chow-fed donor mice. Glucose metabolism was assessed by GTT 7 days after injection. B) Body mass, C) Fasting blood glucose, D) Blood glucose vs. time, and E) Quantified area under the curve during GTT (2g/kg, n=9-10/group). Values are mean ± SEM. *denotes statistical differences between groups ($p<0.05$).

3.3.4 Injection of mice with ileal extracts does not alter insulin secretion in lean or obese mice

Having established that injection of upper gut extracts can lower blood glucose during a GTT in lean mice and obese mice, we next tested if injection of ileal contents altered insulin levels in both chow-fed and HFD-fed models. Lean mice were injected with ileal extracts and a glucose-stimulated insulin secretion test was performed 35 days after ileal injection (Figure 3.3.15, A). Obese mice (that had previously received a first ileal injection during chow-feeding) were injected at 8 weeks of HFD-feeding and a glucose-stimulated insulin secretion test was performed 4 weeks after ileal injection, at 12 weeks total of HFD-feeding (Figure 3.3.16, A). No differences in body mass, fasting blood glucose, HOMA-IR, glucose-stimulated insulin at 10m, 60m, or 120 minutes, insulin area under the curve, or IRI was observed in either lean mice or obese mice injected with ileal extracts (Figure 3.3.15, 3.3.16, B-G), suggesting ileal injection lowers blood glucose during a glucose load, but independent of effects on insulin secretion. It is noteworthy that injection of upper gut extracts consistently lowered glucose levels during a GTT, but the effects on fasting blood glucose are less consistent, since in some experiments injection of mice with ileal extracts from HFD mice lowered fasting blood glucose (Figure 3.3.5, Figure 3.3.12, C), but this did not reach statistical significance in other experiments (Figure 3.3.16, C).

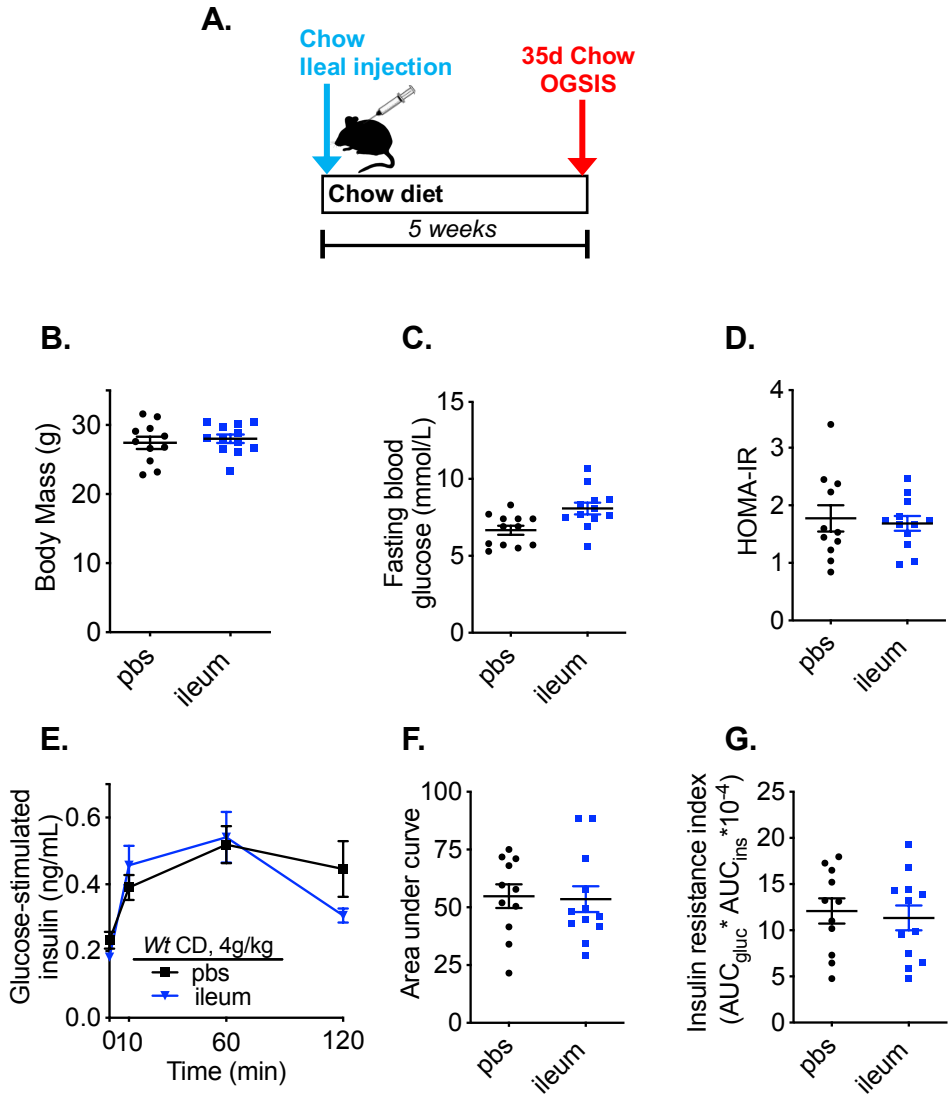

Figure 3.3.15 Intestinal extract injection does not alter insulin secretion in chow-fed mice

A) Experimental model of *Wt* recipient mice fed a chow diet and injected with ileal extracts (200µL, s.c., diluted 5000x) collected from chow-fed donor mice. Oral glucose-stimulated insulin secretion was assessed 35 days after injection. B) Body mass, C) Fasting blood glucose, D) HOMA-IR, E) Blood insulin vs. time and F) Insulin area under the curve. F) Calculated insulin resistance index (IRI). Values are mean ± SEM. *denotes statistical differences between groups ($p<0.05$).

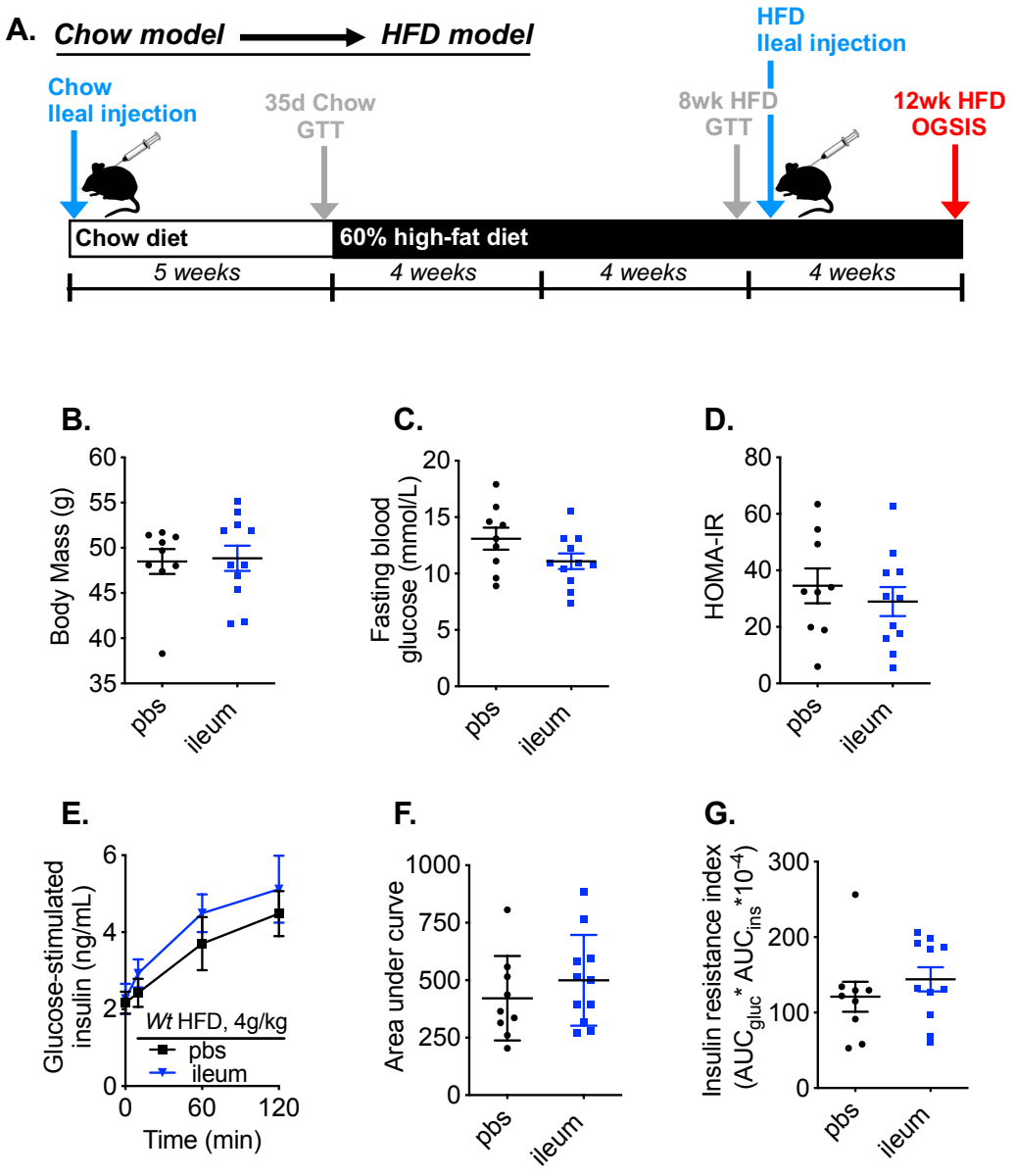

Figure 3.3.16 Intestinal extract injection does not alter insulin secretion in obese mice

A) Experimental model of *Wt* recipient mice fed a 60% HFD and injected with ileal extracts (200µL, s.c., diluted 5000x) collected from chow-fed donor mice. Oral glucose-stimulated insulin secretion was assessed 4 weeks after injection. B) Body mass, C) Fasting blood glucose, D) HOMA-IR, E) Blood insulin vs. time and F) Insulin area under the curve. F) Calculated insulin resistance index (IRI). Values are mean ± SEM. *denotes statistical differences between groups ($p<0.05$).

3.3.5 Bacteria are required for intestinal extracts to lower blood glucose

To determine if bacteria are required for intestinal extracts to later blood glucose, we tested ileal extracts prepared from germ-free donor mice using our injection protocol in chow diet-fed mice. The data presented in Figure 3.3.17 represents three separate collections of germ-free ileal extracts, used to inject three separate cohorts of *Wt* recipient mice. *Wt* recipient mice were specific pathogen free mice that harbored commensal bacteria, only the mice used for preparing intestinal luminal contents were germ free. There was no effect on body mass, fasting blood glucose, or glucose tolerance was observed between PBS-injected controls and mice injected with ileal extracts from germ free mice (Figure 3.3.17, B-E). Our results demonstrate that ileal extracts derived from germ-free mice do not alter blood glucose in *Wt* mice fed a chow diet (Figure 3.3.17). Thus, intestinal extracts require an intact intestinal microbiota to alter blood glucose.

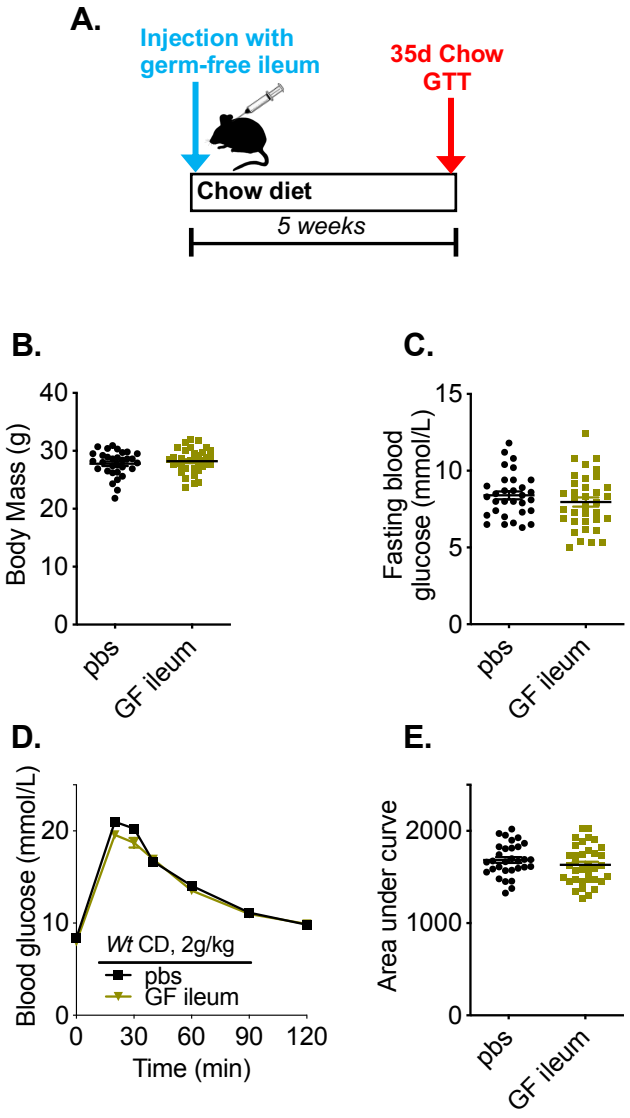

Figure 3.3.17 Glucose tolerizing properties of intestinal extracts require an intact intestinal microbiota

A) Experimental model of *Wt* recipient mice fed a chow diet injected with ileal extracts (200µL, s.c., diluted 50-20,000x) collected from chow-fed germ-free donor mice under sterile conditions. Glucose metabolism was assessed by GTT 35 days after injection. B) Body mass, C) Fasting blood glucose, D) Blood glucose vs. time, and E) Quantified area under the curve during GTT (2g/kg, n=31-35/group from 3 separate experiments with 3 separate germ-free ileal extract collections). Values are mean ± SEM. *denotes statistical differences between groups ($p<0.05$).

3.3.6 Intestinal extract injection requires NOD2-RIPK2 to alter blood glucose

We next tested if MDP acting on NOD2 was the key factor in intestinal extracts that could alter blood glucose. First, we sought to determine if NOD2 was required for upper gut intestinal extracts to alter blood glucose. We prepared ileal extracts from chow diet-fed *Wt* mice and injected these ileal extracts into *Nod2*$^{-/-}$ mice. Our results demonstrate that injection of ileal extracts does not alter blood glucose during a GTT in *Nod2*$^{-/-}$ mice (Figure 3.3.18, D-E). Similar to previous ileal extract injections into *Wt* mice, no differences in body mass or fasting blood glucose were observed. Following assessment of blood glucose control 35 days after ileal injection during chow diet-feeding, *Nod2*$^{-/-}$ mice were switched to HFD and again no differences in blood glucose were observed after 8 weeks of HFD-feeding (Figure 3.3.19).

Nod2$^{-/-}$ mice were refractory to changes in blood glucose after ileal extract injection, hence NOD2 is necessary for changes in blood glucose from intestinal extract injection. We next tested if the well-established NOD2 ligand, MDP is sufficient to lower blood glucose using this injection protocol. We took advantage of our previously published HFD 'intervention style' model that demonstrates 3 consecutive injections of MDP can lower blood glucose during a GTT in obese mice[193,311]. However, we have never previously tested the durability of blood glucose changes induced by MDP and here we determined if the glycemic effects of MDP are long-lasting. Figure 3.3.9 and Figure 3.3.11 previously showed lower blood glucose in obese mice injected with ileal extracts, which can be observed at

4 weeks following a single injection. Thus, we injected HFD-fed mice with three consecutive injections of MDP, as published[193,311], but also included a 4 week follow-up assessment of glucose tolerance (Figure 3.3.20, A). As expected, 3 injections of MDP lowered blood glucose on the 4th day, (i.e. 24 hours after the final injection of MDP), independent of any effect on body mass or fasting blood glucose (Figure 3.3.20, B-E). Interestingly, these 3 injections of MDP caused long lasting effects on blood glucose that included lower blood glucose during a GTT 4 weeks after these 3 injections of MDP (Figure 3.2.21, F-I).

Because we found that multiple injections of MDP can lower blood glucose during a GTT in obese mice 4 weeks following MDP injection, we next wanted to tested a single injection of MDP that more closely resembled the single injection of upper gut intestinal extracts. Thus, we tested the effects on glucose tolerance 24 hours and 4 weeks after a single administration of MDP in a cohort of obese mice (Figure 3.2.21, A). Interestingly, a single injection of MDP increased fasting blood glucose and increased blood glucose during a GTT in obese mice, when tested 24 hours after this single injection, without altering body mass (Figure 3.2.21, B-E). A single injection of MDP had no effect on blood glucose 4 weeks after injection, (Figure 3.2.21, F-I). Our data shows that MDP is not a stand-alone factor that is sufficient to explain the effect of a single injection of upper gut intestinal extract injection on blood glucose, but NOD2 is required in propagating a response that alters blood glucose in response to an injection of upper gut intestinal extract .

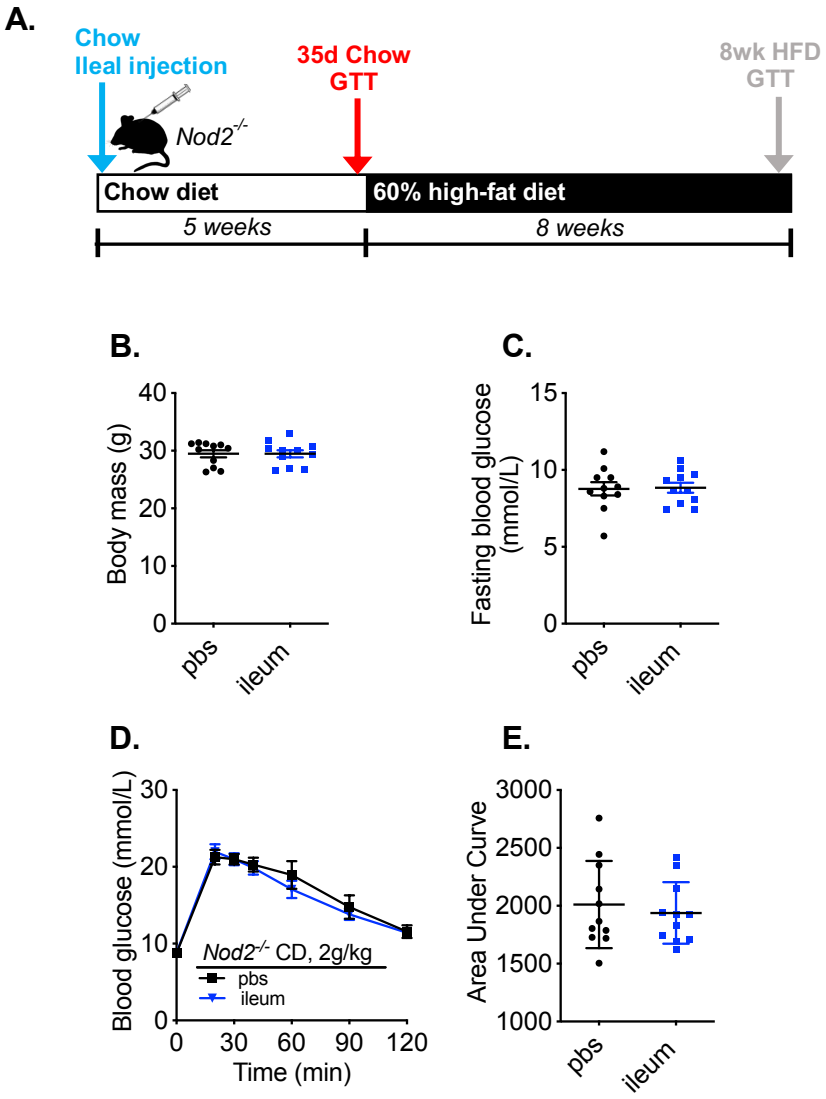

Figure 3.3.18 NOD2 is required for glycemic effects following ileal extract injection

A) Experimental model of *Nod2*$^{-/-}$ recipient mice fed a chow diet injected with ileal extracts (200µL, s.c., diluted 50-20,000x) collected from chow-fed donor mice. Glucose metabolism was assessed by GTT 35 days after injection. B) Body mass, C) Fasting blood glucose, D) Blood glucose vs. time, and E) Quantified area under the curve during GTT (2g/kg, n=11/group). Values are mean ± SEM. *denotes statistical differences between groups ($p<0.05$).

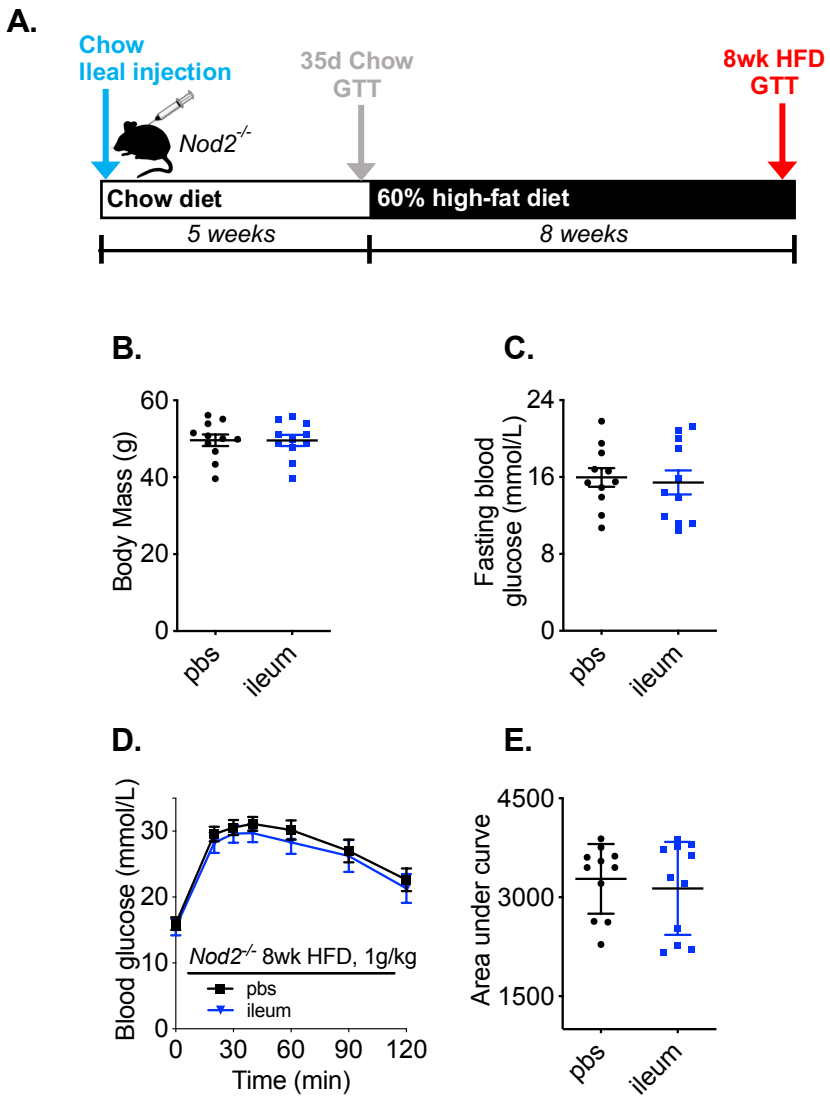

Figure 3.3.19 Absence of glucose phenotype is maintained after 8 weeks of high-fat feeding in *Nod2*$^{-/-}$ mice

A) Experimental model of *Nod2*$^{-/-}$ recipient mice previously injected with ileal extract during chow-feeding. 35 days later, mice were switched to HFD for 8 weeks and glucose metabolism was assessed by GTT. B) Body mass, C) Fasting blood glucose, D) Blood glucose vs. time, and E) Quantified area under the curve during GTT (1g/kg, n=11/group). Values are mean ± SEM. *denotes statistical differences between groups ($p<0.05$).

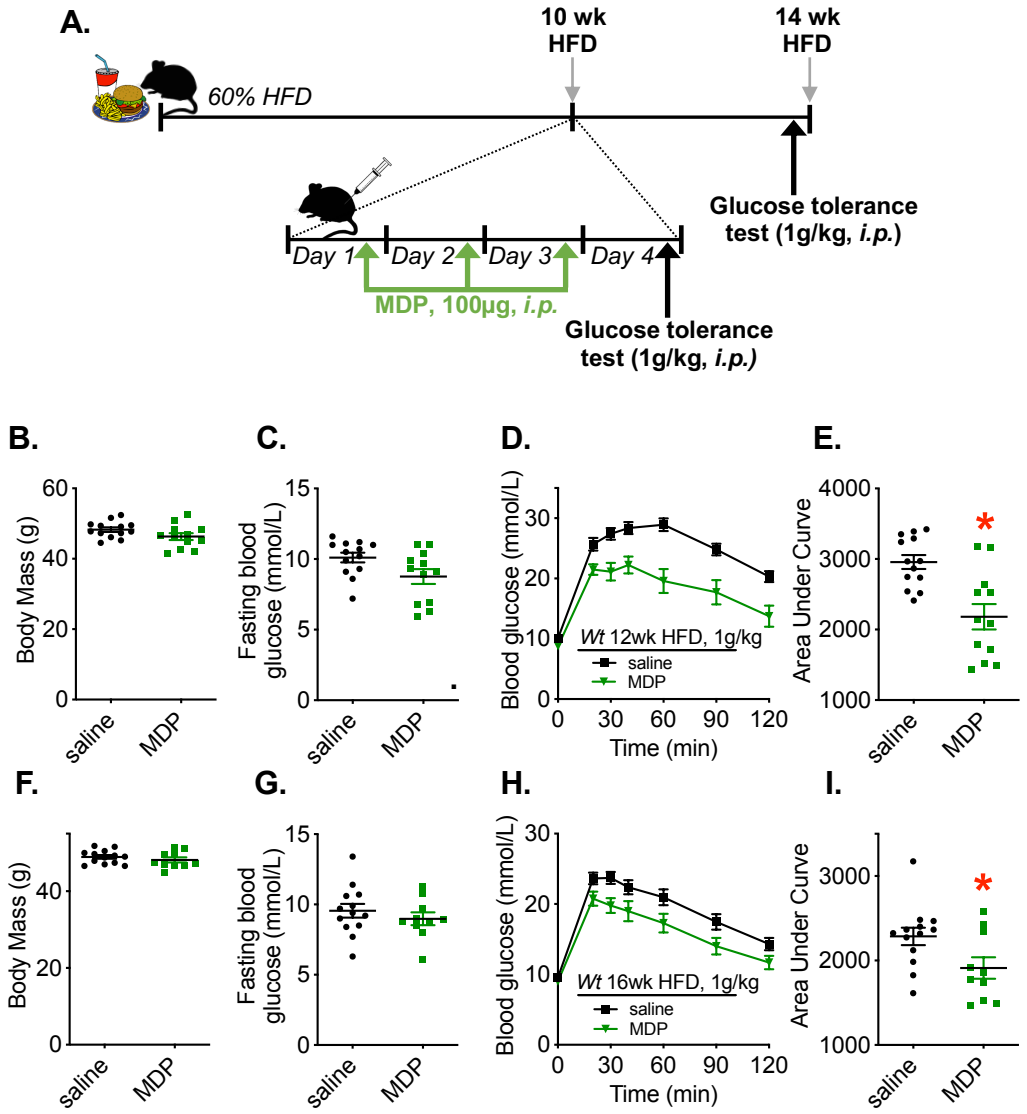

Figure 3.3.20 Repeat MDP treatment acutely decreases blood glucose levels during a GTT in obese mice and persists for 4 weeks

A) Experimental model of *Wt* mice fed a high fat diet for 12 weeks and injected with MDP (100 µg, *i.p*) for 3 days. Glucose tolerance was assessed 24 hours after the final MDP injection, and then again 4 weeks after MDP, at 16 weeks HFD-feeding. B) Body mass, C) Fasting blood glucose, D) Blood glucose vs. time, and E) Quantified area under the curve during GTT 24 h post-MDP. F) Body mass, G) Fasting blood glucose, H) Blood glucose vs. time, and I) Quantified area under the curve during GTT 4 weeks post-MDP, at 14 weeks HFD (1g/kg, n=10-13/group). Values are mean ± SEM. *denotes statistical differences between groups ($p<0.05$).

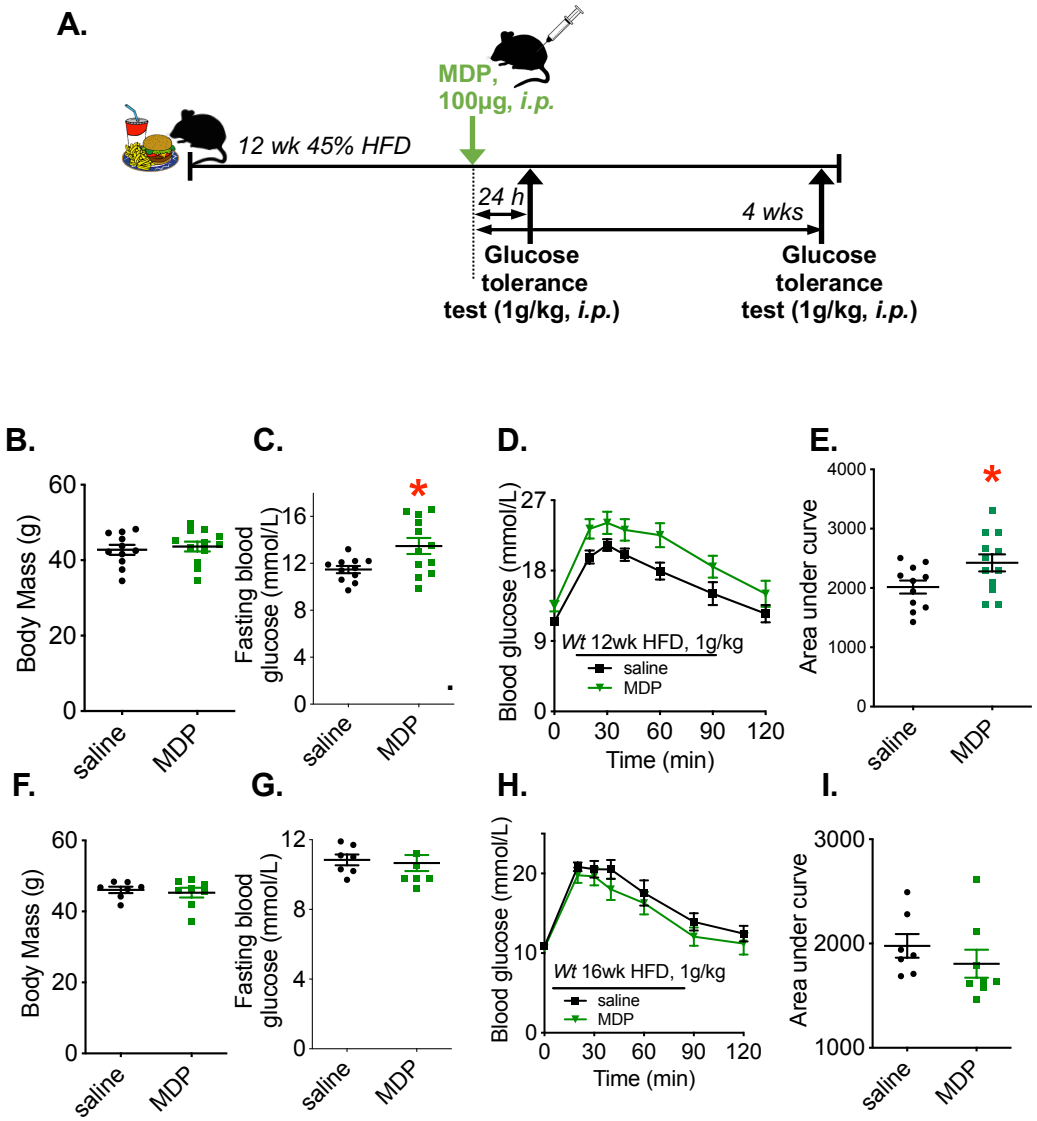

Figure 3.2.21 A single MDP injection acutely increases blood glucose levels during a GTT in obese mice

A) Experimental model of *Wt* mice fed a high fat diet for 12 weeks and injected once with MDP (100 µg, *i.p*). Glucose tolerance was assessed 24 hours after MDP injection, and then again 4 weeks after MDP, at 16 weeks HFD-feeding. B) Body mass, C) Fasting blood glucose, D) Blood glucose vs. time, and E) Quantified area under the curve during GTT 24 h post-MDP. F) Body mass, G) Fasting blood glucose, H) Blood glucose vs. time, and I) Quantified area under the curve during GTT 4 weeks post-MDP, at 14 weeks HFD (1g/kg, n=7-12/group). Values are mean ± SEM. *denotes statistical differences between groups ($p<0.05$).

We next tested if injection of luminal contents obtained the chow diet-fed *Wt* mice into *Ripk2*$^{-/-}$ mice to determine if changes in blood glucose were dependent on a NOD2-RIPK2 signalling pathway. Furthermore, we have recently shown MDP's glycemic effects are dependent on RIPK2, as *Ripk2*$^{-/-}$ are refractory to changes in blood glucose after repeated treatment with MDP[311]. We hypothesized that, similar to *Nod2*$^{-/-}$ mice, ileal extract injection would not alter blood glucose in *Ripk2*$^{-/-}$ mice. We first used tested injection of ileal extracts into chow diet-fed *Ripk2*$^{-/-}$ mice. Unexpectedly, we found that *Ripk2*$^{-/-}$ mice have higher blood glucose following after injection with ileal extracts (Figure 3.3.22, A-E). 35 days after ileal injection during chow diet-feeding, *Ripk2*$^{-/-}$ mice were then switched to HFD and glucose tolerance tests were done after 8 weeks of HFD-feeding (Figure 3.3.23, A). Interestingly, higher blood glucose during a GTT persisted in HFD-fed *Ripk2*$^{-/-}$ mice that were injected once with ileal extracts (Figure 3.3.23).

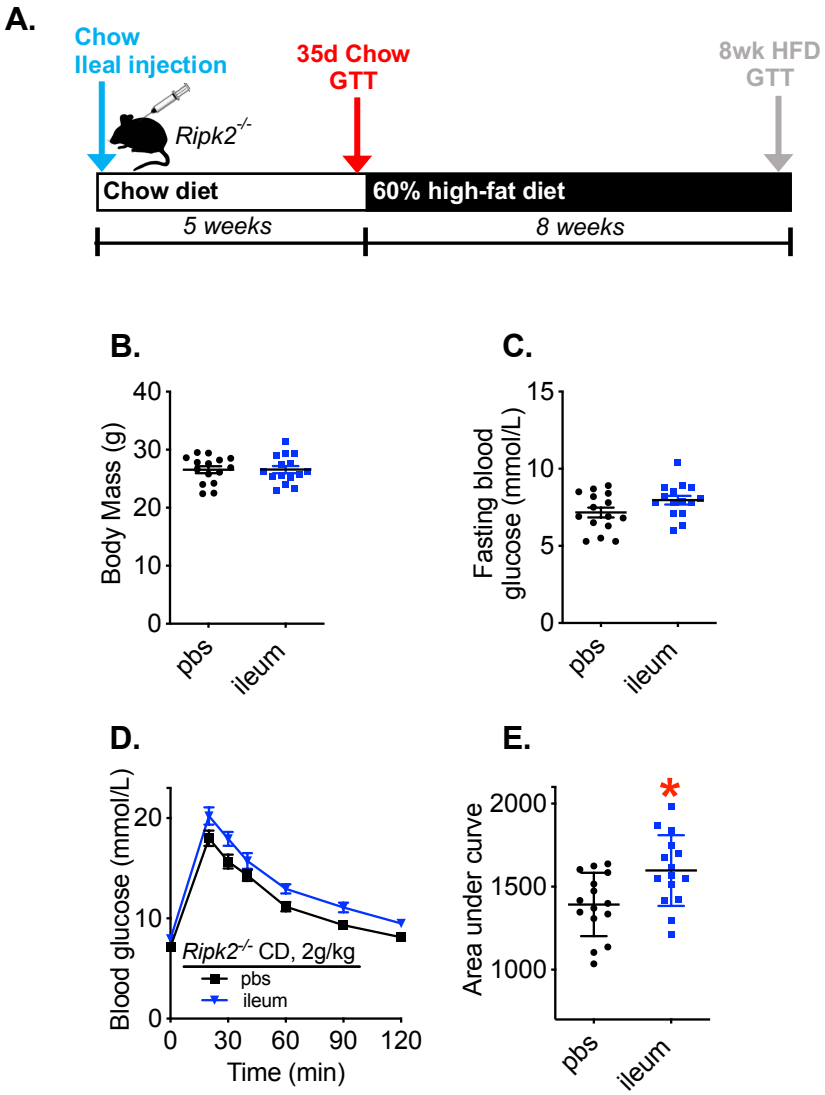

Figure 3.3.22 RIPK2 protects against deleterious glucose control following ileal extract injection

A) Experimental model of *Ripk2*$^{-/-}$ recipient mice fed a chow diet and injected with ileal extracts (200µL, s.c., diluted 5000x) collected from chow-fed donor mice. Glucose metabolism was assessed by GTT 35 days after immunization. B) Body mass, C) Fasting blood glucose, D) Blood glucose vs. time, and E) Quantified area under the curve during GTT (2g/kg, n=15/group). Values are mean ± SEM. *denotes statistical differences between groups ($p<0.05$).

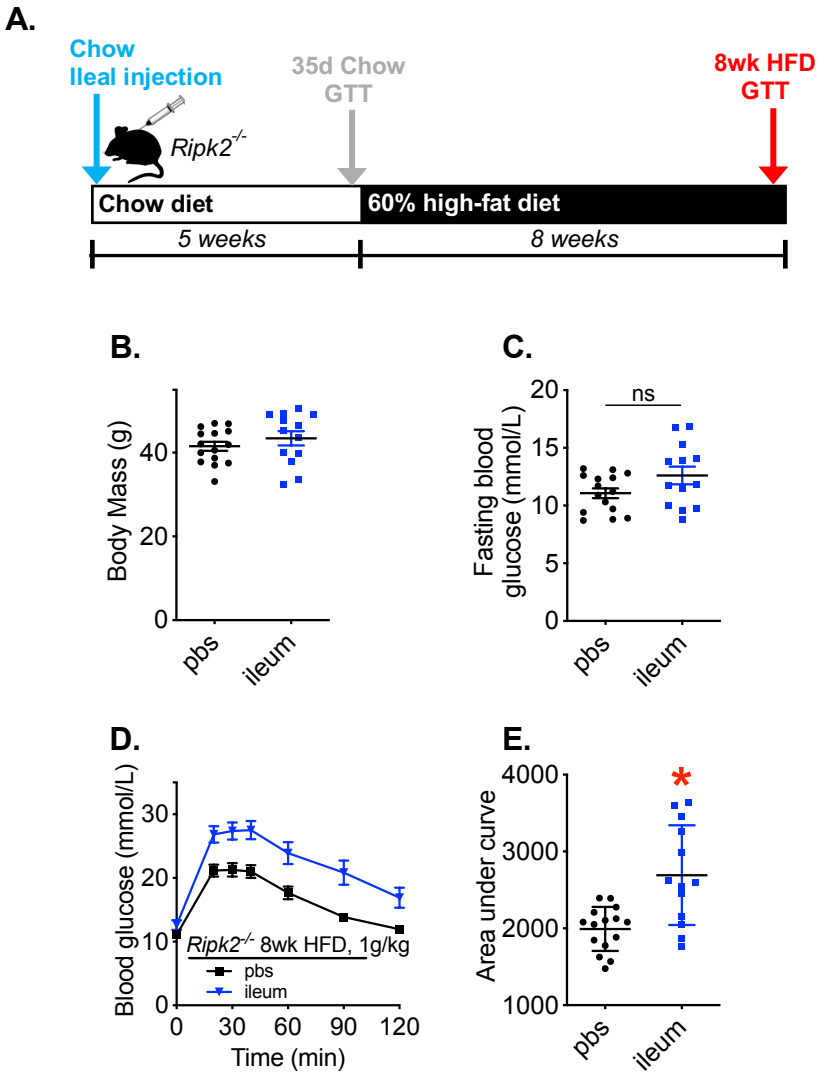

Figure 3.3.23 Changes in blood glucose control persist after 8 weeks of HFD in *Ripk2*$^{-/-}$ mice

A) Experimental model of *Ripk2*$^{-/-}$ recipient mice previously injected with ileal extract during chow-feeding. 35 days later, mice were switched to a HFD for 8 weeks and glucose metabolism was assessed by GTT. B) Body mass, C) Fasting blood glucose, D) Blood glucose vs. time, and E) Quantified area under the curve during GTT (1g/kg, n=13-15/group). Values are mean ± SEM. *denotes statistical differences between groups ($p<0.05$).

RIPK2 is the common downstream adapter for both NOD1 and NOD2 and based on the divergent glucose phenotypes in *Nod2*$^{-/-}$ vs. *Ripk2*$^{-/-}$ mice, we hypothesized that NOD1-RIPK2 signalling mediated worse glucose control following ileal extract injection. Thus, we next tested the glucose response to injection of ileal extracts obtained from chow diet-fed *Wt* mice into *Nod1*$^{-/-}$ mice (Figure 3.3.24, A). Similar to results in *Ripk2*$^{-/-}$ mice, we found that chow diet-fed *Nod1*$^{-/-}$ mice higher blood glucose during a GTT and *Nod1*$^{-/-}$ mice also had higher fasting blood glucose and 35 days after ileal extract injection (Figure 3.3.24, B-E). However, unlike in *Ripk2*$^{-/-}$ mice, there was no difference in blood glucose levels in *Nod1*$^{-/-}$ mice after injection of ileal extracts followed by 8 weeks of HFD-feeding (Figure 3.3.25).

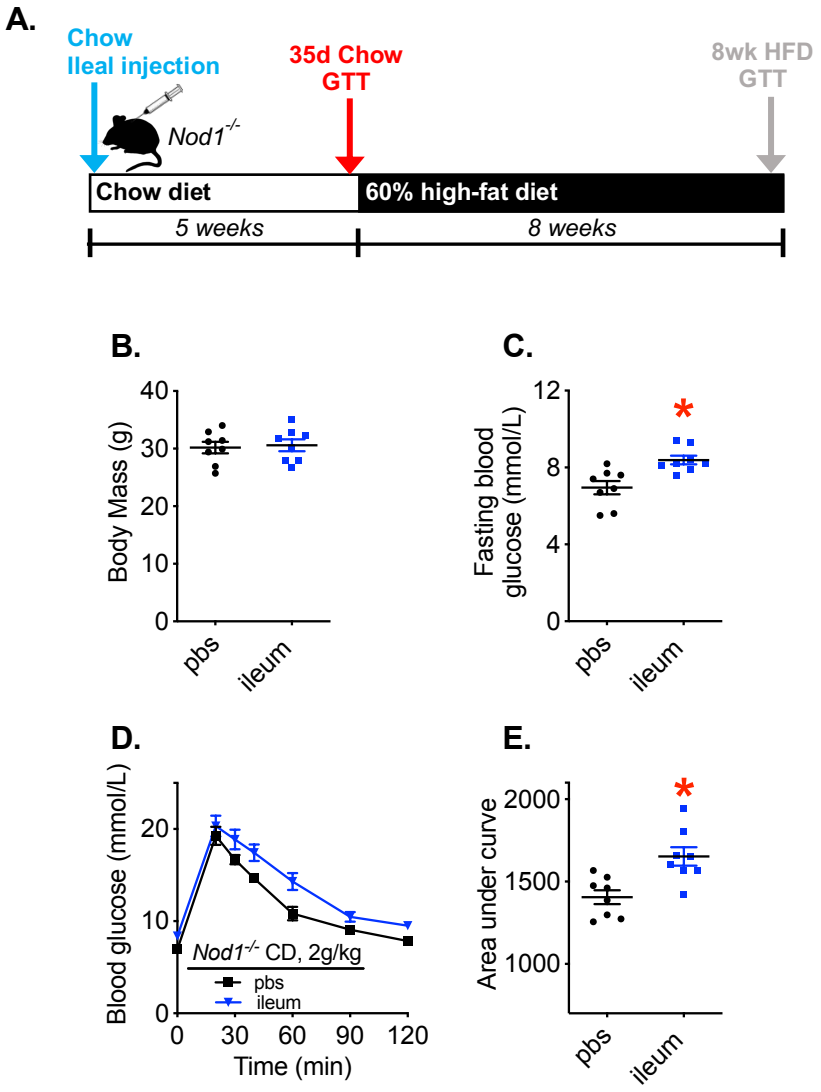

Figure 3.3.24 NOD1 protects against deleterious glucose control following ileal extract injection

A) Experimental model of *Nod1*$^{-/-}$ recipient mice fed a chow diet and injected with ileal extracts (200µL, s.c., diluted 5000x) collected from chow-fed donor mice. Glucose metabolism was assessed by GTT 35 days after immunization. B) Body mass, C) Fasting blood glucose, D) Blood glucose vs. time, and E) Quantified area under the curve during GTT (2g/kg, n=8/group). Values are mean ± SEM. *denotes statistical differences between groups ($p<0.05$).

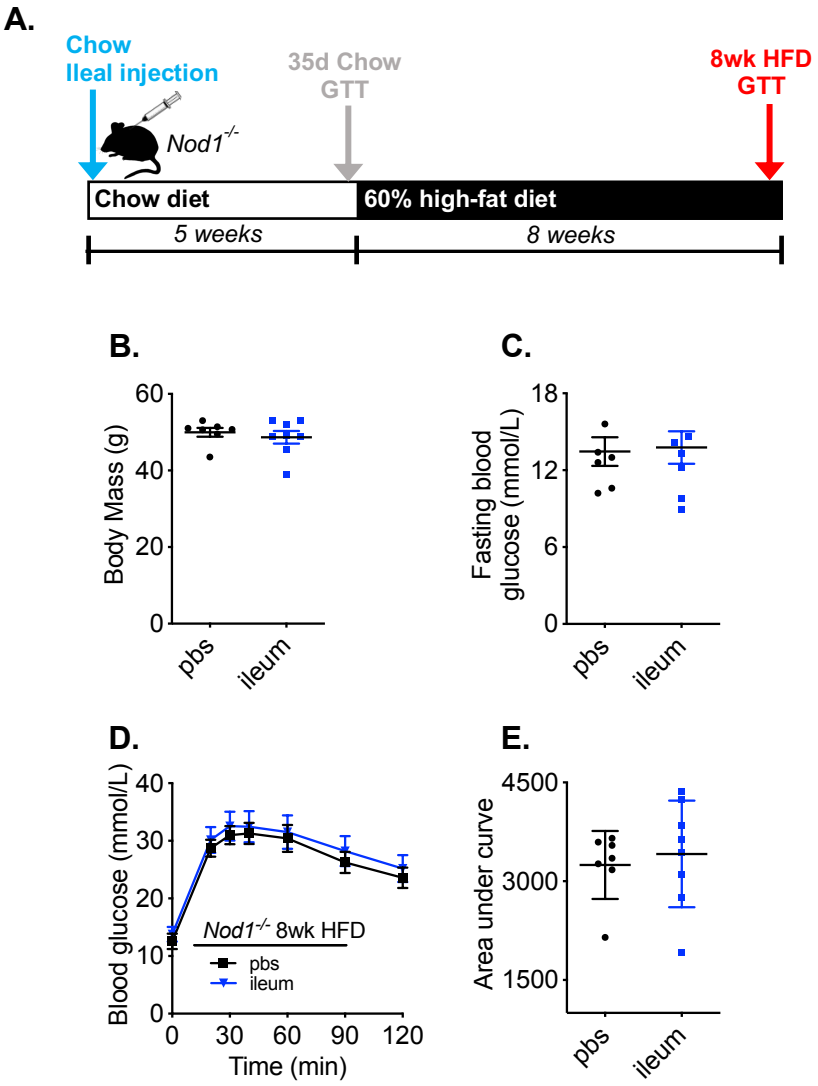

Figure 3.3.25 Changes in blood glucose control are absent after 8 weeks of HFD in *Nod1*$^{-/-}$ mice

A) Experimental model of *Nod1*$^{-/-}$ recipient mice previously injected with ileal extract during chow-feeding. 35 days later, mice were switched to a HFD for 8 weeks and glucose metabolism was assessed by GTT. B) Body mass, C) Fasting blood glucose, D) Blood glucose vs. time, and E) Quantified area under the curve during GTT (1g/kg, n=13-15/group). Values are mean ± SEM. *denotes statistical differences between groups ($p<0.05$).

3.3.7 Quantification of bacterial 16S rRNA in intestinal extracts

Finally, as an assay for estimating total bacterial load in each extract, we quantified bacterial 16S rRNA using qPCR in nucleotides extracted from upper gut extracts derived from conventionalized mice and germ-free mice. The concentration of 16S rRNA in upper gut extracts (duodenal/jejunal extracts or ileal extracts) from specific pathogen free *Wt* mice that harbour a microbiota was 0.7038 ± 0.7962 ng/μL. The concentration of 16S rRNA signal that was obtained in germ-free upper gut extracts was 0.0183 ± 0.02969 ng/μL, which represents the background or level of bacterial contamination during the procedure, reagents and assay (Figure 3.3.26, A).

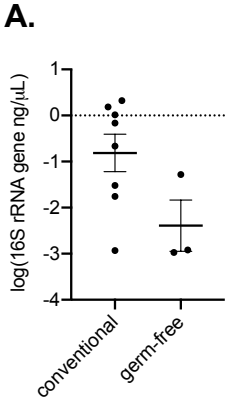

Figure 3.3.26 Quantification of 16S rRNA in intestinal extracts

A) Quantification of 16s rRNA concentration using broad range 16S qPCR in upper gut extracts (derived from duodenum/jejenum or ileum) in *Wt* conventionalized vs. germ-free mice as a estimate of total bacterial load present in intestinal extracts (n=6 conventionalized upper gut extracts, n=3 germ-free upper gut extracts).

CHAPTER 4: Discussion

4.1 Kinase inhibitors of RIPK2 and NOD-mediated immunometabolism

Clinical observations of diabetic cancer patients have revealed that treatment with certain TKIs can lower blood glucose despite various growth factor and oncogenic-related targets of different TKIs[271,273,275,277,319–321]. In addition to different designed targets of TKIs, understanding off-target effects of specific TKIs and can mitigate deleterious drug consequences, but it also provides the opportunity to re-task approved drugs[322,323]. Diabetes and cancer are prevalent causes of morbidity and mortality worldwide and epidemiologic evidence suggests that people with diabetes are at significantly higher risk for many types of cancer[324]. Thus, developing an understanding of how TKIs alter metabolic pathways, such as glucose and insulin homeostasis, via on- or -off target kinase inhibition is important for both safe and effective application in clinical settings, but also to evaluate the potential for re-tasking clinically approved TKIs for metabolic disease. Investigating how specific TKIs can alter inflammatory responses relevant to blood glucose regulation is required to advance the therapeutic potential for different TKIs in metabolic disease and may reveal mechanisms of how TKIs work in cancer by altering metabolism. TKIs have a diverse yet overlapping catalog of kinase targets and understanding the effects of various subsets of TKIs on critical nodes in immunity and metabolism could prioritize the development strategy of these drugs for treatment of metabolic diseases, including diabetes.

TKIs can exert anti-inflammatory effects, and there is a growing interest in expanding the utility of TKIs to combat inflammatory disease[240,241,249–252,254,325]. It

is plausible that TKI-induced changes in inflammatory status mediate effects on blood glucose regulation and insulin resistance, but it is not yet clear which inflammatory pathways link certain TKIs to changes in metabolic homeostasis. TKIs have multiple off-target effects, including inhibition of RIPK2[262]. For example, TKIs designed to inhibit EGFR signalling have been identified as equipotent RIPK2 inhibitors and TKIs such as ponatinib or sorafenib are even more potent type II inhibitors of RIPK2[197,252,325]. TKIs that target RIPK2 are relevant to obesity-induced metabolic disease because RIPK2 propagates inflammatory signals in response to bacterial cell-wall derived PGN and different types of muropeptides of this bacterial cell wall component can promote dysglycemia via NOD1[60,190] or promote glucose-lowering effects via NOD2[193,311]. While RIPK2 is well known to propagate inflammatory signals in response to NOD1 or NOD2 activation, prior to the initiation of this research project, the role of RIPK2 in metabolic perturbations downstream of NOD1 or NOD2 had yet to be established. Thus, our first aim in this thesis project was to establish if RIPK2 was required for metabolic consequences of NOD1 and/or NOD2 signalling and investigate if certain TKIs (reported to inhibit RIPK2) could lower NOD1-mediated inflammation and attenuate related metabolic defects. It was not known if TKIs that targeted RIPK2 would lower NOD1-mediated dysglycemia or conversely if these TKIs would block the glucose-lowering and insulin sensitizing effects of MDP via NOD2 activation. We found that RIPK2 was required for NOD1 ligand-induced lipolysis and poor glucose control caused by NOD1 activation in mice. We also found that TKIs that

target RIPK2 could block NOD2 ligand-induced glucose-lowering during low-level endotoxemia in mice. By comparing gefitinib (which inhibits RIPK2) and imatinib (which does not inhibit RIPK2), we found that inhibition of RIPK2 was the defining characteristic of TKIs that attenuated PGN-induced changes in inflammation and metabolism regardless of the type of muropeptide in the bacterial cell wall.

Beyond RIPK2, there is evidence for the involvement of other proteins inhibited by TKIs in pre-diabetes and diabetes, such as c-Abl, PDGFR, EGFR and VEGFR2, which are all common targets of various TKIs. It is shown that inhibition of c-Abl can protect pancreatic β cells from apoptosis-promoting agents *in vitro* and enhances basal and glucose-stimulated insulin production in a mouse β cell line[292,326]. The PDGF-PDGFR pathway can mediate β cell proliferation in mice and humans and inhibition of PDGFR has been shown to promote adipogenesis and adiponectin secretion in human mesenchymal stromal cells[327,328]. Furthermore, VEGFR inhibition reduces T-cell migration and pancreatic insulitis in spontaneously diabetic Torii rats[329]. However, one important limitation is that only considering a TKIs designed target kinase or even just the most potent kinase target neglects consideration of the multitude of other kinases and pathways affected by TKI treatment. For example, treatment of diet-induced obese mice with PD153035 reduces M1 macrophage infiltration into adipose tissue and improves insulin sensitivity[283]. It was hypothesized that inhibition of EGFR (the main target PD153035 is designed against) underlies the observed therapeutic effects. However, we show that PD153035 is an effective inhibitor of NOD1 signalling at relevant

concentrations, among many other off-target effects of PD153035[262]. To abate confounding targets of TKIs, we based the initial experiments on data from a comprehensive analysis of how kinase inhibitors alter the activity of the majority of human kinases[262], and then used genetic knockout mouse models to determine that our results were specific to RIPK2, NOD1 or NOD2. We used a reductionist approach to determine if certain TKIs attenuated lipolysis and metabolic tissue inflammation in response to a single microbial-based inflammatory trigger (i.e. bacterial cell wall-derived PGN). We directly compared a muropeptide that activates NOD1 to another bacterial cell wall component, LPS, that promotes inflammation and lipolysis by acting on TLR4[330–333]. LPS-induced lipolysis and LPS-induced inflammation do not require RIPK2. Hence, this comparison yielded important insight into how TKIs could contribute to metabolic inflammation because only TKIs with a reported inhibitory effect on RIPK2 attenuated inflammation and lipolysis in response to NOD1, but these TKIs did not alter LPS-induced effects.

It is important to understand how immune pathways underpin TKI-induced changes in glycemia because different immune responses can either promote or protect against insulin resistance and dysglycemia. Our results show that RIPK2 is required for NOD1-mediated inflammation and dysglycemia, and that certain TKIs, such as gefitinib, block bacterial cell wall PGN-induced inflammation and lipolysis in adipocytes and inflammation in macrophages (Figure 4.1).

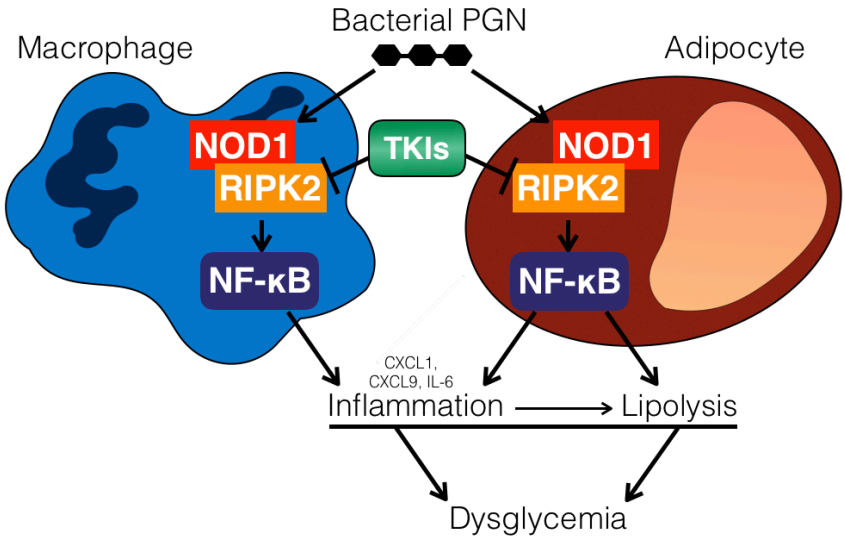

Figure 4.1 Tyrosine kinase inhibitors of RIPK2 attenuate NOD1-mediated immunometabolism

Inflammatory and metabolic effects of TKIs that inhibit RIPK2 in adipocytes and macrophages. RIPK2 is required for increased inflammatory cytokine production and lipolysis induced by bacterial peptidoglycan that acts on NOD1. Certain tyrosine kinase inhibitors (ie. gefitinib) inhibit RIPK2 in both macrophages and adipocytes thereby suppressing lipolysis, reducing inflammation and attenuationg dysglycemia caused by bacterial cell wall components.

Activation of NOD1 activation induces pro-inflammatory pathways leading to production of cytokines and chemokines such as TNFα and CXCL1, CXCL9 and CXCL10 in immune cells, adipocytes and hepatocytes[60,334]. In preliminary experiments, we took advantage of SB203580, an established RIPK2 inhibitor[335]. We show that numerous TKIs are more potent than SB203580 in attenuating NOD1-mediated lipolysis. We also show that SB203580 inhibits both NOD1 and LPS-induced responses in metabolic and immune cells. SB203580 has also been shown to be effective in attenuating TNFα-induced insulin resistance in endothelial

cells via p38 inhibition, demonstrating lack of specificity of this inhibitor for RIPK2[336]. In contrast, all of our results were consistent with the TKI gefitinib attenuating only NOD1-mediated inflammation and lipolysis, but gefitinib did not alter LPS-induced responses. These results show the specificity of gefitinib for NOD/RIPK2 responses compared to those for endotoxin.

It is important to consider multiple sources and triggers of inflammation in metabolic disease, including bacterial cell wall components such as muropeptides and LPS, since obesity-related metabolic endotoxemia can promote dysglycemia[178]. When probing the effects of NOD1-mediated dysglycemia, our model demonstrates that activation of NOD1 lowers fasting blood glucose coincident with significant glucose intolerance (i.e. increase in blood glucose levels in response to a glucose challenge). The mechanisms for divergent changes in fasting glucose versus glucose tolerance are unknown. However, it is noteworthy that many inflammatory triggers, such as LPS, promote insulin resistance and glucose intolerance, while simultaneously lowering fasting glucose[337,338]. NOD1 ligand-mediated changes in blood glucose are similar to glucose responses observed during acute endotoxemia. Acute, transient decreases in fasting blood glucose from both of these inflammatory triggers could occur through increased insulin-independent glucose utilization during inflammation. Acute LPS exposure lowers the expression and activity of enzymes involved in glucose production, such as glucose-6-phosphatase (G6Pase) and phosphoenolpyruvate carboxykinase (PEPCK)[339]. Furthermore, NF-κB is induced following LPS exposure, which can further limit glucose production by

nitric oxide production and desensitization to glucagon, leading to hypoglycemia[339,340]. Interestingly, TNFα can also stimulate the same effect as acute LPS exposure, although neutralization of TNFα does not completely reverse the metabolic alterations that arise in response to endotoxin challenge[341]. This is interesting because these results and our experiments using NOD1 ligands and TKIs that inhibit RIPK2 all suggest that at least part of the effect of bacterial sensing in adipocytes (either NOD1-activating muropeptides or LPS activating on TLR4) to increase lipolysis is through direct actions on PRRs within adipocytes rather than secondary effects mediated by secreted cytokines that could come from adipocytes or other immune cells that reside in adipose tissue.

Augmented pro-inflammatory cytokines and MAPK activation induced by inflammatory triggers leads to reduced insulin signalling, which manifests as impaired phosphorylation of IRS-1, Akt and AS160, and reduces insulin-stimulated glucose transport and inhibits suppression of lipolysis[342]. We speculate that many mechanisms underlying NOD1-induced glucose lowering are analogous to those postulated for LPS, including NF-κB activation and overlapping profiles of cytokine release, contributing to alterations in glucose homeostasis. Our results are consistent with this model since a NOD1 ligand activated NF-κB and lowered phosphorylation of Akt in adipocytes, but the RIPK2-inhibitory TKI gefitinib attenuated these NOD1-mediated effects on inflammatory and insulin signalling.

Certain TKIs can lower blood glucose in some, but not all individuals and mechanisms underlying heterogeneity in the patient response is lacking[343]. The

causes of obesity and diabetes are multifactorial, and there are limitations in applying these findings broadly to metabolic disease. Inflammation can participate in insulin resistance during chronic obesity, but it is dispensable for short-term diet-induced insulin resistance[344]. Also, long-term but not short-term exposure to the microbiota from obese mice promotes host insulin resistance[345]. It is also important to consider compartmentalization of immune responses in different tissues during obesity, which is positioned to dictate PAMP or DAMP-related insulin resistance or protection from excessive insulin resistance[125,126]. *Therefore, both the duration of obesity and site-specific inflammation may dictate if a certain TKI alters blood glucose.* In addition, many triggers of inflammation do not depend on RIPK2. We show here that endotoxin-induced inflammation occurs independently of RIPK2, and this is consistent with previous reports showing that RIPK2 mediates NOD1 or NOD2, but not TLR-induced inflammation[199]. We extend these findings to metabolic cells such as adipocytes and show that gefitinib only inhibits NOD1-ligand, but not TLR4 ligand-induced inflammatory and lipolysis.

Within RIPK2-dependent signalling pathways, work from our lab and others have previously shown divergence in NOD1 versus NOD2-mediated effects on obesity-related metabolic inflammation and dysglycemia signalling pathways[60,139,193,196,311]. Acute activation of NOD2 with MDP prior to endotoxin has an insulin sensitizing effect and lowers blood glucose during a glucose challenge[193,311]. Having first shown that RIPK2 inhibition by TKIs attenuates NOD1-mediated metabolic defects, we next wanted to determine if the same TKIs

could block potential insulin sensitizing effects of NOD2 activation. We found that RIPK2 was required for NOD2-mediated glucose lowering during endotoxemia, and that TKI gefitinib, but not imatinib, blocked the glycemic consequences of NOD2 activation. This was an important consideration for future research goals that aimed to investigate the effect of RIPK2-specific and non-RIPK2 specific TKIs in obesity. The cross talk between different cell types and magnitude of contributions of NOD1 versus NOD2 immunometabolism in modifying glycemic control during obesity are not well understood. Thus, the potential value for targeting RIPK2 therapeutically in diabetes depends on the relative importance of pro-inflammatory NOD1 signalling compared to anti-inflammatory NOD2 signalling and their individual contributions to glycemic control and insulin sensitivity in metabolic disease states. It is plausible that TKIs that do not inhibit RIPK2, such as imatinib, possess greater therapeutic potential in diabetes treatment because therapeutic contributions from NOD2 signalling remains intact. Conversely, it is also plausible that inhibition of RIPK2 by certain TKIs, such as gefitinib, may mediate their therapeutic benefit via attenuation of metabolically deleterious contributions of NOD1 signalling. The source of the inflammation and RIPK2 should be considered in the multifactorial causes and pathways involved in metabolic inflammation and blood glucose control, which can be altered by specific TKIs.

4.2 Metabolic effects of kinase inhibitors during obesity

In addition to their designated kinase target, TKIs inhibit many off-target kinases and this may underpin their divergent effects on blood glucose and insulin. The next aim of this work was to understand how RIPK2 modifies the effects of certain TKIs on blood glucose and insulin during diet-induced obesity in mouse models. We previously demonstrated that the TKI gefitinib attenuates both NOD1-mediated adipocyte lipolysis and dysglycemia in mice, which are hallmarks of metabolic disease. We initially hypothesized that inhibition of the NOD1-RIPK2 signalling axis would contribute to the beneficial effect of the TKI gefitinib on glycemia during obesity. However, RIPK2 is also required to propagate downstream signalling from NOD2 and work from our lab has already shown that MDP is an insulin-sensitizing postbiotic that engages NOD2[193,311]. The overall effect of RIPK2 depends on the relative importance of NOD1 signalling compared to NOD2 signalling and their combined contributions to glycemic control and insulin sensitivity in metabolic disease states, which is not well understood.

We investigated the effects on blood glucose during a glucose challenge in cohorts of *WT*, *Nod1*$^{-/-}$, *Nod2*$^{-/-}$ and *Ripk2*$^{-/-}$ mice. Contrary to our initial hypothesis, gefitinib treatment improved glucose control in all the obese mice that we tested, indicating that this TKI lowers blood glucose independent of NOD1, NOD2 or RIPK2. Interestingly, gefitinib treatment lowered plasma insulin during a glucose challenge, but this was only observed in *Ripk2*$^{-/-}$ mice treated with gefitinib. This is an important stand-alone result since lowering of hyperinsulinemia (especially with

coincident lowering of blood glucose) is positioned to attenuate both insulin resistance and obesity and possibly even diabetic complications[52,54,346]. Thus, these results suggest that deletion of RIPK2 improves the insulin sensitizing effect of this TKI because glucose-lowering occurs concurrently with lower blood insulin in *Ripk2*$^{-/-}$ mice treated with gefitinib. An alternative possibility is that deletion of RIPK2 increases drug availability for other kinases.

We next tested imatinib in obese HFD-fed mice, since this TKI has no reported inhibitory activity against RIPK2 *in vitro*[262]. We previously demonstrated that imatinib does not inhibit glycemic or lipolytic consequences of NOD1-RIPK2 signalling[190], nor glycemic consequences of NOD2-RIPK2 signalling. Imatinib lowered obesity-induced glucose tolerance, but *increased* insulin secretion during glucose challenge. This data suggests that imatinib works through a mechanism distinct from gefitinib to improve glycemic control during obesity. Imatinib reduces blood glucose levels but increases glucose-stimulated insulin secretion whereas gefitinib lowers blood glucose levels without a concomitant increase in insulin. Augmented insulin secretion by imatinib is consistent with reports that inhibition of c-Abl, either with imatinib or c-Abl siRNA knockdown, enhances insulin secretion in β-cell *in vitro*[292]. Furthermore, two case reports in cancer patients being treated with the TKIs dasatinib and sunitinib, which inhibit c-Abl to a similar or greater degree compared to imatinib, have been reported to increase serum c-peptide levels (a marker of insulin secretion)[274,279]. It has been proposed that imatinib alleviates specific cellular-stress mechanisms that offer protection against

β-cell failure and prolongs or enhances the ability of the pancreas to secrete high amounts of insulin to counter insulin resistance at the level of the tissues. Beyond improved glycemic control, assessing a TKI's individual effect on insulin is an important consideration when re-tasking TKIs as a therapeutic for obesity-induced insulin resistance or diabetic complications. Hyperinsulinemia itself has been implicated in the pathogenesis of insulin resistance and increasing evidence suggests high circulating insulin levels promote obesity, metabolic dysfunction and stress responses within insulin secreting or insulin responsive cells[53,55,80,347].

Additional molecular targets common to many TKIs have been investigated, such as PDGFRβ and c-Kit. In studies that investigated the anti-hyperglycemic effects of imatinib and sunitinib in models of Type 1 Diabetes, glucose lowering effects were replicated by specific antibodies to PDGFRβ, but not c-Kit , suggesting that PDGFRβ inhibition may play a role in mediating some antidiabetic effects, at least in animal models of Type 1 Diabetes[284,285]. Interestingly, gefitinib does not have reported inhibitory activity against c-Kit or PDGFRβ[262]. Treatment with gefitinib or imatinib did not result in widespread changes in gene expression of inflammatory- and ER stress-related markers in metabolic tissues. Based on the numerous targets of each TKI, it is plausible that different TKIs work through different mechanisms to exert divergent effects on insulin secretion versus improved insulin sensitivity in peripheral tissues to manifest effects on blood glucose regulation.

It is important that all our results using gefitinib or imatinib occurred despite no change in body mass or adiposity. We used male mice with obesity established after 10 weeks of HFD for experiments involving repeated treatment with TKIs. We confirmed that our selected doses did not impact food consumption, body mass, or adiposity in obese mice across the duration of the treatment period. It is possible that the doses used here would alter body mass in other mouse models. Despite the dose of imatinib required to improve blood glucose (250mg/kg) being 5-fold higher than the dose of gefitinib (50mg/kg), comparable serum concentrations were observed after the 8th treatment (6.167 ± 1.308 μg/mL and 4.257 ± 0.165 μg/mL, respectively), at which point glucose control was assessed in all mice.

We previously showed that RIPK2 was the defining factor that mediated changes in blood glucose caused by bacterial muropeptides, but here we demonstrate that NOD-RIPK2 signalling is not the defining molecular target of TKIs that underpins their effects on blood glucose in obese mice. Multiple TKIs, including gefitinib and imatinib, lower blood glucose in obese mice, independent of RIPK2. However, RIPK2 participated in TKI-induced lowering of blood insulin in response to an oral glucose load. Thus, RIPK2 can discriminate the effects of some TKIs on insulin, but ultimately, the molecular target(s) that promote glucose-lowering remain elusive. Our data provides evidence that RIPK2 is a target that limits the insulin sensitizing potential of certain TKIs. Furthermore, we show different TKIs, including ones that do not inhibit RIPK2, such as imatinib, can manifest improved blood glucose control via different mechanisms including

augmented insulin secretion (Figure 4.2). It is possible that other TKIs that work via the same molecular target(s) as gefitinib to lower blood glucose, but do not inhibit RIPK2, could be well-positioned to lower blood glucose *and* lower blood insulin.

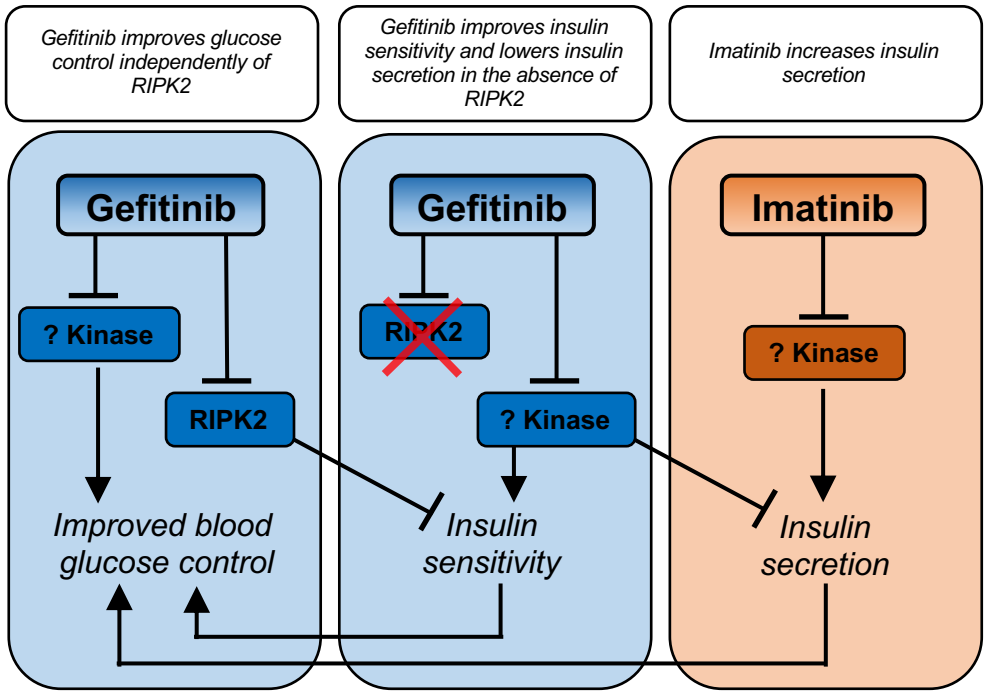

Figure 4.2 Inhibition of RIPK2 limits the insulin sensitizing potential of a TKI

TKIs operate independently of NOD1-RIPK2 or NOD2-RIPK2 signalling to lower blood glucose. TKIs, such as gefitinib, that inhibit RIPK2 signalling lower glucose stimulated insulin secretion only in obese *Ripk2*$^{-/-}$, but not WT mice. RIPK2 inhibition limits the ability of gefitinib to simultaneously lower insulin and glucose and hence, limits the insulin sensitizing potential of this TKI. Other TKIs, such as imatinib decrease blood glucose in obese mice by increasing insulin secretion to achieve lower blood glucose, independent of actions on RIPK2.

The ability of TKIs and their targets to lower both insulin and glucose warrants further investigation for re-tasking TKIs in diabetes treatment. Because

each TKI has its own unique profile of selectivity and specificity, we propose individual TKIs being investigated for diabetes should be evaluated for their effects on blood glucose control and insulin dynamics, as well as their potential to inhibit RIPK2. Taken together, our results suggest that an in-depth exploration of how TKIs alter *both* insulin and glucose metabolism is necessary to efficiently harness the therapeutic potential of these drugs in obesity and diabetes.

4.3 Upper intestinal commensal microbe components alter glucose homeostasis via NOD-RIPK2

Previous work from our lab has identified MDP as a potent microbial-derived insulin sensitizing postbiotic that requires intact NOD2 signalling to improve diet-induced inflammation and metabolic dysfunction[193,311], and further work has shown these effects to be dependent on RIPK2[311]. Hence, we shifted the focus of our work from drugs (i.e. TKIs) back to microbes, but within the final thesis chapter we investigated the effects of crude extracts from entre bacterial community resident in the gut instead of purified muropeptides. We became interested in work published by a collaborating lab that demonstrated injection of mice with the luminal contents collected from ileal segments protected against diet-induced glucose intolerance and insulin resistance[228]. However, the "sensitizing" factor present in the extracts and the host receptors required for alterations in blood glucose were not defined in this previous work. Given our lab's data demonstrating that microbially-derived MDP promotes glucose and insulin tolerance, we sought

to determine if glucose and insulin tolerizing effects of intestinal injection were dependent on the presence of gut microbes, and if these effects were mediated by NOD2-RIPK2 signalling axes.

The experimental design established by Pomie, et al.[228] involved a single injection of dilute luminal ileal contents 35 days prior to initiating HFD-feeding, and glucose tolerance was assessed after 1 and 2 months of HFD. Interestingly, we assessed glucose tolerance in chow-fed mice 35 days after a single injection, *prior* to switching to HFD-feeding, and observed that lean mice that received an injection of ileal contents had lower blood glucose during a GTT (i.e. our 'Chow Injection' model). Importantly, this established the efficacy of our ileal extracts to lower blood glucose. The initial work done by Pomie, et al.[228] utilized a diabetogenic HFD containing 72% fat and <1% carbohydrate that favours rapid development of hyperglycemia without significant body weight gain[313–315]. However, after assessing glucose tolerance in lean mice, we chose to investigate if there was a protective effect of intestinal injection in the context of obesity by using a 60% HFD that promotes rapid and durable weight gain (i.e. our 'HFD Injection' model). However, we found that a single injection of ileal contents was insufficient to improve glucose control after an addition 4 weeks of HFD feeding. There are many reasons that could explain the difference in our results compared to improvements in glucose control that lasted upwards of 2 months of HFD-feeding on the diabetogenic diet by others[228]. One possibility is that a single exposure to luminal

ileal contents (by injection) is insufficient to protect against diet-induced hyperglycemia when coincident with obesity.

Pomie, et al.[228] showed that the intestinal injection protocol induced the proliferation of CD4 and CD8 T cells in lymphoid organs followed by the development of immunological memory, and the glucose tolerance phenotype was transmissible via adoptive transfer of immune cells from injected mice into naïve recipient mice. This demonstration of microbe-immune axis providing strong evidence that the observed glycemic effects were mediated by the adaptive immune system. Given the timing required for involvement of the adaptive immune system, which is generally 30 days[348], we tested if an earlier time point after injection did not alter glycemia. We assessed glucose tolerance 7 days after intestinal injection (i.e. an early time point preceding activation of the adaptive immune response) in our Chow Injection model and found no differences in blood glucose between control mice and mice injected with ileal contents. Considering the involvement of the adaptive immune response and immunological memory was important in establishing a subsequent HFD model of intestinal injection because we hypothesized that a second intestinal injection event during obesity could possibly trigger an immunological memory and re-establish the glucose-lowering phenotype previously observed during chow diet-feeding. Thus, in our HFD Injection model, we delivered a second identical injection of luminal contents after 8 weeks of HFD-feeding and assess glucose tolerance 4 weeks later, after 12 weeks of HFD-feeding. We found that obese mice that received a second injection of ileal contents had

improved glucose control 4 weeks after the injection and after a total of 12 weeks of HFD feeding, which suggests that immunological memory (or another mechanism) engaged by a second injection is particularly important in mediating the glycemic response to intestinal injection during obesity. Furthermore, we tested a cohort of naïve obese mice (i.e. *did not* receive an injection of ileal contents prior to HFD-feeding). In contrast to obese mice that had received a secondary injection of ileal contents at 8 weeks of HFD, a single injection of ileal contents at 8 weeks of HFD was insufficient to promote glucose tolerance at 12 weeks in these mice. One of our most interesting results is the fact that 2 injections of ileal contents lowered blood glucose during a GTT even after prolonged diet-induced obesity (i.e. 16 weeks of HFD). Taken together, these data suggest immunological memory (or another mechanism) in response to repeated exposure to the cocktail of factors present in an extract made from ileal contents of mice rather than the timing of ileal injection, is the key factor in promoting glucose tolerance during obesity. It is enticing to speculate that a critical factor determining glycemic effects of ileal injection during obesity is how repeated injections involve initial exposure to an antigen followed by a boost injection containing the previously-introduced antigen, similar to vaccination strategies. Although we assessed glucose tolerance 7 days after the first ileal injection during chow-feeding, glucose tolerance wasn't assessed any earlier than 4-weeks after the secondary injection in our models of intestinal luminal extracts in HFD-fed mice. It would be interesting to determine if improved glucose control occurs sooner after administration of the second ileal contents

injection (during obesity) as a result of more rapid and robust activation of adaptive immunity due to a potential immunological memory response.

We also sought to assess the effect of intestinal luminal extracts on insulin tolerance in mice using our Chow Injection model. An ITT was performed after 42 days, one week after the 35-day GTT, and no effect of ileal injection on insulin tolerance was observed. However, an effect on insulin tolerance can't be entirely ruled out at the 35-day time-point, when glucose tolerance is also present. We conducted this test a week later because recurrent fasting within a week could have promoted weight loss and improved insulin sensitivity in mice[349].

We next attempted to resolve which host receptors that mediate the glucose-lowering effects of injection of intestinal luminal extracts. We found that, in contrast to WT mice, *Nod2*$^{-/-}$ mice were refractory to improved glucose control after injection of intestinal luminal contents. MDP is the ligand for NOD2 and our result in *Nod2*$^{-/-}$ mice suggests that MDP may be a component of ileal extracts that promotes lower blood glucose during a GTT. Our previously established demonstrates that 3 consecutive injections of MDP can acutely lower blood glucose during a GTT in obese mice by the 4th day in HFD-fed mice[193,311], but the durability of these changes had not been tested. Thus, we tested the durability of the MDP phenotype following 3 consecutive injections and found 3 MDP injections caused lower blood glucose during a GTT that also persisted for 4 weeks. A single injection of intestinal luminal extracts lowers blood glucose during a GTT 4 weeks after the injection in chow fed mice. In contrast, when we tested a single injection of MDP,

in the same style/protocol as a single injection of intestinal luminal extracts in HFD-fed mice, we found it acutely raised blood glucose during a GTT 1 day later, and had no long-lasting effects on glycemia after 4 weeks. This data consistent with a model where multiple administrations of MDP or injection of intestinal luminal extracts tolerizes the immune system to subsequent stressors (i.e. diet-induced obesity), but it appears that MDP is not a stand-alone, critical component of intestinal extracts that is sufficient to cause the improvements in glucose tolerance. Nevertheless, NOD2 sensing of intestinal luminal contents is required for this cocktail of factors to improve glucose control after injection in mice.

Based on this, we next sought to test if injection of intestinal luminal extracts in *Ripk2*$^{-/-}$ mice, as we have previously shown *Ripk2*$^{-/-}$ mice are refractory to changes in blood glucose after repeated treatment with MDP[311]. We hypothesized that, injection of intestinal luminal extracts derived from the ileum would not alter blood glucose in *Ripk2*$^{-/-}$ mice, similar to *Nod2*$^{-/-}$ mice. Unexpectedly, we found that *Ripk2*$^{-/-}$ mice have higher blood glucose during a GTT following after injection with ileal extracts, and interestingly, when *Ripk2*$^{-/-}$ mice were switched to a HFD and left for 8 weeks, the higher blood glucose persisted in these obese *Ripk2*$^{-/-}$ mice. Based on the divergent phenotypes in *Nod2*$^{-/-}$ vs. *Ripk2*$^{-/-}$ mice, we hypothesized that a NOD1-RIPK2 signalling axis mediated the worse glucose control following ileal extract injection and next tested our ileal injection protocol in *Nod1*$^{-/-}$ mice. Similar to *Ripk2*$^{-/-}$ mice, *Nod1*$^{-/-}$ mice exhibited higher blood glucose during GTT after injection of intestinal luminal extracts.

We propose a model where the intestinal luminal contents contain a complex milieu of postbiotic components derived from the commensal microbiota that can either raise or lower glycemia, where NOD1-RIPK2 versus NOD2-RIPK2 immune responses dictate how these postbiotics control blood glucose. RIPK2 resides at the fulcrum of a signalling axes that dictates a long-lasting immune response to bacterial components and subsequent net effects on glycemic control. *Nod2*$^{-/-}$ mice are refractory to glucose lowering after intestinal extract injection, suggesting an unknown bacterial component works with MDP to lower glycemia via NOD2 signalling. It is not yet clear if and how MDP works with other postbiotics as a contributing factor to the NOD2-mediated blood glucose-lowering. In contrast, *Nod1*$^{-/-}$ and *Ripk2*$^{-/-}$ mice exhibit increased blood glucose following intestinal extract injection, suggesting that a NOD1-RIPK2 signalling axis protects against an unknown bacterial component that increases glycemia. In a *WT* mouse, with intact NOD2-RIPK2 signalling that promotes lowered blood glucose via intestinal injection, and intact NOD1-RIPK2 signalling that protects against increased blood glucose via intestinal injection, the net effect on glycemic control is observed as decreased blood glucose during GTT (Figure 4.3).

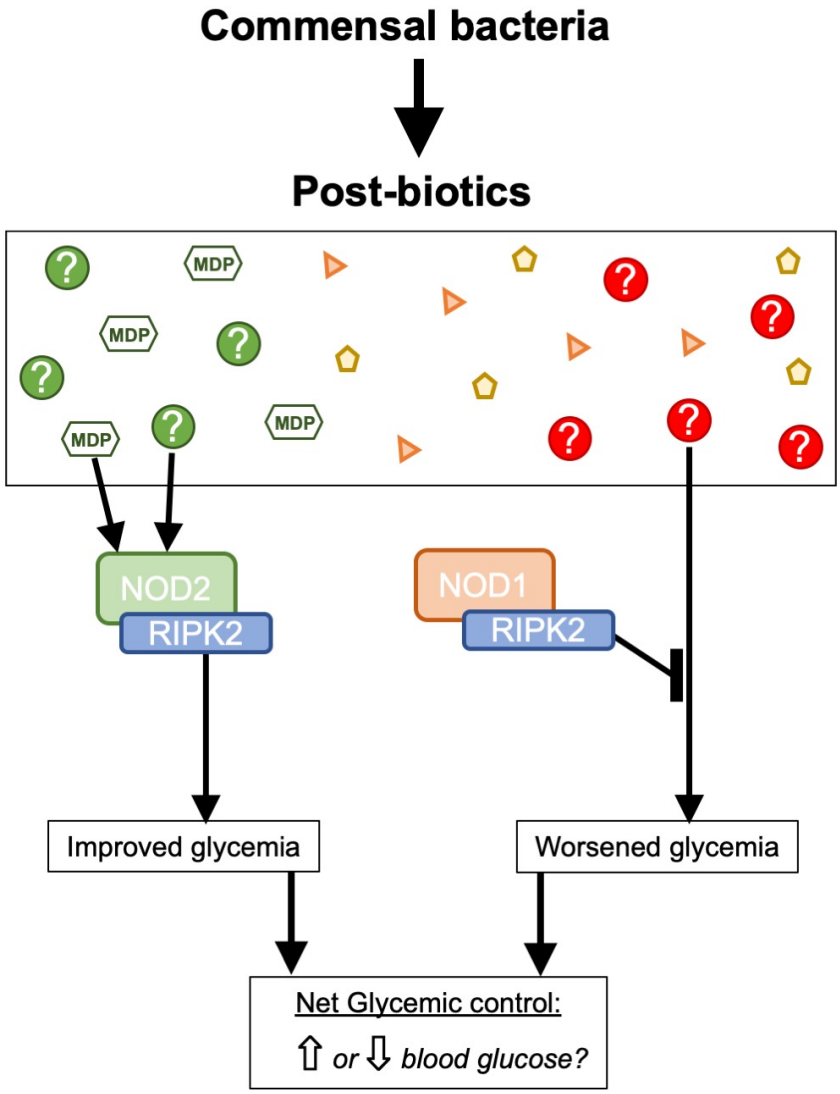

Figure 4.3 Post-biotic components derived from the microbiota can alter blood glucose homeostasis and is influenced by distinct NOD-RIPK2 signalling pathways

Different post-biotic components can improve or impair glycemic control. *WT* mice exhibit lower blood glucose in response to intestinal extract injection, but *Nod2*$^{-/-}$ mice are refractory to intestinal extract injection, suggesting an unknown bacterial component promotes lower glycemia via NOD2 signalling. In contrast, *Nod1*$^{-/-}$ and *Ripk2*$^{-/-}$mice exhibit increased blood glucose in response to intestinal extract injection, suggesting that a NOD1-RIPK2 axis protects against bacterial components that impair glucose control.

4.4 Research limitations and future directions

Data presented in this thesis relied on cell culture and mice and scrutiny of the models used is warranted. Work from our lab and others have previously shown that *Nod1*$^{-/-}$ mice are protected from insulin resistance during obesity[60,139], while inflammation and insulin resistance is exacerbated in obese *Nod2*$^{-/-}$ mice[196]. A study that compared *Ripk2*$^{-/-}$ mice to littermate control mice showed that RIPK2 deletion resulted in exacerbated obesity and worse insulin resistance when mice were fed a HFD[350]. These results should be considered in the context of this thesis. For example, testing glucose-lowering therapeutics in mouse strains (i.e. *Nod1*$^{-/-}$ mice) that are already protected from diet-induced glucose intolerance may prevent or mitigate the potential for observing differences between treatment and control groups. Our experiments showed that the dose and duration of gefitinib that we used caused improved glucose control and we were able to detect improved glycemic control with a TKI intervention in obese *Nod1*$^{-/-}$, *Nod2*$^{-/-}$ and *Ripk2*$^{-/-}$ mice.

Furthermore, recent awareness surrounding the influence of gut microbiota in metabolic and immune homeostasis has prompted the use of littermate mice as control for comparing the effect of gene deletions, especially when investigating the contribution of a specific gene to a phenotype[351]. As a control to overcome this limitation, we compared the effects of treatment and vehicle groups *within* a genotype for all experiments, never *between* multiple genotypes.

The majority of experiments in this thesis was performed in adult-aged male mice, which limits the applicability of results to different human populations. While

male mice were used exclusively in TKI studies to elucidate a role for NOD-RIPK2 signalling, clinical data demonstrates both male and female diabetic cancer patients have improved glycemic control during TKI therapy, suggesting that the observed glucose lowering effects observed in our TKI intervention model are likely not sex-specific. This is an important future direction to test in TKIs in males versus females across various times of the life-course.

The first and second aims of this research project elucidated important effects of TKIs during acute NOD1 or NOD2 activation and determined that NOD1-RIPK2 or NOD2-RIPK2 signalling axes do not contribute to the glucose-lowering actions of these drugs. However, we did not resolve a specific mechanism underlying the observed changes in glucose control by TKIs. We did not observe widespread changes in inflammatory or ER-stress expression profiles in key metabolic tissues (liver, adipose, muscle or pancreas) with TKI intervention, nor did we detect augmented insulin signalling in liver or adipose tissues, as suggested in previous reports[281–283]. Based on the divergence in TKI's effects on glucose and insulin, a more thorough analysis of how the pancreas could be mediating these effects is warranted. At the time these studies were performed, whole pancreas was collected and used for gene expression analysis. However, this is a limiting approach because pancreatic islet cell mass makes up a small fraction of the total pancreatic cell mass and thus, isolation and analysis of distinct pancreatic cell types could reveal important insights into how different TKIs have opposing effects on blood glucose and insulin levels.

Our data, in combination with other animal models of TKI treatment in T1D and T2D and clinical reports, highlight the heterogeneous effects various TKIs can have on blood glucose and blood insulin. This is a critical consideration when selecting TKIs for treating diabetic cancer patients and also for maximizing their therapeutic potential when investigating TKIs for metabolic disease treatment. Further research is needed to thoroughly examine an individual TKI's effects on blood glucose and blood insulin, and a critical understanding of the molecular pathways that underpin each TKI's effect on glucose and insulin is warranted.

The final aim of the research project investigated how postbiotic components derived from the commensal gut microbiota can alter blood glucose homeostasis via NOD-RIPK2 signalling pathways. Importantly, we have resolved some of the host receptors involved in mediated contrasting glycemic responses to intestinal immunization, but future work should aim to elucidate the postbiotic components that drive lower blood glucose, via NOD2 potentially synergizing with other innate immune receptors. Future work should aim to define postbiotics that drive increased blood glucose, via NOD1 in conjunction with other receptors. It will be important to link these innate immune responses to the adaptive immune responses, shown by others to be a critical node in relaying improved glucose control after injection of intestinal liminal contents[228].

An important limitation in our study was our experimental design when testing the glycemic effects of a single injection of MDP in HFD-fed mice and comparing to the glycemic effects of intestinal extracts in HFD-fed mice. Our

results demonstrate that 2 injections of intestinal luminal contents, separated by several weeks, is required to lower glycemia in HFD-fed mice (see Figure 3.3.9 and Figure 3.3.11). In contrast, when testing MDP, we only tested a single administration of MDP at 8 weeks of HFD in mice that had not had a prior injection of MDP (i.e. during chow feeding). Thus, an important future experiment to conduct is to replicate the exact experimental design used with ileal extracts to directly compare with MDP (i.e. a single administration of MDP during chow-feeding, 5 weeks before switching to HFD, and a second administration of MDP at 8 weeks of HFD before assessing glucose tolerance at 12 weeks of HFD. See Figure 3.3.3 for experimental design).

Future studies should focus on defining cell-specific-immune responses and tissues-specific metabolic responses to intestinal luminal contents injection. In addition, the sex-specific effects of intestinal luminal contents injection need to be better defined. We tested our intestinal injection protocol in a cohort of female mice and found that injection with ileal contents lowers blood glucose during a GTT in mice regardless of sex. Nevertheless, a detailed comparison of the source of intestinal luminal extracts from males versus females across different stages of the life course and their effects on both male and female mice after luminal extract injection is warranted.

4.5 Summary

The ultimate goal of this work aimed to understand how NOD-RIPK2 signalling axes mediate the effect of certain drugs (i.e. TKIs) or bugs (i.e. the effect of intestinal luminal contents injection) on blood glucose and insulin homeostasis. TKIs are a class of drugs that have been shown to significantly alter blood glucose control, but the mechanisms underlying these effects was ill-defined. While RIPK2 was well-established as a mediator that propagates inflammatory signals from NOD1 and NOD2, it was unknown if RIPK2 was required for the *metabolic* consequences of NOD1 or NOD2 signalling, particularly those modified by specific TKIs. We demonstrated that RIPK2 is required to mediate the acute effects of NOD1 or NOD2 signalling on glucose control, and showed that specific TKIs, such as gefitinib, attenuate NOD1-mediated inflammation, lipolysis and dysglycemia. We found that other TKIs, such as imatinib, do not alter the metabolic consequences of NOD1 activation. During obesity, we made the surprising finding that gefitinib improved glycemic control in *WT*, *Nod1*$^{-/-}$, *Nod2*$^{-/-}$ and *Ripk2*$^{-/-}$ mice. However, we found that inhibition of RIPK2 limits the insulin-sensitizing potential of gefitinib during obesity. Taken together, this suggests that inhibition of either NOD-RIPK2 signalling pathway by TKIs does not contribute to improved glycemic control, but that inhibition of RIPK2 by TKIs does alter dynamic insulin responses during a glucose load, which needs to be considered in diabetic cancer patients. When investigating the effects of imatinib, a distinct TKI that does not inhibit RIPK2, we found that imatinib lowered glucose but increased insulin during a glucose

challenge, providing evidence that various TKIs mat work in distinct mechanisms, via distinct kinase targets, to manifest their effects on blood glucose. This foundational information may help refine TKI design for potential re-tasking to treat T2D or its complications. Finally, we have demonstrated that injection of the luminal contents from the upper guts of mice can improve glucose control. We confirmed that microbes had to present in the gut for this improvement in glucose control and found that NOD-RIPK2 signalling axis dictates whether these microbial derived products improve or worsen blood glucose after injection into mice. Together, this work helps to characterize the immune pathways underlying microbial-mediated regulation of glucose and insulin homeostasis and contributes to an important understanding of the immune and metabolic consequences of NODs and RIPK2 in responding to microbial factors and tyrosine kinase inhibitors.

CHAPTER 5: References

1. Bentham, J. *et al.* Worldwide trends in body-mass index, underweight, overweight, and obesity from 1975 to 2016: a pooled analysis of 2416 population-based measurement studies in 128·9 million children, adolescents, and adults. *Lancet* **390**, 2627–2642 (2017).
2. Haslam, D. W. & James, W. P. T. Obesity. *Lancet* **366**, 1197–1209 (2005).
3. Aune, D. *et al.* BMI and all cause mortality: Systematic review and non-linear dose-response meta-analysis of 230 cohort studies with 3.74 million deaths among 30.3 million participants. *BMJ (Online)* **353**, i2156 (2016).
4. Pratley, R. E. & Weyer, C. The role of impaired early insulin secretion in the pathogenesis of Type II diabetes mellitus. *Diabetologia* **44**, 929–45 (2001).
5. Johnson, F. & Wardle, J. Variety, Palatability, and Obesity. *Adv. Nutr.* **5**, 851–859 (2014).
6. Owen, N., Sparling, P. B., Healy, G. N., Dunstan, D. W. & Matthews, C. E. Sedentary behavior: Emerging evidence for a new health risk. *Mayo Clinic Proceedings* **85**, 1138–1141 (2010).
7. Martínez-González, M. Á., Martínez, J. A., Hu, F. B., Gibney, M. J. & Kearney, J. Physical inactivity, sedentary lifestyle and obesity in the European Union. *Int. J. Obes.* **23**, 1192–1201 (1999).
8. Blüher, M. Obesity: global epidemiology and pathogenesis. *Nature Reviews Endocrinology* **15**, 288–298 (2019).
9. Choquet, H. & Meyre, D. Molecular Basis of Obesity: Current Status and Future Prospects. *Curr. Genomics* **12**, 154–168 (2012).
10. Montague, C. T. *et al.* Congenital leptin deficiency is associated with severe early-onset obesity in humans. *Nature* **387**, 903–908 (1997).
11. Clément, K. *et al.* A mutation in the human leptin receptor gene causes obesity and pituitary dysfunction. *Nature* **392**, 398–401 (1998).
12. Farooqi, I. S. *et al.* Dominant and recessive inheritance of morbid obesity associate with melanocortin 4 receptor deficiency. *J. Clin. Invest.* **106**, 271–279 (2000).
13. Krude, H. *et al.* Severe early-onset obesity, adrenal insufficiency and red hair pigmentation caused by POMC mutations in humans. *Nat. Genet.* **19**, 155–157 (1998).
14. Locke, A. E. *et al.* Genetic studies of body mass index yield new insights for obesity biology. *Nature* **518**, 197–206 (2015).
15. Mahajan, A. *et al.* Genome-wide trans-ancestry meta-analysis provides insight into the genetic architecture of type 2 diabetes susceptibility. *Nat. Genet.* **46**, 234–244 (2014).
16. Börjeson, M. The Aetiology of Obesity in Children: A Study of 101 twin

Pairs. *Acta Pædiatrica* **65**, 279–287 (1976).

17. Stunkard, A. J., Harris, J. R., Pedersen, N. L. & McClearn, G. E. The Body-Mass Index of Twins Who Have Been Reared Apart. *N. Engl. J. Med.* **322**, 1483–1487 (1990).
18. Panzeri, I. & Pospisilik, J. A. Epigenetic control of variation and stochasticity in metabolic disease. *Molecular Metabolism* **14**, 26–38 (2018).
19. Hu, Z. *et al.* Effects of maternal dietary patterns during pregnancy on early childhood growth trajectories and obesity risk: The CANDLE study. *Nutrients* **12**, (2020).
20. Xu, X. *et al.* A genome-wide methylation study on obesity: Differential variability and differential methylation. *Epigenetics* **8**, 522–533 (2013).
21. Aslibekyan, S. *et al.* Epigenome-wide study identifies novel methylation loci associated with body mass index and waist circumference. *Obesity* **23**, 1493–1501 (2015).
22. Wang, X. *et al.* An epigenome-wide study of obesity in African American youth and young adults: novel findings, replication in neutrophils, and relationship with gene expression. *Clin. Epigenetics* **10**, 3 (2018).
23. Rönn, T. *et al.* Impact of age, BMI and HbA1c levels on the genome-wide DNA methylation and mRNA expression patterns in human adipose tissue and identification of epigenetic biomarkers in blood. *Hum. Mol. Genet.* **24**, 3792–3813 (2015).
24. Wang, Q. *et al.* Brown adipose tissue activation is inversely related to central obesity and metabolic parameters in adult human. *PLoS One* **10**, (2015).
25. Carter, P. J., Taylor, B. J. & Williams, S. M. Longitudinal analysis of sleep in relation to BMI and body fat in children: the FLAME study. *BMJ* **342**, d2712 (2011).
26. Grandner, M. A., Schopfer, E. A., Sands-Lincoln, M., Jackson, N. & Malhotra, A. Relationship between sleep duration and body mass index depends on age. *Obesity* **23**, 2491–2498 (2015).
27. Domecq, J. P. *et al.* Drugs commonly associated with weight change: A systematic review and meta-analysis. *J. Clin. Endocrinol. Metab.* **100**, 363–370 (2015).
28. Duncan, D. T. *et al.* Characteristics of walkable built environments and BMI z-scores in children: Evidence from a large electronic health record database. *Environ. Health Perspect.* **122**, 1359–1365 (2015).
29. Papas, M. A. *et al.* The Built Environment & Obesity. *Epidemiol. Rev.* **29**, 129–143 (2007).

30. Heindel, J. J., Newbold, R. & Schug, T. T. Endocrine disruptors and obesity. *Nature Reviews Endocrinology* **11**, 653–661 (2015).

31. Ley, R. E. *et al.* Obesity alters gut microbial ecology. *Proc. Natl. Acad. Sci. U. S. A.* **102**, 11070–11075 (2005).

32. Backhed, F. *et al.* The gut microbiota as an environmental factor that regulates fat storage. *Proc. Natl. Acad. Sci.* **101**, 15718–15723 (2004).

33. Turnbaugh, P. J. *et al.* An obesity-associated gut microbiome with increased capacity for energy harvest. *Nature* **444**, 1027–1031 (2006).

34. Turnbaugh, P. J., Bäckhed, F., Fulton, L. & Gordon, J. I. Diet-Induced Obesity Is Linked to Marked but Reversible Alterations in the Mouse Distal Gut Microbiome. *Cell Host Microbe* **3**, 213–223 (2008).

35. Doré, J. & Blottière, H. The influence of diet on the gut microbiota and its consequences for health. *Current Opinion in Biotechnology* **32**, 195–199 (2015).

36. Ley, R. E. Obesity and the human microbiome. *Curr. Opin. Gastroenterol.* **26**, 5–11 (2010).

37. Cefalu, W. T. *et al.* Advances in the science, treatment, and prevention of the disease of obesity: Ref lections from a diabetes care editors' expert forum. *Diabetes Care* **38**, 1567–1582 (2015).

38. Bray, G. A. Effect of caloric restriction on energy expenditure in obese patients. *Lancet* **2**, 397–398 (1969).

39. Delany, J. P., Hansen, B. C., Bodkin, N. L., Hannah, J. & Bray, G. A. Long-Term Calorie Restriction Reduces Energy Expenditure in Aging Monkeys. *Journals Gerontol.* **54**, B5–B11 (1999).

40. Redman, L. M. *et al.* Metabolic and behavioral compensations in response to caloric restriction: Implications for the maintenance of weight loss. *PLoS One* **4**, (2009).

41. King, N. A. *et al.* Metabolic and behavioral compensatory responses to exercise interventions: Barriers to weight loss. *Obesity* **15**, 1373–1383 (2007).

42. Lark, D. S. *et al.* Reduced nonexercise activity attenuates negative energy balance in mice engaged in voluntary Exercise. *Diabetes* **67**, 831–840 (2018).

43. Leibel, R. L. *et al.* Biologic responses to weight loss and weight regain: Report from an American diabetes association research symposium. in *Diabetes* **64**, 2299–2309 (American Diabetes Association Inc., 2015).

44. Cohen, D. A. Neurophysiological pathways to obesity: Below awareness and beyond individual control. *Diabetes* **57**, 1768–1773 (2008).

45. Richard, D. Cognitive and autonomic determinants of energy homeostasis

in obesity. *Nature Reviews Endocrinology* **11**, 489–501 (2015).

46. Timper, K. & Brüning, J. C. Hypothalamic circuits regulating appetite and energy homeostasis: Pathways to obesity. *Dis. Model. Mech.* **10**, 679–689 (2017).
47. Ioannides-Demos, L. L., Proietto, J. & McNeil, J. J. Pharmacotherapy for obesity. *Drugs* **65**, 1391–1418 (2005).
48. Campbell, J. E. & Drucker, D. J. Pharmacology, Physiology, and Mechanisms of Incretin Hormone Action. *Cell Metab.* **17**, 819–37 (2013).
49. Drucker, D. J., Habener, J. F. & Juul Holst, J. Discovery, Characterization, and Clinical Development of the Glucagon-Like Peptides. *J. Clin. Invest.* **127**, 4217–4227 (2017).
50. Chang, S. H. *et al.* The effectiveness and risks of bariatric surgery an updated systematic review and meta-analysis, 2003-2012. *JAMA Surgery* **149**, 275–287 (2014).
51. Katzmarzyk, P. T. The Canadian Obesity Epidemic: An Historical Perspective. *Obes. Res.* **10**, 666–674 (2002).
52. Page, M. M. & Johnson, J. D. Mild suppression of hyperinsulinemia to treat obesity and insulin resistance. *Trends in Endocrinology and Metabolism* **29**, 389–399 (2018).
53. Page, M. M. *et al.* Reducing insulin via conditional partial gene ablation in adults reverses diet-induced weight gain. *FASEB J.* **32**, 1196–1206 (2018).
54. Templeman, N. M. *et al.* Reduced circulating insulin enhances insulin sensitivity in old mice and extends lifespan. *Cell Rep.* **20**, 451–463 (2017).
55. Szabat, M. *et al.* Reduced Insulin Production Relieves Endoplasmic Reticulum Stress and Induces β Cell Proliferation. *Cell Metab.* **23**, 179–193 (2016).
56. Butler, A. E. *et al.* β-cell deficit and increased β-cell apoptosis in humans with type 2 diabetes. *Diabetes* **52**, 102–110 (2003).
57. Jellinger, P. S. Metabolic consequences of hyperglycemia and insulin resistance. *Insulin* **4**, 2–14 (2009).
58. World Health Organization. *Global Report on Diabetes*. (World Health Organization, 2016).
59. Klip, A. & Pâquet, M. R. Glucose transport and glucose transporters in muscle and their metabolic regulation. *Diabetes Care* **13**, 228–243 (1990).
60. Schertzer, J. D. *et al.* NOD1 activators link innate immunity to insulin resistance. *Diabetes* **60**, 2206–15 (2011).
61. Nielsen, T. S., Jessen, N., Jørgensen, J. O. L., Møller, N. & Lund, S. Dissecting adipose tissue lipolysis: Molecular regulation and implications

for metabolic disease. *Journal of Molecular Endocrinology* **52**, (2014).

62. Czech, M. P., Tencerova, M., Pedersen, D. J. & Aouadi, M. Insulin signalling mechanisms for triacylglycerol storage. *Diabetologia* **56**, 949–964 (2013).
63. Saltiel, A. R. & Kahn, C. R. Insulin signalling and the regulation of glucose and lipid metabolism. *Nat. Insight* **414**, 799–806 (2001).
64. Keane, K. & Newsholme, P. Metabolic regulation of insulin secretion. in *Vitamins and Hormones* **95**, 1–33 (Academic Press Inc., 2014).
65. Jensen, M. V. *et al.* Metabolic cycling in control of glucose-stimulated insulin secretion. *American Journal of Physiology - Endocrinology and Metabolism* **295**, E1287 (2008).
66. Newsholme, P. & Krause, M. Nutritional Regulation of Insulin Secretion: Implications for Diabetes. *Clinical Biochemist Reviews* **33**, 35–47 (2012).
67. Newsholme, P., Gaudel, C. & McClenaghan, N. H. Nutrient regulation of insulin secretion and β-cell functional integrity. *Adv. Exp. Med. Biol.* **654**, 91–114 (2010).
68. Taniguchi, C. M., Emanuelli, B. & Kahn, C. R. Critical nodes in signalling pathways: insights into insulin action. *Nat. Rev. Mol. Cell Biol.* **7**, 85–96 (2006).
69. Van Obberghen, E. *et al.* Surfing the insulin signaling web. *Eur. J. Clin. Invest.* **31**, 966–977 (2001).
70. White, M. F. The IRS-signalling system: A network of docking proteins that mediate insulin action. in *Insulin Action* 3–11 (Springer US, 1998). doi:10.1007/978-1-4615-5647-3_1
71. Brüning, J. C., Winnay, J., Cheatham, B. & Kahn, C. R. Differential signaling by insulin receptor substrate 1 (IRS-1) and IRS-2 in IRS-1-deficient cells. *Mol. Cell. Biol.* **17**, 1513–1521 (1997).
72. Alessi, D. R. *et al.* Characterization of a 3-phosphoinositide-dependent protein kinase which phosphorylates and activates protein kinase Bα. *Curr. Biol.* **7**, 261–269 (1997).
73. Manning, B. D. & Toker, A. AKT/PKB Signaling: Navigating the Network. *Cell* **169**, 381–405 (2017).
74. Sano, H. *et al.* Insulin-stimulated phosphorylation of a Rab GTPase-activating protein regulates GLUT4 translocation. *J. Biol. Chem.* **278**, 14599–14602 (2003).
75. Puigserver, P. *et al.* Insulin-regulated hepatic gluconeogenesis through FOXO1-PGC-1α interaction. *Nature* **423**, 550–555 (2003).
76. Maehama, T. & Dixon, J. E. PTEN: A tumour suppressor that functions as a phospholipid phosphatase. *Trends in Cell Biology* **9**, 125–128 (1999).

77. Boucher, J., Kleinridders, A. & Kahn, C. R. Insulin Receptor Signaling in Normal and Insulin-Resistant States. *Cold Spring Harb. Perspect. Biol.* **6**, a009191 (2014).

78. Powell, D. J., Hajduch, E., Kular, G. & Hundal, H. S. Ceramide Disables 3-Phosphoinositide Binding to the Pleckstrin Homology Domain of Protein Kinase B (PKB)/Akt by a PKCθ-Dependent Mechanism. *Mol. Cell. Biol.* **23**, 7794–7808 (2003).

79. Copps, K. D. & White, M. F. Regulation of insulin sensitivity by serine/threonine phosphorylation of insulin receptor substrate proteins IRS1 and IRS2. *Diabetologia* **55**, 2565–2582 (2012).

80. Czech, M. P. Insulin action and resistance in obesity and type 2 diabetes. *Nat. Med.* **23**, 804–814 (2017).

81. Newgard, C. B. Metabolomics and Metabolic Diseases: Where Do We Stand? *Cell Metab.* **25**, 43–56 (2017).

82. Samuel, V. T. & Shulman, G. I. The pathogenesis of insulin resistance: Integrating signaling pathways and substrate flux. *Journal of Clinical Investigation* **126**, 12–22 (2016).

83. Aguirre, V. *et al.* Phosphorylation of Ser307 in Insulin Receptor Substrate-1 Blocks Interactions with the Insulin Receptor and Inhibits Insulin Action. *J. Biol. Chem.* **277**, 1531–1537 (2002).

84. Dresner, A. *et al.* Effects of free fatty acids on glucose transport and IRS-1-associated phosphatidylinositol 3-kinase activity. *J. Clin. Invest.* **103**, 253–259 (1999).

85. Roden, M. *et al.* Mechanism of free fatty acid-induced insulin resistance in humans. *J. Clin. Invest.* **97**, 2859–2865 (1996).

86. Gao, Z. *et al.* Serine phosphorylation of insulin receptor substrate 1 by inhibitor κB kinase complex. *J. Biol. Chem.* **277**, 48115–21 (2002).

87. Gual, P. *et al.* Hyperosmotic stress inhibits insulin receptor substrate-1 function by distinct mechanisms in 3T3-L1 adipocytes. *J. Biol. Chem.* **278**, 26550–26557 (2003).

88. Schenk, S., Saberi, M. & Olefsky, J. M. Insulin sensitivity: Modulation by nutrients and inflammation. *Journal of Clinical Investigation* **118**, 2992–3002 (2008).

89. Cani, P. D. *et al.* Metabolic endotoxemia initiates obesity and insulin resistance. *Diabetes* **56**, 1761–1772 (2007).

90. Zhang, K. & Kaufman, R. J. From endoplasmic-reticulum stress to the inflammatory response. *Nature* **454**, 455–462 (2008).

91. Boura-Halfon, S. & Zick, Y. Phosphorylation of IRS proteins, insulin action, and insulin resistance. *American Journal of Physiology -*

Endocrinology and Metabolism **296**, (2009).

92. Muoio, D. M. & Newgaard, C. B. Molecular and metabolic mechanisms of insulin resistance and B-cell failure in type 2 diabetes. *Nat. Rev. Mol. Cell Biol.* **9**, 193–205 (2008).
93. Lee, Y. H., Giraud, J., Davis, R. J. & White, M. F. c-Jun N-terminal kinase (JNK) mediates feedback inhibition of the insulin signaling cascade. *J. Biol. Chem.* **278**, 2896–2902 (2003).
94. Griffin, M. E. *et al.* Free fatty acid-induced insulin resistance is associated with activation of protein kinase C θ and alterations in the insulin signaling cascade. *Diabetes* **48**, 1270–1274 (2000).
95. Ehses, J. A. *et al.* Increased number of islet-associated macrophages in type 2 diabetes. *Diabetes* **56**, 2356–2370 (2007).
96. Larsen, C. M. *et al.* Interleukin-1-receptor antagonist in type 2 diabetes mellitus. *N. Engl. J. Med.* **356**, 1517–1526 (2007).
97. Ehses, J. A. *et al.* IL-1 antagonism reduces hyperglycemia and tissue inflammation in the type 2 diabetic GK rat. *Proc. Natl. Acad. Sci. U. S. A.* **106**, 13998–14003 (2009).
98. Sloan-Lancaster, J. *et al.* Double-blind, randomized study evaluating the glycemic and anti-inflammatory effects of subcutaneous LY2189102, a neutralizing IL-1β antibody, in patients with type 2 diabetes. *Diabetes Care* **36**, 2239–2246 (2013).
99. Kahn, S. E. The relative contributions of insulin resistance and beta-cell dysfunction to the pathophysiology of Type 2 diabetes. *Diabetologia* **46**, 3–19 (2003).
100. Halban, P. A. *et al.* β-Cell failure in Type 2 Diabetes: Postulated mechanisms and prospects for prevention and treatment. *Diabetes Care* **37**, 1751–1758 (2014).
101. Porte, D. & Kahn E, S. E. β-cell dysfunction and failure in Type 2 Diabetes: Potential mechanisms. in *Diabetes* **50**, S160 (American Diabetes Association, 2001).
102. Poitout, V. & Robertson, R. P. Minireview: Secondary β-cell failure in Type 2 Diabetes - A convergence of glucotoxicity and lipotoxicity. *Endocrinology* **143**, 339–342 (2002).
103. Maedler, K. *et al.* Glucose-induced β cell production of IL-1β contributes to glucotoxicity in human pancreatic islets. *J. Clin. Invest.* **110**, 851–860 (2002).
104. Böni-Schnetzler, M. *et al.* Free fatty acids induce a proinflammatory response in islets via the abundantly expressed interleukin-1 receptor I. *Endocrinology* **150**, 5218–5229 (2009).

105. Westermark, P. *et al.* Amyloid fibrils in human insulinoma and islets of Langerhans of the diabetic cat are derived from a neuropeptide-like protein also present in normal islet cells. *Proc. Natl. Acad. Sci. U. S. A.* **84**, 3881–3885 (1987).

106. Cooper, G. J. S. *et al.* Purification and characterization of a peptide from amyloid-rich pancreases of Type 2 Diabetic patients. *Proc. Natl. Acad. Sci. U. S. A.* **84**, 8628–8632 (1987).

107. Park, Y. J. *et al.* Deletion of Fas protects islet beta cells from cytotoxic effects of human islet amyloid polypeptide. *Diabetologia* **55**, 1035–1047 (2012).

108. Park, Y. J. *et al.* The role of caspase-8 in amyloid-induced beta cell death in human and mouse islets. *Diabetologia* **57**, 765–775 (2014).

109. Hotamisligil, G. S., Shargill, S. & Spiegelman, B. M. Adipose expression of Tumor Necrosis Factor-Alpha: Direct role in obesity-linked insulin resistance. *Science (80-.).* **259**, 87–91 (1993).

110. Hotamisligil, G. S. Inflammation and metabolic disorders. *Nature* **444**, (2006).

111. Osborn, O. & Olefsky, J. M. The cellular and signaling networks linking the immune system and metabolism in disease. *Nat. Med.* **18**, 363–74 (2012).

112. Mathis, D. Immunological goings-on in visceral adipose tissue. *Cell Metabolism* **17**, 851–859 (2013).

113. Odegaard, J. I. & Chawla, A. Pleiotropic actions of insulin resistance and inflammation in metabolic homeostasis. *Science* **339**, 172–177 (2013).

114. Fox, M. J., Kuzma, J. F. & Washam, W. T. Transitory diabetic syndrome associated with meningococcic meningitis. *Arch. Intern. Med.* **79**, 614–621 (1947).

115. Ebstein, W. Zur therapie des Diabetes mellitus, insbesondere über die Anwendung des salicylsauren Natron bei demselben. *Berliner Klin. Wochenschrift* **13**, 337–340 (1876).

116. Raymond, R. M., Harkema, J. M. & Emerson Jr, T. E. Mechanism of Increased Glucose Uptake by Skeletal Muscle During E. Coli Endotoxin Shock in the Dog. *Circ. Shock* **8**, 77 (1981).

117. Drobny, E. C., Abramson, E. C. & Baumann, G. Insulin receptors in acute infection: A study of factors conferring insulin resistance. *J. Clin. Endocrinol. Metab.* **58**, 710–716 (1984).

118. Kopp, E. & Ghosh, S. Inhibition of NF-κB by sodium salicylate and aspirin. *Science (80-.).* **265**, 956–959 (1994).

119. Hundal, R. S. *et al.* Mechanism by which high-dose aspirin improves

glucose metabolism in Type 2 Diabetes. *J. Clin. Invest.* **109**, 1321–1326 (2002).

120. Hotamisligil, G. S. Foundations of Immunometabolism and Implications for Metabolic Health and Disease. *Immunity* **47**, (2017).
121. Yongmei Xi, Y. Z. Fat Body Development and its Function in Energy Storage and Nutrient Sensing in Drosophila melanogaster. *J. Tissue Sci. Eng.* **06**, (2015).
122. Kurz, C. L. & Tan, M. W. Regulation of aging and innate immunity in C. elegans. *Aging Cell* **3**, 185–193 (2004).
123. Søndergaard, L. Homology between the mammalian liver and the Drosophila fat body. *Trends Genet.* **9**, 193 (1993).
124. Leclerc, V. & Reichhart, J. M. The immune response of Drosophila melanogaster. *Immunological Reviews* **198**, 59–71 (2004).
125. Cavallari, J. F., Denou, E., Foley, K. P., Khan, W. I. & Schertzer, J. D. Different Th17 immunity in gut, liver, and adipose tissues during obesity: the role of diet, genetics, and microbes. *Gut Microbes* **7**, (2016).
126. Mcphee, J. B. & Schertzer, J. D. Immunometabolism of obesity and diabetes: microbiota link compartmentalized immunity in the gut to metabolic tissue inflammation. *Clin. Sci.* **129**, 1083–1096 (2015).
127. Shoelson, S. E., Lee, J. & Goldfine, A. B. Inflammation and insulin resistance. *Journal of Clinical Investigation* **116**, 1793–1801 (2006).
128. Gregor, M. F. & Hotamisligil, G. S. Inflammatory mechanisms in obesity. *Annu. Rev. Immunol.* **29**, 415–445 (2011).
129. Yuan, M. *et al.* Reversal of obesity- and diet-induced insulin resistance with salicylates or targeted disruption of Ikkbeta. *Science* **293**, 1673–7 (2001).
130. Uysal, K. T., Wiesbrock, S. M., Marino, M. W. & Hotamisligil, G. S. Protection from obesity-induced insulin resistance in mice lacking TNF-α function. *Nature* **389**, 610–614 (1997).
131. Ventre, J. *et al.* Targeted Disruption of the Tumor Necrosis Factor-Alpha Gene: Metabolic Consequences in Obese and Nonobese Mice. *Diabetes* **46**, 1526–1531 (1997).
132. Johnson, A. M. F. & Olefsky, J. M. The origins and drivers of insulin resistance. *Cell* **152**, 673–684 (2013).
133. Boden, G., Chen, X., Ruiz, J., White, J. V. & Rossetti, L. Mechanisms of fatty acid-induced inhibition of glucose uptake. *J. Clin. Invest.* **93**, 2438–2446 (1994).
134. Shi, H. *et al.* TLR4 links innate immunity and fatty acid – induced insulin resistance. *J. Clin. Invest.* **116**, 3015–3025 (2006).

135. Wen, H. *et al.* Fatty acid-induced NLRP3-ASC inflammasome activation interferes with insulin signaling. *Nat. Immunol.* **12**, 408–15 (2011).

136. Lancaster, G. I. *et al.* Evidence that TLR4 Is Not a Receptor for Saturated Fatty Acids but Mediates Lipid-Induced Inflammation by Reprogramming Macrophage Metabolism. *Cell Metab.* **27**, (2018).

137. Lee, J. Y. *et al.* Saturated Fatty Acid Activates but Polyunsaturated Fatty Acid Inhibits Toll-like Receptor 2 Dimerized with Toll-like Receptor 6 or 1. *J. Biol. Chem.* **279**, 16971–16979 (2004).

138. Amar, J. *et al.* Energy intake is associated with endotoxemia in apparently healthy men. *Am. J. Clin. Nutr.* (2008).

139. Chan, K. L. *et al.* Circulating NOD1 Activators and Hematopoietic NOD1 Contribute to Metabolic Inflammation and Insulin Resistance. *Cell Rep.* **18**, 2415–2426 (2017).

140. Aroor, A. R. & DeMarco, V. G. Oxidative stress and obesity: The chicken or the egg? *Diabetes* **63**, 2216–2218 (2014).

141. Furukawa, S. *et al.* Increased oxidative stress in obesity and its impact on metabolic syndrome. *J. Clin. Invest.* **114**, 1752–1761 (2004).

142. Ozcan, U. *et al.* Endoplasmic reticulum stress links obesity, insulin action, and Type 2 Diabetes. *Science (80-.).* **306**, 457–61 (2004).

143. Hu, P., Han, Z., Couvillon, A. D., Kaufman, R. J. & Exton, J. H. Autocrine Tumor Necrosis Factor Alpha Links Endoplasmic Reticulum Stress to the Membrane Death Receptor Pathway through IRE1α-Mediated NF-κB Activation and Down-Regulation of TRAF2 Expression. *Mol. Cell. Biol.* **26**, 3071–3084 (2006).

144. Deng, J. *et al.* Translational Repression Mediates Activation of Nuclear Factor Kappa B by Phosphorylated Translation Initiation Factor 2. *Mol. Cell. Biol.* **24**, 10161–10168 (2004).

145. Arkan, M. C. *et al.* IKK- β links inflammation to obesity-induced insulin resistance. *Nat. Med.* **11**, 191–198 (2005).

146. Weissmann, L. *et al.* IKKε is key to induction of insulin resistance in the hypothalamus, and its inhibition reverses obesity. *Diabetes* **63**, 3334–3345 (2014).

147. Kwon, H. *et al.* Adipocyte-Specific IKKβ Signaling Suppresses Adipose Tissue Inflammation through an IL-13-Dependent Paracrine Feedback Pathway. *Cell Rep.* **9**, 1574–1583 (2014).

148. Mosser, D. M. The many faces of macrophage activation. *J. Leukoc. Biol.* **73**, 209–212 (2003).

149. Weisberg, S. P. *et al.* Obesity is associated with macrophage accumulation in adipose tissue. *J. Clin. Invest.* **112**, 1796–808 (2003).

150. Olefsky, J. M. & Glass, C. K. Macrophages, Inflammation, and Insulin Resistance. *Annu. Rev. Physiol.* **72**, 219–246 (2010).

151. Xu, H. *et al.* Chronic inflammation in fat plays a crucial role in the development of obesity-related insulin resistance. *J. Clin. Invest.* **112**, 1821–30 (2003).

152. De Victoria, E. O. M. *et al.* Macrophage content in subcutaneous adipose tissue: Associations with adiposity, age, inflammatory markers, and whole-body insulin action in healthy Pima Indians. *Diabetes* **58**, 385–393 (2009).

153. Sherwin, R. S. *et al.* Epinephrine and the regulation of glucose metabolism: Effect of diabetes and hormonal interactions. *Metabolism* **29**, 1146–1154 (1980).

154. Freitas-Lopes, M., Mafra, K., David, B., Carvalho-Gontijo, R. & Menezes, G. Differential Location and Distribution of Hepatic Immune Cells. *Cells* **6**, 48 (2017).

155. Cai, D. *et al.* Local and systemic insulin resistance resulting from hepatic activation of IKK--β and NF-κB. *Nat. Med.* **11**, 183–190 (2005).

156. Magkos, F. *et al.* Intrahepatic diacylglycerol content is associated with hepatic insulin resistance in obese subjects. *Gastroenterology* **142**, (2012).

157. Konstantynowicz-Nowicka, K., Harasim, E., Baranowski, M. & Chabowski, A. New evidence for the role of ceramide in the development of hepatic insulin resistance. *PLoS One* **10**, (2015).

158. Eipel, C., Abshagen, K. & Vollmar, B. Regulation of hepatic blood flow: The hepatic arterial buffer response revisited. *World Journal of Gastroenterology* **16**, 6046–6057 (2010).

159. DeFronzo, R. A. & Tripathy, D. Skeletal muscle insulin resistance is the primary defect in type 2 diabetes. *Diabetes care* **32 Suppl 2**, S157 (2009).

160. Febbraio, M. A. *et al.* Glucose ingestion attenuates interleukin-6 release from contracting skeletal muscle in humans. *J. Physiol.* **549**, 607–612 (2003).

161. Röhl, M. *et al.* Conditional disruption of IκB kinase 2 fails to prevent obesity-induced insulin resistance. *J. Clin. Invest.* **113**, 474–481 (2004).

162. Sell, H., Dietze-Schroeder, D., Kaiser, U. & Eckel, J. Monocyte chemotactic protein-1 is a potential player in the negative cross-talk between adipose tissue and skeletal muscle. *Endocrinology* **147**, 2458–2467 (2006).

163. Plomgaard, P. *et al.* Tumor Necrosis Factor-α Induces Skeletal Muscle Insulin Resistance in Healthy Human Subjects via Inhibition of Akt Substrate 160 Phosphorylation. *Diabetes* **54**, 2939–2945 (2005).

164. Kelley, D. E., Goodpaster, B. H. & Storlien, L. Muscle Triglyceride and

Insulin Resistance. *Annu. Rev. Nutr.* **22**, 325–346 (2002).

165. Krssak, M. *et al.* Intramyocellular lipid concentrations are correlated with insulin sensitivity in humans: A 1H NMR spectroscopy study. *Diabetologia* **42**, 113–116 (1999).
166. Itani, S. I., Ruderman, N. B., Schmieder, F. & Boden, G. Lipid-induced insulin resistance in human muscle is associated with changes in diacylglycerol, protein kinase C, and IκB-α. *Diabetes* **51**, 2005–2011 (2002).
167. Eguchi, K. & Nagai, R. Islet inflammation in type 2 diabetes and physiology. *Journal of Clinical Investigation* **127**, 14–23 (2017).
168. Giannoukakis, N., Rudert, W. A., Trucco, M. & Robbins, P. D. Protection of human islets from the effects of interleukin-1β by adenoviral gene transfer of an IκB repressor. *J. Biol. Chem.* **275**, 36509–36513 (2000).
169. Eldor, R. *et al.* Conditional and specific NF-κB blockade protects pancreatic beta cells from diabetogenic agents. *Proc. Natl. Acad. Sci. U. S. A.* **103**, 5072–5077 (2006).
170. Obici, S. & Rossetti, L. Minireview: Nutrient Sensing and the Regulation of Insulin Action and Energy Balance. *Endocrinology* **144**, 5172–5178 (2003).
171. Obici, S., Zhang, B. B., Karkanias, G. & Rossetti, L. Hypothalamic insulin signaling is required for inhibition of glucose production. *Nat. Med.* **8**, 1376–1382 (2002).
172. Winer, D. A., Luck, H., Tsai, S. & Winer, S. The intestinal immune system in obesity and insulin resistance. *Cell Metabolism* **23**, 413–426 (2016).
173. Ding, S. *et al.* High-fat diet: Bacteria interactions promote intestinal inflammation which precedes and correlates with obesity and insulin resistance in mouse. *PLoS One* **5**, (2010).
174. Luck, H. *et al.* Regulation of obesity-related insulin resistance with gut anti-inflammatory agents. *Cell Metab.* **21**, 527–542 (2015).
175. Johnson, A. M. F. *et al.* High fat diet causes depletion of intestinal eosinophils associated with intestinal permeability. *PLoS One* **10**, (2015).
176. Sonnenberg, G. F. & Artis, D. Innate Lymphoid Cell Interactions with Microbiota: Implications for Intestinal Health and Disease. *Immunity* **37**, 601–610 (2012).
177. Zheng, Y. *et al.* Interleukin-22 mediates early host defense against attaching and effacing bacterial pathogens. *Nat. Med.* **14**, 282–289 (2008).
178. Cani, P. D. *et al.* Changes in gut microbiota control metabolic endotoxemia-induced inflammation in high-fat diet-induced obesity and diabetes in mice. *Diabetes* **57**, 1470–81 (2008).

179. Takeuchi, O. & Akira, S. Pattern Recognition Receptors and Inflammation. *Cell* **140**, 805–820 (2010).

180. Kawai, T. & Akira, S. The role of pattern-recognition receptors in innate immunity: Update on toll-like receptors. *Nature Immunology* **11**, 373–384 (2010).

181. Girardin, S. E. *et al.* Peptidoglycan molecular requirements allowing detection by Nod1 and Nod2. *J. Biol. Chem.* **278**, 41702–8 (2003).

182. Girardin, S. E. *et al.* Nod1 detects a unique muropeptide from gram-negative bacterial peptidoglycan. *Science* **300**, 1584–7 (2003).

183. Chamaillard, M. *et al.* An essential role for NOD1 in host recognition of bacterial peptidoglycan containing diaminopimelic acid. *Nat. Immunol.* **4**, 702–707 (2003).

184. Philpott, D. J., Sorbara, M. T., Robertson, S. J., Croitoru, K. & Girardin, S. E. NOD proteins: Regulators of inflammation in health and disease. *Nature Reviews Immunology* **14**, 9–23 (2014).

185. Kobayashi, K. *et al.* RICK/Rip2/CARDIAK mediates signalling for receptors of the innate and adaptive immune systems. *Nature* **416**, 194–9 (2002).

186. McCarthy, J. V., Ni, J. & Dixit, V. M. RIP2 Is a Novel NF-kappa B-activating and Cell Death-inducing Kinase. *J. Biol. Chem.* **273**, 16968–16975 (1998).

187. Lysenko, E. S. *et al.* Nod1 signaling overcomes resistance of S. pneumoniae to opsonophagocytic killing. *PLoS Pathog.* **3**, 1073–1081 (2007).

188. Hugot, J. P. *et al.* Association of NOD2 leucine-rich repeat variants with susceptibility to Crohn's disease. *Nature* **411**, 599–603 (2001).

189. Yang, S. *et al.* Pellino3 ubiquitinates RIP2 and mediates Nod2-induced signaling and protective effects in colitis. *Nat. Immunol.* **14**, 927–936 (2013).

190. Duggan, B. M. *et al.* Tyrosine kinase inhibitors of RIPK2 attenuate bacterial cell wall-mediated lipolysis, inflammation and dysglycemia. *Sci. Rep.* **7**, 1578 (2017).

191. Vandanmagsar, B. *et al.* The NLRP3 inflammasome instigates obesity-induced inflammation and insulin resistance. *Nat. Med.* **17**, 179–88 (2011).

192. Henriksbo, B. D. *et al.* Fluvastatin causes NLRP3 inflammasome-mediated adipose insulin resistance. *Diabetes* **63**, 3742–7 (2014).

193. Cavallari, J. F. *et al.* Muramyl Dipeptide-Based Postbiotics Mitigate Obesity-Induced Insulin Resistance via IRF4. *Cell Metab.* **25**, 1063–1074 (2017).

194. Chi, W. *et al.* Bacterial peptidoglycan stimulates adipocyte lipolysis via NOD1. *PLoS One* **9**, e97675 (2014).

195. Zhou, Y. J. *et al.* Increased NOD1, but not NOD2, activity in subcutaneous adipose tissue from patients with metabolic syndrome. *Obesity* **23**, 1394–1400 (2015).

196. Denou, E. *et al.* Defective NOD2 peptidoglycan sensing promotes diet-induced inflammation, dysbiosis, and insulin resistance. *EMBO Mol. Med.* **7**, 259–74 (2015).

197. Tigno-aranjuez, J. T., Asara, J. M. & Abbott, D. W. Inhibition of RIP2's tyrosine kinase activity limits NOD2-driven cytokine responses. *Genes Dev.* **24**, 2666–2677 (2010).

198. Chin, A. I. *et al.* Involvement of receptor-interacting protein 2 in innate and adaptive immune responses. *Nature* **416**, 190–4 (2002).

199. Park, J.-H. *et al.* RICK/RIP2 Mediates Innate Immune Responses Induced through Nod1 and Nod2 but Not TLRs. *J. Immunol.* **178**, 2380–2386 (2007).

200. Medzhitov, R. & Janeway, C. Innate immune recognition: mechanisms and pathways. *Immunol. Rev.* **173**, 89–97 (2000).

201. Bertrand, M. J. M. *et al.* Cellular Inhibitors of Apoptosis cIAP1 and cIAP2 Are Required for Innate Immunity Signaling by the Pattern Recognition Receptors NOD1 and NOD2. *Immunity* **30**, 789–801 (2009).

202. Krieg, A. *et al.* XIAP mediates NOD signaling via interaction with RIP2. *Proc. Natl. Acad. Sci. U. S. A.* **106**, 14524–14529 (2009).

203. Abbott, D. W. *et al.* Coordinated Regulation of Toll-Like Receptor and NOD2 Signaling by K63-Linked Polyubiquitin Chains. *Mol. Cell. Biol.* **27**, 6012–6025 (2007).

204. Windheim, M., Lang, C., Peggie, M., Plater, L. A. & Cohen, P. Molecular mechanisms involved in the regulation of cytokine production by muramyl dipeptide. *Biochem. J.* **404**, 179–190 (2007).

205. Hasegawa, M. *et al.* A critical role of RICK/RIP2 polyubiquitination in Nod-induced NF-κB activation. *EMBO J.* **27**, 373–383 (2008).

206. Liu, T., Zhang, L., Joo, D. & Sun, S. C. NF-κB signaling in inflammation. *Signal Transduction and Targeted Therapy* **2**, 1–9 (2017).

207. Tao, M. F. *et al.* ITCH K63-Ubiquitinates the NOD2 Binding Protein, RIP2, to Influence Inflammatory Signaling Pathways. *Curr. Biol.* **19**, 1255–1263 (2009).

208. Harris, T. E. & Lawrence, J. C. TOR signaling. *Science's STKE : Signal Transduction Knowledge Environment* **212**, re15 (2003).

209. Lozupone, C. A., Stombaugh, J. I., Gordon, J. I., Jansson, J. K. & Knight,

R. Diversity, stability and resilience of the human gut microbiota. *Nature* **489**, 220–30 (2012).

210. Kamada, N. & Núñez, G. Regulation of the Immune System by the Resident Intestinal Bacteria. *Gastroenterology* **146**, 1477–1488 (2014).
211. Caesar, R. *et al.* Gut-derived lipopolysaccharide augments adipose macrophage accumulation but is not essential for impaired glucose or insulin tolerance in mice. *Gut* **61**, 1701–1707 (2012).
212. Kennedy, E. A., King, K. Y. & Baldridge, M. T. Mouse microbiota models: Comparing germ-free mice and antibiotics treatment as tools for modifying gut bacteria. *Front. Physiol.* **9**, 1534 (2018).
213. Yoo, S. *et al.* Comparison of dietary intakes associated with metabolic syndrome risk factors in young adults: the Bogalusa Heart Study. *Am J Clin Nutr* **80**, 841–849 (2004).
214. Rinaldi, A. E. M. *et al.* Dietary factors associated with metabolic syndrome and its components in overweight and obese Brazilian school children: A cross-sectional study. *Diabetol. Metab. Syndr.* **8**, 58 (2016).
215. Turnbaugh, P. J. *et al.* The effect of diet on the human gut microbiome: A metagenomic analysis in humanized gnotobiotic mice. *Sci. Transl. Med.* **1**, 6ra14-6ra14 (2009).
216. Faith, J. J., McNulty, N. P., Rey, F. E. & Gordon, J. I. Predicting a human gut microbiota's response to diet in gnotobiotic mice. *Science (80-.).* **333**, 101–104 (2011).
217. Chassaing, B. *et al.* Dietary emulsifiers impact the mouse gut microbiota promoting colitis and metabolic syndrome. *Nature* **519**, 92–96 (2015).
218. Ley, R. E., Turnbaugh, P. J., Klein, S. & Gordon, J. I. Microbial ecology: Human gut microbes associated with obesity. *Nature* **444**, 1022–1023 (2006).
219. Festi, D. *et al.* Gut microbiota and metabolic syndrome. *World Journal of Gastroenterology* **20**, 16079–16094 (2014).
220. He, M. & Shi, B. Gut microbiota as a potential target of metabolic syndrome: The role of probiotics and prebiotics. *Cell and Bioscience* **7**, 1–14 (2017).
221. Vrieze, A. *et al.* Transfer of intestinal microbiota from lean donors increases insulin sensitivity in individuals with metabolic syndrome. *Gastroenterology* **143**, 913-916.e7 (2012).
222. Kootte, R. S. *et al.* Improvement of Insulin Sensitivity after Lean Donor Feces in Metabolic Syndrome Is Driven by Baseline Intestinal Microbiota Composition. *Cell Metab.* **26**, 611-619.e6 (2017).
223. Everard, A. *et al.* Cross-talk between Akkermansia muciniphila and

intestinal epithelium controls diet-induced obesity. *Proc. Natl. Acad. Sci. U. S. A.* **110**, 9066–9071 (2013).

224. Plovier, H. *et al.* A purified membrane protein from Akkermansia muciniphila or the pasteurized bacterium improves metabolism in obese and diabetic mice. *Nat. Med.* **23**, 107–113 (2017).
225. Depommier, C. *et al.* Supplementation with Akkermansia muciniphila in overweight and obese human volunteers: a proof-of-concept exploratory study. *Nat. Med.* **25**, 1096–1103 (2019).
226. Illuri, V. D. S., Layden, B. T. & Aleppo, G. Extreme insulin resistance in critically ill patient with sepsis. *Clinical Diabetes* **34**, 158–160 (2016).
227. Van Cromphaut, S., Vanhorebeek, I. & Berghe, G. Glucose Metabolism and Insulin Resistance in Sepsis. *Curr. Pharm. Des.* **14**, 1887–1899 (2008).
228. Pomié, C. *et al.* Triggering the adaptive immune system with commensal gut bacteria protects against insulin resistance and dysglycemia. *Mol. Metab.* **5**, 392–403 (2016).
229. Rena, G., Hardie, D. G. & Pearson, E. R. The mechanisms of action of metformin. *Diabetologia* **60**, 1577–1585 (2017).
230. Pollak, M. The effects of metformin on gut microbiota and the immune system as research frontiers. *Diabetologia* **60**, 1662–1667 (2017).
231. Shin, N. R. *et al.* An increase in the Akkermansia spp. population induced by metformin treatment improves glucose homeostasis in diet-induced obese mice. *Gut* **63**, 727–735 (2014).
232. Forslund, K. *et al.* Disentangling type 2 diabetes and metformin treatment signatures in the human gut microbiota. *Nature* **528**, 262–266 (2015).
233. Cameron, A. R. *et al.* Anti-Inflammatory Effects of Metformin Irrespective of Diabetes Status. *Circ. Res.* **119**, 652–665 (2016).
234. Vasamsetti, S. B. *et al.* Metformin inhibits monocyte-to-macrophage differentiation via AMPK-mediated inhibition of STAT3 activation: Potential role in atherosclerosis. *Diabetes* **64**, 2028–2041 (2015).
235. Cabreiro, F. *et al.* Metformin retards aging in C. elegans by altering microbial folate and methionine metabolism. *Cell* **153**, 228–239 (2013).
236. Albert, M. A., Danielson, E., Rifai, N. & Ridker, P. M. Effect of statin therapy on C-reactive protein levels: The pravastatin inflammation/CRP evaluation (PRINCE): A randomized trial and cohort study. *J. Am. Med. Assoc.* **286**, 64–70 (2001).
237. Karmaus, P. W. F. *et al.* Effects of rosuvastatin on the immune system in healthy volunteers with normal serum cholesterol. *JCI Insight* **4**, (2019).
238. Henriksbo, B. D. & Schertzer, J. D. Is immunity a mechanism contributing to statin-induced diabetes? *Adipocyte* **4**, (2015).

239. Liao, Y.-H. *et al.* HMG-CoA reductase inhibitors activate caspase-1 in human monocytes depending on ATP release and P2X7 activation. *J. Leukoc. Biol.* **93**, 289–299 (2013).

240. Kontzias, A., Laurence, A., Gadina, M. & O'Shea, J. J. Kinase inhibitors in the treatment of immune-mediated disease. *F1000 Med. Rep.* **4**, 5 (2012).

241. Patterson, H., Nibbs, R., McInnes, I. & Siebert, S. Protein kinase inhibitors in the treatment of inflammatory and autoimmune diseases. *Clin. Exp. Immunol.* **176**, 1–10 (2014).

242. Adams, J. A. Kinetic and Catalytic Mechanisms of Protein Kinases. *Chem. Rev.* **101**, 2271–2290 (2001).

243. Manning, G., Whyte, D. B., Martinez, R., Hunter, T. & Sudarsanam, S. The protein kinase complement of the human genome. *Science* **298**, 1912–1934 (2002).

244. Dhanasekaran, N. & Premkumar Reddy, E. Signaling by dual specificity kinases. *Oncogene* **17**, 1447–1455 (1998).

245. Hanks, S. K. & Hunter, T. The eukaryotic protein kinase superfamily: kinase (catalytic) domain structure and classification 1 . *FASEB J.* **9**, 576–596 (1995).

246. Wu, P., Nielsen, T. E. & Clausen, M. H. FDA-approved small-molecule kinase inhibitors. *Trends Pharmacol. Sci.* **36**, 422–439 (2015).

247. Lahiry, P., Torkamani, A., Schork, N. J. & Hegele, R. A. Kinase mutations in human disease: Interpreting genotype-phenotype relationships. *Nature Reviews Genetics* **11**, 60–74 (2010).

248. Roskoski, R. Properties of FDA-approved small molecule protein kinase inhibitors: A 2020 update. *Pharmacological Research* **152**, 104609 (2020).

249. Guntur, V. P. & Reinero, C. R. The potential use of tyrosine kinase inhibitors in severe asthma. *Curr. Opin. Allergy Clin. Immunol.* **12**, 68–75 (2012).

250. Mesa, R. A. Ruxolitinib, a selective JAK1 and JAK2 inhibitor for the treatment of myeloproliferative neoplasms and psoriasis. *IDrugs* **13**, 394–403 (2010).

251. Sidhu, M. *et al.* Small molecule tyrosine kinase inhibitors for the treatment of intestinal inflammation. *Inflamm. Bowel Dis.* **17**, 2416–2426 (2011).

252. Tigno-Aranjuez, J. T. *et al.* In vivo inhibition of RIPK2 kinase alleviates inflammatory disease. *J. Biol. Chem.* **289**, 29651–29664 (2014).

253. Kirkwood, K. L. *et al.* A p38α selective mitogen-activated protein kinase inhibitor prevents periodontal bone loss. *J. Pharmacol. Exp. Ther.* **320**, 56–63 (2007).

254. Nachbur, U. *et al.* A RIPK2 inhibitor delays NOD signalling events yet

prevents inflammatory cytokine production. *Nat. Commun.* **6**, 6442 (2015).

255. Wollin, L., Maillet, I., Quesniaux, V., Holweg, A. & Ryffel, B. Antifibrotic and Anti-inflammatory Activity of the Tyrosine Kinase Inhibitor Nintedanib in Experimental Models of Lung Fibrosis. *J. Pharmacol. Exp. Ther.* **349**, 209–220 (2014).
256. Fountas, A., Diamantopoulos, L. N. & Tsatsoulis, A. Tyrosine kinase inhibitors and diabetes: A novel treatment paradigm? *Trends Endocrinol. Metab.* **26**, 643–656 (2015).
257. Prada, P. O. & Saad, M. J. Tyrosine kinase inhibitors as novel drugs for the treatment of diabetes. *Expert Opin. Investig. Drugs* **22**, 751–63 (2013).
258. Mokhtari, D. & Welsh, N. Potential utility of small tyrosine kinase inhibitors in the treatment of diabetes. *Clin. Sci. (Lond).* **118**, 241–247 (2010).
259. Noble, M. E. M., Endicott, J. A. & Johnson, L. N. Protein Kinase Inhibitors: Insights into Drug Design from Structure. *Science (80-.).* **305**, 1800–1805 (2004).
260. Garuti, L., Roberti, M. & Bottegoni, G. Non-ATP Competitive Protein Kinase Inhibitors. *Curr. Med. Chem.* **17**, 2804–2821 (2010).
261. Cox, K. J., Shomin, C. D. & Ghosh, I. Tinkering outside the kinase ATP box: Allosteric (type IV) and bivalent (type V) inhibitors of protein kinases. *Future Medicinal Chemistry* **3**, 29–43 (2011).
262. Davis, M. I. *et al.* Comprehensive analysis of kinase inhibitor selectivity. *Nat. Biotechnol.* **29**, 1046–51 (2011).
263. van Erp, N. P., Gelderblom, H. & Guchelaar, H. J. Clinical pharmacokinetics of tyrosine kinase inhibitors. *Cancer Treatment Reviews* **35**, 692–706 (2009).
264. Peng, B., Lloyd, P. & Schran, H. Clinical Pharmacokinetics of Imatinib. *Clin. Pharmacokinet.* **44**, 879–894 (2005).
265. Swaisland, H. C. *et al.* Single-Dose Clinical Pharmacokinetic Studies of Gefitinib. *Clin. Pharmacokinet.* **44**, 1165–1177 (2005).
266. Swaisland, H. *et al.* Pharmacokinetics and tolerability of the orally active selective epidermal growth factor receptor tyrosine kinase inhibitor ZD1839 in healthy volunteers. *Clin. Pharmacokinet.* **40**, 297–306 (2001).
267. Soldavini, J. & Kaunitz, J. D. Pathobiology and Potential Therapeutic Value of Intestinal Short-Chain Fatty Acids in Gut Inflammation and Obesity. *Dig Dis Sci* **58**, 2756–2766 (2013).
268. Taoka, H. *et al.* Role of bile acids in the regulation of the metabolic pathways. *World J Diabetes July World J Diabetes* **10**, 260–270 (2016).
269. Tolentino, M. S., Tolentino, A. J. & Tolentino, M. J. Current and

investigational drugs for the treatment of diabetic retinopathy. *Expert Opin. Investig. Drugs* **25**, 1011–1022 (2016).

270. Khamaisi, M., Schrijvers, B. F., De Vriese, A. S., Raz, I. & Flyvbjerg, A. The emerging role of VEGF in diabetic kidney disease. *Nephrol. Dial. Transplant* **18**, 1427–30 (2003).
271. Agostino, N. M. *et al.* Effect of the tyrosine kinase inhibitors (sunitinib, sorafenib, dasatinib, and imatinib) on blood glucose levels in diabetic and nondiabetic patients in general clinical practice. *J. Oncol. Pharm. Pract.* **17**, 197–202 (2011).
272. Brooks, M. B. Erlotinib and gefitinib, small-molecule EGFR inhibitors. New uses for old drugs? *Br. J. Diabetes Vasc. Dis.* **12**, 195–196 (2012).
273. Veneri, D., Franchini, M. & Bonora, E. Imatinib and regression of type 2 diabetes. *N. Engl. J. Med.* **352**, 1049–1050 (2005).
274. Ono, K. *et al.* Rapid amelioration of hyperglycemia facilitated by dasatinib in a Chronic Myeloid Leukemia patient with Type 2 Diabetes Mellitus. *Intern. Med.* **51**, 2763–2766 (2012).
275. Breccia, M. *et al.* Fasting glucose improvement under dasatinib treatment in an accelerated phase chronic myeloid leukemia patient unresponsive to imatinib and nilotinib. *Leuk. Res.* **32**, 1626–8 (2008).
276. Haap, M. *et al.* Symptomatic hypoglycemia during imatinib mesylate in a non-diabetic female patient with gastrointestinal stromal tumor. *J. Endocrinol. Invest.* **30**, 688–692 (2007).
277. Salaroli, A., Loglisci, G., Serrao, A., Alimena, G. & Breccia, M. Fasting glucose level reduction induced by imatinib in chronic myeloproliferative disease with TEL-PDGFR? rearrangement and type 1 diabetes. *Ann. Hematol.* **91**, 1823–1824 (2012).
278. Templeton, A., Brandle, M., Cerny, T. & Gillessen, S. Remission of diabetes while on sunitinib treatment for renal cell carcinoma. *Ann. Oncol.* **19**, 824–825 (2007).
279. Huda, M. S. B., Amiel, S. A., Ross, P. & Aylwin, S. J. B. Tyrosine kinase inhibitor sunitinib allows insulin independence in long-standing Type 1 Diabetes. *Diabetes Care* **37**, e87–e88 (2014).
280. Billemont, B. *et al.* Blood glucose levels in patients with metastatic renal cell carcinoma treated with sunitinib. *Br. J. Cancer* **99**, 1380–1382 (2008).
281. Han, M. S. *et al.* Imatinib mesylate reduces ER stress and induces remission of diabetes in db / db Mice. *Diabetes* **58**, 329–336 (2009).
282. Hägerkvist, R., Jansson, L. & Welsh, N. Imatinib mesylate improves insulin sensitivity and glucose disposal rates in rats fed a high-fat diet. *Clin. Sci. (Lond).* **114**, 65–71 (2008).

283. Prada, P. O. *et al.* EGFR tyrosine kinase inhibitor (PD153035) improves glucose tolerance and insulin action in high-fat diet-fed mice. *Diabetes* **58**, 2910–9 (2009).

284. Louvet, C. *et al.* Tyrosine kinase inhibitors reverse type 1 diabetes in nonobese diabetic mice. *Proc. Natl. Acad. Sci. USA* **105**, 18895–18900 (2008).

285. Lau, J. *et al.* Inhibition of c-Kit is not required for reversal of hyperglycemia by imatinib in NOD mice. *PLoS One* **9**, e84900 (2014).

286. Choung, S. *et al.* Epidermal growth factor receptor inhibition attenuates non-alcoholic fatty liver disease in diet-induced obese mice. *PLoS One* **14**, e0210828 (2019).

287. Ito, Y. *et al.* Nilotinib exacerbates diabetes mellitus by decreasing secretion of endogenous insulin. *Int. J. Hematol.* **97**, 135–8 (2013).

288. Zdenek, R. *et al.* Comparison of glucose and lipid metabolism abnormality during nilotinib, imatinib and dasatinib therapy – Results of Enigma 2 study. *Blood* **124**, 1813–1813 (2014).

289. Sequist, L. V. *et al.* Rociletinib in EGFR-mutated non–small-cell lung cancer. *N. Engl. J. Med.* **372**, 1700–1709 (2015).

290. Zykadia™ (ceritinib) [prescribing information]. *Novartis Pharm. Corp.* (2014).

291. Sakuma, I., Nagano, H., Yoshino, I., Yokote, K. & Tanaka, T. Ceritinib aggravates glycemic control in insulin-treated patients with diabetes and metastatic ALK-positive lung cancer. *Intern. Med.* **58**, 817–820 (2019).

292. Xia, C. Q. *et al.* C-Abl inhibitor imatinib enhances insulin production by β cells: c-Abl negatively regulates insulin production via interfering with the expression of NKx2.2 and GLUT-2. *PLoS One* **9**, e97694 (2014).

293. Lutz, S. Z., Ullrich, A., Häring, H. U., Ullrich, S. & Gerst, F. Sunitinib specifically augments glucose-induced insulin secretion. *Cell. Signal.* **36**, 91–97 (2017).

294. Fontaine, D. A. & Davis, D. B. Attention to background strain Is essential for metabolic research: C57BL/6 and the International Knockout Mouse Consortium. *Diabetes* **65**, 25–33 (2016).

295. Matthews, D. R. *et al.* Homeostasis model assessment: insulin resistance and β-cell function from fasting plasma glucose and insulin concentrations in man. *Diabetologia* **28**, 412–419 (1985).

296. Sim, K. *et al.* Improved Detection of Bifidobacteria with Optimised 16S rRNA-Gene Based Pyrosequencing. *PLoS One* **7**, e32543 (2012).

297. Gasic, S., Tian, B. & Green, A. Tumor necrosis factor α stimulates lipolysis in adipocytes by decreasing Gi protein concentrations. *J. Biol. Chem.* **274**,

6770–5 (1999).

298. Hoffman, B. B., Chang, H., Farahbakhsh, Z. & Reaven, G. Inhibition of lipolysis by adenosine is potentiated with age. *J. Clin. Invest.* **74**, 1750–5 (1984).

299. Ohisalo, J. J. Effects of Adenosine on Lipolysis in Human Subcutaneous Fat Cells. *J. Clin. Endocrinol. Metab.* **52**, 359–363 (1981).

300. Koppe, L. *et al.* p-Cresyl sulfate promotes insulin resistance associated with CKD. *J. Am. Soc. Nephrol.* **24**, 88–99 (2013).

301. Okamoto, H., Obici, S., Accili, D. & Rossetti, L. Restoration of liver insulin signaling in Insr knockout mice fails to normalize hepatic insulin action. *J. Clin. Invest.* **115**, 1314–1322 (2005).

302. Wang, M. *et al.* Salidroside improves glucose homeostasis in obese mice by repressing inflammation in white adipose tissues and improving leptin sensitivity in hypothalamus. *Sci. Rep.* **6**, (2016).

303. Shimizu, I. *et al.* Excessive cardiac insulin signaling exacerbates systolic dysfunction induced by pressure overload in rodents. *J. Clin. Invest.* **120**, 1506–1514 (2010).

304. Simon, M. M. *et al.* A comparative phenotypic and genomic analysis of C57BL/6J and C57BL/6N mouse strains. *Genome Biol.* **14**, R82 (2013).

305. Mekada, K. *et al.* Genetic differences among C57BL/6 substrains. *Exp. Anim.* **58**, 141–9 (2009).

306. Duckett, D. R. & Cameron, M. D. Metabolism considerations for kinase inhibitors in cancer treatment. *Expert Opin. Drug Metab. Toxicol.* **6**, 1175–1193 (2010).

307. Wang, Z. *et al.* Pharmacokinetics interaction between imatinib and genistein in rats. *Biomed Res. Int.* **2015**, 368976 (2015).

308. Bi, Y., Deng, J., Murry, D. J. & An, G. A whole-body physiologically based pharmacokinetic model of gefitinib in mice and scale-up to humans. *AAPS J.* **18**, 228–238 (2016).

309. Zheng, N. *et al.* Simultaneous determination of gefitinib and its major metabolites in mouse plasma by HPLC-MS/MS and its application to a pharmacokinetics study. *J. Chromatogr. B Anal. Technol. Biomed. Life Sci.* **1011**, 215–222 (2016).

310. Wang, S., Guo, P., Wang, X., Zhou, Q. & Gallo, J. M. Preclinical pharmacokinetic/pharmacodynamic models of gefitinib and the design of equivalent dosing regimens in EGFR wild-type and mutant tumor models. *Mol. Cancer Ther.* **7**, 407–417 (2008).

311. Cavallari, J. F. *et al.* Postbiotics for NOD2 require non-hematopoietic RIPK2 to improve blood glucose and metabolic inflammation in mice. *Am.*

J. Physiol. Endocrinol. Metab. **318**, e579-585 (2020).

312. Tran, H. Q., Ley, R. E., Gewirtz, A. T. & Chassaing, B. Flagellin-elicited adaptive immunity suppresses flagellated microbiota and vaccinates against chronic inflammatory diseases. *Nat. Commun.* **10**, 1–15 (2019).
313. Garidou, L. *et al.* The Gut Microbiota Regulates Intestinal CD4 T Cells Expressing RORγt and Controls Metabolic Disease. *Cell Metab.* **22**, 100–112 (2015).
314. Amar, J. *et al.* Intestinal mucosal adherence and translocation of commensal bacteria at the early onset of type 2 diabetes: molecular mechanisms and probiotic treatment. *EMBO Mol. Med.* **3**, 559–72 (2011).
315. Burcelin, R., Crivelli, V., Dacosta, A., Roy-Tirelli, A. & Thorens, B. Heterogeneous metabolic adaptation of C57BL/6J mice to high-fat diet. *Am. J. Physiol. - Endocrinol. Metab.* **282**, (2002).
316. Albenberg, L. G. & Wu, G. D. Diet and the intestinal microbiome: Associations, functions, and implications for health and disease. *Gastroenterology* **146**, 1564–1572 (2014).
317. Mowat, A. M. & Agace, W. W. Regional specialization within the intestinal immune system. *Nature Reviews Immunology* **14**, 667–685 (2014).
318. James, K. R. *et al.* Distinct microbial and immune niches of the human colon. *Nat. Immunol.* **21**, 343–353 (2020).
319. Brooks, M. B. Erlotinib appears to produce prolonged remission of insulin-requiring type 2 diabetes associated with metabolic syndrome and chronic kidney disease. *Br. J. Diabetes Vasc. Dis.* **12**, 87–90 (2012).
320. Breccia, M., Muscaritoli, M., Aversa, Z., Mandelli, F. & Alimena, G. Imatinib mesylate may improve fasting blood glucose in Ph+ Chronic Myelogenous Leukemia patients responsive to treatment. *J. Clin. Oncol.* **22**, 4653–4654 (2004).
321. Costa, D. B. & Huberman, M. S. Improvement of Type 2 Diabetes in a lung cancer patient treated with erlotinib. *Diabetes Care* **29**, 1711 (2006).
322. Drucker, D. J. *et al.* Never Waste a Good Crisis: Confronting Reproducibility in Translational Research. *Cell Metab.* **24**, 348–360 (2016).
323. Prinz, F., Schlange, T. & Asadullah, K. Believe it or not: how much can we rely on published data on potential drug targets? *Nat. Rev. Drug Discov.* **10**, 712–712 (2011).
324. Giovannucci, E. *et al.* Diabetes and Cancer: A Consensus Report. *CA. Cancer J. Clin.* **60**, 207–221 (2010).
325. Canning, P. *et al.* Inflammatory Signaling by NOD-RIPK2 Is Inhibited by

Clinically Relevant Type II Kinase Inhibitors. *Chem. Biol.* **22**, 1174–84 (2015).

326. Hägerkvist, R., Makeeva, N., Elliman, S. & Welsh, N. Imatinib mesylate (Gleevec) protects against streptozotocin-induced diabetes and islet cell death in vitro. *Cell Biol. Int.* **30**, 1013–1017 (2006).
327. Chen, Y. T. *et al.* Platelet-derived growth factor receptor signaling activates pericyte-myofibroblast transition in obstructive and post-ischemic kidney fibrosis. *Kidney Int.* **80**, 1170–1181 (2011).
328. Fitter, S., Vandyke, K., Gronthos, S. & Zannettino, A. C. W. Suppression of PDGF-induced PI3 kinase activity by imatinib promotes adipogenesis and adiponectin secretion. *J. Mol. Endocrinol.* **48**, 229–240 (2012).
329. Mukai, E. *et al.* Enhanced vascular endothelial growth factor signaling in islets contributes to β cell injury and consequential diabetes in spontaneously diabetic Torii rats. *Diabetes Res. Clin. Pract.* **106**, 303–11 (2014).
330. Zu, L. *et al.* Bacterial endotoxin stimulates adipose lipolysis via toll-like receptor 4 and extracellular signal-regulated kinase pathway. *J. Biol. Chem.* **284**, 5915–26 (2009).
331. Zeuke, S., Ulmer, A. J., Kusumoto, S., Katus, H. A. & Heine, H. TLR4-mediated inflammatory activation of human coronary artery endothelial cells by LPS. *Cardiovasc. Res.* **56**, 126–134 (2002).
332. Medzhitov, R. Recognition of microorganisms and activation of the immune response. *Nature* **449**, 819–826 (2007).
333. Lakhani, S. A. & Bogue, C. W. Toll-like receptor signaling in sepsis. *Current Opinion in Pediatrics* **15**, 278–282 (2003).
334. Masumoto, J. *et al.* Nod1 acts as an intracellular receptor to stimulate chemokine production and neutrophil recruitment in vivo. *J. Exp. Med.* **203**, 203–213 (2006).
335. Argast, G. M., Fausto, N. & Campbell, J. S. Inhibition of RIP2/RIck/CARDIAK activity by pyridinyl imidazole inhibitors of p38 MAPK. *Mol. Cell. Biochem.* **268**, 129–40 (2005).
336. Li, G., Barrett, E. J., Barrett, M. O., Cao, W. & Liu, Z. Tumor Necrosis Factor-α Induces Insulin Resistance in Endothelial Cells via a p38 Mitogen-Activated Protein Kinase-Dependent Pathway. *Endocrinology* **148**, 3356–3363 (2007).
337. Raetzsch, C. F. *et al.* Lipopolysaccharide inhibition of glucose production through the Toll-like receptor-4, myeloid differentiation factor 88, and nuclear factor κB pathway. *Hepatology* **50**, 592–600 (2009).
338. Tweedell, A. *et al.* Metabolic response to endotoxin in vivo in the

conscious mouse: role of interleukin-6. *Metabolism.* **60**, 92–8 (2011).

339. Waltner-Law, M., Daniels, M. C., Sutherland, C. & Granner, D. K. NF-κB Inhibits Glucocorticoid and cAMP-mediated Expression of the Phosphoenolpyruvate Carboxykinase Gene. *J. Biol. Chem.* **275**, 31847–31856 (2000).
340. Horton, R. A., Knowles, R. G. & Titheradge, M. A. Endotoxin Causes Reciprocal Changes in Hepatic Nitric Oxide Synthesis, Gluconeogenesis, and Flux through Phosphoenolpyruvate Carboxykinase. *Biochem. Biophys. Res. Commun.* **204**, 659–665 (1994).
341. Vogel, S. N., Henricson, B. E. & Neta, R. Roles of interleukin-1 and tumor necrosis factor in lipopolysaccharide-induced hypoglycemia. *Infect. Immun.* **59**, 2494–8 (1991).
342. Liang, H., Hussey, S. E., Sanchez-Avila, A., Tantiwong, P. & Musi, N. Effect of lipopolysaccharide on inflammation and insulin action in human muscle. *PLoS One* **8**, e63983 (2013).
343. Malek, R. & Davis, S. N. Tyrosine kinase inhibitors under investigation for the treatment of type II diabetes. *Expert Opin. Investig. Drugs* **25**, 287–96 (2016).
344. Lee, Y. S. *et al.* Inflammation is necessary for long-term but not short-term high-fat diet-induced insulin resistance. *Diabetes* **60**, 2474–83 (2011).
345. Foley, K. P. *et al.* Long term but not short term exposure to obesity related microbiota promotes host insulin resistance. *Nat. Commun.* **9**, 1–15 (2018).
346. Nassar, I., Pasupati, T., Judson, J. P. & Segarra, I. Reduced exposure of imatinib after coadministration with acetaminophen in mice. *Indian J. Pharmacol.* **41**, 167–172 (2009).
347. Mehran, A. E. *et al.* Hyperinsulinemia Drives Diet-Induced Obesity Independently of Brain Insulin Production. *Cell Metab.* **16**, 723–737 (2012).
348. *Janeway's Immunobiology, Ninth Edition.* (Garland Science: New York, New York., 2016).
349. Liu, B., Page, A. J., Hutchison, A. T., Wittert, G. A. & Heilbronn, L. K. Intermittent fasting increases energy expenditure and promotes adipose tissue browning in mice. *Nutrition* **66**, 38–43 (2019).
350. Wang, X.-A. *et al.* CARD3 deficiency exacerbates diet-induced obesity, hepatosteatosis, and insulin resistance in male mice. *Endocrinology* **154**, 685–697 (2013).
351. Holmdahl, R. & Malissen, B. The need for littermate controls. *Eur. J. Immunol.* **42**, 45–47 (2012).